

this document downloaded from

vulcanhammer.net

Since 1997, your complete
online resource for
information geotechnical
engineering and deep
foundations:

The Wave Equation Page for
Piling

*Online books on all aspects of
soil mechanics, foundations and
marine construction*

Free general engineering and
geotechnical software

And much more...

Terms and Conditions of Use:

All of the information, data and computer software ("information") presented on this web site is for general information only. While every effort will be made to insure its accuracy, this information should not be used or relied on for any specific application without independent, competent professional examination and verification of its accuracy, suitability and applicability by a licensed professional. Anyone making use of this information does so at his or her own risk and assumes any and all liability resulting from such use. The entire risk as to quality or usability of the information contained within is with the reader. In no event will this web page or webmaster be held liable, nor does this web page or its webmaster provide insurance against liability, for any damages including lost profits, lost savings or any other incidental or consequential damages arising from the use or inability to use the information contained within.

This site is not an official site of Prentice-Hall, Pile Buck, the University of Tennessee at Chattanooga, or Vulcan Foundation Equipment. All references to sources of software, equipment, parts, service or repairs do not constitute an endorsement.

**Visit our
companion site**

<http://www.vulcanhammer.org>



ANALYSIS OF Laterally Loaded Drilled Shafts in Rock

A Dissertation

Presented to

The Graduate Faculty of The University of Akron

In Partial Fulfillment

of the Requirements for the Degree

Doctor of Philosophy

Ke Yang

May, 2006

ANALYSIS OF Laterally Loaded Drilled Shafts in Rock

Ke Yang

Dissertation

Approved:

Advisor
Dr. Robert Liang

Committee Member
Dr. Wieslaw Binienda

Committee Member
Dr. Ernian Pan

Committee Member
Dr. Yueh-Jaw Lin

Committee Member
Dr. Chien-Chung Chan

Accepted:

Department Chair
Dr. Wieslaw Binienda

Dean of the College
Dr. George Haritos

Dean of the Graduate School
Dr. George Newkome

Date

ABSTRACT

Drilled shafts socketed into rock are widely used as foundations for bridges and other important structures. Rock-socketed drilled shafts are also used to stabilize a landslide. The main loads applied on the drilled shafts are axial compressive or uplift loads as well as lateral loads with accompanying moments. Although there exist several analysis and design methods especially for rock-socketed drilled shafts under lateral loading, these methods were developed with assumptions without actual validations with field load test results. Some of the methods have been found to provide unsafe designs when compared to recently available field test data. Therefore, there is a need to develop a more rational design approach for laterally loaded drilled shafts socketed in rock.

A hyperbolic non-linear p-y criterion for rock is developed in this study that can be used in conjunction with existing computer programs, such as COM624P, LPILE, and FBPIER, to predict the deflection, moment, and shear responses of a shaft under the applied lateral loads. Considerations for the effects of joints and discontinuities on the rock mass modulus and strength are included in the p-y criterion. Evaluations based on comparisons between the predicted and measured responses of full-scale lateral load tests on fully instrumented drilled shafts have shown the applicability of the proposed p-y

criterion and the associated methods for determining the required input of rock parameters.

In addition to the development of a hyperbolic p - y criterion for rock, a method for predicting lateral capacities of drilled shafts in rock and/or soils is developed for assessing the safety margin of the designed shafts against the design loads. A computer program LCPILE is developed using VC++ to facilitate computations. An elastic solution based on a variational approach is also developed for determining drilled shaft elastic deflection due to applied lateral loads in a two-layer soil layer system. The computational algorithm was coded in a Mathematica file for easy application.

Finally, Briaud's method for deriving p - y curves of rock from pressuremeter or dilatometer test results is evaluated using available field test data. A modification to the Briaud's method is recommended for applications in rocks.

DEDICATION

To my wife, my father and mother, who made all of this possible, for their endless encouragement and patience.

ACKNOWLEDGEMENTS

As I approach the end of my graduate tenure, I am left with profound feelings of accomplishment, excitement, and gratitude to a number of people whose support has been significant in completing this dissertation.

My advisor Professor Robert Y. Liang, has been a constant source of inspiration, motivation and guidance throughout the past three and a half years. I have learned so much from his keen insight, his research and problem solving abilities, and his amazing energy. What I learned from him is not only the knowledge, but also the way to be a positive and energetic person.

Thanks in large part to the kindness and mentoring provided by the committee members: Dr. Wieslaw Binienda, Dr. Ernian Pan, Dr. Yueh-Jaw Lin, and Dr. Chien-Chung Chan. Additionally, the great help from Dr. Jamal Nusairat is highly appreciated.

My wife, parents, and brother have been extremely supportive of my studies, and have always been encouraging and understanding. I am also grateful to my wonderful friends in Akron, Ohio. Their aid has been invaluable during the period of this work.

TABLE OF CONTENTS

	Page
LIST OF TABLES	xiii
LIST OF FIGURES	xvi
 CHAPTER	
I. INTRODUCTION.....	1
1.1 Statement of the Problem	1
1.2 Objectives.....	3
1.3 Scope of the Work.....	4
1.4 Outlines of the Dissertation.....	6
II. LITERATURE REVIEW	8
2.1 Analysis Methods of Laterally Loaded Rock-Socketed Drilled Shafts	8
2.1.1 Introduction.....	8
2.1.2 Brief Description of the Existing Methods	10
2.1.3 Comments on the Existing Analysis Methods	23
2.2 Bedrocks of Ohio	26
2.2.1 The Distribution of Rocks in Ohio.....	26
2.2.2 The Shales in Ohio	30
2.2.3 Limestone and Dolomite.....	34

2.3 Mechanical Characteristics of Rock and Its Classifications	35
2.3.1 The types of rocks	35
2.3.2 Features for Rock Characterization.....	35
2.3.3 Rock Mass Classifications	38
III. LATERAL LOAD TEST RESULTS AND DATA ANALYSES	49
3.1 Lateral Load Test at Dayton.....	49
3.1.1 Test Site.....	49
3.1.2 Test Setup and Procedure.....	52
3.1.3 Lateral Load Test Results.....	53
3.2 Lateral Load Test at Pomeroy-Mason.....	57
3.2.1 Test Site.....	57
3.2.2 Test Set-up and Test Procedure.....	62
3.2.3 Lateral Load Test Results.....	64
3.3 Methods for Deriving P-y Curves From Lateral Load Test Results	70
3.3.1 Introduction.....	70
3.3.2 Method for Deriving Deflection from Strain Gage Readings.....	72
3.3.3 Determination of Moment Profiles	73
3.3.4 Methods for Deriving P (Net Resistance)	74
3.3.5 Evaluation Using Field Test Data	81
3.3.6 Evaluation Using Hypothetical Cases.....	88
3.3.7 Optimum Strain Gage Spacing.....	90
3.3.8 Effect of Measurement Error	92
3.3.9 Conclusions on Methods for Deriving p-y Curves	94

3.4 Analyses of the Load Tests	95
3.4.1 Evaluation of Experimental P-y Curves.....	95
3.4.2 Evaluation of Reese Interim Rock p-y Criterion.....	100
3.5 Summary and Conclusions.....	104
IV. LATERAL CAPACITY OF DRILLED SHAFTS IN ROCK	105
4.1 3-D Finite Element Modeling and Validation.....	106
4.1.1 3-D FEM Modeling.....	107
4.1.2 Validation of the 3D FEM Model	111
4.2 Failure Modes of Rock Subjected to Loading from Laterally Loaded Drilled Shafts	115
4.2.1 Failure of Isotropic and Homogeneous Rock without Overburden Soils.....	115
4.2.2 Failure of Jointed Rock without Overburden Soils.....	124
4.2.3 Failure of Isotropic and Jointed Rock with Overburden Soils.....	129
4.3 Rock Strength Criteria.....	129
4.3.1 Hoek-Brown Criterion	130
4.3.2 Converting Hoek-Brown Criterion to Mohr-Coulomb Criterion.....	132
4.4 Side Shear Resistance	132
4.4.1 Empirical Equations for Axially Loaded Drilled Shaft in Rock	134
4.4.2 Suggested Empirical Equation for Side Resistance in Horizontal Direction.....	136
4.5 Ultimate Resistance of Rock Mass	138
4.5.1 Ultimate Resistance of Rock Near Surface.....	138
4.5.2 Ultimate Rock Resistance at Great Depth.....	140

4.5.3 Ultimate Resistance of Jointed Rock	141
4.6 New Method for Predicting Lateral Capacity of Drilled Shafts in Rock	142
4.6.1 Free Head Boundary	142
4.6.2 Fixed Head Boundary	145
4.7 Ultimate Reaction of Soils	148
4.7.1 Ultimate Resistance of Clay	148
4.7.2 Ultimate Resistance of Sand	150
4.7.3 Ultimate Resistance of c - ϕ Soils	151
4.8 Validation of the Derived Capacity Prediction Method.....	152
4.9 Summary and Conclusions.....	155
V. ELASTIC SOLUTION OF LATERALLY LOADED DRILLED SHAFTS IN ROCK.....	157
5.1 Determination of Rock Mass Deformability	157
5.1.1 Introduction.....	157
5.1.2 Goodman Jack Test.....	158
5.1.3 Selection of In-Situ Test Method	163
5.1.4 Existing Empirical Equations.....	165
5.1.5 Parameters for Determination of E_m	167
5.1.6 Proposed Empirical Equation.....	169
5.1.7 Recommended Methodology for Determination of Deformation Modulus of Rock	170
5.2 Initial Modulus of Subgrade Reaction of Rock Mass	171
5.2.1 Introduction.....	171
5.2.2 FEM Model and Parametric Study.....	173

5.2.3 Suggested Empirical Equation	179
5.2.4 Validation of the Empirical Equation	180
5.3 Numerical Solution for Laterally Loaded Piles in A Two Layer Soil Profile.....	184
5.3.1 Introduction.....	184
5.3.2 Definition of the Problem	186
5.3.3 Variational Solution	187
5.3.4 Validations	191
5.3.5 Methods for Determining Input Parameters.....	195
5.3.6 Case Study.....	195
5.4 Summary and Conclusions.....	198
VI. P-Y CRITERION FOR ROCK MASS	200
6.1 General Shape of P-y Curve in Rock	200
6.2 Determination of p_u	202
6.2.1 Failure Modes	202
6.2.2 P_u Near Surface	204
6.2.3 P_u at Great Depth.....	205
6.2.4 P_u of Jointed Rock.....	206
6.3 Initial Tangent to P-y Curve K_i	206
6.4 Rock Mass Properties.....	207
6.4.1 Strength Parameters	207
6.4.2 Rock-Shaft Interface Strength.....	209
6.4.3 Rock Mass Modulus E_m	209

6.5 Construction of P-y curves for Rock Mass	209
6.6 Comparison of the Proposed P-y Criterion with That of Gabr et al. (2002).....	210
6.7 Case Studies	211
6.7.1 Dayton Load Test.....	213
6.7.2 Pomeroy-Mason Load Test.....	217
6.7.3 Load Tests at North Carolina	221
6.8 Conclusions	226
VII. DERIVING P-Y CURVE FROM DILATOMETER TESTS.....	227
7.1 Pressuremeter and Dilatometer	227
7.1.1 Modulus of Rock Mass	232
7.1.2 Limit Pressure	232
7.1.3 Undrained Shear Strength	232
7.1.4 Friction Angle	234
7.2 Deriving p-y Curves from Pressuremeter/Dilatometer Test Results.....	238
7.3 Evaluation	244
VIII. SUMMARIES AND CONCLUSIONS.....	252
8.1 Summaries.....	252
8.2 Conclusions.....	253
8.3 Future Studies.....	255
REFERENCES	257

LIST OF TABLES

Table	Page
2-1 Engineering Properties of Rocks in Ohio.....	33
2-2 Simplified Rock Classification.....	36
2-3 Factors influencing Rock Mass Behavior.....	37
2-4 Classification Parameters and Their Rating (After Bieniawski, 1976).....	41
2-5 Rock Mass Rating System (Bieniawski, 1989)	42
2-6 GSI Ranges for General Rocks (Marinos and Hoek, 2000)	44
2-7 GSI Ranges for Typical Sandstones (Marinos and Hoek, 2000).....	45
2-8 GSI Ranges for Typical Siltstones, Claystones and Clay Shales (Marinos and Hoek, 2000)	46
2-9 GSI Ranges for Typical Limestones (Marinos and Hoek, 2000).....	47
2-10 GSI Estimates for Heterogeneous Rock Masses Such as Flysch (Marinos and Hoek, 2000)	48
3-1 RMR Ratings and GSI Values of Rock at Dayton Test Site.....	51
3-2 RMR Ratings and GSI Values of Rock Based on Boring S-9.....	59
3-3 RMR Ratings and GSI Values of Rock Based on Boring S-10.....	62
3-4 Compiled Lateral Load Test Database.....	82
3-5 Cumulative Shaft Head Deflection Errors based on Various Methods.....	87

3-6	Cumulative Moment Errors based on Various Methods.....	87
3-7	Soil Parameters of Hypothetical Cases.....	88
3-8	Cumulative Errors of p-y Curves of Hypothetical Cases.....	89
3-9	Rock Properties for LPILE Analysis.....	100
3-10	Test Drilled Shafts Information.....	102
4-1	Rock Mass Properties.....	112
4-2	Summary of Rock Strength Criteria.....	130
4-3	Values of Constant m_i for Intact Rock (After Marinos and Hoek, 2000).....	131
4-4	Roughness Classes (After Pells et al., 1980)	135
4-5	Recommended Values of K by Kulhawy et al. (1983) and Kulhawy (1991)	151
4-6	Recommended Values of δ by Kulhawy et al. (1983) and Kulhawy (1991)	151
4-7	Test Drilled Shaft Information.....	153
4-8	Input rock mass parameters of the load tests.....	153
4-9	Comparison of Lateral Capacities of Test Drilled Shafts.....	154
5-1	Values of Constant $K(v)$ for $\beta=45^\circ$	160
5-2	Values of T^* (Heuze and Amadei, 1985)	163
5-3	Empirical Equations for Estimating the Deformation Modulus of Rock Mass.....	166
5-4	The Strength of the Relation between E_M and Parameters (Kayabasi et al. 2003)	168
5-5	Properties of Rock Masses in Ironton-Russell.....	168
5-6	Predictions and Ratios of Predicted over Measured Modulus of Rock Masses.....	169

5-7	Summary of Lateral Load Test Drilled Shafts.....	181
5-8	Modulus of Rock Masses Based on Pressuremeter Test.....	182
5-9	Modulus of Rock Masses Based on Empirical Equation.....	182
5-10	Measured and Predicted Initial Modulus of Subgrade Reaction.....	183
5-11	Summary of Definitions Related to Subgrade Reaction Theory.....	186
6-1	Comparison of P-y Criteria.....	212
6-2	Input Rock Mass Parameters of Dayton Load Test.....	213
6-3	Input Rock Mass Parameters of Pomeroy-Mason Load Test.....	217
6-4	Input Rock Mass Parameters of I-40 Load Test.....	222
6-5	Input Rock Mass Parameters of I-85 Load Test.....	223
7-1	Preliminary estimates of ϕ'_{cv} (Robertson and Hughes, 1986).....	236
7-2	The Rheological Factor α for Various Soils (Baguelin et al., 1978)	239

LIST OF FIGURES

Figure	Page
1-1	Drilled shaft and soil models of p-y analysis.....3
1-2	Flow chart of the work..... 5
2-1	Distribution of ultimate lateral force per unit length (after Carter and Kulhawy 1992)13
2-2	Rock-shaft model (a) Shaft and soil/rock mass system; (b) Coordinate system and displacement components; (c) Shear force $V(z)$ and moment $M(z)$ acting on shaft at z (Zhang et al. 2000) 16
2-3	Consideration of yielding of soil and/or rock mass by decomposition of loading (after Zhang et al. 2000) 18
2-4	Components of rock mass resistance (Zhang et al. 2000) 19
2-5	Typical forces on wedge23
2-6	The elastoplastic and brittle behavior of rock mass25
2-7	Geological map of Ohio, showing the pattern of surface rocks across the state 28
2-8	Cross section through the rocks of central Ohio from the Indiana-Ohio border to the Ohio River (taken from Feldmann et al., 1996) 28
2-9	Generalized column of bedrock units in Ohio.....29
2-10	Classification of shales for embankment construction (Wood and Deo, 1975) 32
3-1	Soil and rock layer profiles at Dayton test site 51

3-2	Instrumentation of load test at Dayton	53
3-3	Load-deflection curves at the top of shafts.....	54
3-4	Deflection-depth curves of shaft #3.....	55
3-5	Deflection-depth curves of shaft #4.....	55
3-6	Compression strain profiles of shaft #4.....	56
3-7	Tension strain profiles of shaft #4.....	57
3-8	Boring S-9	60
3-9	Boring S-10.....	61
3-10	Instrumentation and load test setup.....	64
3-11	Measured load-deflection curves at loading point of Pomeroy-Mason test.....	65
3-12	Deflection-depth profiles of drilled shaft #1 at Pomeroy-Mason test.....	66
3-13	Deflection-depth profiles of drilled shaft #2 at Pomeroy-Mason test.....	67
3-14	Tension strain profiles of test shaft #1 of Pomeroy-Mason test.....	68
3-15	Compression strain profiles of test shaft #1 of Pomeroy-Mason test.....	68
3-16	Tension strain profiles of test shaft #2 of Pomeroy-Mason test.....	69
3-17	Compression strain profiles of test shaft #2 of Pomeroy-Mason test.....	69
3-18	Procedure for reducing moment data to p using piecewise polynomial (after Dunnavant, 1986)	75
3-19	Linear shape functions.....	77
3-20	Elimination of outlier moment profiles.....	83

3-21	Comparison of deflections from strain readings and inclinometer for test PomS1.....	83
3-22	P vs. depth profile of test MaumeeS1.....	85
3-23	P vs. depth profile of test CDOTC1.....	86
3-24	Definition of deflection prediction error.....	86
3-25	Comparison of p-y curves.....	90
3-26	Optimum spacing of strain gages.....	92
3-27	Four types of moment error profiles.....	93
3-28	Cumulative p-y curve errors due to moment errors.....	94
3-29	Experimental p-y curves for shaft #4 of Dayton load test.....	96
3-30	Experimental p-y curves for shaft #1 of Pomeroy-Mason load test.....	96
3-31	Experimental p-y curves for shaft #2 of Pomeroy-Mason load test.....	97
3-32	Equivalent load combinations.....	98
3-33	Prediction of load-deflection curves of shaft #4 of Dayton load test using experimental p-y curves.....	98
3-34	Prediction of load-deflection curves of shaft #1 of Pomeroy-Mason load test using experimental p-y curves.....	99
3-35	Prediction of load-deflection curves of shaft #2 of Pomeroy-Mason load test using experimental p-y curves.....	99
3-36	Prediction of load-deflection curve of shaft #4 of Dayton load test using Reese weak rock p-y criterion.....	102
3-37	Prediction of load-deflection curve of shaft #1 of Pomeroy-Mason load test using Reese weak rock p-y criterion.....	103
3-38	Prediction of load-deflection curve of shaft #2 of Pomeroy-Mason load test using Reese weak rock p-y criterion.....	103

4-1	Finite element meshes of a drilled shaft-rock system	107
4-2	Finite elements for (a) drilled shaft, (b) surrounding rock, and (c) outside boundary of rock.....	108
4-3	Cap model: yield surface in the p-t plane (ABAQUS, 1998).....	110
4-4	Drilled shaft dimension and rock profiles of the load test at Dayton.....	111
4-5	Mesh convergence.....	113
4-6	Comparison of load-deflection curves at shaft head.....	114
4-7	Comparison of deflection profiles at the load of (a) 1126 kips and (b) 705 kip	114
4-8	The forward movement of rock mass.....	116
4-9	Front view of upward movement of rock mass.....	117
4-10	Y direction stress distribution in xz plane.....	118
4-11	Maximum shear stress distribution on yz plane.....	119
4-12	Proposed wedge type failure model for the top layer of rock.....	119
4-13	Stress distribution at Y direction of in-depth rock layer.....	121
4-14	The predefined cracks.....	122
4-15	The stress redistribution at Y direction of in-depth rock layer after crack.....	122
4-16	Friction distribution on the shaft-rock interface.....	123
4-17	Suggested stress distribution at failure at great depth	124
4-18	Tensile stress on xz plane for jointed rock mass case.....	127
4-19	Maximum shear stress concentrations for jointed rock mass case.....	127
4-20	Concrete and rock joint.....	134

4-21	Displacement behavior of drilled shafts in rock (Johnston and Lam, 1989a).....	137
4-22	Increased normal stress due to lateral load.....	137
4-23	The Rock-Shaft Model.....	143
4-24	Lateral capacity calculation models for drilled shafts in rocks.....	144
4-25	Capacity of rigid drilled shaft at fixed head boundary.....	146
4-26	Capacity of intermediate length drilled shaft at fixed head boundary.....	147
4-27	Capacity of long drilled shaft at fixed head boundary.....	148
4-28	Distribution of lateral reaction stresses.....	149
5-1	The schematic of loading of Goodman Jack (Heuze, 1984)	159
5-2	Modulus reduction vs. hydraulic pressure for various borehole diameters (a) undersize – the pressure must be decreased by about 14% for a given E_{app}/E_{act} as recalculated by Heuze et al.(1985). (b) oversize holes.....	162
5-3	Correction for platen bending of the jack (after Heuze and Amadei, 1985)	163
5-4	Proposed empirical equation using GSI.....	171
5-5	Initial modulus of subgrade reaction for various moduli of rock.....	175
5-6	Initial modulus of subgrade reaction for various Poisson's ratio.....	175
5-7	P-y curves along with depth	176
5-8	Initial modulus of subgrade reaction for various rock-shaft interface frictions.....	177
5-9	K_i varies with shaft diameter.....	178
5-10	Initial modulus of subgrade reaction for various shaft-rock relative stiffness.....	179

5-11	Comparison of FEM computed and predicted subgrade reaction modulus.....	180
5-12	Comparison of load-deflection curves of North Carolina load test.....	181
5-13	Validation of empirical equation using field test data.....	184
5-14	Two-layer soil profile with four possible variations.....	187
5-15	Soil-pile system.....	187
5-16	Comparison with Reese and Matlock solutions– varying soil stiffness	192
5-17	Comparisons with Davisson and Gill method for free head condition	193
5-18	Comparison with Davisson and Gill solution for fixed head condition	194
5-19	Shaft and soil profiles of the case study.....	196
5-20	Interpretation of subgrade reaction modulus of rock.....	197
5-21	Comparison of shaft head deflections.....	198
6-1	P-y curves deduced from shaft #4 of load test at Dayton.....	201
6-2	P-y curves deduced from Shaft #2 of load test at Pomeroy-Mason.....	201
6-3	Schematics of a hyperbolic p-y curve.....	202
6-4	Failure mode for rock near ground surface.....	203
6-5	Failure mode of rock at great depth.....	204
6-6	Hyperbolic p-y curves of Dayton site.....	214
6-7	Comparison of load-deflection of test shaft #4 at Dayton load test.....	215
6-8	Comparison of load-Maximum moment of test shaft #4 at Dayton load test.....	215

6-9	Comparisons of deflection-depth curves of shaft #4 at Dayton test.....	216
6-10	Comparisons of moment-depth curves of shaft #4 at Dayton test.....	216
6-11	Hyperbolic p-y curves of Pomeroy-Mason site.....	219
6-12	Comparison of load-deflection at the loading point for Pomeroy-Mason test.....	219
6-13	Comparison of load-Maximum moment of Pomeroy-Mason load test.....	220
6-14	Comparisons of deflection-depth curves of shaft #2 at Pomeroy-Mason test.....	220
6-15	Comparisons of moment-depth curves of shaft #2 at Pomeroy-Mason test.....	221
6-16	Layout of I-40 load test.....	222
6-17	Layout of I-85 load test.....	222
6-18	Comparison of load-deflection curves of I-40 short shaft.....	224
6-19	Comparison of load-deflection curves of I-40 long shaft.....	224
6-20	Comparison of load-deflection curves of I-85 short shaft.....	225
6-21	Comparison of load-deflection curves of I-85 long shaft.....	225
7-1	Menard G-Am pressuremeter from RocTest.....	228
7-2	PROBEX-1 Dilatometer from RocTest.....	228
7-3	Calibration for volume and pressure losses.....	229
7-4	Typical pressuremeter/dilatometer test curve.....	231
7-5	Determination of limit pressure from inverse of volume versus pressure.....	233
7-6	P-y curves from pressuremeter (Baguelin et al., 1978)	240

7-7	Steps for constructing p-y curve from pressuremeter test.....	241
7-8	Determination of the critical depth (Smith, 1983)	243
7-9	Reduction factor for depth within critical depth (Smith, 1983).....	244
7-10	Shaft and soil profiles of the case study.....	245
7-11	Dilatometer test results of the case study (after Cho et al., 2001).....	246
7-12	P-y curves from dilatometer tests of Cho et al. (2001).....	246
7-13	Comparison of the measured and predicted deflections at shaft top.....	247
7-14	Derived p-y curves from dilatometers for I-40 short shaft.....	248
7-15	Derived p-y curves from dilatometers for I-40 long shaft.....	248
7-16	Derived p-y curves from dilatometers for I-85 short shaft.....	249
7-17	Derived p-y curves from dilatometers for I-85 long shaft.....	249
7-18	Comparison of load-deflection curves of I-40 short shaft.....	250
7-19	Comparison of load-deflection curves of I-40 long shaft.....	250
7-20	Comparison of load-deflection curves of I-85 short shaft.....	251
7-21	Comparison of load-deflection curves of I-85 long shaft.....	251

CHAPTER I

INTRODUCTION

1.1 Statement of the Problem

Drilled shafts socketed into rock are widely used as foundations for bridges and other important structures. Rock-socketed drilled shafts are also used to stabilize slopes. The main loads applied to the drilled shafts are axial compressive or uplift loads as well as lateral loads with accompanying moments. For axially loaded drilled shafts socketed into rock, numerous research efforts have been conducted in the past, especially for the determinations of side shear resistance.

However, for laterally loaded drilled shafts, there is a lack of validated, rational analysis and design methods. It has been a customary practice to adopt the techniques developed for laterally loaded piles in soil to solve the problem of rock-socketed drilled shafts under lateral loading (Gabr, 1993). This practice has created erroneous designs and often leads to excessive socket length. Although there exist several analysis and design methods specially for rock-socketed drilled shafts under lateral loading, including those by Carter and Kulhawy (1992), Reese (1997), Zhang et al. (2000), and Gabr et al. (2002); however, these methods were developed with limited validations against field lateral load test data.

Several researchers (such as DiGioia and Rojas-Gonzalez, 1993; Dykeman and Valsangkar, 1996; and Cho et al., 2001) have evaluated the methods of Carter and Kulhawy (1992) and Reese (1997) using their lateral load test data. They concluded that the two methods provided very unconservative results. Zhang et al. (2000)'s analysis method has not been evaluated by others due to the complexity of the method and the needs of a computer program. The assumption of an elastic-perfectly plastic model for rock masses by Zhang et al. (2000) prohibited its wide application, especially for weak rock masses which can not be exactly characterized by elastic-perfectly plastic model.

In addition to the need to develop analysis methods for predicting lateral shaft deflections, there is also a need for the development of methods for estimating lateral capacity of shafts. Very few methods (Carter and Kulhawy, 1992; and To et al., 2003) have been developed for estimating lateral capacity of piles in rock. Additionally, several other researchers, such as Reese (1997) and Zhang et al. (2000), have proposed methods to predict the ultimate lateral resistance of rock per unit shaft length. However, Carter and Kulhawy's (1992) method does not consider the effect of secondary structures of rock mass; and the method of To et al. (2003) is only suitable for two sets of parallel joints and rigid piles.

The lack of validated design methods stimulates the need to develop a more rational design approach for laterally loaded drilled shafts in rock. Additionally, a method for predicting ultimate capacity of drilled shafts in rock mass needs to be developed.

The p-y method has been widely and successfully used for the design of laterally loaded drilled shafts in soils for decades. This method is based on a numerical solution of a physical model based on a beam on Winkler foundation, shown in Fig. 1-1. The

structural behavior of the drilled shafts is modeled as a beam, while the soil-shaft interaction is represented by discrete, non-linear springs.

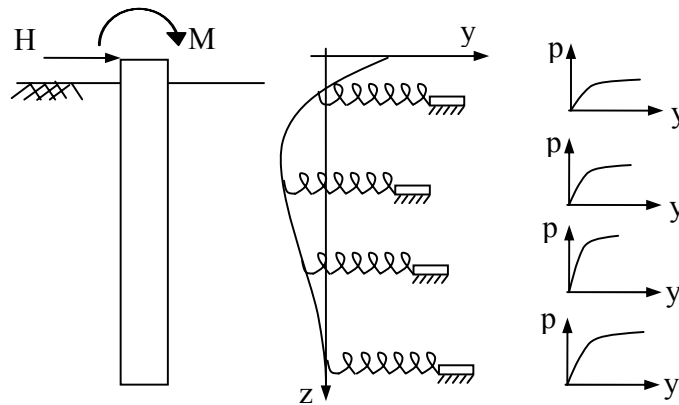


Figure 1-1 Drilled shaft and soil models of p-y analysis

It is believed that the non-linear p-y approach is the best way to analyze and design laterally loaded drilled shafts in rock, if a rational and appropriate p-y criterion for rock masses can be developed. Therefore, this study will focus on the development of p-y curves for rock masses. There are two ways that one can generate p-y criterion: one is to use fundamental rock properties along with basic rock-shaft interaction mechanics; and the second is to derive the p-y curves using in-situ tests, such as pressuremeter or dilatometer tests.

1.2 Objectives

The objectives of this research are to:

- 1) Develop a method to predict the lateral capacity of drilled shafts in rock masses.
- 2) Develop a simple elastic solution for predicting deflections of laterally loaded drilled shafts in rock in a two-layer soil/rock profile.

- 3) Develop a p-y criterion for rock mass.
- 4) Identify the best field or laboratory test methods for determining rock mass properties used in the developed p-y criterion. Necessary correlations between rock properties and the p-y curve parameters will also be established.
- 5) Perform full-scale field lateral load tests on fully instrumented drilled shafts to obtain reliable and comprehensive field test data for validating the p-y criterion.
- 6) Review and recommend a best approach for deriving site specific p-y curves of rock mass from pressuremeter or dilatometer test data.

1.3 Scope of the Work

The work involved in this study mainly consists of two parts: one is the theoretical work to develop a p-y criterion for rock and evaluation of an existing approach for deriving site specific p-y curves using dilatometer tests; the other is to conduct full-scale field lateral load tests. A lateral capacity prediction method and elastic solution for estimating shaft deflection under lateral loads are developed as well. Additionally, an evaluation is carried out to identify the most suitable method for deriving p-y curves based on test results of a fully instrumented lateral load test. Specifically, the work to be done are outlined as follows and depicted in Figure 1-2.

A literature review on the design and analysis methods of laterally loaded drilled shafts and piles in rock is performed. The types of rock of interest and rock classification systems are identified. To construct a hyperbolic p-y curve, it is necessary to obtain the initial slope and ultimate rock reaction. The determination of ultimate rock reaction involves a 3D finite element analysis to identify the possible failure modes of rocks

subjected to movement of laterally loaded drilled shafts. Rock strength criteria and side shear resistance between rock and shaft are carefully identified. To obtain the initial slope of p-y curves, a correlation between the slope and deformation modulus of rock masses is established using a parametric study based on a 3D FEM model. Finally, based on the ultimate rock reaction and initial slope of p-y curve, a hyperbolic p-y criterion for rock mass is proposed.

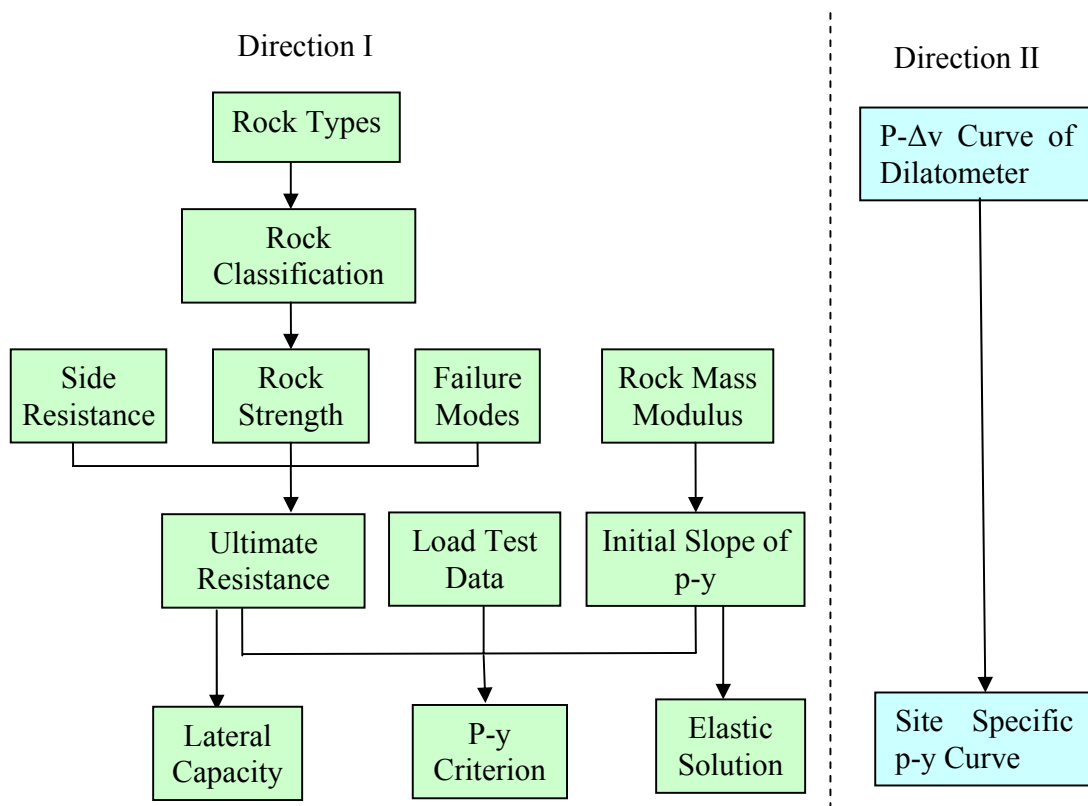


Figure 1-2 Flow chart of the work

In addition to the development of a p-y criterion of rock, a method for predicting lateral capacity of drilled shafts in rock and an elastic solution for estimation of drilled shaft deflections in a two-layer soil/rock profile under lateral loads are proposed.

Two field lateral load tests are conducted to facilitate the development and validation of the p-y criterion for rock mass. An evaluation of various existing methods for deriving p-y curves from the results of an instrumented lateral load test is carried out to identify the best method.

Finally, the existing methods for deriving site specific p-y curves for soils from pressuremeter and dilatometer tests are reviewed and examined with lateral load test results of rock-socketed drilled shafts. The most suitable method is then recommended for deriving p-y curves from pressuremeter and dilatometer tests.

1.4 Outlines of the Dissertation

Chapter II presents the literature review on analysis methods of laterally loaded drilled shafts/piles in rock. Also, typical Ohio bedrock, and rock classification systems are reviewed.

Chapter III presents the results of two full-scale lateral load tests on instrumented drilled shafts socketed in rock. The best suitable method for deriving p-y curves from the load test results is identified and it is used to derive the site-specific p-y curves of the two load test sites. At the end of this chapter, the existing Reese (1997) interim p-y criterion is evaluated against the results of the two lateral load tests.

The developed method for determination of ultimate resistance of rock mass against laterally loaded shafts is presented in Chapter IV, in which the failure modes of rock in response to laterally loaded drilled shafts, rock strength criterion, and side shear resistance will be elucidated. A 3D finite element modeling technique is established and validated against a lateral load test. Simulations using 3-D FEM modeling technique

enable the identification of failure modes of rock mass. Finally, a method for predicting lateral capacity of drilled shafts in rock and/or soil is proposed.

An elastic solution for predicting the deflections of laterally loaded drilled shaft in a two-layer soil/rock system is proposed in Chapter V, in which a correlation equation for estimating the modulus of rock mass based on modulus of intact rock and a rock classification system is also developed. Additionally, a correlation equation for estimating the subgrade reaction modulus of rock mass based on a 3D finite element parametric study is established as well.

Chapter VI presents the development of a new hyperbolic p-y criterion for rock mass. A validation of the proposed p-y criterion of rock is carried out by comparing the predictions against actual lateral load tests results.

Chapter VII provides an evaluation of several existing methods for interpreting the properties of rock mass and driving p-y curves from pressuremeter or dilatometer tests. The most suitable method for deriving p-y curves for rock from dilatometer tests is recommended based on the evaluation findings.

Chapter VIII presents summaries and conclusions of the research work.

CHAPTER II

LITERATURE REVIEW

2.1 Analysis Methods of Laterally Loaded Rock-Socketed Drilled Shafts

2.1.1 Introduction

To date, there are few published analysis methods for the lateral response of rock-socketed drilled shafts. It has been a customary practice to adopt the p-y analysis with p-y criterion developed for soils to solve the problem of rock-socketed drilled shafts (Gabr, 1993). Currently, two categories of analysis methods for laterally loaded rock-socketed drilled shafts have been developed. One category treats rock as a continuum mass (Carter and Kulhawy 1992; and Zhang et al 2000), the other one discretizes the rock mass into a set of non-linear springs (Reese 1997; and Gabr et al. 2002).

Carter and Kulhawy (1992) proposed a method that treats rock mass as a homogeneous elastic continuum. Parametric solutions for the load-displacement relationships were generated by using the finite element technique. However, elastic continuum model is only good for small loads. Zhang et al. (2000), therefore, developed a nonlinear continuum approach. The approach adopts and extends the basic idea of Sun (1994) on laterally loaded piles in soil. The elasto-plastic soil/rock response under lateral loads and the linearly variation of deformation modulus of soil/rock along depth were assumed. To consider the yielding, a method based on Hoek-Brown criterion (Hoek and

Brown 1980, 1988) was proposed to calculate the ultimate resistance of rock masses. In practice, however, the rock masses, especially weak rock, show nonlinear and non-homogeneous properties which can not be fully captured by an elasto-plastic model.

The second category of analysis method, such as p-y method, discretizes the rock masses into a series of nonlinear springs. The p-y method was extended to the analysis of single rock-socketed drilled shaft under lateral loading by Reese (1997). An interim p-y criterion for weak rock was proposed. Thereafter, Gabr et al. (2002) proposed a p-y criterion for weak rock based on their field test data.

In addition to the above mentioned analysis methods for solving load-deflection relationship at the drilled shaft head, methods for estimating ultimate rock reaction have also been proposed. Carter and Kulhawy (1992) presented a method to determine the rock capacity by using cohesion and friction angle of rock. This method was based on a theory of expansion of a long cylindrical cavity in an elasto-plastic, dilatant material. The method requires input of Poisson's ratio, shear modulus and dilation angle. By assuming distribution of ultimate rock resistance along the depth of a shaft, the ultimate lateral capacity of a rock-socketed drilled shaft was obtained by summing the capacity of compressive resistance and shear resistance between shaft and rock. Carter and Kulhawy (1992)'s method on rock resistance, treats rock mass as a homogeneous and elasto-plastic material, without considering secondary structures of rock mass, such as cracks and fractures.

Reese (1997) considered the secondary structure of rock mass by using a rock strength reduction factor which can be determined from Rock Quality Designation (RQD). However, Reese (1997)'s method for estimating ultimate rock reaction per unit

length ignored the contribution of shear resistance between shaft and rock. Additionally, RQD can not fully represent all the secondary rock structures, such as spacing and condition of discontinuities.

Zhang et al. (2000) proposed a method to estimate the ultimate reaction of rock masses per unit shaft length using Hoek-Brown rock strength criterion (Hoek and Brown 1988), in which RQD and other secondary rock structures were included. However, simple rock resistance distribution along the shaft circumference under lateral loads was assumed (Carter and Kulhawy 1992). It seems that Zhang et al. (2000)'s method for estimation of lateral capacity of rock-socketed drilled shaft considered most of characteristics of rock mass; however, the authors did not investigate possible failure modes of rock mass, especially possible sliding failures along pre-existing joints. Regarding the sliding failure on joints, To et al. (2003) proposed a method to estimate the lateral load capacity of drilled shafts in jointed rock. The block theory (Goodman and Shi 1985) was used to identify the failure block, and the static limit equilibrium was used to obtain the ultimate capacity. The Coulomb failure criterion was utilized to model the sliding failure on joints.

2.1.2 Brief Description of the Existing Methods

2.1.2.1 Carter and Kulhawy (1992)

Carter and Kulhawy (1992) performed a parametric study to obtain deflection u and rotation angle θ at the shaft head. The solutions for these two variables were expressed as a function of effective Young's modulus E_e and an equivalent shear modulus G^* , by using finite element technique. The drilled shaft is idealized as a cylindrical elastic inclusion with effective Young's modulus E_e , which is defined as

$$E_e = \frac{(EI)_c}{\frac{\pi D^4}{64}} \quad (2-1)$$

in which, $(EI)_c$ = the actual bending rigidity of the shaft; D = diameter of the drilled shaft. The rock mass is assumed to be a homogeneous, isotropic elastic material. The equivalent shear modulus is given by

$$G^* = G_r \left(1 + \frac{3}{4} \nu \right) \quad (2-2)$$

where

$$G_r = \frac{E_r}{2(1 + \nu)} \quad (2-3)$$

in which E_r = Young's modulus of rock, and ν = Poisson's ratio of rock.

From the finite element analysis performed by Carter and Kulhawy (1992), it was found that u and θ are largely dependent on the ratio of E_e / G^* and the ratio of the shaft socket length to the diameter L/D . Two categories of shafts, flexible and rigid, were classified by the authors. A flexible pile is one in which the following condition meets:

$$\frac{L}{D} \geq \left(\frac{E_e}{G^*} \right)^{2/7} \quad (2-4)$$

For a flexible drilled shaft, ground-line deflection u and rotation θ induced by the lateral load H and the moment M at shaft top are calculated from the following equations:

$$u = 0.5 \left(\frac{H}{G^* D} \right) \left(\frac{E_e}{G^*} \right)^{-1/7} + 1.08 \left(\frac{M}{G^* D^2} \right) \left(\frac{E_e}{G^*} \right)^{-3/7} \quad (2-5)$$

$$\theta = 1.08 \left(\frac{H}{G^* D^2} \right) \left(\frac{E_e}{G^*} \right)^{-3/7} + 6.4 \left(\frac{M}{G^* D^3} \right) \left(\frac{E_e}{G^*} \right)^{-5/7} \quad (2-6)$$

A drilled shaft is considered to be rigid when

$$\frac{L}{D} \leq 0.05 \left(\frac{E_e}{G^*} \right)^{1/2} \quad (2-7)$$

For a rigid drilled shaft, ground-line deflection u and rotation θ are calculated from the following equations:

$$u = 0.4 \left(\frac{H}{G^* D} \right) \left(\frac{2L}{D} \right)^{-1/3} + 0.3 \left(\frac{M}{G^* D^2} \right) \left(\frac{2L}{D} \right)^{-7/8} \quad (2-8)$$

$$\theta = 0.3 \left(\frac{H}{G^* D^2} \right) \left(\frac{2L}{D} \right)^{-7/8} + 0.8 \left(\frac{M}{G^* D^3} \right) \left(\frac{2L}{D} \right)^{-5/3} \quad (2-9)$$

For the drilled shafts having intermediate rigidity, the authors suggested that the displacements be taken as 1.25 times the larger displacements of those calculated values by treating the shaft as a flexible or a rigid shaft.

For ultimate capacity of rock-socketed drilled shafts, Carter and Kulhawy (1992) proposed a solution in which they suggested that the lateral resistance were derived from side shear τ between shaft and rock, and frontal compressive strength of rock. The authors further suggested that the magnitude of this shear was equal to that produced in axial loading. The assumed distribution of ultimate resistance along the shaft is shown in Fig. 2-1, from which one can see that lateral resistance is equal to $\tau_{\max} D$ at the surface of the rock and is increasing linearly with depth to a magnitude of $(P_L + \tau_{\max}) D$ at a depth of $3D$. Below this depth, the ultimate resistance remains constant with depth. P_L is the limit stress developed in rock, which can be calculated according to the expansion theory of a long cylindrical cavity in an elasto-plastic, cohesive-frictional, dilatant material (Carter et

al. 1986). The following equations were derived by Carter and Kulhawy to determine the lateral capacity of rock-socketed drilled shafts, H_u :

$$H_u = \left(\frac{P_L L}{6} + \tau_{\max} D \right) L \quad \text{for } L < 3D \quad (2-10)$$

$$H_u = \left(\frac{P_L}{2} + \tau_{\max} \right) 3D^2 + (P_L + \tau_{\max})(L - 3D)D \quad \text{for } L > 3D \quad (2-11)$$

where τ_{\max} = maximum unit side resistance; D = diameter of the drilled shaft; and L = length of drilled shafts embedded in rock.

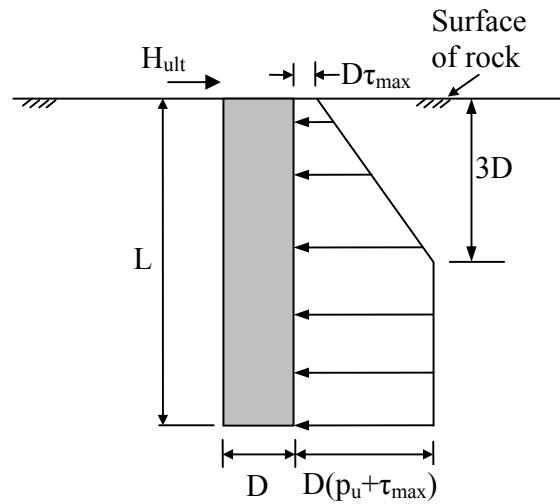


Figure 2-1 Distribution of ultimate lateral force per unit length (after Carter and Kulhawy 1992)

2.1.2.2 Reese (1997)

The p-y method for the analysis of drilled shafts in soils under lateral loading was extended to the analysis of rock-socketed drilled shafts by Reese (1997). In order to characterize the rock response under lateral loading, an interim p-y criterion for weak rock was suggested. Due to the lack of adequate test data, the term “interim” was applied

to this p-y criterion. With this interim p-y criterion, COM624P or LPILE can be run to obtain the lateral response of rock-socketed drilled shafts.

The ultimate reaction, p_u (F/L), of rock was given by

$$p_u = \alpha_r \sigma_{ci} D (1 + 1.4 \frac{z_r}{D}) \quad \text{for } 0 \leq z_r \leq 3D \quad (2-12)$$

$$p_u = 5.2 \alpha_r \sigma_{ci} D \quad \text{for } z_r \geq 3D \quad (2-13)$$

where σ_{ci} = uniaxial compressive strength of intact rock; α_r = strength reduction factor, which is used to account for fracturing of rock mass; D = diameter of the drilled shaft; and z_r = depth below rock surface. The value of α_r is assumed to be 1/3 for RQD of 100% and it increases linearly to unity at a RQD of zero.

The slope of initial portion of p-y curves was given by

$$K_{ir} = k_{ir} E_m \quad (2-13)$$

where K_{ir} = initial tangent to p-y curve; E_m = deformation modulus of rock masses, which may be obtained from a pressuremeter or dilatometer test; and k_{ir} = dimensionless constant. The expressions for k_{ir} , derived by correlation with experimental data, are as follows.

$$k_{ir} = (100 + \frac{400z_r}{3D}) \quad \text{for } 0 \leq z_r \leq 3D \quad (2-14)$$

$$k_{ir} = 500 \quad \text{for } z_r \geq 3D \quad (2-15)$$

A complete description of the interim p-y criterion may be summarized as follows.

$$\text{First segment: } p = K_{ir} y; \quad y \leq y_A \quad (2-16)$$

$$\text{Second segment: } p = \frac{p_u}{2} \left(\frac{y}{y_m} \right)^{0.25}; \quad y \geq y_A \text{ and } p \leq p_u \quad (2-17)$$

$$\text{Third segment: } p = p_u; \quad p \geq p_u \quad (2-18)$$

where

$$y_{rm} = k_{rm} D \quad (2-19)$$

$$y_A = \left[\frac{p_u}{2(y_{rm})^{0.25} K_{ir}} \right]^{1.333} \quad (2-20)$$

in which, k_{rm} = strain at 50% of ultimate load, ranging from 0.0005 to 0.00005.

2.1.2.3 Zhang et al. (2000)

Zhang et al. (2000) proposed a nonlinear continuum method to predict the load-displacement response of rock-socketed drilled shafts under lateral loads by treating soil/rock as an elasto-plastic material. The approach was extended from the basic idea of Sun (1994) on laterally loaded piles in soil.

The model of rock-socketed drilled shafts under lateral loading is shown in Fig. 2-2. The deformation modulus of soils varies linearly from E_{s1} to E_{s2} . Similarly, the deformation modulus of rock mass varies linearly from E_{m1} to E_{m2} at the tip of shaft and stays constant below the shaft tip. By minimizing the energy of rock-shaft system with respect to displacements, the following governing equations were obtained:

$$E_p I_p \frac{d^4 u_s}{dz^4} - 2t_s \frac{d}{dz} \left\{ \left[\eta_s + (1 - \eta_s) \frac{z}{L_s} \right] \frac{du_s}{dz} \right\} + k_s \left[\eta_s + (1 - \eta_s) \frac{z}{L_s} \right] u_s = 0 \quad (0 \leq z \leq L_s) \quad (2-21a)$$

$$E_p I_p \frac{d^4 u_m}{dz^4} - 2t_m \frac{d}{dz} \left\{ \left[\eta_m + (1 - \eta_m) \frac{z - L_s}{L_m} \right] \frac{du_m}{dz} \right\} + k_m \left[\eta_m + (1 - \eta_m) \frac{z - L_s}{L_m} \right] u_m = 0$$

($L_s \leq z \leq L$) (2-21b)

where u_s and u_m = displacement components of the shaft in the soil and in the rock mass, respectively; $E_p I_p$ = flexural rigidity of the shaft; z = depth starting from ground line; L_s = shaft length embedded in soils; L_m = shaft length embedded in rock masses; and

$$\eta_s = \frac{E_{s1}}{E_{s2}} \quad (2-22a)$$

$$\eta_m = \frac{E_{m1}}{E_{m2}} \quad (2-22b)$$

$$t_s = \frac{\pi E_{s2} R^2 m_1}{2(1 + \nu_s)} \quad (2-22c)$$

$$k_s = \frac{\pi(3 - 4\nu_s) E_{s2} m_2}{2(1 + \nu_s)(1 - 2\nu_s)} \quad (2-22d)$$

$$t_m = \frac{\pi E_{m2} R^2 m_1}{2(1 + \nu_m)} \quad (2-22e)$$

$$k_m = \frac{\pi(3 - 4\nu_m) E_{m2} m_2}{2(1 + \nu_m)(1 - 2\nu_m)} \quad (2-22f)$$

in which ν_s and ν_m = Poisson's ratio of soils and rock masses, respectively; m_1 and m_2 = parameters describing the behavior of the elastic foundations.

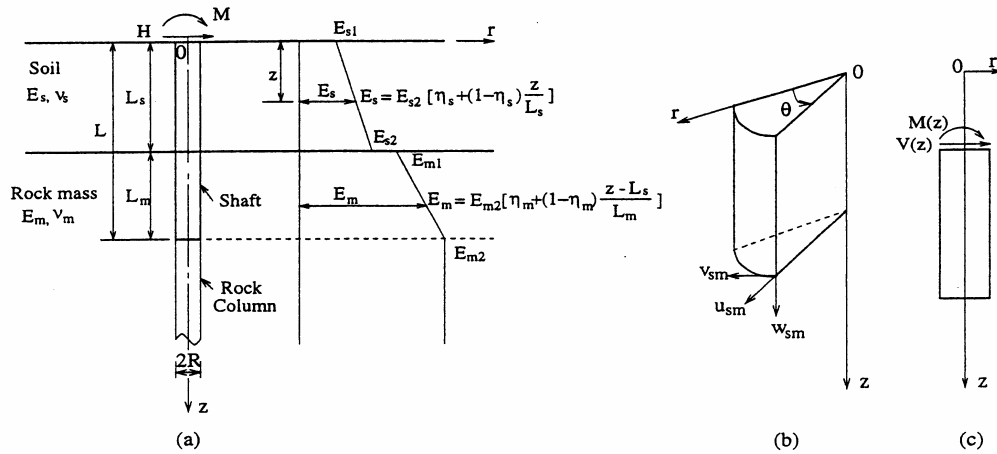


Figure 2-2 Rock-shaft model (a) Shaft and soil/rock mass system; (b) Coordinate system and displacement components; (c) Shear force $V(z)$ and moment $M(z)$ acting on shaft at z (Zhang et al. 2000)

The shear force $V(z)$ acting on the shaft, shown in Fig. 2-2(c), can be obtained as

$$V(z) = E_p I_p \left(\frac{d^3 u_s}{dz^3} \right) - 2t_s \left[\eta_s + (1 - \eta_s) \frac{z}{L_s} \right] \left(\frac{du_s}{dz} \right) \quad (0 \leq z \leq L_s) \quad (2-23a)$$

$$V(z) = E_p I_p \left(\frac{d^3 u_m}{dz^3} \right) - 2t_m \left[\eta_m + (1 - \eta_m) \frac{z - L_s}{L_m} \right] \left(\frac{du_m}{dz} \right) \quad (L_s \leq z \leq L) \quad (2-23b)$$

and the bending moment $M(z)$ acting on the shaft is be given by

$$M(z) = E_p I_p \left(\frac{d^2 u_s}{dz^2} \right) \quad (0 \leq z \leq L_s) \quad (2-24a)$$

$$M(z) = E_p I_p \left(\frac{d^2 u_m}{dz^2} \right) \quad (L_s \leq z \leq L) \quad (2-24b)$$

The governing differential equations and the shear force and bending moment can be solved using classical finite difference method and an iterative process. The above process considers the soil/rock to be elastic. Elastic-perfectly plastic stress-strain relationship, therefore, was proposed to consider the yielding of the soils or rock masses. The method for considering the yielding of soil or rock mass consists of several steps depicted in Fig. 2-3. Firstly, for the applied lateral load H and the moment M , the shaft is analyzed by using the above elastic solutions. Secondly, the lateral reaction force p at certain depth is computed and compared to the ultimate resistance p_u at that depth. If $p > p_u$, take the depth z as the yielding depth z_y . Thirdly, treat the unyielded portion of shaft as a new shaft, and analyze it by using the elastic solution while ignoring the effect of the yielded portion of shaft. Fourthly, repeat steps two and three until no further yielding of soil or rock occurs. Finally, the final results can be obtained by considering the two parts of the shaft separately. The portion of shaft in yielded soil and/or rock mass is analyzed

as a beam with distributed load p_u acting on it. The other part of shaft in the unyielded soil and/or rock mass is analyzed by using the elastic solution.

To compute the ultimate resistance p_u of soil, Zhang et al. (2000) suggested two existing methods for clay and sand, respectively. For clay, the equation proposed by Matlock (1970), and Reese and Welch (1975) was suggested.

$$p_u = N_p C_u D \quad (2-25)$$

where C_u = undrained shear strength of soil; D = diameter of drilled shafts; and

$$N_p = 3 + \frac{\gamma'}{c_u} z + \frac{J}{2R} z \leq 9 \quad (2-26)$$

in which γ' = average effective unit weight of soil above depth z ; R = shaft radius; and J = coefficient ranging from 0.25 to 0.5.

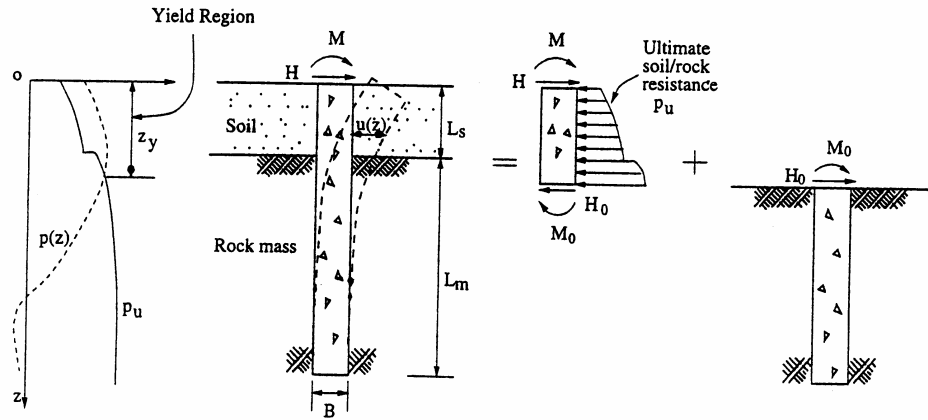


Figure 2-3 Consideration of yielding of soil and/or rock mass by decomposition of loading (after Zhang et al. 2000)

For sand, Zhang et al. (2000) suggested the method of Fleming et al. (1992) as follows.

$$p_u = K_p^2 \gamma' z D \quad (2-27)$$

where $K_p = \tan^2(45^\circ + \phi' / 2)$ = Rankine passive coefficient, in which ϕ' = effective internal friction angle.

To compute the ultimate resistance p_u of rock mass, Zhang et al. (2000) proposed to utilize the assumed resistance distribution (Carter and Kulhawy 1992), shown in Fig. 2-4, and Hoek-Brown rock strength criterion (Hoek and Brown 1988). The assumption for resistance distribution is that the total resistance of rock mass consists of two parts: the side resistance and the front normal resistance. The ultimate resistance p_u can be calculated by

$$p_u = (p_L + \tau_{\max})D \quad (2-28)$$

where D = diameter of the drilled shaft; τ_{\max} = maximum shearing resistance along the sides of the shaft; and p_L = normal limit resistance. τ_{\max} was assumed to be the same as the maximum side resistance under axial loading and can be given by

$$\tau_{\max} = 0.20(\sigma_{ci})^{0.5} \quad (\text{MPa}) \quad \text{for smooth socket} \quad (2-29a)$$

$$\tau_{\max} = 0.80(\sigma_{ci})^{0.5} \quad (\text{MPa}) \quad \text{for rough socket} \quad (2-29b)$$

where σ_{ci} = unconfined compressive strength of the intact rock (MPa).

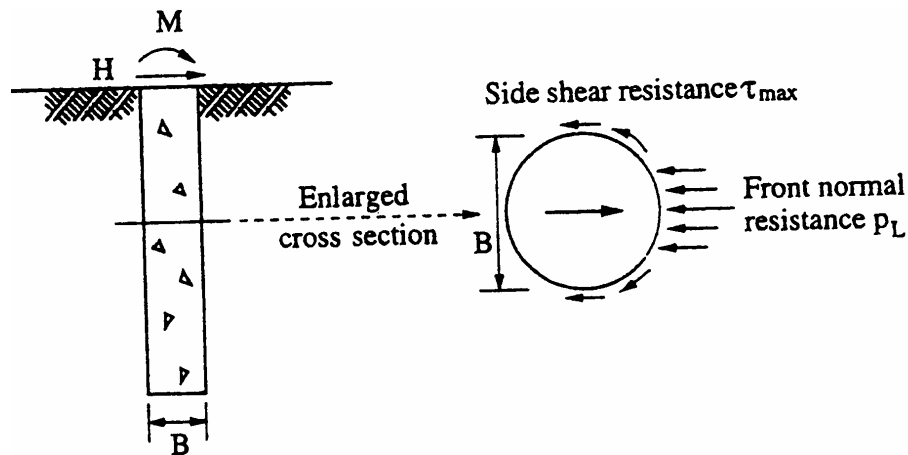


Figure 2-4 Components of rock mass resistance (Zhang et al. 2000)

The strength criterion for rock mass developed by Hoek and Brown (1980, 1988) was adopted to determine the normal limit stress p_L . The Hoek-Brown criterion, which is suitable for intact rock and rock mass, can be given by

$$\sigma'_1 = \sigma'_3 + \sigma_{ci} \left(m_b \frac{\sigma'_3}{\sigma_{ci}} + s \right)^a \quad (2-30)$$

where σ_{ci} = uniaxial compressive strength of the intact rock; σ'_1 and σ'_3 = the major and minor effective principal stresses, respectively; and m_b , s , and a = constants depending on the characteristics of the rock.

For intact rock, $m_b = m_i$, a constant depending on rock type; $s = 1$; and $a = 0.5$. For rock mass, the values of m_b , s , and a can be estimated by correlations with Geological Strength Index (GSI) (Hoek, 1994). In addition to GSI, Rock Mass Rating (RMR) of Bieniawski can also be used to determine the constants m_b , s , and a (Hoek and Brown 1997). With Hoek-Brown's strength criterion, the normal limit stress p_L , which is the major principal effective stress σ'_1 , can be obtained by assuming that the minor principal effective stress is the effective overburden pressure $\gamma' z$.

2.1.2.4 Gabr et al. (2002)

Gabr et al. (2002) proposed a hyperbolic p-y criterion for weak rock based on field tests on small diameter drilled shafts socketed in weak rock. The following procedure can be used to construct a p-y curve according to Gabr et al. (2002).

Step 1: Calculation of Coefficient of Subgrade Reaction

The coefficient of subgrade reaction can be calculated as follows (Vesic, 1961):

$$n_h = \frac{0.65E_m}{D(1-\nu^2)} \left[\frac{E_m D^4}{E_p I_p} \right]^{1/12} \quad (2-31)$$

where D is the diameter of a drilled shaft, ν is Poisson's ratio of rock mass, and GSI is Geological Strength Index.

Step 2: Calculation of Flexibility Factor

A flexibility factor, K_R , is computed as follows (Poulos and Davis, 1972):

$$K_R = \frac{E_p I_p}{E_m L^4} \quad (2-32)$$

where, E_p is modulus of elasticity of shaft, I_p is the moment of inertia of shaft, L is the embedment length of shaft.

Step 3: Calculation of Point of Rotation

The following equation is used to define the turning point as a function of the embedded shaft length:

$$T_0 = (1 + 0.18 \log K_R) L \quad (2-33)$$

where, T_0 is turning point.

Step 4: Calculation of I_T Number

$$I_T = -28 - 383 \log(T_0/L) \quad I_T \geq 1 \quad (2-34)$$

Step 5: Calculation of the Subgrade Reaction

$$k_h = n_h D \quad (0 \leq z \leq T_0) \quad (2-35)$$

$$k_h = I_T n_h D \quad (T_0 < z \leq L) \quad (2-36)$$

Step 6: Calculation of Ultimate Resistance of Rock Mass P_u

The Eq. (2-28) proposed by Zhang et al. (2000) was employed to calculate the ultimate resistance of rock as presented in Section 2.1.2.3. Smooth condition was assumed for all the cases when the side shear resistance is concerned.

Step 7: Construction of the P-y Curve

$$p = \frac{y}{\frac{1}{k_h} + \frac{y}{p_u}} \quad (2-37)$$

2.1.2.5 To, Ernst, and Einstein (2003)

For the drilled shafts socketed into jointed rock, To et al. (2003) assumed a wedge type block failure and Coulomb failure criterion to obtain the lateral capacity of drilled shafts. Goodman and Shi (1985)'s block theory was used to determine the possible failure block for two sets jointed rock mass with the help of AutoCAD or Excel. Due to the complexity of the entire process to obtain the failure block, no details about the block theory will be described here. The assumed mechanisms of sliding failure along the joint plane and tensile failure on the rock mass, preventing the movement of the wedge, are depicted in Fig. 2-5, where W = weight of the wedge; P = axial load of shaft; F = lateral force; T = tensile force due to the fracture of Category II blocks, which is defined as a block that is not removable, but becomes removable if it breaks due to the lateral force exerted by the pier; N_1 = normal force on joint; and R_1 = tangential force on joint.

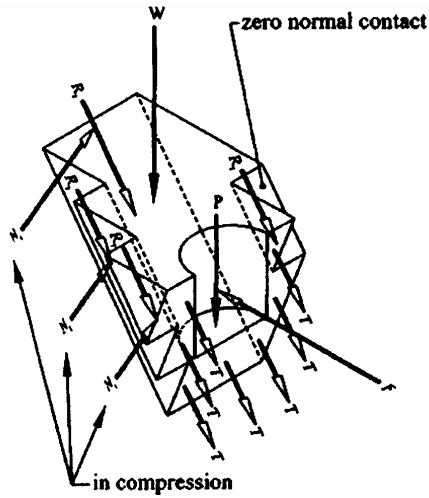


Figure 2-5 Typical forces on wedge

Normal force N and tangential force R can be related by the Coulomb failure criterion as follow:

$$\tau = c + \sigma \tan \phi \quad (2-38)$$

where τ = shear stress; c = cohesion; σ = normal stress; ϕ = friction angle.

Static limit equilibrium relation between the forces on the wedge (Fig. 2-5) was used to solve for ultimate lateral force F .

2.1.3 Comments on the Existing Analysis Methods

2.1.3.1 Carter and Kulhawy (1992)

Carter and Kulhawy (1992) provides solutions for the lateral load-deflection relation at shaft head as well as shaft lateral capacity. For load-deflection prediction, Carter and Kulhawy assumed rock mass as an elastic material, which implies that the solution is only applicable to small loads. The solution for ultimate lateral capacity needs verification. One of the drawbacks of the solution is the requirement of numerous rock

deformation and strength parameters, such as shear modulus, cohesion, friction angle, and dilation angle.

DiGioia and Rojas-Gonzalez (1993) evaluated this method by using their field lateral load test on drilled shafts socketed into rock mass. They found a reasonable agreement between the measured and predicted displacements for these foundations at low load levels (20-30% capacity). However, this method gave predictions that were stiffer than observed at higher load levels. Additionally, Dykeman and Valsangkar (1996) conducted a centrifuge test on eight model socketed shafts and used the test results to evaluate Carter and Kulhawy's method. The comparison showed that Carter and Kulhawy (1992)'s method tend to overestimate the ultimate lateral capacity by a factor of two, while it predicted smaller deflection at shaft head than measured deflection at a given load level. In addition to their own test data, Dykeman and Valsangkar (1996) evaluated Carter and Kulhawy's method by using Frantzen and Stratten (1987)'s field test data. Similar comparison results were found for the predicted deflection at shaft head.

2.1.3.2 Zhang et al. (2000)

The yielding of rock mass was considered in Zhang et al. (2000) method, however, the elasto-perfectly plastic stress-strain relationship can not fully represent the nonlinear behavior of rock masses. As shown in Fig. 2-6, the actual nonlinear behavior may already appear before the stress reaches the peak. For weak rock mass, brittle post-failure may not occur. However, for good quality rock mass, which is likely to behave as a brittle material (Hoek and Brown 1997), the stress will drop after it reaches the peak, as shown in Fig. 2-6. Therefore, despite that yielding of rock was considered in this method, the

behavior of different types of rock mass was not fully represented as an elasto-perfectly plastic model.

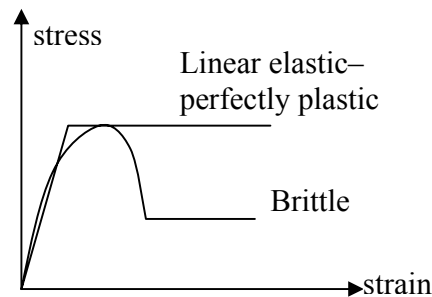


Figure 2-6 The elastoplastic and brittle behavior of rock mass

2.1.3.3 To et al. (2003)

The determination of removable wedge required by this method is a very tedious procedure which involves the use of AutoCAD and EXCEL. Furthermore, only two sets of joints can be considered and the joints in each set should be parallel. The failure mode is restricted to failure at the top portion of rock mass with a free surface at the ground-line.

2.1.3.4 Existing P-y Criteria for Rock

Reese (1997)'s interim rock p-y criterion was not well calibrated due to inadequate test data. The failure modes of rock mass were not well defined; and an estimation of ultimate lateral capacity did not include the effect of friction between rock mass and shaft. Determination of such parameters as constant k_{rm} appears to be empirical. Cho et al. (2001) conducted a lateral load test on rock-socketed drilled shafts. Two drilled shafts, 30 inch in diameter and 10 feet to 13 feet of socket were laterally loaded. Reese (1997)'s interim rock p-y criterion for weak rock was used to construct p-y curves. It was found

that the interim p-y curves underestimated the deflections of shafts when comparing with the measured values.

Although the interim rock p-y criterion was not well established, the p-y method is still a promising method for rock-socketed drilled shaft under lateral loads. Gabr (1993) evaluated two field tests on rock-socketed drilled shafts under lateral loads presented by Carter and Kulhawy (1992) by using p-y analysis and the p-y criterion for stiff clay (Reese et al. 1975). The analysis results showed that p-y approach is analytically attractive because it can approximately model the nonlinearity in the load-displacement response. Gabr et al. (2002) p-y criterion is a most recently proposed p-y criterion for weak rock. However, it has not been further validated with other load tests. The equation for estimating modulus of subgrade reaction was based on Vesic (1961)'s equation for beam on elastic foundation. This is not same as the case of drilled shafts embedded in rock where shaft-rock interaction is more complicated.

2.2 Bedrocks of Ohio

2.2.1 The Distribution of Rocks in Ohio

Six of the groups or systems in the historical classification of rocks are present in the outcrops of Ohio. The geological map, shown in Fig. 2-7, provides the distribution of those rock systems across the state. The six systems of rock are formed in different periods in the history of earth. They are ordered as, from the oldest to youngest, Ordovician, Silurian, Devonian, Mississippian, Pennsylvanian, and Permian (Lamborn et al., 1938). Usually, the older rock systems are bedded under the younger rock systems.

The cross section through the rocks of central Ohio from the Indiana-Ohio border to the Ohio River is shown in Fig. 2-8.

The bedrocks exposed at the surface in Ohio are all of sedimentary types formed from unconsolidated sediments deposited in marine, brackish, or fresh waters (Lamborn et al. 1938). All the common varieties of the sedimentary series can be found, such as limestone, shale, sandstone, dolomite, and conglomerate, as well as many thin beds of coal, clay, and iron ore. In the western half of the State, the bedrock is predominantly limestone and dolomite with minor amounts of calcareous shale. The calcareous shales are most abundant in the southwestern part of the State, where thin limestone interstratified with shale is the usual mode of occurrence. In the northwestern corner of the State, non-calcareous shale is the bedrock lying immediately below the glacial drift.

In contrast to the dominantly calcareous nature of the beds exposed in the western half of Ohio, those in the eastern half are mainly of the clastic or fragmental varieties. Although in the Pennsylvanian and Permian systems of eastern Ohio, thick beds of shale, shaly sandstone, and sandstone are the rule, thin beds of coal, clay, limestone, iron ore, and conglomerate are present. Lens-like bodies of sandstone are widely distributed but lateral gradation to shale is of common occurrence. Shales of varying character are widely distributed both horizontally and vertically on the outcrop (Lamborn et al. 1938). For example, the Conemaugh series of Pennsylvanian System, located in the southeastern of Ohio, ranges from 355 feet to 545 feet and crops out across the center of southeastern Ohio in a belt 10 to 20 miles in width. Bedded marine shales and some thin marine limestones are presented in the lower part of this series, while the upper part includes abundant red calcareous claystones (Fisher et al. 1968). The generalized column of

bedrock in Ohio is presented in Figure 2-9, which was compiled by Hull (1990) and revised by Larsen (2000).

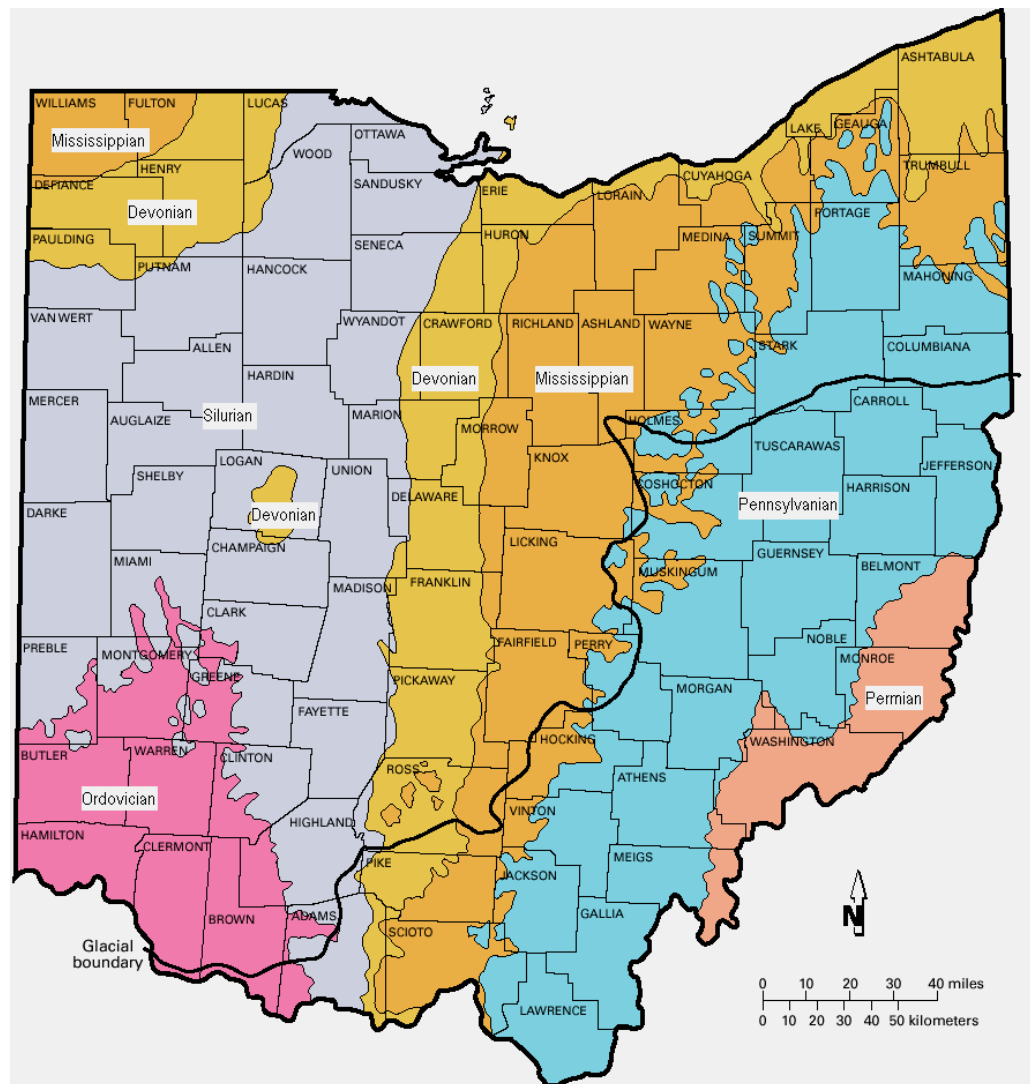


Figure 2-7 Geological map of Ohio, showing the pattern of surface rocks across the state

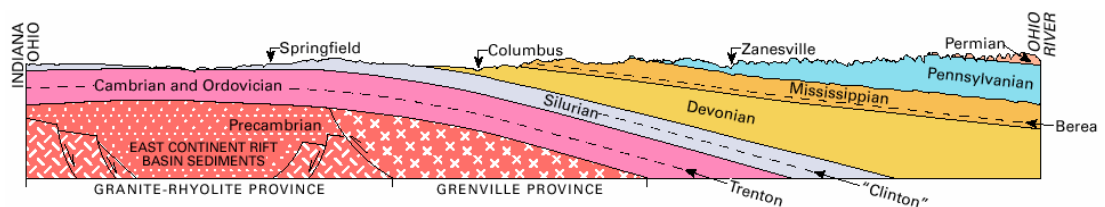


Figure 2-8 Cross section through the rocks of central Ohio from the Indiana-Ohio border to the Ohio River (taken from Feldmann et al., 1996)

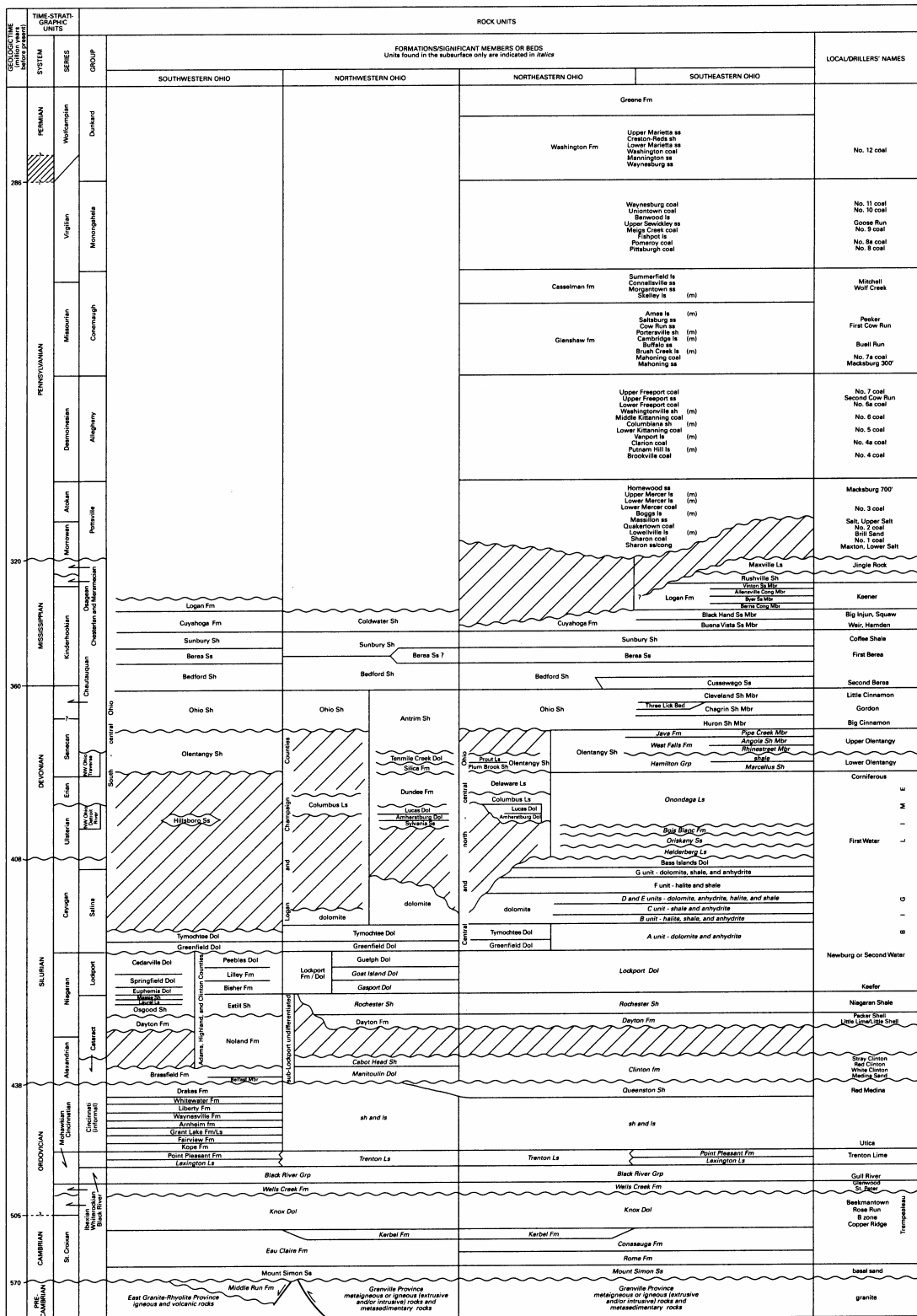


Figure 2-9 Generalized column of bedrock units in Ohio

2.2.2 The Shales in Ohio

2.2.2.1 Introduction

Shale, highly distributed in eastern, southwestern, and northwestern of Ohio, is a variety of sedimentary rock resulted from the consolidation of more or less thinly laminated or bedded silts and clays (Lamborn et al., 1938). In general, shale is less weather resistant than most other varieties of sedimentary rocks.

The composition of shales is variable as it is assemblage of many mineral substances of different chemical composition. The chief mineral constituents found in shale are hydrated aluminum silicates of varying composition, quartz, rutile, apatite, calcite, dolomite, and iron oxides. Organic material is generally present in small amounts. The hydrated silicates and quartz make up a large part of the average shale and in themselves produce a rock which is white, green, or greenish gray in color. Dark bluish gray, dark brown and black colors are usually found when finely divided organic material is presented in the shale. Where iron oxide occurs in the absence of much organic matter, the shale may be buff, yellowish brown, brown, or red in color. Green or greenish gray colors are characteristic of unweathered shale rich in either iron carbonates or chloritic material and poor in organic matter.

Shale beds are associated with sandstone, limestone, coal, and claystone. Shale may gradually become shaly sandstone and finally sandstone as quartz increases in percentage and size of grain. With an increase in the percentage of calcium carbonate, shale transits to limestone. As carbonaceous material becomes greater in amount, shale is transited to bone coal and coal; and as the fissility or shaly structure disappears, siltstone is produced from shale.

2.2.2.2 Shale Classification System

Typical shales possess fissility or the property of splitting with comparative ease along the planes of lamination or bedding. Hand specimens of typical shale are distinguished from sandstones and conglomerates by the smaller grain size and by the fissility; from coal, clay and mudstone by its fissility; and from limestone and dolomite by its fissility and low carbonate content.

Various shale classification systems have been proposed by different investigators from engineering view point, such as Wood and Deo (1975). Wood and Deo (1975) proposed a shale classification system for embankments. Four simple tests were suggested to characterize shales for embankment use: one cycle slaking in water, slake-durability on an initially dry sample, slake-durability on a soaked sample, and a modified sodium sulfate soundness test. The system classifies shales into four groups: rock-like shales, intermediate-1 shales, intermediate-2 shales, and soil-like shales, as shown in Figure 2-10. In Figure 2-10, $(I_d)_d$ is the slake durability index of dry sample; $(I_d)_s$ is the slake durability index of soaked sample; and I_s is the soundness index.

The classification of shales for deep foundations has not been established yet. However, the engineering performance of shales for deep foundation design, such as reduced shear resistance, swelling, reduced bearing capacity, could be correlated to the durability and other properties of shales. If a series of tests on shale strength and durability can be organized and conducted, the correlation between shale-shaft side resistance reduction due to water intrusion and the durability index can be established (not to be done in this study). For instance, Richardson and Wiles (1990) proposed a correlation between the loss of shear strength and results of simple tests (e.g., sieved

slake durability index, natural moisture content, and change in point-load strength) for embankment applications. The effect of slake during drilling or coring of shales should also be taken into account. The cored shales can be used for slake-durability test.

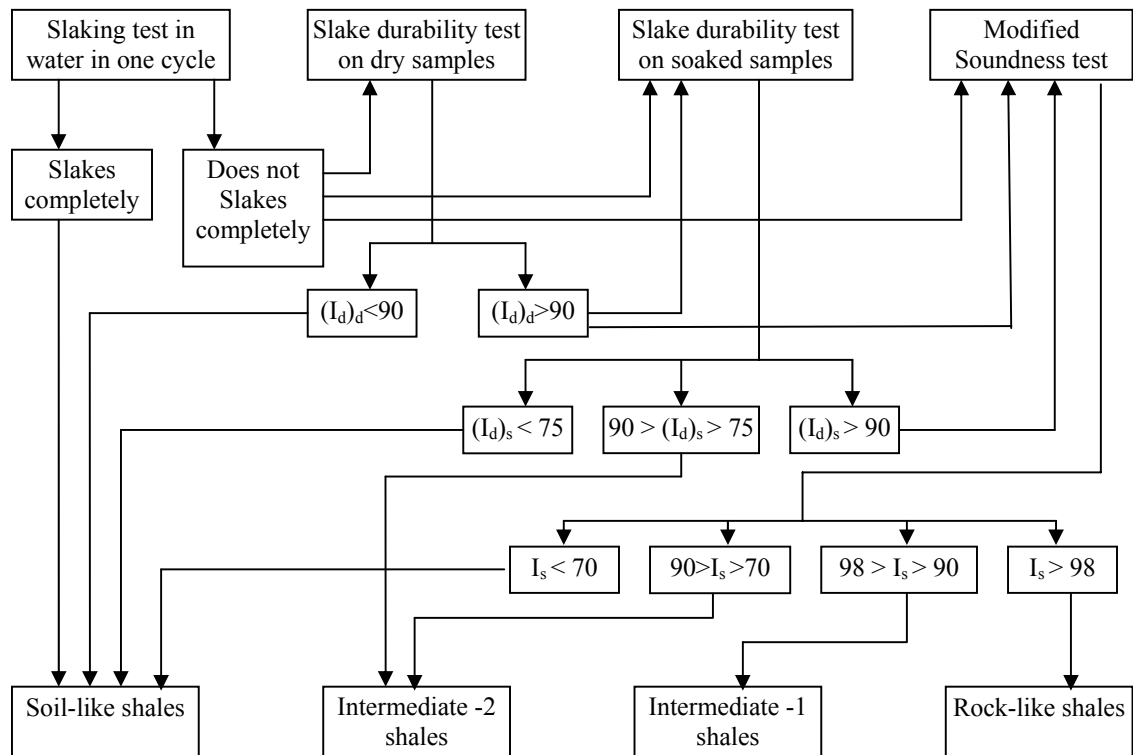


Figure 2-10 Classification of shales for embankment construction (Wood and Deo, 1975)

2.2.2.3 Engineering Properties of Ohio Shales

A compilation of field and lab test results on Ohio shales is presented in Table 2-1, where the unconfined compressive strength, σ_{ci} , and RQD of shales are given.

Hawk and Ko (1980) examined the orthotropic nature of two shales and concluded that the properties of both shales are represented well by a transversely isotropic model, although an isotropic model is also acceptable. Additionally, Sargand and Hazen (1987)

conducted a series of triaxial tests on Ohio grey shales and concluded that the transverse isotropy is an appropriate model to simulate the stress-strain relations of these shales.

Table 2-1 Engineering Properties of Rocks in Ohio

County	Project Name	Depth (ft)	Rock Type	RQD (%)	σ_{ci} (psi)
Erie	ERI60 ⁽¹⁾	26	Medium-hard to hard shale	100	7320
Erie	ERI60 ⁽¹⁾	15	Medium-hard to hard shale	100	6604
Meigs	Pomery Mason ⁽²⁾	29-45	Shale (50%) with interbedded siltstone (50%)	60	905
Meigs	Pomery Mason ⁽²⁾	75-88	Siltstone, hard	56	4611
Noble	Sargand and Hazen ⁽³⁾		Grey shale		2100-3125
Chesapeake	Sargand and Hazen ⁽³⁾		Grey shale		1400-2800

(1): Nusairat, J., Engel, R. L., and Liang, R. Y. (2002).

(2): Data obtained from E.L. Robinson Engineering of Ohio Co. and University of Akron.

(3): Sargand and Hazen (1987). The strengths were obtained with 100 to 200 psi of confining pressure.

2.2.2.4 Effect of Water on Shales

Water plays an important role on engineering properties of shales, such as shear strength and durability. The shearing strength of shale is quite low, deriving from small internal friction of microscopic platy grains as well as cohesion between particles. This cohesion is usually dependent upon a skin of absorbed, oriented water molecules and sometimes also upon surface tension between the water and any air that may exist from time to time in the pores of the coarse phases of the sediment. However, excess water under pressure may reduce the cohesion, either by altering the molecular film of water or by destroying the surface tension as all air spaces become filled with water. Also, pore-water pressure in the silty phases of the rock may spread the grains apart so that internal friction is further diminished. Finally, certain clay minerals have the ability to absorb

water and swell, thus exerting an upward pressure that may reduce shear resistance within a claystone. (Fisher et al., 1968)

Fisher et al. (1968) conducted slake tests, in which equal size cubic shales were immersed in water and observed during a period of three and one-half days, on various Ohio shales cored from southeastern Ohio. Twenty three red shale samples, eight gray shale samples, and eleven green shales were tested. With three exceptions, the red shale samples deteriorated completely; almost all slaked within one hour into chunks one to two mm in diameter, and two-thirds eventually became oozes covering the bottoms of the beakers. Three red shales became oozes within only ten minutes, and almost a dozen flaked badly on the bedding surfaces in the same span of time.

The eight samples of gray shales, under the same treatment, were essentially unaffected. The eleven green shales varied widely in behavior, some slaking within five hours, a few slaking slightly, but most not deteriorating at all.

2.2.3 Limestone and Dolomite

The dolomites and limestones of western Ohio form the bedrock in approximately 20,381 square miles or in nearly one-half of the total area of the State (Stout, 1941). A limestone is a rock composed essentially of calcium carbonate, CaCO_3 , with minor quantities of other basic carbonates, sulphates, sulphides, phosphates, and silicates, and of siliceous and clay-like materials. In general, they range from 80% to 98% calcium carbonate. The limestones are deposited in shallow or comparatively shallow water and are the result of precipitation either by direct exchange or by the agency of organic life.

Dolomite is the prominent carbonate rock throughout the stratigraphic section of western Ohio. Such strata constitute more than 60% of the whole. Dolomite may be

defined as a rock composed largely of magnesium carbonate combined directly with calcium carbonate in the molecular ratio of one to one. Its chemical composition may be written as $\text{MgCa}(\text{CO}_3)_2$. The dolomites marine in origin, were deposited in shallow or comparatively shallow water, and in the main are direct precipitates. Most certainly, they were laid down in the form we now find them and are not secondary, that is, deposited as limestone or limy sediment, then changed to dolomite (Stout, 1941).

2.3 Mechanical Characteristics of Rock and Its Classifications

2.3.1 The types of rocks

There are three basic types of rocks: igneous, sedimentary, and metamorphic. Table 2-2 presents a simplified rock classification system and common rock types.

2.3.2 Features for Rock Characterization

The difficulties in making predictions of the engineering responses of rocks and rock mass derive largely from their discontinuous and variable nature. In fact, rock is distinguished from other engineering materials by the presence of inherent discontinuities, which may control its mechanical behavior. The response of intact rock material itself may be complex and difficult to describe theoretically because the rock consists of an aggregation of grains of material having quite different physical properties. It may contain inter- and intra-granular micro-cracks and may have anisotropic and/or nonlinear mechanical properties (Brown, 1993).

Qualification and quantification of in-situ rock masses are some of the most important aspects of site characterization for design of foundations. These characteristics generally indicate the strength, deformability, and stability of the rock masses. For

economical reason, it is not feasible to fully measure the characteristics of a complex rock masses. The key factors influencing the rock mass behavior are listed in Table 2-3.

Table 2-2 Simplified Rock Classification

Common igneous rocks	Major division	Secondary divisions	Rock types
	Extrusive	Volcanic explosion debris (fragmental) Lava flows and hot siliceous clouds Lava flows (fine-grained texture)	Tuff (lithified ash) and volcanic breccia Obsidian (glass), pumice, and scoria Basalt, andesite, and rhyolite
	Intrusive	Dark minerals dominant Intermediate (25-50% dark minerals) Light color (quartz and feldspar)	Gabbro Diorite Granite
Common sedimentary rocks	Major division	Texture (grain size) or chemical composition	Rock types
	Clastic rocks	Grain size large than 2 mm (pebbles, gravel, cobbles, and boulders) Sand-size grains, 0.0062 to 2 mm Silt-size grain, 0.004 to 0.062 mm Clay-size grains, less than 0.004 mm	Conglomerate (rounded cobbles) or breccia (angular rock fragments) Sandstone Siltstone Claystone and shale
	Chemical and organic rock	Carbonate minerals (e.g., calcite) Halite minerals Sulfate minerals Iron-rich minerals Siliceous minerals Organic products	Limestone Rock salt Gypsum Hematite Chert Coal
Common metamorphic rocks	Major division	Structure (foliated or massive)	Rock types
	Coarse crystalline	Foliated Massive	Gneiss Metaquartzite
	Medium crystalline	Foliated Massive	Schist Marble, quartzite, serpentine, soapstone
	Fine to microscopic	Foliated Massive	Phyllite, slate Hornfels, anthracite coal

Discontinuities, one of the major effects, may influence the engineering response of rock masses in a variety of ways as enumerated below:

- The provision of planes of low shear strength along which slip might occur
- Reducing the overall shear and tensile strengths of the rock masses
- Rendering the overall mechanical response of the rock masses in the sense that individual blocks may be free to rotate or to translate with associated slip and/or separation at block interfaces
- Introducing a wide range of potential failure mechanisms (such as unraveling, toppling, slip or the gravity fall of blocks or wedges)
- Influencing the stress distribution within the rock masses mainly because of their low stiffness and strengths
- Attenuating, reflecting and refracting stress waves arising from blasting
- Controlling to a large extent the fragmentation achieved by excavation processes
- Providing major conduits for the flow of fluids through most masses due to their permeability is orders of magnitude higher than that of intact rocks

Table 2-3 Factors influencing Rock Mass Behavior

Characteristics of Rock	Specimen and Environmental Conditions	State of Stress or Strain	Method of Loading
Rock material structure: lithology, cracks	Moisture content, temperature, and pore-pressure	Magnitude of applied stress or strain	Type of loading: compressive, shear
Rock mass structure: discontinuities	Groundwater conditions and chemical environment	Distribution of stress or strain	Rate of loading: static, dynamic, impact
Properties: mechanical, physical	Specimen size and shape		Pattern of loading: constant load, repetitive (fatigue), pulse

2.3.3 Rock Mass Classifications

In order to evaluate influence of discontinuities in rock masses for a given rock engineering project, it is necessary that the discontinuities in rock masses should be characterized. The International Society for Rock Mechanics selects ten parameters as being of the primary importance for quantitative description of discontinuities in rock masses (Brown, 1981):

- 1) Orientation: attitude of a discontinuity in space, described by the dip direction and dip of the line of steepest declination in plane of discontinuity
- 2) Spacing: perpendicular distance between adjacent discontinuities, normally refers to the mean or modal spacing of a set of joints
- 3) Persistence: discontinuity trace length as observed in an exposure which may give a crude measure of the area extent or penetration length of a discontinuity. Termination in solid rock or against other discontinuities reduces the persistence
- 4) Roughness: Inherent surface roughness and waviness relative to the mean plane of a discontinuity. Both roughness and waviness contribute to the shear strength. Large scale waviness may also alter the dip locally
- 5) Wall strength: equivalent compressive strength of adjacent rock walls of discontinuity may be lower than rock block strength due to weathering or alteration of the walls.
- 6) Aperture: perpendicular distance between adjacent rock walls of a discontinuity, in which the intervening space is air or water filled
- 7) Filling: material that separates the adjacent rock wall of a discontinuity and that is usually weaker than the parent rock. Typical filling materials are sand, silt, clay,

- breccia, gouge and mylonite. Also includes thin mineral coatings and healed discontinuities, e.g. quartz and calcite veins
- 8) Seepage: water flow and free moisture visible in individual discontinuities or in the rock mass as a whole
 - 9) Number of sets: the number of joints comprising the intersecting joint system. The rock mass may be further divided by individual discontinuities
 - 10) Block size: rock block dimensions resulting from the mutual orientation of intersection joint sets, and resulting from the spacing of individual discontinuities may further influence the block size and shape.

To quantify the effect of discontinuities of rock masses, three different rock mass classifications, Rock Mass Quality (Q) system of Norwegian Geotechnical Institute (Barton et al., 1974), Rock Mass Rating (RMR) system of the Council for Scientific and Industrial Research, South Africa (Bieniawski, 1976 and 1989), and Geological Strength Index (GSI) system (Hoek, 1994), have been proposed in literature. All these classification systems were developed initially for tunnel or dam applications. However, they have been used for other engineering applications, such as slope and foundation.

2.3.3.1 Q System

Q system (Barton et al., 1974) is based on six parameters: RQD, number of joint or discontinuity sets (J_n), joint roughness (J_r), joint alteration (J_a), water flow (J_w) and a stress reduction factor (SRF). Because this system is mainly used for tunneling applications in Europe, the details to quantify these parameters will not be discussed here. The rock mass quality (Q) is defined as:

$$Q = \left(\frac{RQD}{J_n} \right) \left(\frac{J_r}{J_a} \right) \left(\frac{J_w}{SRF} \right) \quad (2-39)$$

2.3.3.2 RMR System

There are two versions of RMR system: one is developed by Bieniawski in 1976; the other one is proposed by Bieniawski (1989) which is a modified version of 1976 RMR system. In 1976 version, the major factors used to quantify the rating are:

1. Uniaxial compressive strength of intact rock
2. RQD
3. Spacing of joints
4. Strike and dip orientations of joints
5. Condition of joints
6. Ground water inflow

The RMR_{76} value equals to the summation of the six ratings. Details of the rating system are presented in Table 2-4. The 1989 version of RMR system combines orientations rating and condition of joints rating into one rating as condition of discontinuities. The other items are kept same; however, the values of the ratings are changed. The RMR_{89} value also equals to the summation of five ratings as presented in detail in Table 2-5.

Table 2-4 Classification Parameters and Their Rating (After Bieniawski, 1976)

1	Uniaxial compressive strength of intact rock	> 200 MPa	100-200 MPa	50-100 MPa	25 –50 MPa	< 25 MPa
	Rating	10	5	2	1	0
2	Drill core quality RQD	90%-100%	75%-90%	50%-75%	25%-50%	<25% or highly weathered
	Rating	20	17	14	8	3
3	Spacing of joints	> 3 m	1-3 m	0.3-1 m	50-300 mm	< 50 mm
	Rating	30	25	20	10	5
4	Strike and dip orientations of joints	Very favorable	Favorable	Fair	Unfavorable	Very unfavorable
	Rating	15	13	10	6	3
5	Condition of joints	Very tight: separation<0.1 mm Not continuous		Tight: <1 mm and continuous No gouge	Open: 1-5 mm Continuous Gouge<5 mm	Open >5 mm Continuous Gouge>5 mm
	Rating	15		10	5	0
6	Ground water inflow (per 10m of tunnel length)	None		<25 liters/min	25-125 liters/min	>125 liters/min
	Rating	10		8	5	2
Rock Mass Classes and Other Rating						
Class No.	I	II	III	IV	V	
Description	Very good rock	Good rock	Fair rock	Poor rock	Very poor rock	
Total rating	100-90	90-70	70-50	50-25	<25	

Table 2-5 Rock Mass Rating System (Bieniawski, 1989)

A. CLASSIFICATION PARAMETERS AND THEIR RATINGS									
Parameter			Range of values						
1	Strength of intact rock material	Point-load strength index	>10 MPa	4-10 MPa	2-4 MPa	1-2 MPa	For this low range - uniaxial compressive test is preferred		
		Uniaxial comp. strength	>250 MPa	100-250 MPa	50-100 MPa	25-50 MPa	5-25 MPa	1-5 MPa	< 1 MPa
	Rating		15	12	7	4	2	1	0
2	Drill core Quality <i>RQD</i>		90%-100%	75%-90%	50%-75%	25%-50%	< 25%		
	Rating		20	17	13	8	3		
3	Spacing of discontinuities		> 2 m	0.6-2 . m	200-600 mm	60-200 mm	< 60 mm		
	Rating		20	15	10	8	5		
4	Condition of discontinuities (See E)		Very rough surfaces Not continuous No separation Unweathered wall rock	Slightly rough surfaces Separation < 1 mm Slightly weathered walls	Slightly rough surfaces Separation < 1 mm Highly weathered walls	Slickensided surfaces or Gouge < 5 mm thick or Separation 1-5 mm Continuous	Soft gouge >5 mm thick or Separation > 5 mm Continuous		
	Rating		30	25	20	10	0		
5	Ground water	Inflow per 10 m tunnel length (l/m)	None	< 10	10-25	25-125	> 125		
		(Joint water press/ (Major principal σ)	0	< 0.1	0.1-0.2	0.2-0.5	> 0.5		
		General conditions	Completely dry	Damp	Wet	Dripping	Flowing		
	Rating		15	10	7	4	0		
B. RATING ADJUSTMENT FOR DISCONTINUITY ORIENTATIONS (See F)									
Strike and dip orientations			Very favourable	Favourable	Fair	Unfavourable	Very Unfavourable		
Ratings	Tunnels & mines		0	-2	-5	-10	-12		
	Foundations		0	-2	-7	-15	-25		
	Slopes		0	-5	-25	-50			
C. ROCK MASS CLASSES DETERMINED FROM TOTAL RATINGS									
Rating			100 ← 81	80 ← 61	60 ← 41	40 ← 21	< 21		
Class number			I	II	III	IV	V		
Description			Very good rock	Good rock	Fair rock	Poor rock	Very poor rock		
D. MEANING OF ROCK CLASSES									
Class number			I	II	III	IV	V		
Average stand-up time			20 yrs for 15 m span	1 year for 10 m span	1 week for 5 m span	10 hrs for 2.5 m span	30 min for 1 m span		
Cohesion of rock mass (kPa)			> 400	300-400	200-300	100-200	< 100		
Friction angle of rock mass (deg)			> 45	35-45	25-35	15-25	< 15		
E. GUIDELINES FOR CLASSIFICATION OF DISCONTINUITY conditions									
Discontinuity length (persistence)			< 1 m	1-3 m	3-10 m	10-20 m	> 20 m		
Rating			6	4	2	1	0		
Separation (aperture)			None	< 0.1 mm	0.1-1.0 mm	1-5 mm	> 5 mm		
Rating			6	5	4	1	0		
Roughness			Very rough	Rough	Slightly rough	Smooth	Slickensided		
Rating			6	5	3	1	0		
Infilling (gouge)			None	Hard filling < 5 mm	Hard filling > 5 mm	Soft filling < 5 mm	Soft filling > 5 mm		
Rating			6	4	2	2	0		
Weathering			Unweathered	Slightly weathered	Moderately weathered	Highly weathered	Decomposed		
Ratings			6	5	3	1	0		
F. EFFECT OF DISCONTINUITY STRIKE AND DIP ORIENTATION IN TUNNELLING**									
Strike perpendicular to tunnel axis					Strike parallel to tunnel axis				
Drive with dip-Dip 45-90°			Drive with dip-Dip 20-45°		Dip 45-90°		Dip 20-45°		
Very favourable			Favourable		Very favourable		Fair		
Drive against dip-Dip 45-90°			Drive against dip-Dip 20-45°		Dip 0-20-Irrespective of strike°				
Fair			Unfavourable		Fair				

*Some conditions are mutually exclusive. For example, if infilling is present, the roughness of the surface will be overshadowed by the influence of the gouge. In such cases use A.4 directly.

**Modified after Wickham et al. (1972).

2.3.3.3 GSI System

The RMR values are difficult to estimate for very poor rock, especially for borehole cores that contain relatively few intact core pieces longer than 4 inch (Hoek, 1994). Therefore, GSI system was proposed by Hoek (1994) to replace the RMR rating in developing his rock strength criterion. GSI values are based on the structure of rock mass and the surface condition. For cored weak rock, the physical appearance of material recovered in the core can be used to estimate a GSI value. The details for estimating GSI value are presented in Table 2-6 to Table 2-10.

Additionally, GSI can be converted from Rock Mass Rating (RMR) (see Hoek and Brown, 1997). If Bieniawski (1976) RMR_{76} is used, the rock mass should be assumed to be completely dry and a rating of 10 could be assigned to the groundwater, and adjustment for discontinuity orientation value should be set to zero. If Bieniawski (1989) RMR_{89} is used, the value of 15 should be assigned to groundwater rating and adjustment for discontinuity value is set to zero. Consequently, the following relationship can be established.

$$GSI = RMR_{76} \quad (2-40)$$

$$GSI = RMR_{89} - 5 \quad (2-41)$$

Table 2-6 GSI Ranges for General Rocks (Marinos and Hoek, 2000)

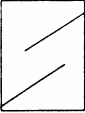
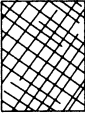




<p>GEOLOGICAL STRENGTH INDEX FOR JOINTED ROCKS (Hoek and Marinos, 2000)</p> <p>From the lithology, structure and surface conditions of the discontinuities, estimate the average value of GSI. Do not try to be too precise. Quoting a range from 33 to 37 is more realistic than stating that GSI = 35. <u>Note that the table does not apply to structurally controlled failures.</u> Where weak planar structural planes are present in an unfavourable orientation with respect to the excavation face, these will dominate the rock mass behaviour. The shear strength of surfaces in rocks that are prone to deterioration as a result of changes in moisture content will be reduced if water is present. When working with rocks in the fair to very poor categories, a shift to the right may be made for wet conditions. Water pressure is dealt with by effective stress analysis.</p>		<p>SURFACE CONDITIONS</p> <p>VERY GOOD Very rough, fresh unweathered surfaces</p> <p>GOOD Rough, slightly weathered, iron stained surfaces</p> <p>FAIR Smooth, moderately weathered and altered surfaces</p> <p>POOR Slackensided, highly weathered surfaces with compact coatings or fillings or angular fragments</p> <p>VERY POOR Slackensided, highly weathered surfaces with soft clay coatings or fillings</p>				
<p>STRUCTURE</p>		<p>DECREASING SURFACE QUALITY →</p>				
<p>DECREASING INTERLOCKING OF ROCK PIECES</p> <p>↓</p>	 <p>INTACT OR MASSIVE - intact rock specimens or massive in situ rock with few widely spaced discontinuities</p>	90			N/A	N/A
	 <p>BLOCKY - well interlocked undisturbed rock mass consisting of cubical blocks formed by three intersecting discontinuity sets</p>	80	70			
	 <p>VERY BLOCKY - interlocked, partially disturbed mass with multi-faceted angular blocks formed by 4 or more joint sets</p>		60			
	 <p>BLOCKY/DISTURBED/SEAMY - folded with angular blocks formed by many intersecting discontinuity sets. Persistence of bedding planes or schistosity</p>		50	40		
	 <p>DISINTEGRATED - poorly interlocked, heavily broken rock mass with mixture of angular and rounded rock pieces</p>			30	20	
	 <p>LAMINATED/SHEARED - Lack of blockiness due to close spacing of weak schistosity or shear planes</p>	N/A	N/A			10

Table 2-7 GSI Ranges for Typical Sandstones (Marinos and Hoek, 2000)

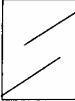
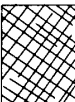




<p>GEOLOGICAL STRENGTH INDEX FOR JOINTED ROCKS (Hoek and Marinos, 2000)</p> <p>From the lithology, structure and surface conditions of the discontinuities, estimate the average value of GSI. Do not try to be too precise. Quoting a range from 33 to 37 is more realistic than stating that GSI = 35. <u>Note that the table does not apply to structurally controlled failures.</u> Where weak planar structural planes are present in an unfavourable orientation with respect to the excavation face, these will dominate the rock mass behaviour. The shear strength of surfaces in rocks that are prone to deterioration as a result of changes in moisture content will be reduced if water is present. When working with rocks in the fair to very poor categories, a shift to the right may be made for wet conditions. Water pressure is dealt with by effective stress analysis.</p>		<p>SURFACE CONDITIONS</p> <p>VERY GOOD Very rough, fresh unweathered surfaces</p> <p>GOOD Rough, slightly weathered, iron stained surfaces</p> <p>FAIR Smooth, moderately weathered and altered surfaces</p> <p>POOR Slackensided, highly weathered surfaces with compact coatings or fillings or angular fragments</p> <p>VERY POOR Slackensided, highly weathered surfaces with soft clay coatings or fillings</p>				
<p>STRUCTURE</p>		<p>DECREASING SURFACE QUALITY →</p>				
<p>DECREASING INTERLOCKING OF ROCK PIECES</p> <p>↓</p>	 <p>INTACT OR MASSIVE - intact rock specimens or massive in situ rock with few widely spaced discontinuities</p>	90	80	70	60	N/A
	 <p>BLOCKY - well interlocked undisturbed rock mass consisting of cubical blocks formed by three intersecting discontinuity sets</p>			1	50	
	 <p>VERY BLOCKY - interlocked, partially disturbed mass with multi-faceted angular blocks formed by 4 or more joint sets</p>				40	
	 <p>BLOCKY/DISTURBED/SEAMY - folded with angular blocks formed by many intersecting discontinuity sets. Persistence of bedding planes or schistosity</p>				30	
	 <p>DISINTEGRATED - poorly interlocked, heavily broken rock mass with mixture of angular and rounded rock pieces</p>				20	
	 <p>LAMINATED/SHEARED - Lack of blockiness due to close spacing of weak schistosity or shear planes</p>	N/A	N/A			10
<p>WARNING:</p> <p>The shaded areas are indicative and may not be appropriate for site specific design purposes. Mean values are not suggested for indicative characterisation; the use of ranges is recommended</p> <p>1. Massive or bedded (no clayey cement present)</p> <p>2. Brecciated (no clayey cement present)</p>						

Table 2-8 GSI Ranges for Typical Siltstones, Claystones and Clay Shales (Marinos and Hoek, 2000)


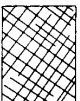




<p>GEOLOGICAL STRENGTH INDEX FOR JOINTED ROCKS (Hoek and Marinos, 2000)</p> <p>From the lithology, structure and surface conditions of the discontinuities, estimate the average value of GSI. Do not try to be too precise. Quoting a range from 33 to 37 is more realistic than stating that GSI = 35. Note that the table does not apply to structurally controlled failures. Where weak planar structural planes are present in an unfavourable orientation with respect to the excavation face, these will dominate the rock mass behaviour. The shear strength of surfaces in rocks that are prone to deterioration as a result of changes in moisture content will be reduced if water is present. When working with rocks in the fair to very poor categories, a shift to the right may be made for wet conditions. Water pressure is dealt with by effective stress analysis.</p>		SURFACE CONDITIONS				
STRUCTURE		DECREASING SURFACE QUALITY →				
		VERY GOOD Very rough, fresh unweathered surfaces	GOOD Rough, slightly weathered, iron stained surfaces	FAIR Smooth, moderately weathered and altered surfaces	POOR Slickensided, highly weathered surfaces with compact coatings or fillings or angular fragments	VERY POOR Slickensided, highly weathered surfaces with soft clay coatings or fillings
	INTACT OR MASSIVE - intact rock specimens or massive in situ rock with few widely spaced discontinuities	90			N/A	N/A
	BLOCKY - well interlocked undisturbed rock mass consisting of cubical blocks formed by three intersecting discontinuity sets	80	70			
	VERY BLOCKY - interlocked, partially disturbed mass with multi-faceted angular blocks formed by 4 or more joint sets		60	50		
	BLOCKY/DISTURBED/SEAMY - folded with angular blocks formed by many intersecting discontinuity sets. Persistence of bedding planes or schistosity			40	30	
	DISINTEGRATED - poorly interlocked, heavily broken rock mass with mixture of angular and rounded rock pieces				20	
	LAMINATED/SHEARED - Lack of blockiness due to close spacing of weak schistosity or shear planes	N/A	N/A		10	
<p>WARNING:</p> <p>The shaded areas are indicative and may not be appropriate for site specific design purposes. Mean values are not suggested for indicative characterisation; the use of ranges is recommended</p> <p>1. Bedded, foliated, fractured 2. Sheared, brecciated</p>						

Table 2-9 GSI Ranges for Typical Limestones (Marinos and Hoek, 2000)


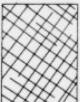





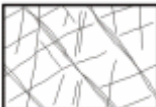
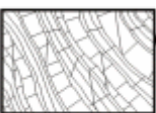
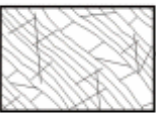
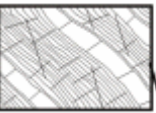
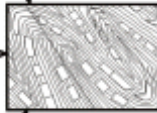
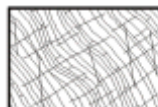
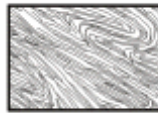
GEOLOGICAL STRENGTH INDEX FOR JOINTED ROCKS (Hoek and Marinos, 2000)		SURFACE CONDITIONS											
From the lithology, structure and surface conditions of the discontinuities, estimate the average value of GSI. Do not try to be too precise. Quoting a range from 33 to 37 is more realistic than stating that GSI = 35. Note that the table does not apply to structurally controlled failures. Where weak planar structural planes are present in an unfavourable orientation with respect to the excavation face, these will dominate the rock mass behaviour. The shear strength of surfaces in rocks that are prone to deterioration as a result of changes in moisture content will be reduced if water is present. When working with rocks in the fair to very poor categories, a shift to the right may be made for wet conditions. Water pressure is dealt with by effective stress analysis.		VERY GOOD Very rough, fresh unweathered surfaces	GOOD Rough, slightly weathered, iron stained surfaces	FAIR Smooth, moderately weathered and altered surfaces	POOR Slickensided, highly weathered surfaces with compact coatings or fillings or angular fragments	VERY POOR Slickensided, highly weathered surfaces with soft clay coatings or fillings							
STRUCTURE		DECREASING SURFACE QUALITY →											
	INTACT OR MASSIVE - intact rock specimens or massive in situ rock with few widely spaced discontinuities	<div>DECREASING INTERLOCKING OF ROCK PIECES</div> <div>↓</div>	90	80	70	60	50	40	30	20	10	N/A	N/A
	BLOCKY - well interlocked undisturbed rock mass consisting of cubical blocks formed by three intersecting discontinuity sets		1	60	50	40	30	20	10	N/A	N/A		
	VERY BLOCKY- interlocked, partially disturbed mass with multi-faceted angular blocks formed by 4 or more joint sets		2	30	20	10	N/A	N/A	N/A	N/A			
	BLOCKY/DISTURBED/SEAMY - folded with angular blocks formed by many intersecting discontinuity sets. Persistence of bedding planes or schistosity		3	N/A	N/A	N/A	N/A	N/A	N/A	N/A			
	DISINTEGRATED - poorly interlocked, heavily broken rock mass with mixture of angular and rounded rock pieces		N/A	N/A	N/A	N/A	N/A	N/A	N/A	N/A	N/A		
	LAMINATED/SHEARED - Lack of blockiness due to close spacing of weak schistosity or shear planes		N/A	N/A	N/A	N/A	N/A	N/A	N/A	N/A	N/A		
WARNING: The shaded areas are indicative and may not be appropriate for site specific design purposes. Mean values are not suggested for indicative characterisation; the use of ranges is recommended													
1. Massive													
2. Thin bedded													
3. Brecciated													

Table 2-10 GSI Estimates for Heterogeneous Rock Masses Such as Flysch (Marinos and Hoek, 2000)

Rock Type:	Flysch	GSI Selection:	50	OK	SURFACE CONDITIONS OF DISCONTINUITIES						
					VERY GOOD	GOOD	FAIR	POOR	VERY POOR		
COMPOSITION AND STRUCTURE											
	A. Thick bedded, very blocky sandstone The effect of pelitic coatings on the bedding planes is minimized by the confinement of the rock mass. In shallow tunnels or slopes these bedding planes may cause structurally controlled instability.										
	B. Sandstone with thin inter-layers of siltstone										
C, D, E and G - may be more or less folded than illustrated but this does not change the strength. Tectonic deformation, faulting and loss of continuity moves these categories to F and H.											

CHAPTER III

LATERAL LOAD TEST RESULTS AND DATA ANALYSES

This chapter presents two lateral load tests on drilled shafts socketed in rock. The two tests were designed and conducted by E.L. Robinson Engineering of Ohio Co. The subsurface investigation and lab test results on rock core samples are provided. The information pertinent to test drilled shafts and instrumentation are also presented. The lateral load test results, including deflections at shaft head at various loading levels, the shaft deflection profiles along depth of shaft, and strain gage readings are presented.

To obtain the most accurate experimental p-y curves from strain gage readings, this chapter also exams the accuracy of various existing methods for deriving p-y curves from lateral load test results, particularly in terms of strain gage readings. Hypothetical cases are used to further verify the findings from actual field load test data.

An existing weak rock p-y criterion proposed by Reese (1997) is evaluated against the two actual lateral load tests results.

3.1 Lateral Load Test at Dayton

3.1.1 Test Site

The lateral load test was performed for assisting the design of a new two span reinforced concrete rib arch bridge as a replacement to an existing single span steel

bridge where East Siebenthaler Avenue crosses the Stillwater River in Dayton, Ohio. In general, both the Illinoian and Wisconsin glaciers covered the site. Glacial deposits in the area are generally less than 30 feet thick. The underlying bedrock was reported to be limestone and shale of the Richmond Formation.

Two borings, B-2 and B-4, were drilled in the approximate location of the lateral load test, with the boring B-2 closer to the test site. As shown in Fig. 3-1, borings B-2 and B-4 encountered fill soils to depths of 3.5 feet and 8 feet, respectively. The fill soils were underlain by natural soils consisting of sandy silt, silt and clay, and silty clay. Borings B-2 and B-4 encountered auger refusal at depth of 13.5 feet and 24 feet, respectively. Then, the borings were cored to depths of 28.5 feet and 40 feet, respectively.

The bedrock encountered in the borings consists of soft to medium gray shale interbedded with hard gray limestone. The limestone interbeds are typically less than 1 foot thick. The gray shale is slightly weathered to decomposed, weakly calcareous, and very thinly laminated. It is broken to very broken, becoming massive near the completion depths of the borings. The lateral load test drilled shafts were fully constructed in the gray shale interbedded with limestone after excavation at the site.

One direct shear test was performed on a representative sample of the gray shale obtained from boring B-4. The residual angle of internal friction of 24° was obtained by shearing the sample along a bedding plane. Another sample of the massive gray shale from boring B-4 was subjected to an unconfined compression test and was found to have an unconfined compressive strength of 5668 psi. The elastic modulus of the gray shale is 590 ksi based on the unconfined compression test results. The possible lowest and largest RMR₈₉ ratings of the bedrock at the test site are estimated based on the rock properties

presented in Fig. 3-1. These ratings are shown in Table 3-1. The GSI values in the table were obtained by correlations with RMR_{89} using the equation $GSI = RMR_{89} - 5$ and by setting the water rating as 15.

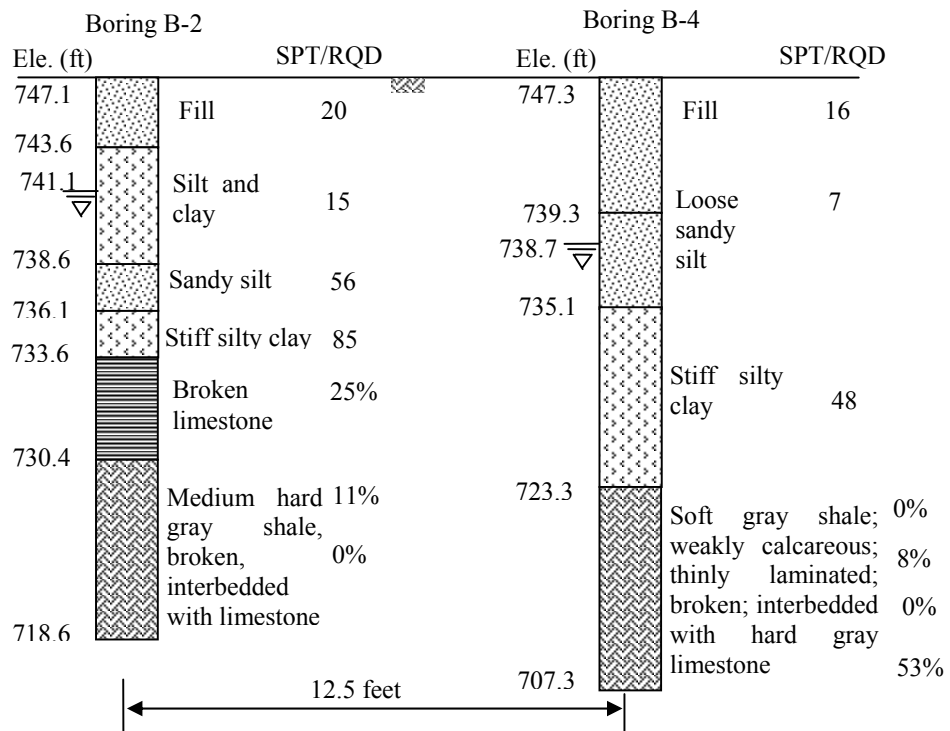


Figure 3-1 Soil and rock layer profiles at Dayton test site

Table 3-1 RMR Ratings and GSI Values of Rock at Dayton Test Site

Elevations (ft)	(2)	(3)	(4)	(5)	(6)	RMR ₈₉			GSI		
						Min.	Max.	Mean	Min.	Max.	Mean
721-728	4	3 - 5	5 - 15	5 - 20	0	17	44	30.5	27	54	40.5
728-739	4 - 7	13	5 - 15	20 - 25	0	42	60	51	52	70	61
(2): Strength rating; (3): RQD rating; (4): Spacing rating; (5): Discontinuity rating; (6): Ground water rating											

3.1.2 Test Setup and Procedure

Two 6 feet diameter drilled shafts were constructed and tested under lateral loads at Dayton site. The shaft was reinforced with 36 #11 primary and #6 spiral bars. The test site was excavated to the depth so that the two drilled shafts were fully constructed in shale without any overlying soils. The elevation of the top of the drilled shafts and the excavated ground surface was 721 feet. The embedment length of the two drilled shafts was 18 feet. The center-to-center distance between two test shafts is 18 feet. Fig. 3-2 shows the layout of the two test shafts. The 28-day compressive strength of concrete was around 4500 psi.

Both drilled shafts were instrumented with inclinometers for measuring the deflection of the shaft with depth and dial gages for measuring the deflection at shaft head. In total, three and two dial gages were installed for measuring the deflections at the top of shaft #4 and shaft #3, respectively. The shaft #4 was instrumented with 10 vibrating wire strain gages along the depth of shaft for monitoring the rebar strains. The strain reading will be used to determine the shaft moments and soil reactions at each gage elevation. A CR10X Campbell Scientific Data Logger was used to collect strain gage readings during lateral loading. The gages were placed at a depth interval of either 2 feet or 3 feet, as shown in Fig. 3-2.

The lateral load was applied by pushing the two drilled shafts apart via a jack and reaction beam placed between them. A load cell was installed between shaft #4 and the jack to measure the actual applied lateral loads. The loading sequence consisted of applying the lateral load in increments of 50 kips or 100 kips, followed by an unloading. The maximum load was 1126 kips. Each load was held until the rate of deflection at the

top of shaft was less than 0.04 inch/min and the inclinometer reading of each shaft was taken.

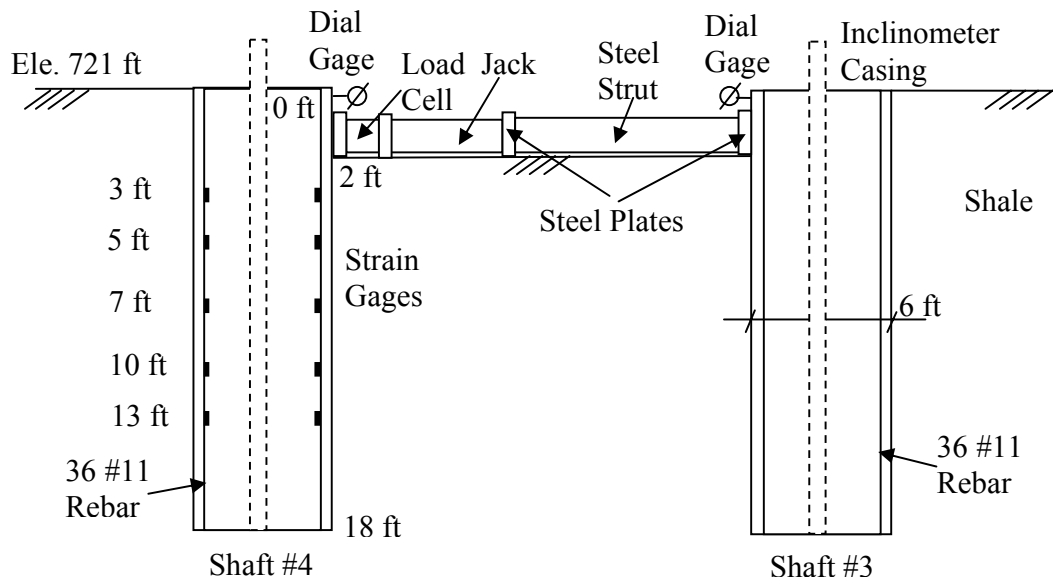


Figure 3-2 Instrumentation of load test at Dayton

3.1.3 Lateral Load Test Results

The measured lateral load test results include the two load-deflection curves at the top of the two shafts, deflection versus depth profiles measured from inclinometers at each load level, and strain gage readings at each load level.

3.1.3.1 Load-Deflection Curves at Shaft Top

Fig. 3-3 presents the load-deflection response measured at the top of each shaft during incremental lateral loading. The deflections were averaged from the three dial gage readings for shaft #4 and two dial gage readings for shaft #3 at each loading level. The relatively similar response of the two shafts indicates the spatial homogeneity of the rock mass. It can be seen that the load-deflection curve behaves nonlinearly even at small deflections due to nonlinear response of weak rock masses. There was one cycle of lateral

load due to the loss of jacking pressure and back up at the load level of 700 kips. This resulted in a sudden increase of deflections of both shafts. It can be concluded that the cyclic loading would increase the lateral deflections. After unloading, both shafts registered 0.05 inch of permanent deflection at the top of shaft.

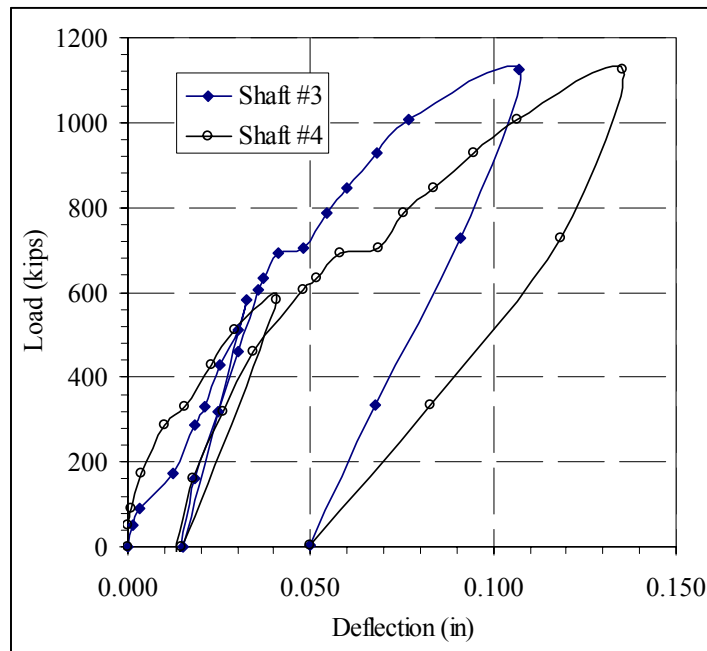


Figure 3-3 Load-deflection curves at the top of shafts

3.1.3.2 Deflection Profiles

The deflection versus depth profiles of shaft #3 and shaft #4 deduced from inclinometer readings by assuming the deflection at the bottom of the inclinometer tube as zero are presented in Figs. 3-4 and 3-5, respectively. Lateral deflections were mobilized on most part of the two shafts along depth under lateral loads. Both shafts behaved like an intermediate shaft between a rigid shaft which exhibits linear displacement profile along the shaft length and a flexible shaft which displays fixity in the lower portion of the shaft. For some loading levels, the inclinometer readings are

considered to be unreasonable. For example, the deflections at the load of 173 kips were less than the deflections at the load of 93 kips as shown in Fig. 3-4.

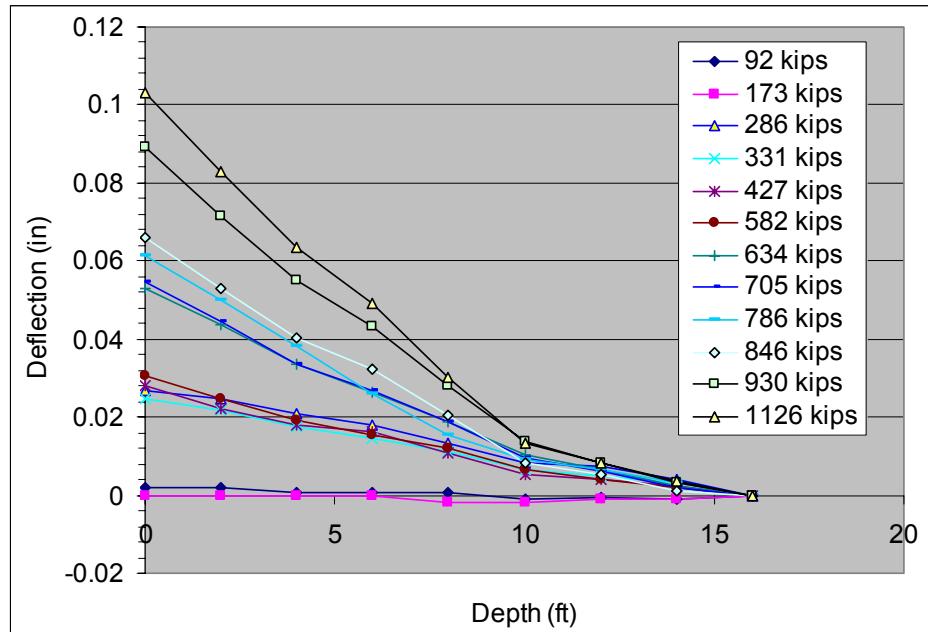


Figure 3-4 Deflection-depth curves of shaft #3

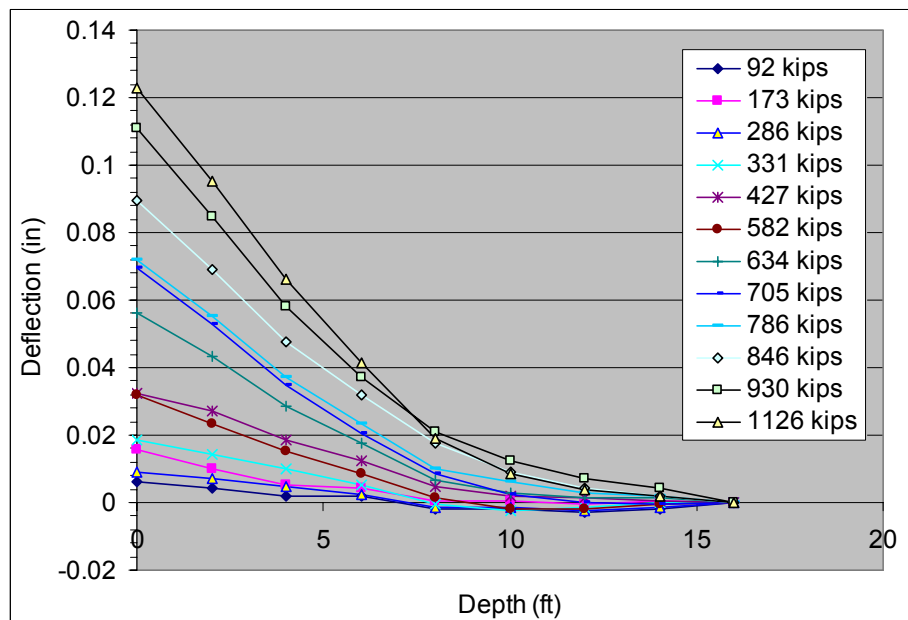


Figure 3-5 Deflection-depth curves of shaft #4

3.1.3.3 Strain Profiles

The strain readings were recorded by a data logger connected to a laptop. The compression strain and tension strain profiles of shaft #3 and shaft #4 under various loading levels are presented in Fig. 3-6 and 3-7, respectively. When the load was increased from 510 kips to 582 kips, a sudden increase of tension strain at the depth of 8 feet was noticed, as shown in Fig. 3-7. This could be due to concrete cracking in the shaft.

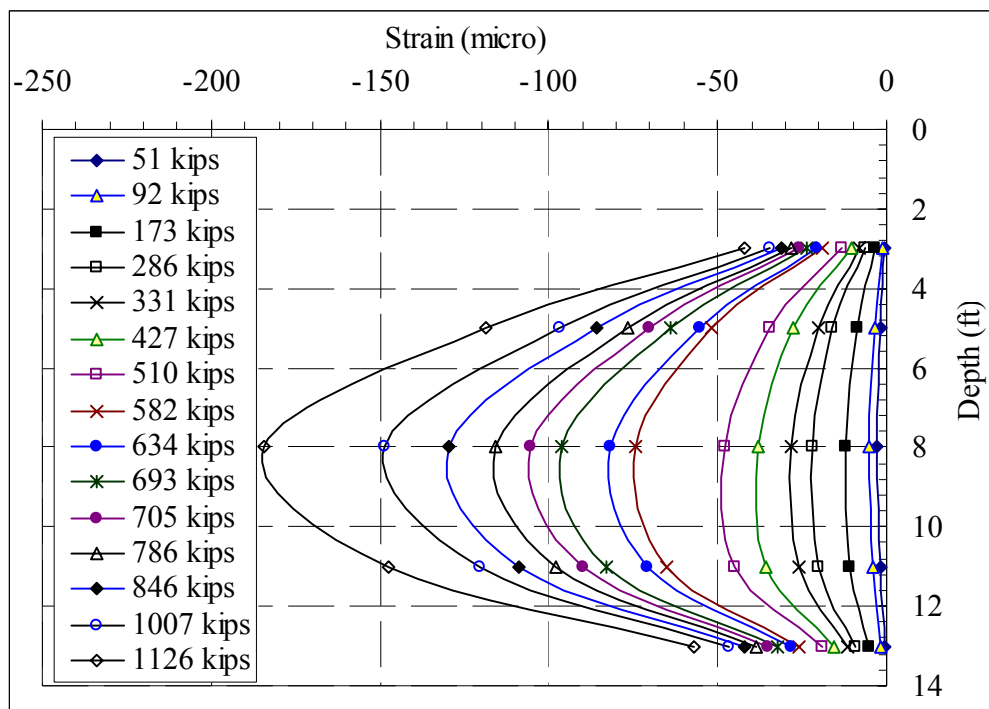


Figure 3-6 Compression strain profiles of shaft #4

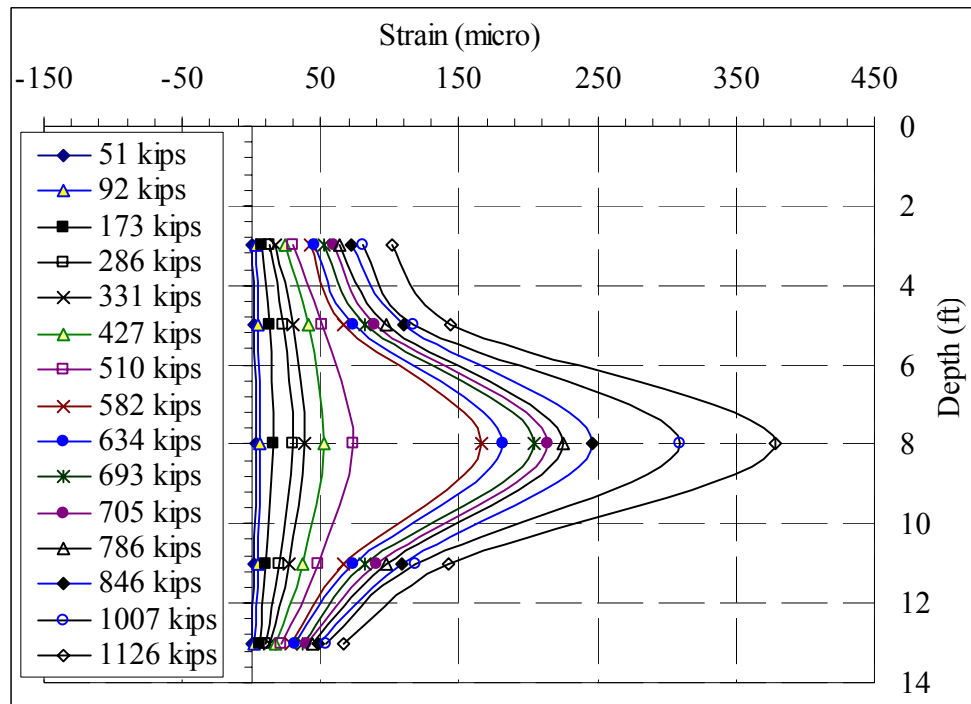


Figure 3-7 Tension strain profiles of shaft #4

3.2 Lateral Load Test at Pomeroy-Mason

3.2.1 Test Site

The Ohio Department of Transportation (ODOT), together with the West Virginia Department of Transportation (WVDOT) and the Federal Highway Administration (FHWA) worked on design and construction of a replacement bridge for the U.S. Route 33 Bridge over the Ohio River between Pomeroy, Ohio and Mason, West Virginia. The new structure will be a three-span cable-stay bridge with a reinforced concrete superstructure and substructure. The cable stay towers are to be supported by groups of drilled shafts. Considering the large wind load and possible ship impact on the bridge piers, the lateral loads will be one of the key design loads for the bridge deep foundation.

Due to lack of competent design methods available for analyzing laterally loaded drilled shafts in rock, a lateral load test was carried out on two drilled shafts constructed for the West Virginia cable stay tower.

Two Borings S-9 and S-10 near the test drilled shafts were advanced from a floating platform at the Station 29+95.5, 24 feet right and Station 30+18.7, 28.4 feet left, respectively. During soil boring, water surface elevations of 538.0 feet and 537.9 feet were observed, respectively. The water was 28.8 feet deep in S-9 and 28.3 feet deep in S-10.

In Boring S-9, from the river bottom to a depth of 38.9 feet (below the water surface), a layer of coarse and fine sand (A-3a) and fine sand (A-3) was encountered. This layer was described as grayish brown and orangish brown, wet and loose. Water contents varied from 20 to 24 percent and SPT N-values ranged from 4 to 8 blows per foot. Underlying the aforementioned soil in S-9 and at the surface in S-10, gravel with sand (A-1-b) was observed. This material extended to depths of 57.2 and 56.9 feet in Borings S-9 and S-10, respectively. The gravel with sand was described as brown, wet and loose to medium dense. Water contents ranged from 13 to 20 percent and SPT N-values varied from 4 to 16 blows per foot, with an average of 9 blows per foot.

Bedrock was encountered below the soils described above at a depth of 57.2 feet below the water surface in S-9 and at 56.9 feet in S-10. The rock core recovered was described as shale with interbedded siltstone from bedrock surface to depths of 75.9 and 73.6 feet below the water surface in S-9 and S-10, respectively. Shale (mudstone) was observed in S-9 from 75.9 to 102.9 feet and in S-10 from 73.6 to 103.7 feet below the water surface. Siltstone was recovered underlying the shale to a depth of 123.3 and 118.4

feet below the water surface in S-9 and S-10, respectively. The borings were terminated at these depths. The weathered rock zone was observed in the uppermost 3 feet below the rock surface, approximately. The rock core samples were used for unconfined compression tests. The details of Borings S-9 and S-10 are provided in Fig. 3-8 and 3-9, respectively.

The possible highest and lowest RMR_{89} ratings are estimated based on the rock properties indicated in Fig. 3-8 and 3-9. They are summarized in Tables 3-2 and 3-3 for S-9 and S-10, respectively. The top elevations of the rock are adjusted according to the drilling observations during the construction of drilled shafts. The GSI values correlated from RMR_{89} using the equation $GSI = RMR_{89} - 5$ and by setting the water rating as 15 are also provided in Tables 3-2 and 3-3.

Table 3-2 RMR Ratings and GSI Values of Rock Based on Boring S-9

Elevations (ft)	(2)	(3)	(4)	(5)	(6)	RMR ₈₉			GSI		
						Min.	Max.	Mean	Min.	Max.	Mean
490.8 – 469	4	8	5	10-20	0	27	37	32	37	47	42
469 – 461.4	7	8	5	10-20	0	30	40	35	40	50	45
461.4-453.5	0	13	5	10	0	28	28	28	38	38	38
453.5-442.8	0	3	5	10	0	18	18	18	28	28	28
442.8-434	2	17	5	10	0	34	34	34	44	44	44
(2): Strength rating; (3): RQD rating; (4): Spacing rating; (5): Discontinuity rating; (6): Ground water rating											

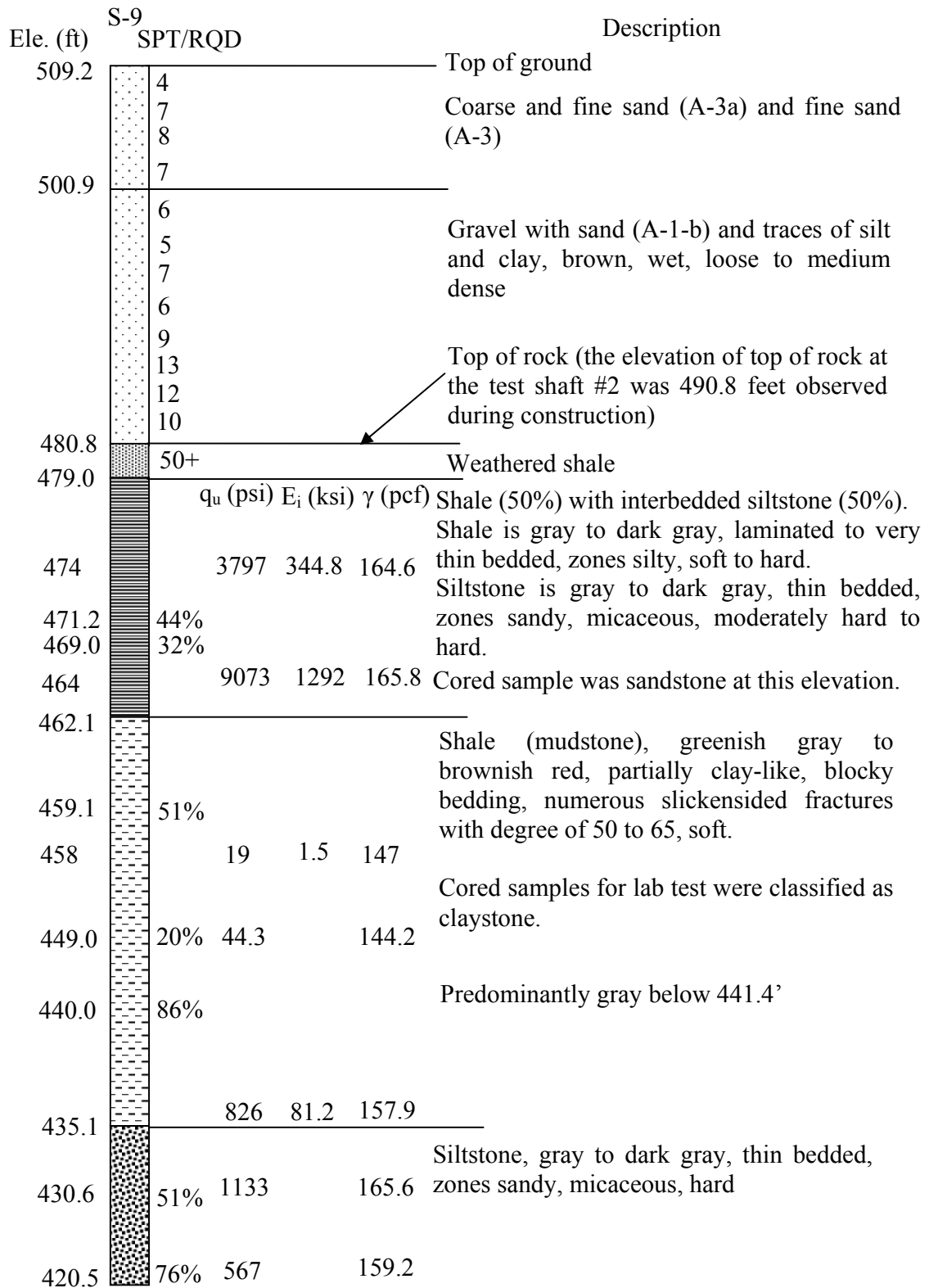


Figure 3-8 Boring S-9
60

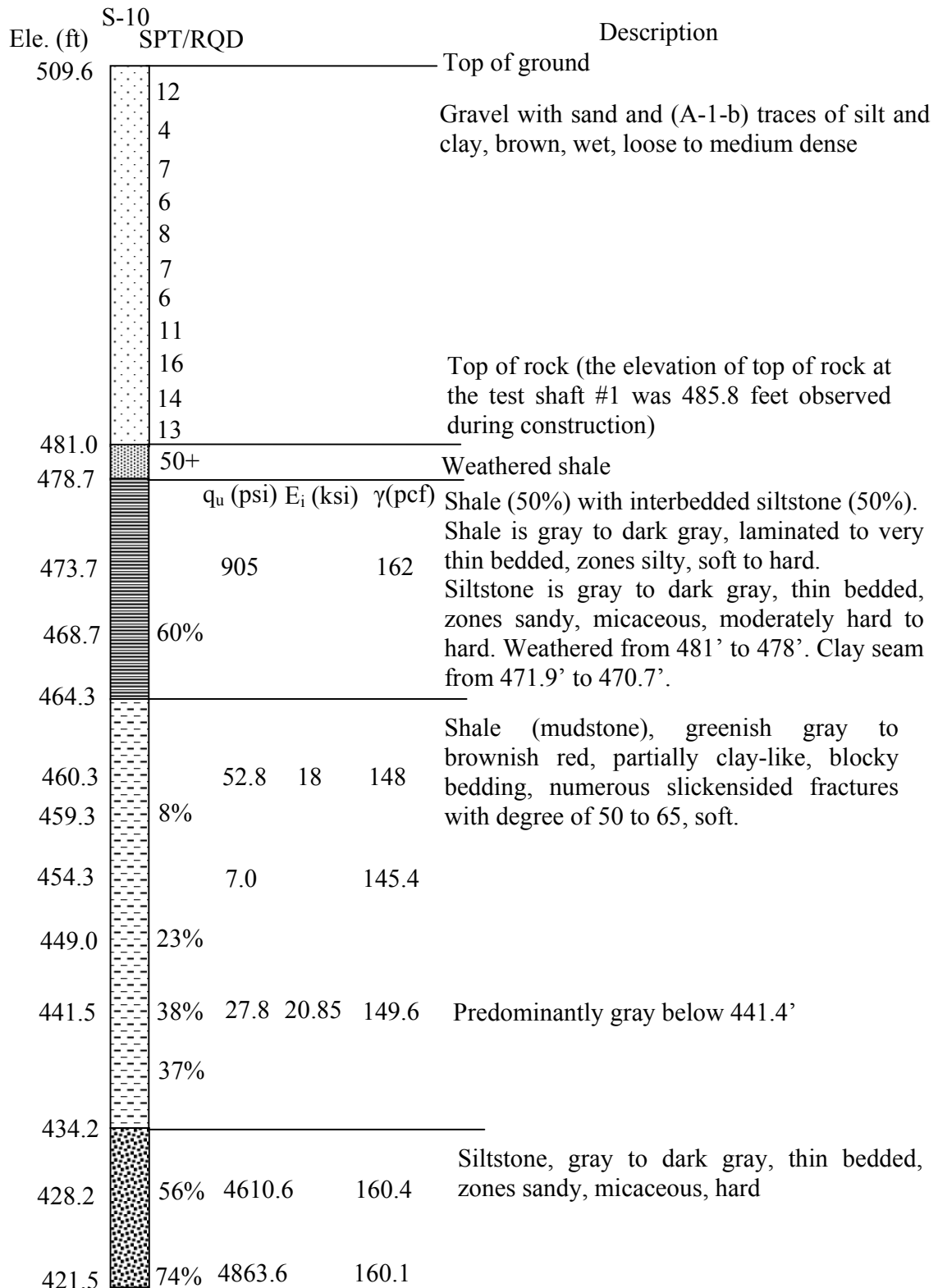


Figure 3-9 Boring S-10

Table 3-3 RMR Ratings and GSI Values of Rock Based on Boring S-10

Elevations (ft)	(2)	(3)	(4)	(5)	(6)	RMR ₈₉			GSI		
						Min.	Max.	Mean	Min.	Max.	Mean
485.8-464.3	2	13	5	10-20	0	30	40	35	40	50	45
464.3-457.3	0	3	5	10	0	18	18	18	28	28	28
457.3-447.9	0	3	5	10	0	18	18	18	28	28	28
447.9-445.8	0	8	5	10	0	23	23	23	33	33	33
(2): Strength rating; (3): RQD rating; (4): Spacing rating; (5): Discontinuity rating; (6): Ground water rating											

3.2.2 Test Set-up and Test Procedure

The test drilled shaft #1 was constructed at Station 29+00 offset 33'-1" left; and the test drilled shaft #2 was located at Station 29+00 offset 38'-8" right. Therefore, the Boring S-9 is closer to the test drilled shaft #2 and the Boring S-10 is closer to the test drilled shaft #1. Due to the variability of the site, the top elevations of bedrock at the test drilled shaft #1 and shaft #2 were observed as 485.8 feet and 490.8 feet during construction, respectively. The elevation of ground surface of shaft #1 was 511.8 feet. The total length of the test drilled shaft #1 and shaft #2 was 101.4 feet and 112.9 feet, respectively. Rock socket length was 40 feet and 56.8 feet, respectively. The distance between the top of the two test drilled shafts and the loading point during test was 3 feet. The thickness of the soil layers at test drilled shaft #1 and shaft #2 was 26 feet and 18.8 feet.

The unconfined compressive strength of concrete was 5115 psi. The diameter of the drilled shaft socketed in bedrock was 8 feet. The reinforcement of the rock-socket portion was 28 #18 bars and the cover was 4 inch. The portion of the two drilled shafts above the bedrock has a diameter of 8.5 feet with a 1 inch thickness of casing and 28 #18 bars. The equivalent modulus of drilled shafts in rock is 4250 ksi. To fully mobilize the rock-shaft interaction and isolate the overburden soils, an 11 feet diameter casing was used to form a gap between the test drilled shaft #2 and the soils above bedrock. This means all the lateral forces were resisted by the bedrock during the lateral load test.

Both drilled shafts were instrumented with inclinometers for measuring the deflection along shaft length and dial gages for measuring the deflection at loading point. Two dial gages were installed for each test drilled shaft. The test drilled shaft #1 and #2 was instrumented with 13 and 10 levels of vibrating wire strain gages along the shaft length for monitoring the rebar strains. Two CR10X Campbell Scientific Data Loggers were used to collect strain gage readings during test. The details of the instrumentation are provided in Fig. 3-10.

The testing loads were applied by tensioning a tendon connecting the two drilled shafts. The two shafts move toward each other during test. A load cell was installed between shaft #1 and the jack to measure the actual applied lateral loads. The maximum load applied was 275 kips. Each load increment was held until the deflection at the top of shafts was stable and the inclinometer reading of each drilled shaft was taken.

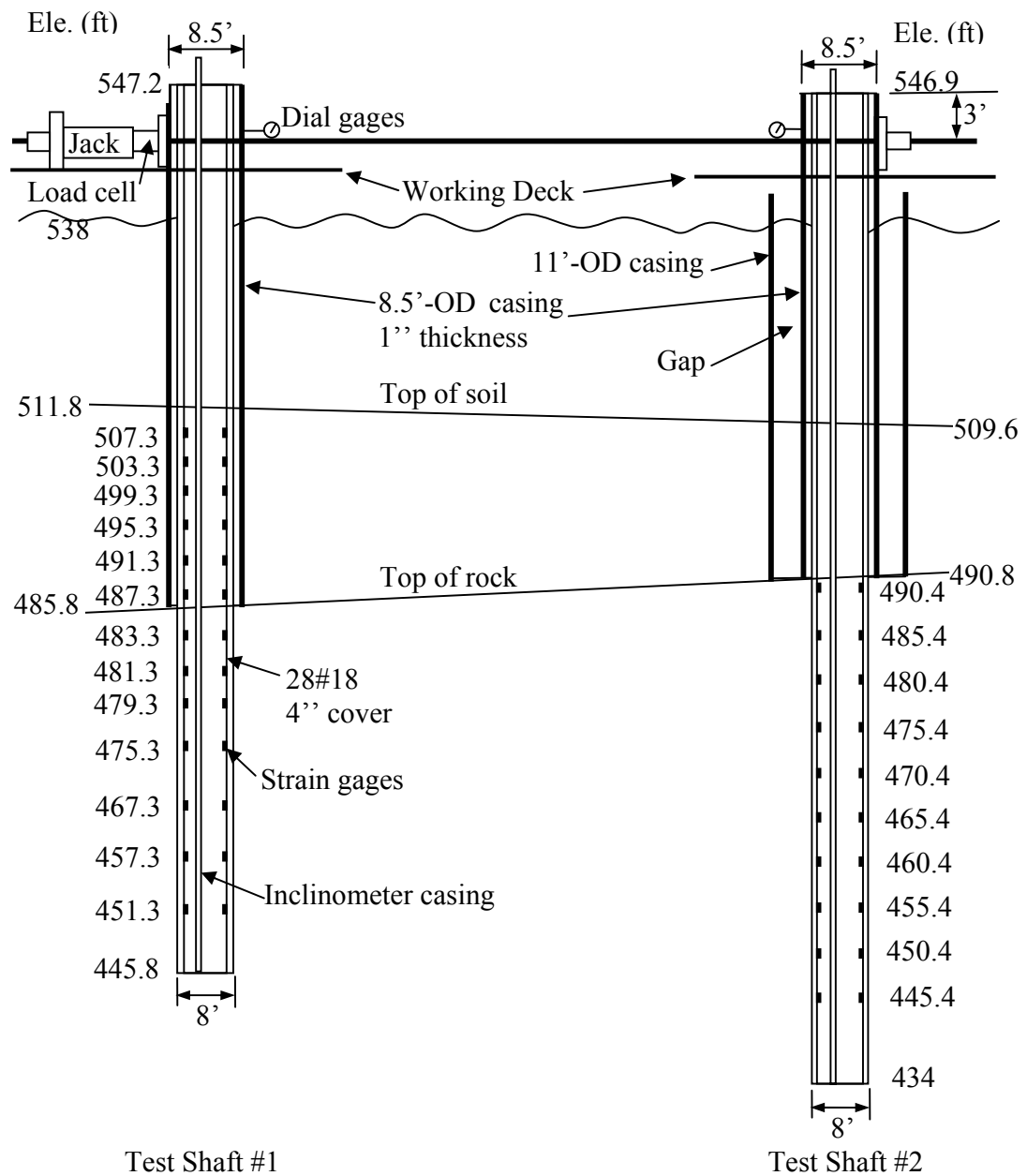


Figure 3-10 Instrumentation and load test setup

3.2.3 Lateral Load Test Results

The measured data during lateral load test on the two drilled shafts include load-deflection curves at the loading point, deflection versus depth profiles measured from inclinometers, and strain gage readings along shaft length.

Fig. 3-11 presents the load-deflection response measured at the loading point during incremental lateral loading. The deflections were taken as an average of the two dial gage readings for each shaft at each loading level. It can be seen that the deflections at the loading point of shaft #2 is much larger than those of shaft #1 due to the use of casing in shaft #2 for isolation of soils. The maximum deflections at the 275 kips load level of shaft #1 and shaft #2 are 1.725 inch and 3.73 inch, respectively.

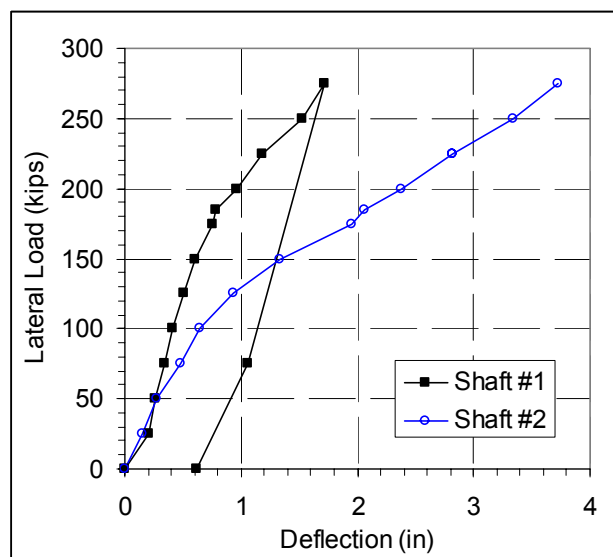


Figure 3-11 Measured load-deflection curves at loading point of Pomeroy-Mason test

The deflection profiles of test shaft #1 and shaft #2 along shaft length, deduced from inclinometer readings by assuming that the deflection at the bottom of the inclinometer tube was zero, are presented in Fig. 3-12 and 3-13, respectively. From Fig. 3-12, it can be seen that the deflection at the bedrock elevation is very small. This means that most of applied lateral load was resisted by the soils for shaft #1. However, for shaft #2, the lateral loads were resisted by the rock due to the use of casing to isolate soil reactions.

The strain readings were recorded by a data logger connected to a laptop during test. The compression strain and tension strain profiles of shaft #1 under various loading

levels are presented in Figs. 3-14 and 3-15, respectively. The depth shown in figure starts from the top of the drilled shafts. When the load was increased from 175 kips to 200 kips, a sudden increase of tension strain at the depth of 56 feet was noticed. The maximum tension strain was recorded as 938 micros. This could be due to concrete cracking in the shaft, as sound of concrete cracking was clearly audible during test at this load increment. The tension and compression strain profiles of test shaft #2 are provided in Figs. 3-16 and 3-17, respectively. Similarly, a sudden increase of tension strain accompanying a cracking sound was observed at the loading level of 175 kips, as shown in Fig. 3-16.

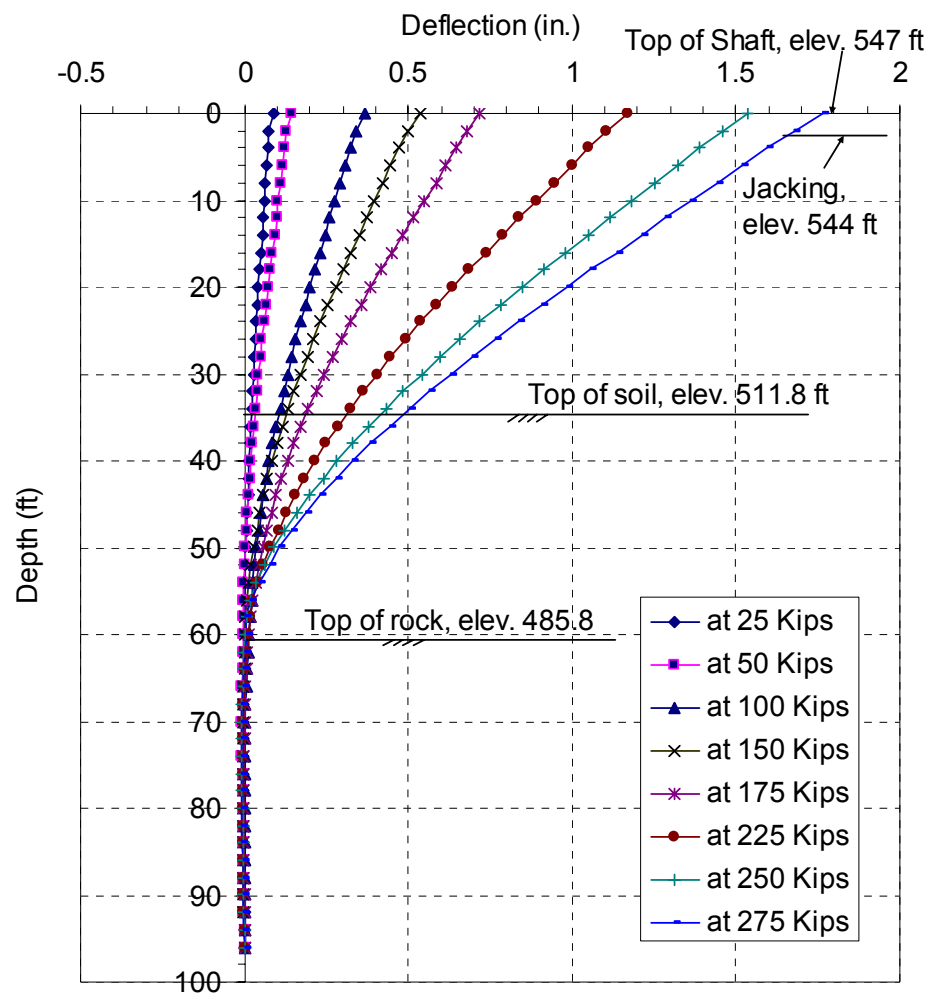


Figure 3-12 Deflection-depth profiles of drilled shaft #1 at Pomeroy-Mason test

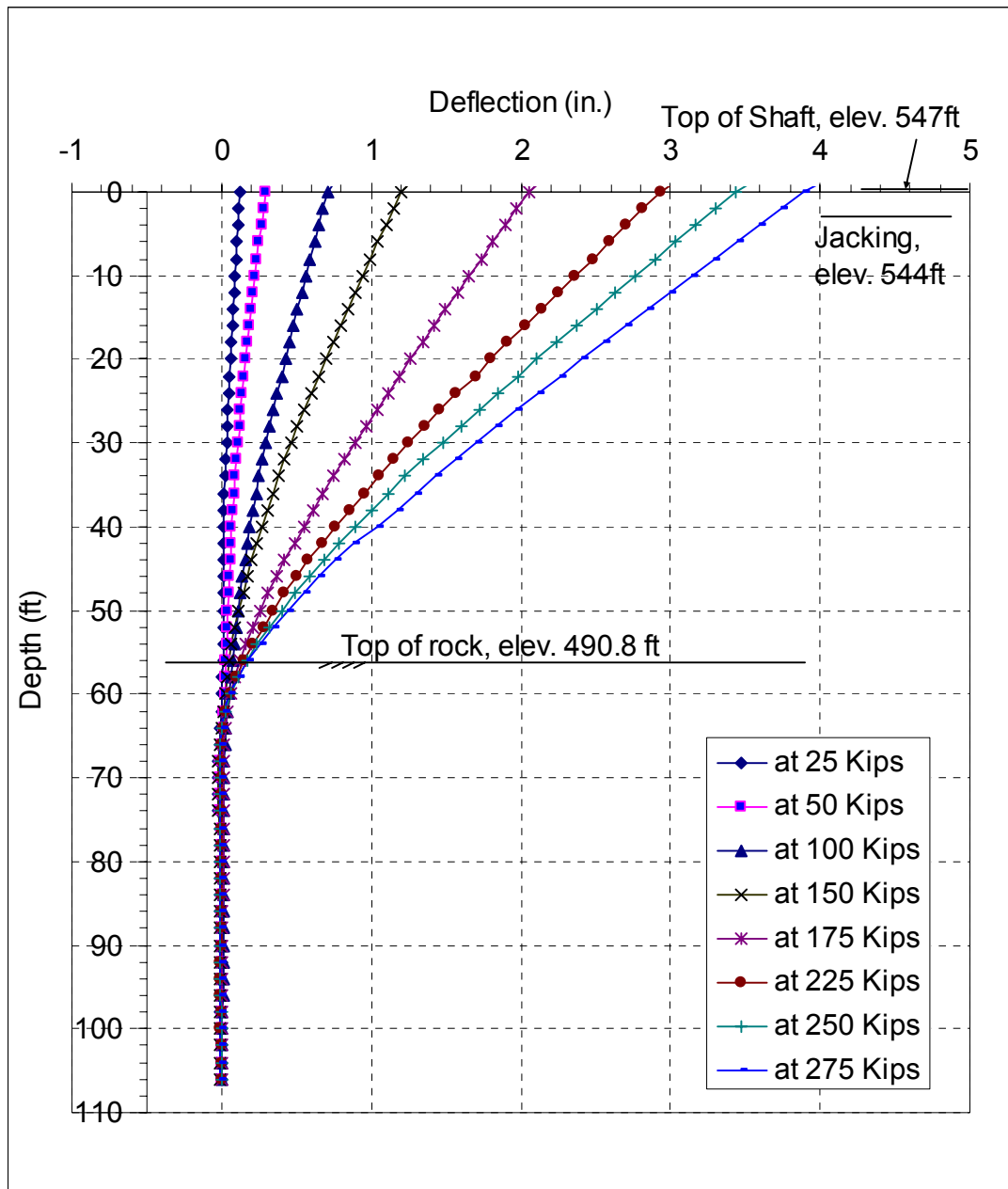


Figure 3-13 Deflection-depth profiles of drilled shaft #2 at Pomeroy-Mason test

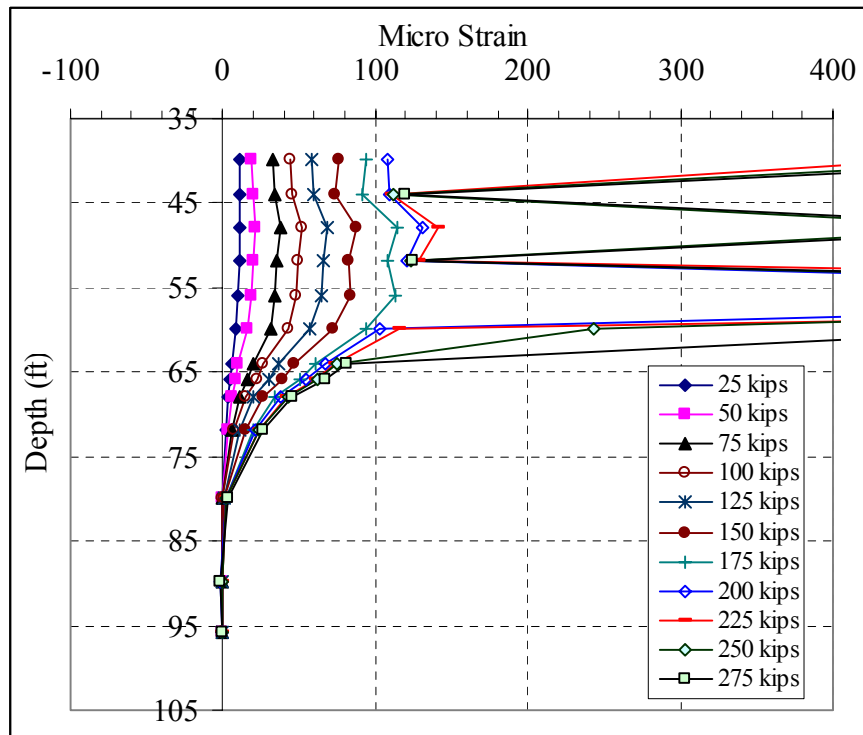


Figure 3-14 Tension strain profiles of test shaft #1 of Pomeroy-Mason test

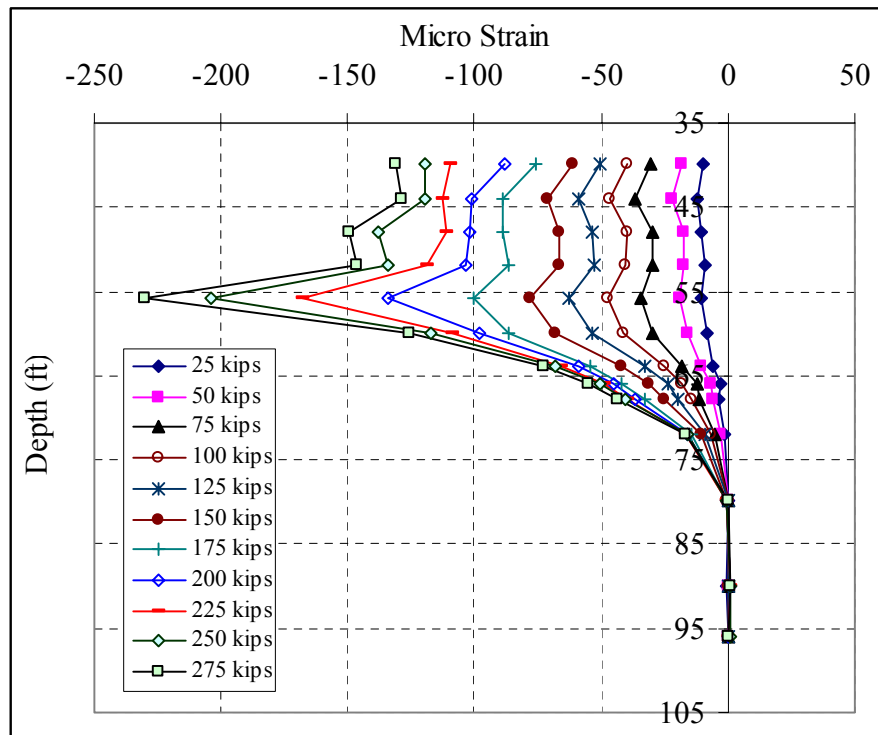


Figure 3-15 Compression strain profiles of test shaft #1 of Pomeroy-Mason test

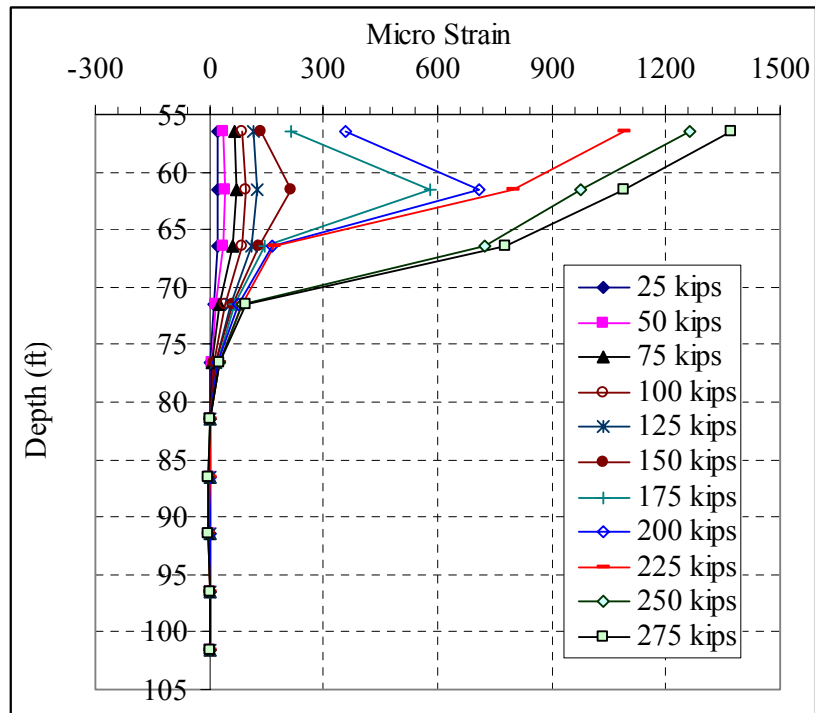


Figure 3-16 Tension strain profiles of test shaft #2 of Pomeroy-Mason test

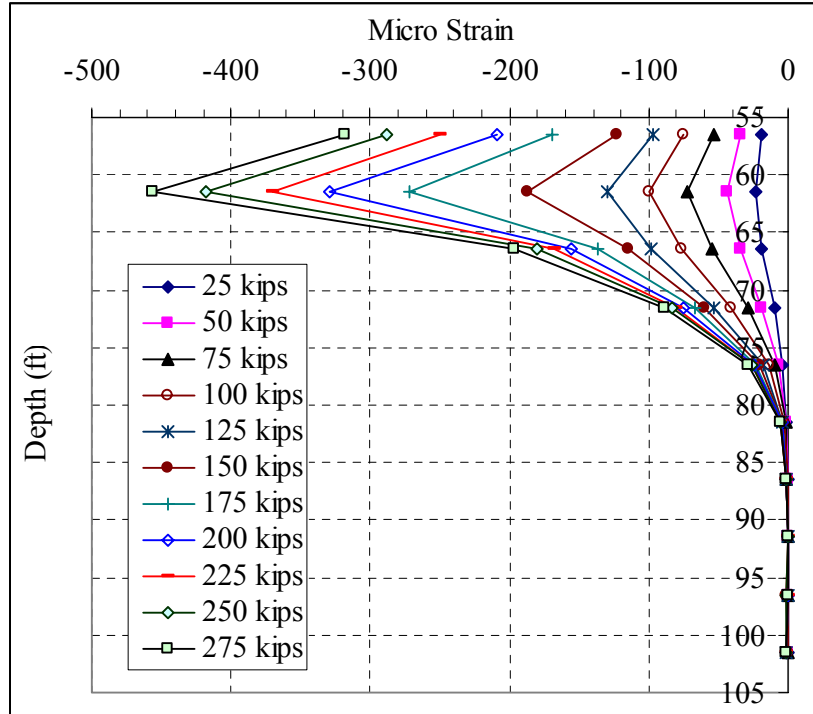


Figure 3-17 Compression strain profiles of test shaft #2 of Pomeroy-Mason test

3.3 Methods for Deriving P-y Curves From Lateral Load Test Results

3.3.1 Introduction

Site specific p-y curves derived from instrumented lateral load tests are necessary for a situation when the site geological condition may differ from those that were used to derive existing p-y criteria.

Derivations of p-y curves using strain gage readings from fully instrumented lateral load tests usually involve three steps: deriving deflection versus depth profile using double integrating technique on the curvature versus depth profile of a drilled shaft from strain data; determining the moment versus depth profile based on curvature versus depth profile; and finally deriving p, soil resistance per unit length of a shaft, using double differentiating technique on the moment versus depth profile. Mathematically, these three steps can be written as follows.

$$y = \int (\int \phi dz) dz \quad (3-1)$$

$$M = EI\phi \quad (3-2)$$

$$p = -\frac{d^2 M}{dz^2} \quad (3-3)$$

where y is deflections along depth of a drilled shaft; p is net soil resistance per unit length of the drilled shaft; M is shaft moment at depth z; EI is section modulus of the shaft, ϕ is the curvature of the shaft, which can be obtained as the difference between compression and tension strains measured at the same depth of the shaft divided by the distance between these two strain gages.

Mathematically, double integration of discrete data points (curvature data points) with respect to depth generally would not introduce significant numerical inaccuracy.

However, double differentiation of discrete curvature data points would generally result in amplification of measurement errors and consequently inaccurate p . Therefore, several techniques have been proposed to minimize numerical errors due to double differentiation, such as high order global polynomial curve fitting (Reese and Welch, 1975), piecewise polynomial curve fitting (Matlock and Ripperger 1956), cubic spline (Dou and Byrne, 1996), weighted residuals method (Wilson, 1998), and smoothed weighted residuals method (Yang, et al. 2005). However, these methods for deriving p - y curves from strain data have not been systematically compared and evaluated. In fact, there is a lack of guidance for best method in deducing p - y curves based on strain data obtained from load tests.

In this section, the existing methods for deriving p - y curves are summarized. Eight field lateral load tests on instrumented drilled shafts in soils and/or rocks are compiled to evaluate these methods. Comparisons of load-deflection curves of drilled shafts between measured values and predicted values based on those derived experimental p - y curves using various existing methods are performed. Additionally, four hypothetical cases based on assumed p - y curves from existing p - y criteria (Matlock, 1970; Reese and Welch, 1975; et al.) and known moment profiles from COM624P (Wang and Reese, 1993) are used to further evaluate these derivation methods by comparing deduced experimental p - y curves with those assumed p - y curves. It is found that piecewise polynomial curve fitting technique provides the most accurate p - y curves.

A procedure for determining an optimum strain gage spacing for planning instrumentation of a lateral load test is suggested. Additionally, a parametric study shows

that the errors of those derived p-y curves are mainly due to inaccurate determination of moment profiles from strain gage readings.

3.3.2 Method for Deriving Deflection from Strain Gage Readings

The lateral displacements of a drilled shaft along depth at each lateral load can be deduced from strain gage readings by using Eq. (3-1). The displacements from inclinometer readings are not directly used, because it was found from experiences that some inclinometers tend to provide smaller deflections of a shaft under larger lateral loads. However, the inclinometer readings could be used as an independent check on the accuracy of the deflections deduced from strain gage readings.

The 5th order polynomial function given in Eq. (3-4) has been successfully used by Wilson (1998) to fit the discrete strain points. This technique, therefore, is adopted herein to fit discrete curvature data points along shaft depth using the least-square method.

$$\phi = a + bz + cz^{2.5} + dz^3 + ez^4 + fz^5 \quad (3-4)$$

where a, b, c, d, e, f are curve fitting constants.

The deflections can be obtained by double integrating the above fitted curvature versus depth profile. Two boundary conditions are required to determine two integrating constants involved in the double integration. Based on the evaluation (to be discussed later), it is found that the boundary combination ($y_0, y_{tip}=0$) for a long pile (ratio of shaft length over diameter, $L/D \geq 10$, according to Boghrat, 1990) and the combination ($y_0, y_{fixity}=0$) for a short pile ($L/D < 10$) would provide the best deduced deflections by comparing with inclinometer readings. Additionally, combination (y_0, θ_0) can be used for a short drilled shaft when combination ($y_0, y_{fixity}=0$) is not available. The meanings of these boundary conditions are as follows: y_0 is the measured deflection at the ground line;

θ_0 is the measured shaft tilt at the ground line; $y_{tip}=0$ means the deflection at the tip of a drilled shaft is assumed to be zero; $y_{fixity}=0$ means that deflection is set to zero at a fixity point where the deflection of the shaft is close to zero according to the inclinometer readings.

The problems associated other combinations are observed during the evaluation as follows. Combination ($y_{tip}=0$, $\theta_{tip}=0$) may result in deflections at the ground line to be different from the measured shaft deflections. Combination (y_0 , $y_{fixity}=0$) may result in large negative deflections at the tip of a long drilled shaft, which is deemed unreasonable. Combination (y_0 , θ_0) provides none zero deflections at the tip of a long drilled shaft which may affect accuracy of shaft-head slope measurement. A similar conclusion was reported by Dunnavant (1986). However, combination (y_0 , θ_0) can be used for a short drilled shaft when a fixity point is not known.

3.3.3 Determination of Moment Profiles

The nonlinearity of shaft stiffness is usually represented by $M-\phi$ relationship, which can be inferred from field data by comparing measured values of ϕ to known values of M at various loading levels, as was done by Reese and Welch (1975). When a lateral load test is performed with a large loading eccentricity (distance between the loading point and ground line), a pair of strain gages can be mounted at the ground line level to obtain a representative $M-\phi$ relationship of the shaft.

Although it is preferred to use field measured moment-curvature relationship; nevertheless, it may not always available. In this case, the relationship between M and ϕ can be obtained from theory of reinforced concrete, where stress-strain curves for both

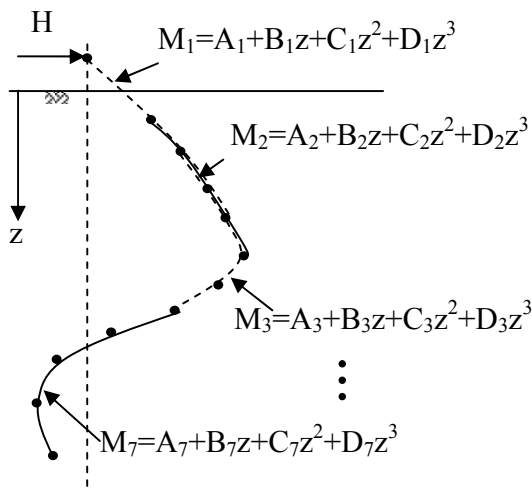
reinforcing steels and concrete or predefined stress-strain models are used to compute $M-\phi$ curves (Wang and Reese, 1993).

3.3.4 Methods for Deriving P (Net Resistance)

3.3.4.1 Piecewise Polynomial Curve Fitting

Both Matlock and Ripperger (1956) and Dunnavant (1986) have used piecewise cubic polynomial function to fit discrete moment data. The procedure described by Dunnavant (1986) is presented in Fig. 3-18, where piecewise cubic polynomial with a window of 5 points is employed to fit measured moment data using the least-square technique. That is every 5 successive moment data points along the shaft length are fitted to one cubic polynomial curve. The double differentiation of the local fitted polynomial curve with respect to the middle point yields p (the unit reaction of soil) at that point. The p of upper three points and bottom three points is obtained from the smoothed local cubic polynomial moment curve using the top five points and bottom five points, respectively.

The zero moment at the loading point or a known value of moment at the ground line should also be included in the moment profiles. The piecewise polynomial curve fitting is a local curve fitting technique, which avoids the requirement to capture the global trend of scattered data in global polynomial curve fitting approach. However, this method requires minimum of five discrete data points along shaft length.



- (1) Least-square technique is used to fit cubic polynomials to groups of give contiguous moment values.
- (2) The first polynomial, M_1 , is differentiated twice to evaluate p at the 3 moment levels closest to the surface (including the loading level). Other polynomials, such as M_2 , are used to evaluate p at the group center point. The polynomial for the five

Figure 3-18 Procedure for reducing moment data to p using piecewise polynomial (after Dunnavant, 1986)

3.3.4.2 High Order Global Polynomial Curve Fitting

Single high order polynomials have been used to fit moment profiles by Reese and Welch (1975) and Wilson (1998). According to Wilson (1998), a five order polynomial with an exponent of 2.5 rather than 2 on the quadratic term using least-square technique, as shown in Eq. (3-5), provided the most reasonable p profiles. The non-integer form of polynomial will yield a zero soil resistance at the ground surface assuming depth z is zero at the ground surface. The value of p can then be obtained by double differentiating Eq. (3-5) with respect to z .

$$M = a + bz + cz^{2.5} + dz^3 + ez^4 + fz^5 \quad (3-5)$$

The advantage of the method is its simplicity of application. However, the technique is applicable only if the trend of moment profile can be captured, especially the moment data points near the ground surface.

3.3.4.3 Weighted Residuals Method

Weighted residuals (WR) method was introduced to derive p from moment profiles by Wilson (1998). The WR method is not a curve fitting technique; rather it is a numerical differentiation method based on minimizing weighted residuals, as is often used in finite element method. The main idea of WR method is to find an approximate function $a(z)$ to represent the actual function $u(z)$ over some interval $z=0$ to $z=L$. Generally, $u(z) \neq a(z)$, and the difference can be defined as $a(z)-u(z)=R(z)$, the residual. While $R(z)$ may not be zero anywhere in the range of z , $a(z)$ can be selected such that $R(z)$ is zero in an average sense by enforcing the following condition.

$$\int_0^L R(z)\Psi(z)dz = 0 \quad (3-6)$$

where $\psi(z)$ is a weighting function. This is commonly referred to as saying $u(z) = a(z)$ “weakly”.

WR method is used to obtain shear force profiles by differentiating the moment profiles one time. Then, another differentiation on the derived shear force profiles using WR method results in the soil/rock reaction profiles, $p(z)$. As described by Wilson (1998), the shaft can be considered as discretized finite elements with nodes at each location with measured bending moment value. If $f(z)$ represents the actual bending moment distribution of the shaft as a function of depth, then $f(z)$ is known at the nodes. Then, the shear force $g(z)$ as the first derivative of the bending moment distribution is defined as:

$$g(z) = \frac{df(z)}{dz} = f'(z) \quad (3-7)$$

If $g(z)=f'(z)$ “weakly”, then

$$\int_0^L \{g(z) - f'(z)\} \Psi(z) dz = 0 \quad (3-8)$$

where $\psi(z)$ is a weighting function. Both $f(z)$ and $g(z)$ are written as linear combinations of shape functions of finite element type, e.g. linear “hat” functions as shown in Fig. 3-19.

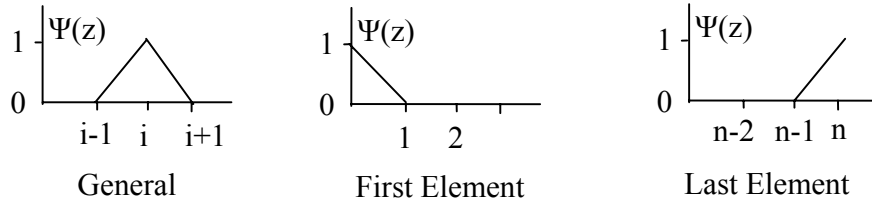


Figure 3-19 Linear shape functions

For each node along the shaft, weighting function $\psi(z)$ is taken to be the shape function to generate a system of linear equations for the coefficients of $f(z)$ and $g(z)$. This can be written as:

$$f(z) = \sum_{i=0}^n f_i \Psi_i(z), \text{ and} \quad (3-9)$$

$$g(z) = \sum_{i=0}^n g_i \Psi_i(z) \quad (3-10)$$

where i is the node number and ranges from 0 to n ; f_i is the measured moment; z is the depth along the shaft; and $\psi(z)$ is the shape function for node i . Substituting Eqs. (3-9) and (3-10) into Eq. (3-8), Wilson (1998) developed a system of equations that can be used to solve for the values of $g(z)$ at each node. The solution to those equations is provided herein.

The measured moment values inferred from strain gage readings at depth z_i are $f(z_i)$. According to the shape function expressed in Fig. 3-19, the bending moment between adjacent nodes i and $i+1$ can be expressed as follows:

$$f(z) = f(z_i) \frac{z_{i+1} - z}{z_{i+1} - z_i} + f(z_{i+1}) \frac{z - z_i}{z_{i+1} - z_i} \quad (3-11)$$

Substituting Eqs. (3-9) and (3-10) into Eq. (3-8), one can obtain:

$$\int_0^L \left\{ \sum_{i=0}^n g_i \Psi(z) - \frac{d \sum_{i=0}^n f_i \Psi(z)}{dz} \right\} \Psi(z) dz = 0 \quad (3-12)$$

By expanding Eq. (3-12), the following equation can be obtained for the first element.

$$\int_{z_0}^{z_1} \frac{\{[f(z_1) - f(z_0)] - [(z_1 - z)g(z_0) + (z - z_0)g(z_1)]\}(z_1 - z)}{(z_1 - z_0)^2} dz = 0 \quad (3-13)$$

For the last element, we have:

$$\int_{z_{n-1}}^{z_n} \frac{\{[f(z_n) - f(z_{n-1})] - [(z_n - z)g(z_{n-1}) + (z - z_{n-1})g(z_n)]\}(z - z_{n-1})}{(z_n - z_{n-1})^2} dz = 0 \quad (3-14)$$

Also, for the general elements, the following equation based on Eq. (3-12) can be obtained.

$$\begin{aligned} & \int_{z_{i-1}}^{z_i} \frac{\{[f(z_i) - f(z_{i-1})] - [(z_i - z)g(z_{i-1}) + (z - z_{i-1})g(z_i)]\}(z - z_{i-1})}{(z_i - z_{i-1})^2} dz + \\ & \int_{z_i}^{z_{i+1}} \frac{\{[f(z_{i+1}) - f(z_i)] - [(z_{i+1} - z)g(z_i) + (z - z_i)g(z_{i+1})]\}(z_{i+1} - z)}{(z_{i+1} - z_i)^2} dz = 0 \end{aligned} \quad (3-15)$$

where $f(z_i)$ = measured value of bending moment at node i in the drilled shaft; $g(z_i)$ = shear force at node i ; z_i = the depth of node i .

The Eqs. (3-13) to (3-15) can be rewritten as follows, respectively.

$$\frac{f_1 - f_0}{(z_1 - z_0)^2} \left(\frac{z_1^2}{2} + \frac{z_0^2}{2} - z_0 z_1 \right) - \frac{g_0}{(z_1 - z_0)^2} \frac{(z_1 - z_0)^3}{3} - \frac{g_1}{(z_1 - z_0)^2} \left[\frac{1}{6} (z_1^3 - z_0^3) - \frac{z_0 z_1}{2} (z_1 - z_0) \right] = 0 \quad (3-16)$$

$$\frac{f_n - f_{n-1}}{(z_n - z_{n-1})^2} \left(\frac{z_n^2}{2} + \frac{z_{n-1}^2}{2} - z_{n-1}z_n \right) - \frac{g_{n-1}}{(z_n - z_{n-1})^2} \left[\frac{1}{6} (z_n^3 - z_{n-1}^3) - \frac{z_{n-1}z_n}{2} (z_n - z_{n-1}) \right] - \frac{g_n}{(z_n - z_{n-1})^2} \frac{(z_n - z_{n-1})^3}{3} = 0 \quad (3-17)$$

$$\begin{aligned} & \frac{f_i - f_{i-1}}{(z_i - z_{i-1})^2} \left(\frac{z_i^2}{2} + \frac{z_{i-1}^2}{2} - z_{i-1}z_i \right) - \frac{g_{i-1}}{(z_i - z_{i-1})^2} \left[\frac{1}{6} (z_i^3 - z_{i-1}^3) - \frac{z_{i-1}z_i}{2} (z_i - z_{i-1}) \right] - \\ & \frac{g_i}{(z_i - z_{i-1})^2} \frac{(z_i - z_{i-1})^3}{3} + \frac{f_{i+1} - f_i}{(z_{i+1} - z_i)^2} \left(\frac{z_{i+1}^2}{2} + \frac{z_i^2}{2} - z_i z_{i+1} \right) - \frac{g_i}{(z_{i+1} - z_i)^2} \frac{(z_{i+1} - z_i)^3}{3} - \\ & \frac{g_{i+1}}{(z_{i+1} - z_i)^2} \left[\frac{1}{6} (z_{i+1}^3 - z_i^3) - \frac{z_i z_{i+1}}{2} (z_{i+1} - z_i) \right] = 0 \end{aligned} \quad (3-18)$$

The above equation group that includes $3n$ equations can be expressed using matrices as follows:

$$[A]\{G\} = \{B\} \quad (3-19)$$

$$\begin{bmatrix} a_{00} & a_{01} & & & \\ & & \dots & \dots & \dots \\ & & & a_{i-1} & a_i & a_{i+1} \\ & & & & \dots & \dots & \dots \\ & & & & & a_{n-1} & a_n \end{bmatrix} \begin{Bmatrix} g_0 \\ g_1 \\ \vdots \\ g_{i-1} \\ g_i \\ g_{i+1} \\ \vdots \\ g_{n-1} \\ g_n \end{Bmatrix} = \begin{Bmatrix} b_0 \\ b_1 \\ \vdots \\ b_{i-1} \\ b_i \\ b_{i+1} \\ \vdots \\ b_{n-1} \\ b_n \end{Bmatrix} \quad (3-20)$$

where

$$a_{00} = \frac{1}{3} (z_1 - z_0) \quad (3-21)$$

$$a_{01} = \frac{1}{6} (z_1 - z_0) \quad (3-22)$$

$$b_0 = \frac{1}{2} (f_1 - f_0) \quad (3-23)$$

$$a_{i i-1} = \frac{1}{6}(z_i - z_{i-1}) \quad (3-24)$$

$$a_{ii} = \frac{1}{3}(z_{i+1} - z_{i-1}) \quad (3-25)$$

$$a_{i i+1} = \frac{1}{6}(z_{i+1} - z_i) \quad (3-26)$$

$$b_i = \frac{1}{2}(f_{i+1} - f_{i-1}) \quad (3-27)$$

$$a_{n n-1} = \frac{1}{6}(z_n - z_{n-1}) \quad (3-28)$$

$$a_{n n} = \frac{1}{3}(z_n - z_{n-1}) \quad (3-29)$$

$$b_n = \frac{1}{2}(f_n - f_{n-1}) \quad (3-30)$$

As a result, each element in coefficient matrix $[A]$ and vector $\{B\}$ can be determined based on the above equations, and the solution $\{G\}$ is expressed as:

$$\{G\} = [A]^{-1} \{B\} \quad (3-31)$$

Note that the bending moment distribution $f(z)$ is approximated as piecewise linear function using the weighting or shape function $\psi(z)$. The WR approximation to derivative of $f(z)$, however, is piecewise linear, and can be applied a second time to obtain a piecewise linear approximation on the second derivative. Thus, a double differentiation of moment profiles using WR method can result in the soil/rock reaction profiles, $p(z)$. The WR method has been coded into the software Matlab to obtain shear force profiles and soil/rock reaction profiles based on the measured values of moment.

3.3.4.4 Smoothed Weighted Residuals Method

An improvement on WR method can be achieved by using the 2D negative exponential smoothing function of commercial available software, Sigmaplot, to smooth the data points before WR differentiation is applied. The smoothing process can provide a smooth trend of measured moment data. Additionally, it can interpolate as many data points as needed to make the spacing of moment data points smaller. A study by Yang, et al. (2005) has shown that this improved technique helps generation of smooth p-y curves.

3.3.4.5 Cubic Spline Curve Fitting

A cubic spline was employed to fit the discrete moment data points to derive p by Mezazigh and Levacher (1998). The cubic spline is perhaps the simplest interpolation function of discrete test data that can be double differentiated. However, since a spline fits every point exactly, it is therefore prone to errors of measurement. In this dissertation, cubic spline curve fitting technique will not be examined.

3.3.5 Evaluation Using Field Test Data

A total of eight field lateral load tests results on fully instrumented drilled shafts in soils and/or rocks have been compiled herein for evaluating the various methods for deriving p-y curves. A summary of these load tests is presented in Table 3-4. Four methods for deriving p, including piecewise polynomial, 5th order global polynomial, weighted residuals (WR), and smoothed weighted residuals (SWR), are evaluated.

To deduce p-y curves, the y vs. depth profiles are first obtained by double integrating curvature vs. depth profiles using the 5th order polynomial curve fitting method. The relationship between moment and curvature is obtained by comparing measured curvatures at the ground surface level and the known applied moments for load

tests PomS1 and PomS2. Extrapolation is used when curvature is greater than the maximum curvature measured at the ground surface. For other load tests, M- ϕ curves are obtained using the LPILE computer program by inputting the drilled shaft geometry, concrete strength, and reinforcement.

Due to possible measurement errors, variability of concrete stiffness, and inaccurate moment-curvature relationships, some moment profiles are considered as outlier. For such load tests data (e.g., CDOTS1), these outlier moment versus depth curves were discarded, as illustrated in Fig. 3-20.

Table 3-4 Compiled Lateral Load Test Database

No.	Test Shaft	Diameter (ft)	Total Length (ft)	Location	Reference
1	PomS1	8	101	Pomeroy, OH	This chapter
2	PomS2	8	112.9	Pomeroy, OH	This chapter
3	CDOTC1	2.5	16.7	Denver, CO	Nusairat, et al. (2004)
4	CDOTC2	2.5	16.7	Denver, CO	Nusairat, et al. (2004)
5	CDOTS1	2.5	21	Denver, CO	Nusairat, et al. (2004)
6	CDOTS2	2.5	21	Denver, CO	Nusairat, et al. (2004)
7	DaytonS4	6	18	Dayton, OH	This chapter
8	MaumeeS1	8	93	Toledo, OH	Yang and Liang (2005)

3.3.5.1 Deflection versus Depth

The deflections deduced from strain gage readings are checked against the deflections measured by inclinometers. In general, the deflections deduced from strain readings match the deflections from inclinometer readings. A representative comparison for test PomS1 is shown in Fig. 3-21.

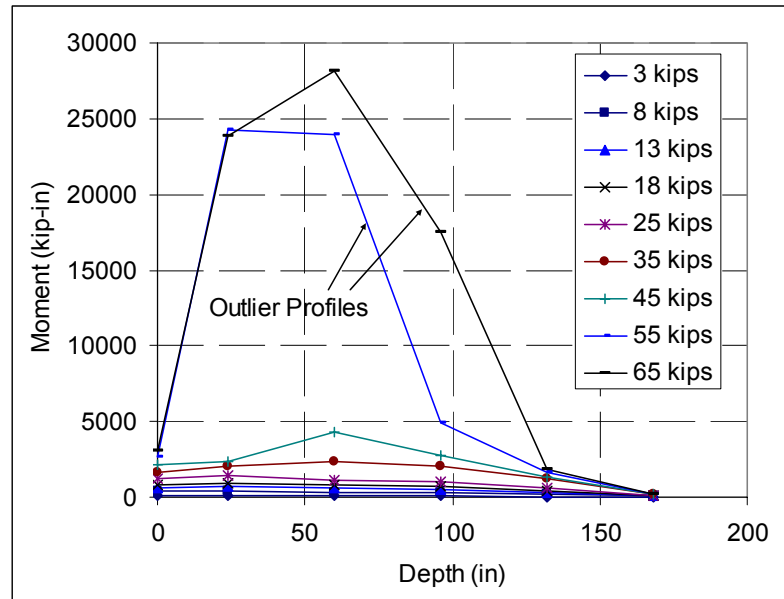


Figure 3-20 Elimination of outlier moment profiles

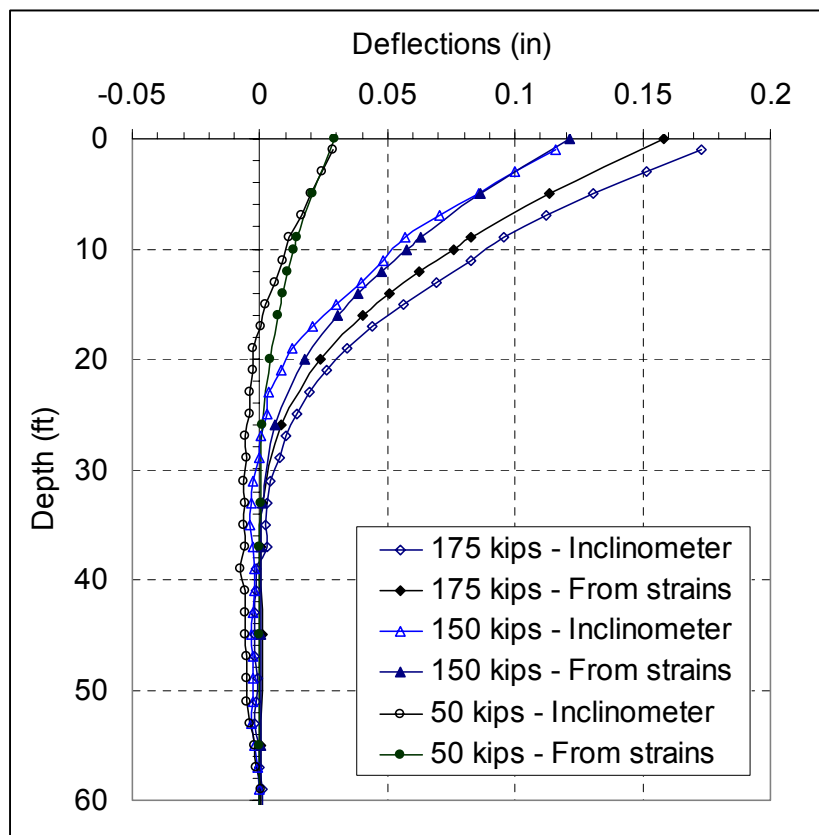


Figure 3-21 Comparison of deflections from strain readings and inclinometer for test PomS1

3.3.5.2 P versus Depth Profile

The derived p values near the ground surface from WR and SWR methods are negative for test data from MaumeeS1, CDOTS2, and PomS1, as shown in Fig. 3-22 for MaumeeS1. Similarly, the p values near the ground surface of PomS1 are also negative when global polynomial curve fitting method is used. Furthermore, SWR method results in irregular spikes in p vs. depth profiles for tests data of CDOTC1 and CDOTC2, as shown in Fig. 3-23 for CDOTC1.

Based on the above observations, it is concluded that WR and SWR methods are not capable of producing reasonable p v. depth profiles for some of the load tests. On the other hand, the piecewise polynomial curve fitting method seems to be able to provide a reasonable result.

3.3.5.3 Load-Deflection Curve at Shaft Head

The predicted load-deflection curves at the ground line (or shaft head) by inputting the deduced p - y curves into LPILE (or COM624P) program are compared with the measured. The method proposed by Murchison and O'Neill (1984) is employed to quantify prediction error. The prediction error is defined as the difference between the measured and predicted deflections at the ground line divided by the measured deflections at the same loading level, as shown in Fig. 3-24. Specifically, the errors at four loading levels (i.e., $0.25H_{\max}$, $0.5H_{\max}$, $0.75H_{\max}$, and H_{\max}), are computed and summed. It should be noted that H_{\max} is usually taken as the maximum applied load; however, for tests, such as CDOTS1, where elimination of outlier data has resulted in the use of highest reasonable loads as H_{\max} .

The calculated cumulative errors for each load test data are summarized in Table 3-5. It can be seen that piecewise polynomial curve fitting method yields the smallest cumulative errors. If test CDOTS1 is ignored due to its inaccurate moment versus depth profiles, the average calculated error of the four loading levels of the remaining seven tests using the piecewise polynomial method deduced p-y curves is about 29%.

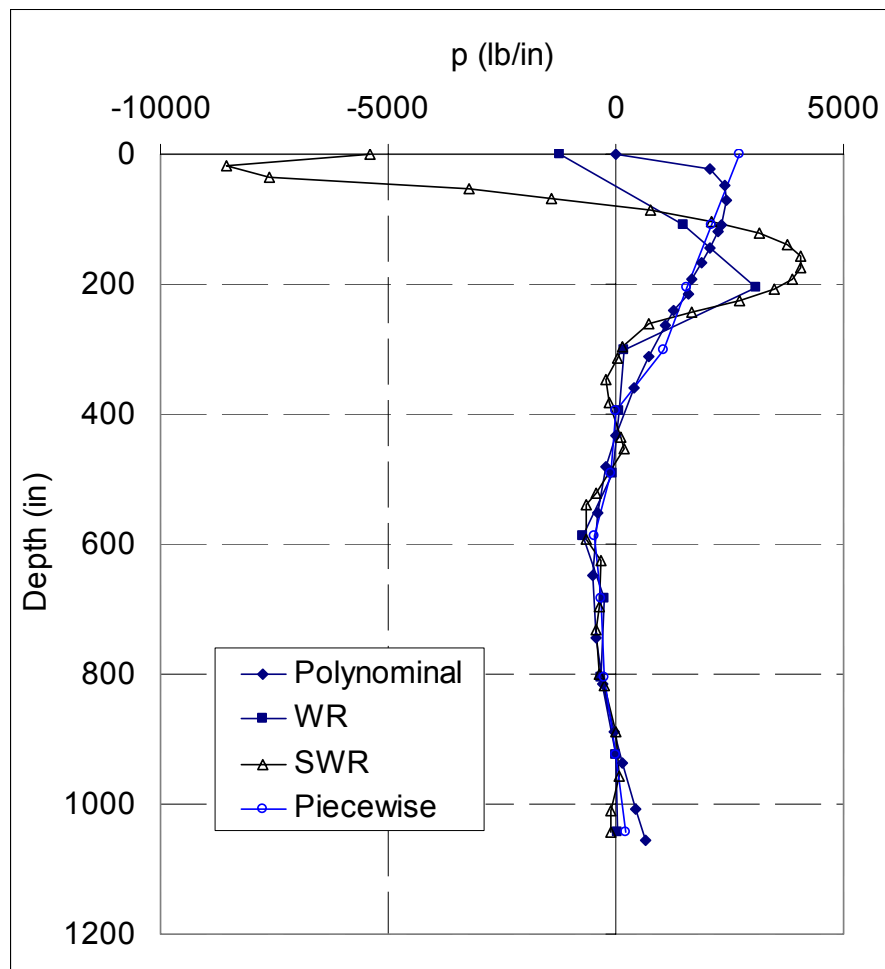


Figure 3-22 P vs. depth profile of test MaumeeS1

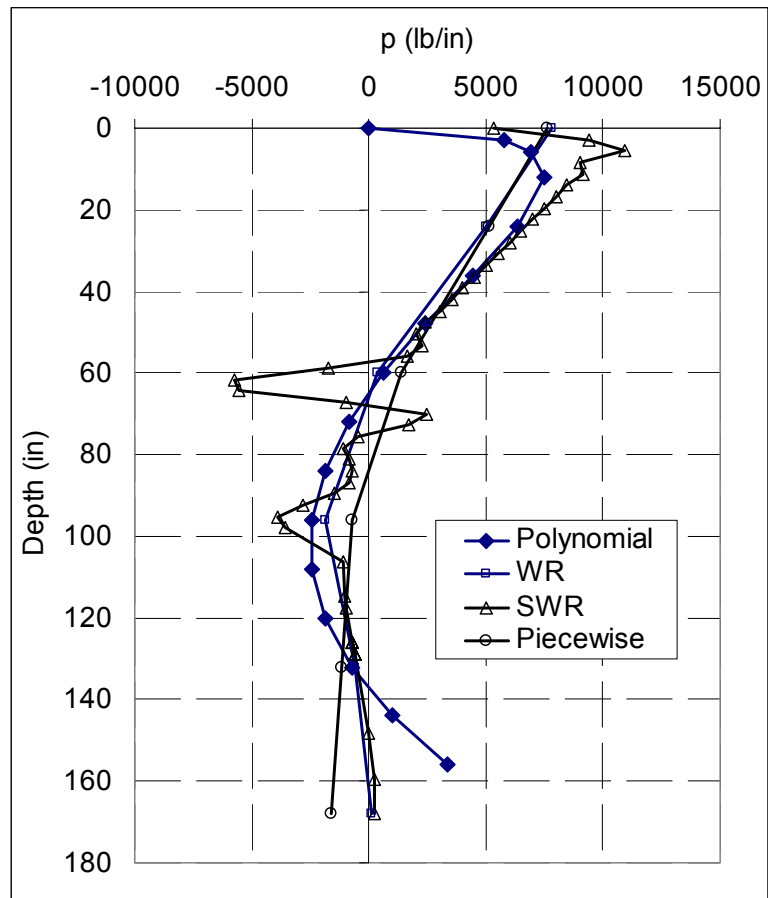


Figure 3-23 P vs. depth profile of test CDOTC1

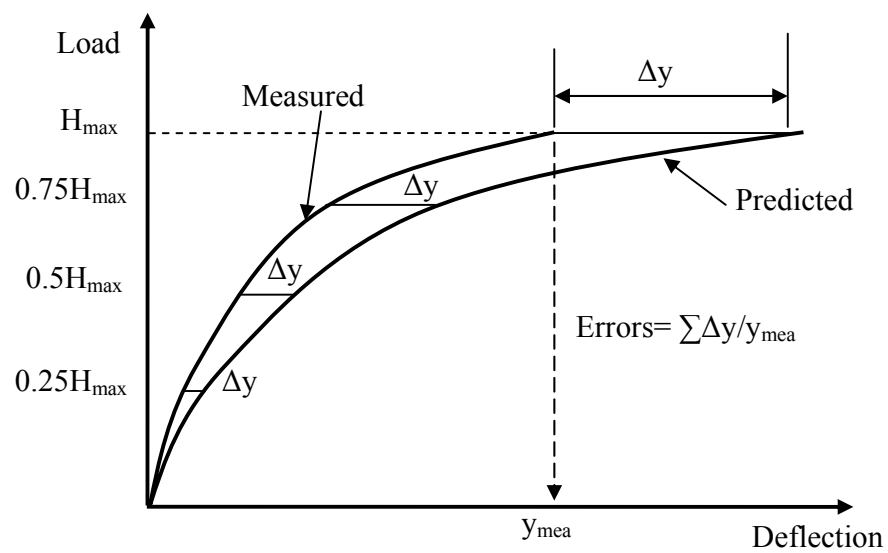


Figure 3-24 Definition of deflection prediction error

Table 3-5 Cumulative Shaft Head Deflection Errors based on Various Methods

Test Shaft	Polynomial	WR	SWR	Piecewise
PomS1	6.3	6.3	2.7	3.0
PomS2	0.9	1.0	0.8	0.9
CDOTC1	1.3	1.4	2.0	0.7
CDOTC2	1.7	2.3	1.9	1.9
CDOTS1	8.4	5.2	9.9	8.5
CDOTS2	0.5	1.4	0.4	0.5
DaytonS4	0.6	1.2	0.5	0.4
MaumeeS1	0.5	3.8	1.0	0.5
Total	20.3	22.6	19.2	16.5

3.3.5.4 Maximum Moment in Drilled Shafts

In addition to deflection prediction, the maximum moments of drilled shafts under the four loading levels predicted using COM624P based on experimental p-y curves are compared with the corresponding maximum moments based on strain gage readings. The moment prediction errors, defined as the moment difference divided by the measured moments, are summarized in Table 3-6. It can be seen that the difference among these four methods is not significant with SWR providing the smallest error.

Table 3-6 Cumulative Moment Errors based on Various Methods

Test Shaft	Polynomial	WR	SWR	Piecewise
PomS1	0.6	1.3	0.9	0.9
PomS2	0.3	0.3	0.3	0.3
CDOTC1	0.7	0.8	0.8	0.7
CDOTC2	0.8	1.0	0.8	0.7
CDOTS1	0.3	0.2	0.2	0.2
CDOTS2	2.4	1.3	2.1	2.2
DaytonS4	0.0	0.1	0.1	0.1
MaumeeS1	1.3	1.3	0.4	1.6
Total	6.3	6.3	5.6	6.8

3.3.6 Evaluation Using Hypothetical Cases

3.3.6.1 Hypothetical Cases

LPILE (or COM624P) was used with the prescribed (assumed) p-y curves to simulate results of a lateral load test, from which moment versus depth profiles under various lateral loads were obtained. These moment profiles were then used to deduce p versus depth profile. The p-y curves could then be obtained by using y versus depth profiles from the simulation. By comparing the deduced p-y curves using various derivation methods with the prescribed (assumed) p-y curves, one could then assess the accuracy of various p derivation methods. Three p derivation methods, including piecewise polynomial, global 5th order polynomial, and WR method, are included in this evaluation study. SWR method was not evaluated, because it yields almost the same results as WR method, if a small spacing of moment data points is chosen.

Four hypothetical cases are chosen for four types of p-y curves that could be prescribed in COM624P program. The drilled shaft used in these four hypothetical cases has a diameter of 3 ft and embedment length of 30 ft. The reinforcement of the shaft is 12 #14. The soil used for each case is a homogeneous soil layer. The soil parameters for the selected four p-y criteria are summarized in Table 3-7. The spacing of moment data points used for deducing p is prescribed as 12 inch.

Table 3-7 Soil Parameters of Hypothetical Cases

Case No.	p-y criteria (COM624P)	S_u (psi)	ϕ (°)	γ' (pci)	ϵ_{50}	k_s (pci)
1	Stiff clay above water	20	-	0.072	0.004	1000
2	Stiff clay below water	20	-	0.035	0.004	1000
3	Sand	-	36	0.072	-	90
4	Soft clay	2	-	0.052	0.02	20
S_u – undrained shear strength, ϕ – friction angle, γ' – effective unit weight, ϵ_{50} – strain at 50% of maximum principle stress, k_s – coefficient of initial slope of p-y curves.						

3.3.6.2 Comparison of p-y Curves

The deduced p-y curves are compared with the prescribed p-y curves in Fig. 3-25. It can be seen that the global 5th order polynomial derived p-y curves deviate significantly from the prescribed p-y curves. The piecewise polynomial derived p-y curves closely match the prescribed p-y curves except for case 2. It also shows that WR method provides a good result.

To quantify the accuracy of these three methods investigated, the errors of the derived p-y curves are computed. Using the same definition of error of load-deflection curves given in Fig. 3-24, the p-y curve error is defined as $\Delta p/p_{\text{prescribed}}$, where $p_{\text{prescribed}}$ is the p from prescribed p-y curves and Δp is the difference between the p from prescribed and the derived. The errors at deflections of $0.25y_m$, $0.5y_m$, $0.75y_m$, and y_m , where y_m is the maximum y of prescribed p-y curves, are calculated for each p-y curve. The cumulative errors of four p-y curves at four different depths (1 ft, 4 ft, 7 ft, and 10 ft) for each case are calculated and summarized in Table 3-8. It can be seen that the piecewise polynomial method yields the smallest error, while the global polynomial method leads to the largest error.

Table 3-8 Cumulative Errors of p-y Curves of Hypothetical Cases

Case No.	Polynomial	WR	Piecewise
1	4.6	1.0	0.2
2	83.5	16.4	16.5
3	4.0	1.0	0.6
4	3.5	0.8	0.4
Total	95.5	19.1	17.8

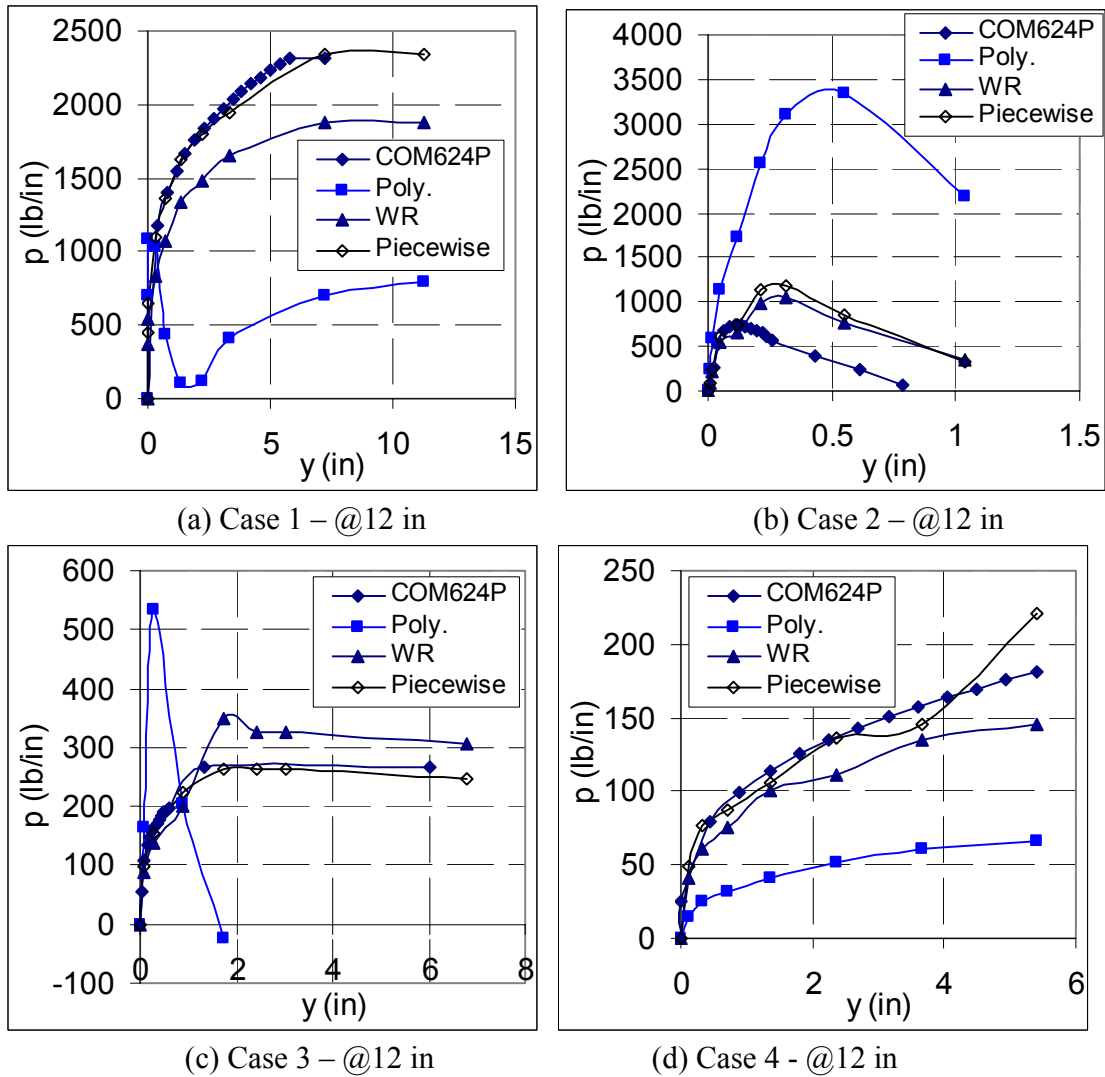


Figure 3-25 Comparison of p-y curves

3.3.7 Optimum Strain Gage Spacing

The spacing of strain gages is important for deriving accurate p-y curves from lateral load tests. A sparsely distributed strain data points may result in inaccurate p-y curves; on the other hand, too closely spaced strain gage distribution may be cost prohibitive. An optimum spacing of strain gages, which balances the cost and accuracy of the deduced p-y curves, is needed in planning of any instrumentation project for a lateral load test. The

following procedure is suggested for determining an optimum strain gage spacing for a particular lateral load test so that accurate p-y curves can be derived with minimum cost spent on strain gages. The first step is to select p-y criterion from the pool of existing criteria in LPILE program that fit to the soil condition at test site. Next, generate the moment vs. depth profiles of the pile at various loads using LPILE program with the prescribed p-y curves. Then, deduce p-y curves using the piecewise polynomial curve fitting method and LPILE generated moment vs. depth profiles. In this step, different trial moment spacings should be used to obtain different sets of p-y curves. Finally, compare the deduced p-y curves with the prescribed p-y curves used in step one and determine an optimum moment (or strain gage) spacing accordingly.

To illustrate the suggested procedure, an example case with homogenous soil is employed. Moment spacings varying from 1 ft to 7 ft are investigated. To account for the effect of drilled shaft diameter on optimum spacing, additional two cases are introduced with drilled shafts diameter of 6 ft and 9 ft. The ratio of shaft length over diameter is kept as 10 for both additional cases. The soil and shaft strength parameters are kept the same as those used for the hypothetical case 1.

The cumulative errors of deduced p-y curves at four depths based on piecewise polynomial method for various chosen moment data point spacing is presented in Fig. 3-26. It can be seen that 3 ft, 4 ft and 5 ft of spacing can minimize the errors of the deduced p-y curves and be taken as the optimum spacing for a drilled shaft with diameter of 3 ft, 6 ft, and 9 ft, respectively.

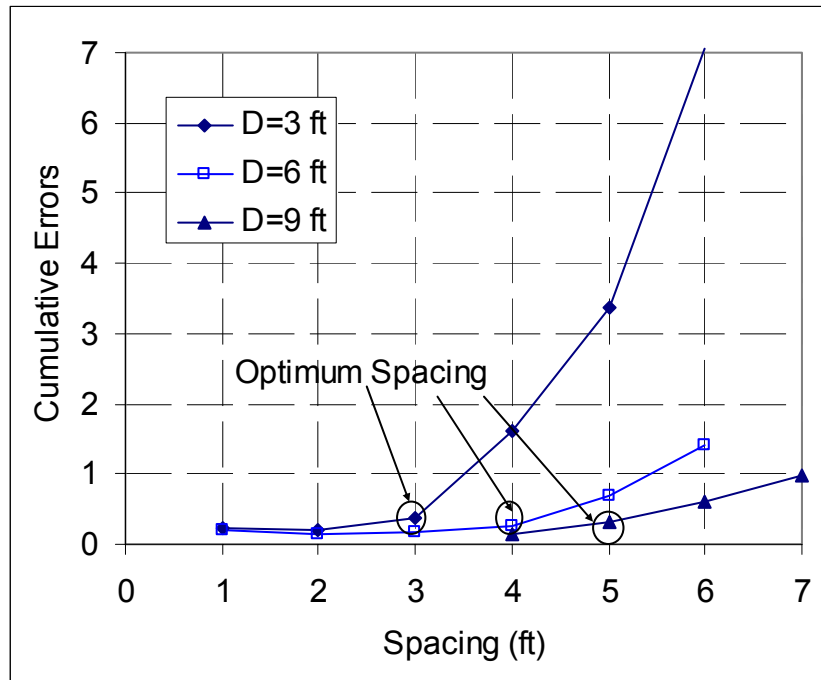


Figure 3-26 Optimum spacing of strain gages

It should be noted that above recommended method for determining optimum strain gage spacing is only valid when the moment vs. depth profiles can be accurately determined from strain gage readings. A lateral load test usually only mobilizes the deflection at top soil layers; therefore, it is preferred to use smaller gage spacing near ground surface and larger spacing for the bottom portion of the drilled shafts in order to obtain moment versus depth profile as accurately as possible.

3.3.8 Effect of Measurement Error

To study the effect of error of measured moment profiles on the deduced p-y curves, a parametric study is performed. According to Eq. (3-2), the errors of moment-depth profiles from strain gage readings may be due to two possible reasons: the error of strain gage measurement and inaccurate estimate of shaft stiffness EI. The worst moment profiles could be appearance of wavy types of profiles due to unstable strain gage

readings. As far as the errors due to shaft stiffness, three possible situations may occur, including under estimating EI, over estimating EI before cracking, and over estimating EI at positions where crack appears. A diagram of these four possible measurement errors of moment is sketched in Fig. 3-27.

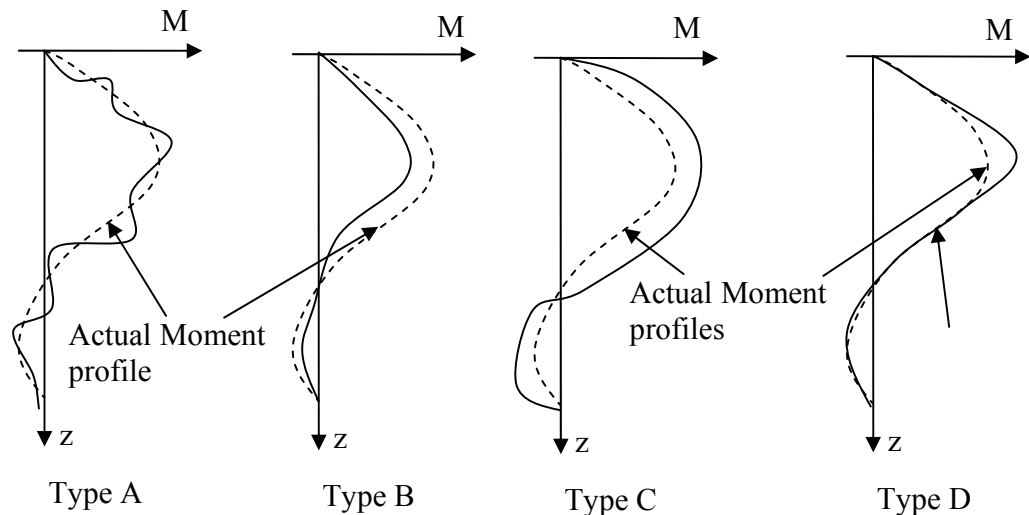


Figure 3-27 Four types of moment error profiles

The hypothetical case 1 is used to investigate the effect of moment errors on the deduced p-y curves by modifying the moment profiles from COM624P. Two feet of spacing of moment data points is used. The errors of moment are varied from 5% to 20%. The p-y curves deduced from the modified moment profiles using piecewise polynomial method are compared with the prescribed p-y curves in the initial LPILE analysis. The cumulative p-y curve errors of four deflections (i.e., $0.25y_m$, $0.5y_m$, $0.75 y_m$, and y_m) at four depths (i.e., 2 ft, 6 ft, 10 ft, and 14 ft) are presented in Fig. 3-28. It can be seen that the wavy type of moment error induces the largest error in the deduced p-y curves among these four types of moment error. The cumulative errors caused by other three types of error are about the same.

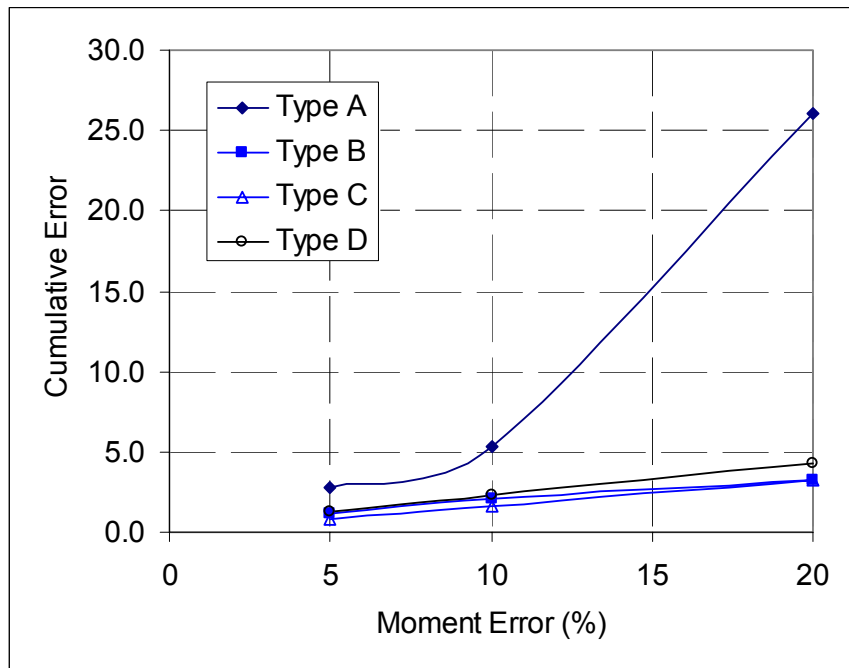


Figure 3-28 Cumulative p-y curve errors due to moment errors

The cumulative errors of the deduced p-y curve for the four cases are greater than 3.3 for 20% of moment error, which is much larger than the cumulative error of 0.2 when accurate moment profiles is used as shown in Table 3-8. This implies that the errors of deduced p-y curves are mainly due to inaccurate determination of moment profiles from strain gage readings when an appropriate method is used to deduce the p-y curves.

3.3.9 Conclusions on Methods for Deriving p-y Curves

Based on the work presented in this section, the following conclusions can be made:

1. WR and SWR methods tend to yield unreasonable p vs. depth profiles for 5 out of 8 tests. Some of the problems are negative p values near ground surface and irregular spikes. On the other hand, piecewise polynomial curve fitting method yields reasonable results.
2. The deduced p-y curves using WR method leads to the largest errors on the predicted

- load-deflection curve of drilled shafts. The p-y curves deduced from the piecewise polynomial curve fitting method on the other hand yields the smallest error.
3. Regarding the prediction of maximum moment of a drilled shaft, the p-y curves deduced by SWR method yields the smallest errors. However, the difference of maximum moment prediction errors of all four methods is not significant.
 4. The piecewise cubic polynomial curve fitting method provides the smallest error of the deduced p-y curves for the 4 hypothetical cases. On the other hand, global 5th order polynomial curve fitting provides the largest error.
 5. Based on the evaluation studies presented, piecewise cubic polynomial curve fitting method is recommended as a method for deriving p versus depth.
 6. A procedure is outlined for determining optimum strain gage spacing for developing site-specific instrumentation plans.
 7. The parametric study suggests that the error of the deduced p-y curves are mainly due to inaccurate determination of moment profiles from strain gage readings, provided that an appropriate method for deducing p is used.

3.4 Analyses of the Load Tests

The lateral load tests presented earlier in this chapter are used to deduce p-y curves and to evaluate interim p-y criterion for weak rock developed by Reese (1997).

3.4.1 Evaluation of Experimental P-y Curves

By using piecewise polynomial curve fitting technique, the p-y curves for shaft #4 of Dayton load test and those for shaft #1 and shaft #2 of Pomeroy-Mason load test at various depths are derived and presented in Figs. 3-29, 3-30, and 3-31, respectively.

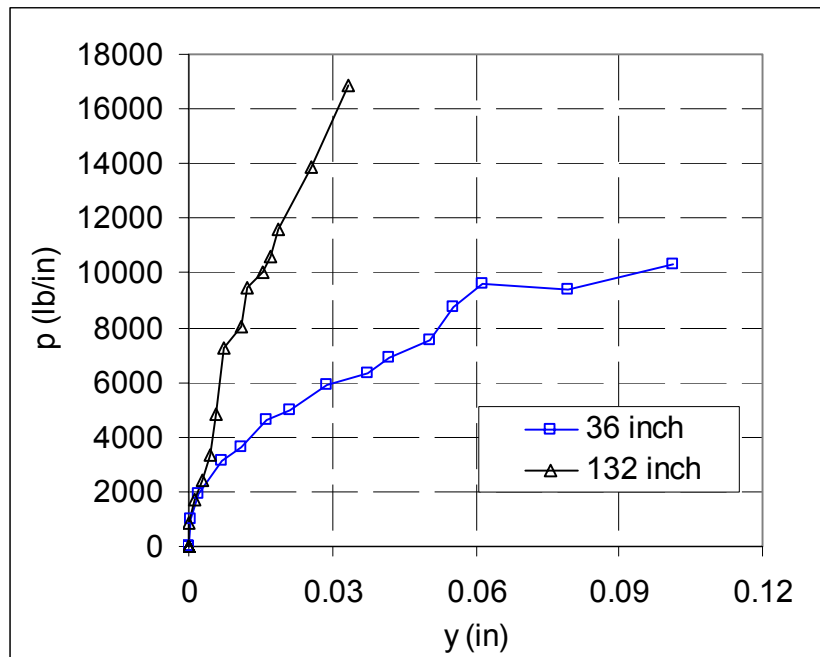


Figure 3-29 Experimental p-y curves for shaft #4 of Dayton load test

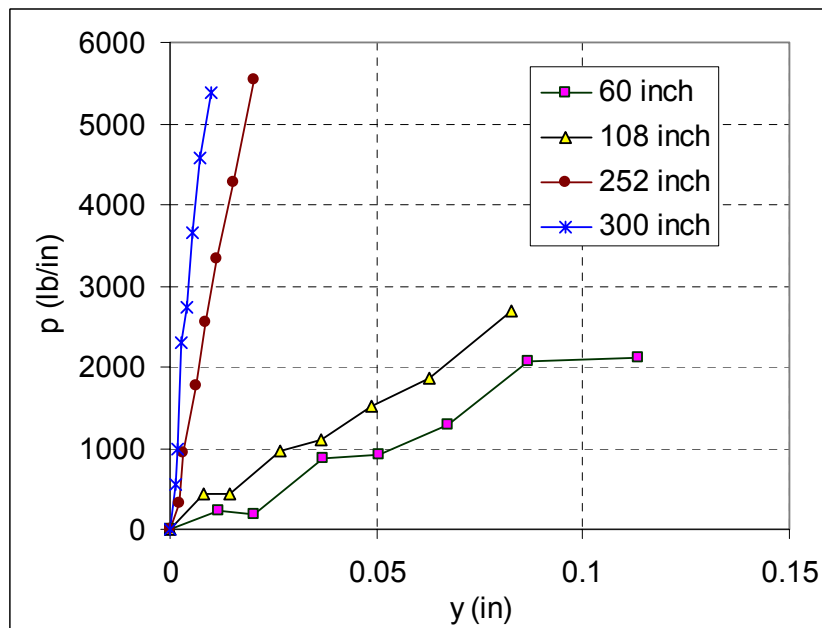


Figure 3-30 Experimental p-y curves for shaft #1 of Pomeroy-Mason load test

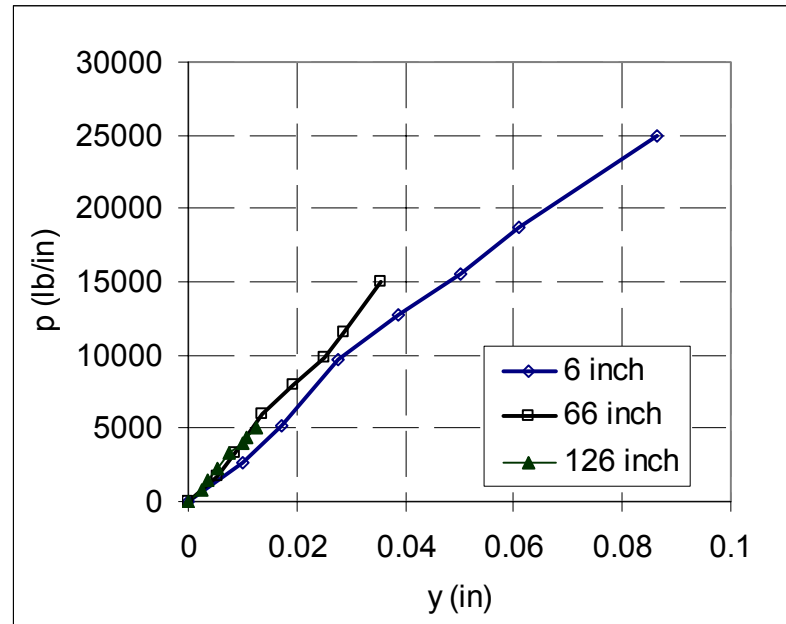


Figure 3-31 Experimental p-y curves for shaft #2 of Pomeroy-Mason load test

To verify the accuracy of these derived p-y curves, an analysis using LPILE with these p-y curves was made to compare with actual measured load-deflection curves. The lateral load was not applied at the top of the shaft for Dayton load test, while the program LPILE requires the input load be applied at the shaft top, as shown in Fig. 3-32(a). Therefore, to facilitate analysis using LPILE, an equivalent load combination, including a same value of lateral load at the top of shaft and an additional moment, is used to represent the actual applied lateral load, as shown in Fig. 3-32(b). For the load test at Pomeroy-Mason, the deflections were measured at the loading point; therefore, the loading point will be taken as the top of the shaft for the analysis using LPILE. The effect of casing above rock layer at Pomeroy-Mason load test is considered in LPILE analysis. The nonlinear pile stiffness option is chosen to account for the reduction of stiffness of concrete shaft after the appearance of crack.

The load-deflection curves at the top of shaft predicted by LPILE using the derived p-y curves are provided in Figs. 3-33, 3-34, and 3-35 for the three test drilled shafts. Even though, the predicted deflections are less than the measured values at large load levels for shaft #2 of Pomeroy-Mason load test. In general, the predicted load-deflections curves match those measured curves. This provides validation that the recommended method for deriving p-y curves can be used to obtain reasonable site specific p-y curves.

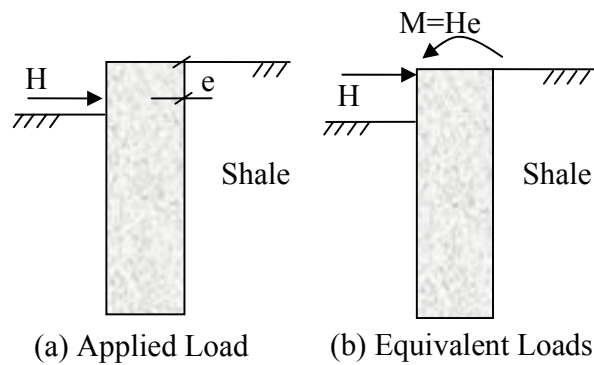


Figure 3-32 Equivalent load combinations

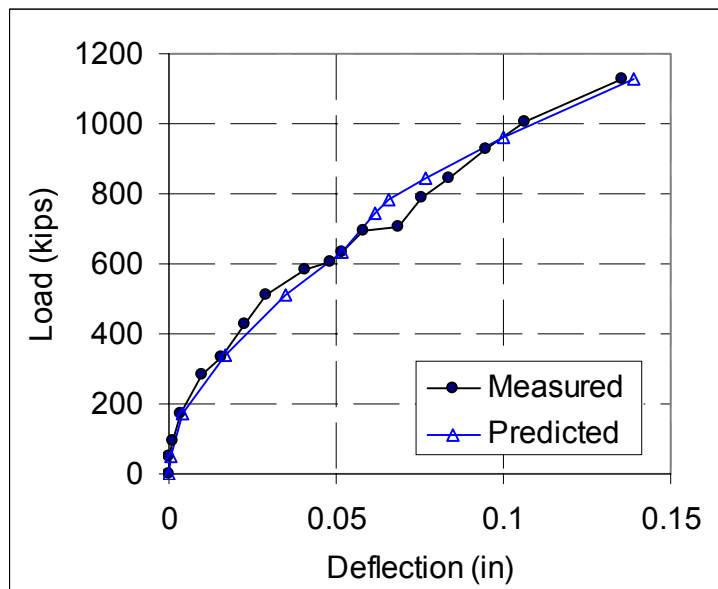


Figure 3-33 Prediction of load-deflection curves of shaft #4 of Dayton load test using experimental p-y curves

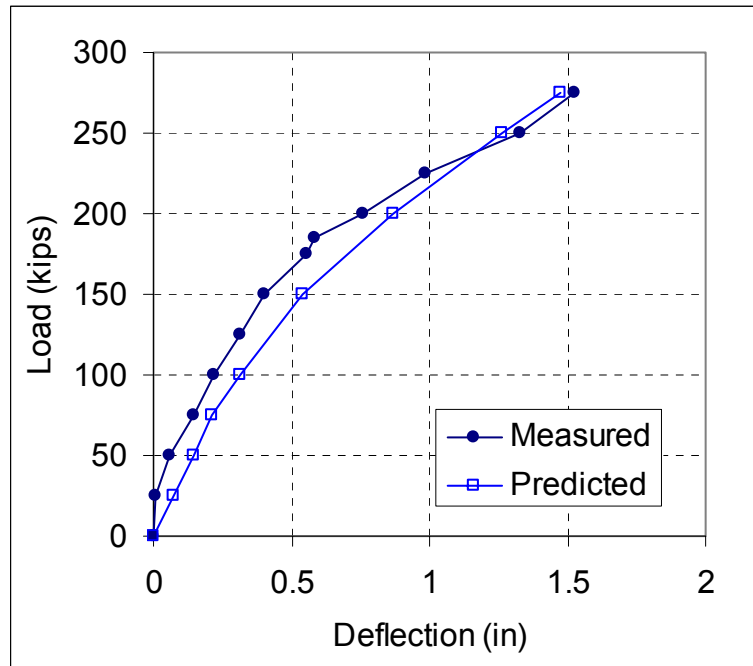


Figure 3-34 Prediction of load-deflection curves of shaft #1 of Pomeroy-Mason load test using experimental p-y curves

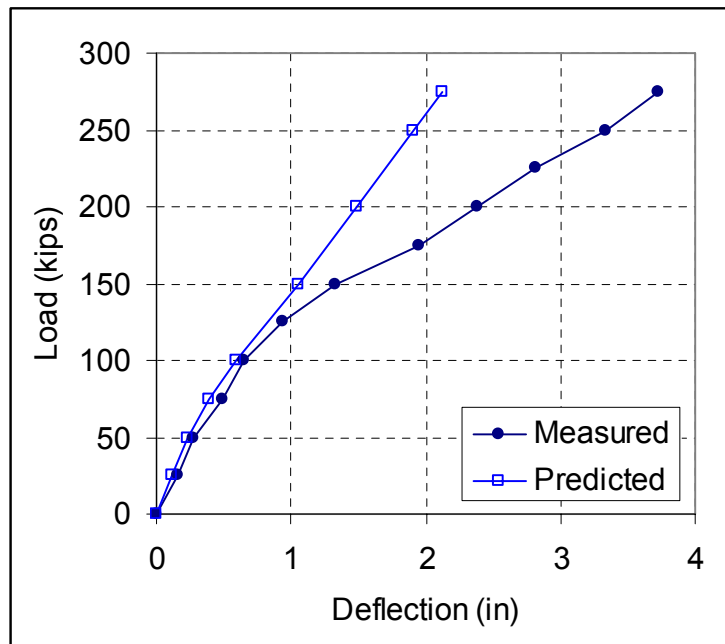


Figure 3-35 Prediction of load-deflection curves of shaft #2 of Pomeroy-Mason load test using experimental p-y curves

3.4.2 Evaluation of Existing p-y Criterion

The interim p-y criterion for weak rock proposed by Reese (1997) is evaluated by using LPILE analysis to predict field test data. The main rock properties required by Reese p-y criterion are γ' (effective unit weight), RQD, q_u (unconfined compressive strength), E_m (modulus of rock mass), and k_{rm} (strain at 50% ultimate load). A range of 0.0005 to 0.00005 of k_{rm} was suggested by Reese (1997). Because of the lack of measured k_{rm} , a value of 0.0005 was used. The values of E_m are obtained by correlations with E_i . Further discussion on this correlation is provided in chapter V. The main parameters need to represent the weak rock p-y curves using Reese criterion are tabulated in Tables 3-9 to 3-11 for the three test shafts. The depth is from the top of rock for shaft #4 at Dayton and shaft #2 at Pomeroy-Mason. However, the depth for shaft #1 at Pomeroy-Mason is from the ground level.

Table 3-9 Rock Properties for LPILE Analysis

Test Shaft	Depths (ft)	γ' (pci)	RQD	E_m (psi)	q_u (psi)	k_{rm}	Type
Shaft #4 Dayton	0 – 7	0.038	8%	38142	5668	0.0005	Shale
	7 – 18	0.038	53%	98102	5668	0.0005	Shale
Shaft #1 Pomeroy – Mason	0 – 17.3	0.035	SPT =7.1	-	$\phi = 30$	$k = 20$	Sand
	17.3 – 26	0.035	SPT =13.5	-	$\phi = 32$	$k = 60$	Sand
	26 – 47.5	0.057	60%	6462	905	0.0005	Shale/Siltstone
	47.5 – 54.5	0.049	8%	654	52.8	0.0005	Shale(Mudstone)
	54.5 – 63.9	0.047	23%	654	7.0	0.0005	Shale(Mudstone)
	63.9 – 66	0.05	38%	954	27.8	0.0005	Shale(Mudstone)
Shaft #2 Pomeroy – Mason	0 – 21.9	0.059	44%	23885	3797	0.0005	Shale
	21.9 – 29.4	0.06	32%	102807	9073	0.0005	Sandstone
	29.4 – 37.3	0.049	51%	88.3	19	0.0005	Claystone
	37.3 – 48	0.047	20%	55.7	44.3	0.0005	Claystone
	48 – 56.8	0.055	86%	6170.9	826.2	0.0005	Claystone

The information of test shafts used in LPILE analysis is summarized in Table 3-10. By inputting properties of rock, soil, and shaft (summarized in Table 3-9 and Table 3.10) into LPILE, the load-deflection curves at the loading point can be obtained. Nonlinear shaft stiffness option is selected. The comparisons of the predicted load-deflection curves and the measured curves are provided in Figs. 3-36 through 3-38. The predicted deflections are larger than the measured values for shaft #1 of Pomeroy-Mason load test according to Fig. 3-37. However, it should be noted that a 26 feet thick layer of sand exists above the rock mass when shaft #2 was under test. This may impede full interaction of drilled shaft and rock, as evidenced in Fig. 3-12 where the deflection at the top rock almost is close to 0.

On the other hand, the predicted deflections are much less than the measured values for the other two test shafts. This may be due to inaccurate determination of input parameters or due to the unsuitability of Reese weak rock p-y criterion for the two tests. To explore the first reason, the rock parameters are adjusted to match the measured results. As shown in Fig. 3-36 and Fig. 3-38, good matches are obtained when the modulus and unconfined compressive strength of top rock layer of Dayton site and those of Pomeroy-Mason site are reduced to 2% and 1% of the original values provided in Table 3-9, respectively. One can see that a dramatic reduction of rock properties is needed to match the load test results.

Table 3-10 Test Drilled Shafts Information

Test Shaft	Depths (ft) start from loading point	Diameter (ft)	Loading Eccentricity (ft)	Reinforcement	Concrete Strength (psi)
Shaft #4 Dayton	0 - 18	6	0	34#11	4500
Shaft #1 Pomeroy - Mason	0 - 58.4	8.5	32.4	28#18 with 1 inch thick casing	5115
	58.4 - 98.4	8	32.4	28#18	5115
Shaft #2 Pomeroy - Mason	0 - 53.1	8.5	53.1	28#18 with 1 inch thick casing	5115
	53.1 - 109.9	8	53.1	28#18	5115

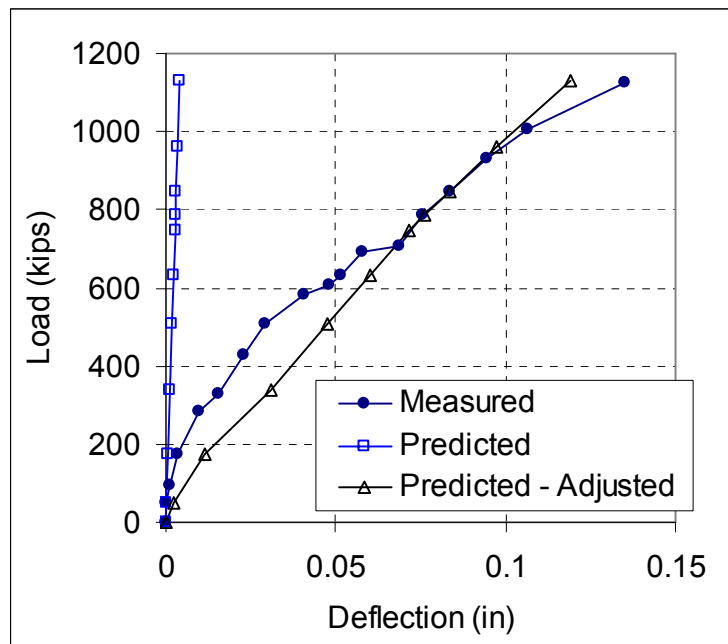


Figure 3-36 Prediction of load-deflection curve of shaft #4 of Dayton load test using Reese weak rock p-y criterion

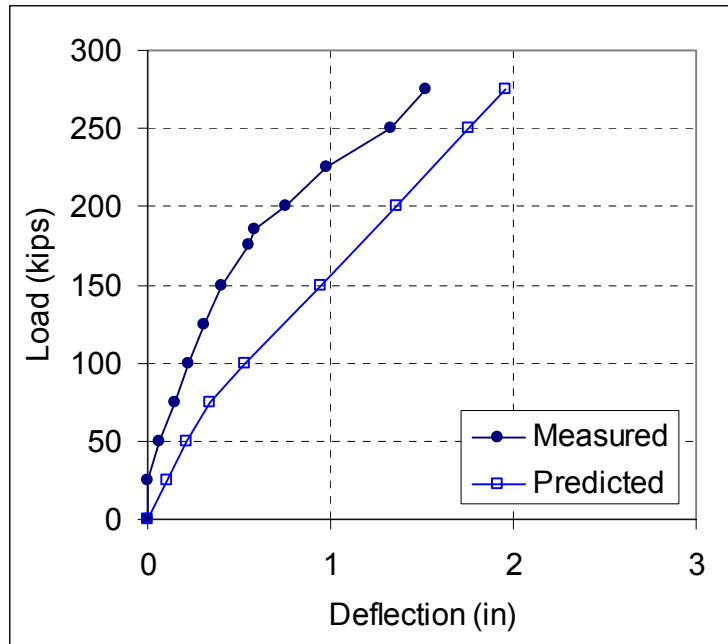


Figure 3-37 Prediction of load-deflection curve of shaft #1 of Pomeroy-Mason load test using Reese weak rock p-y criterion

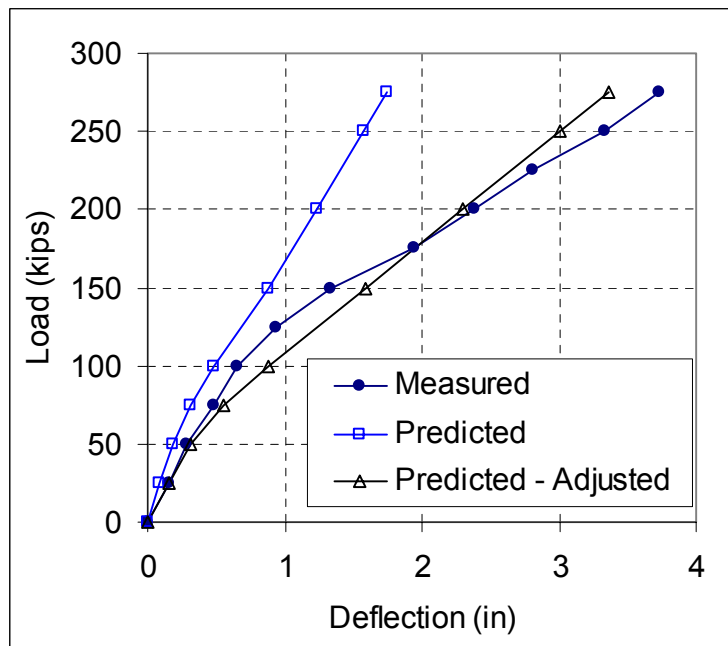


Figure 3-38 Prediction of load-deflection curve of shaft #2 of Pomeroy-Mason load test using Reese weak rock p-y criterion

3.5 Summary and Conclusions

In this chapter, two lateral load tests results of fully instrumented drilled shafts at Dayton site and Pomeroy-Mason site were presented. The details of instrumentation used and load test procedures were also presented. Based on an extensive evaluation of several existing methods, the piecewise polynomial curve fitting technique is recommended for deriving p-y curves from strain data obtained during lateral load test. The accuracy of the deduced p-y curves using the recommended procedure was validated against the two load tests. Additionally, the interim weak rock p-y criterion proposed by Reese (1997) was evaluated as well. The following conclusions can be made.

1. Due to lack of actual lateral load tests of drilled shafts in rock, the two lateral load tests results presented here contribute to understanding and development of pertinent p-y curves.
2. The recommended method for deriving p-y curves from strain data of load test includes using high order polynomial curve fitting to obtain y and using piecewise polynomial curve fitting to obtain p. The superior results of this recommended method was supported by the smallest error on the predictions of load-deflection curves among all other methods.
3. The deduced p-y curves from actual load test data is shown to result in reasonable predictions of the lateral response of drilled shafts for the two load tests.
4. The evaluation of the interim weak rock p-y criterion (Reese, 1997) indicates that this p-y criterion tends to under predict the deflections of drilled shafts in rock.

CHAPTER IV

LATERAL CAPACITY OF DRILLED SHAFTS IN ROCK

The ultimate capacity of laterally loaded drilled shafts in rock has received very little attention in literature. The reason, as pointed out by Carter and Kulhawy (1992), perhaps is that the lateral design is governed largely by displacement considerations. Nevertheless, reliable estimate of lateral capacity is still very important, so that the margin of safety on capacity consideration can be ascertained. Moreover, deriving p-y curve criteria requires that theoretical values of ultimate resistance of rock.

In order to develop theoretical equations for computing the ultimate capacity, it is essential to identify failure modes of rock surrounding the laterally loaded drilled shaft. For this purpose, a 3-D finite element model (FEM) is developed to simulate the response of laterally loaded drilled shafts in rock. The load test result from Dayton site is employed to validate the FEM simulation techniques. Based on calibrated FEM analysis techniques, stress and deformation fields around the shaft are used to develop failure modes of rocks surrounding laterally loaded shafts. Both Hoek-Brown strength criterion of rock mass and an empirical equation for estimating the side shear resistance of shaft/rock interface are employed to derive the theoretical equations for compute the ultimate resistance of rock. Finally, a method for estimating ultimate lateral capacity of a drilled shaft in rock and/or soils is developed.

4.1 3-D Finite Element Modeling and Validation

Although, there are several analytical methods available for analyzing the response of laterally loaded drilled shafts in rock, such as p-y analysis (Reese, 1997) and elasto-plastic solution (Zhang, et al. 2000), finite element method (FEM) nevertheless provides a powerful tool for simulating complete nonlinear and plastic behavior of rocks subjected to laterally loaded drilled shafts. In early stage of FEM applications, Randolph (1981) presented a 2D FEM solution by modeling soil as an elastic continuum and the pile as an elastic beam. With the advances of FEM computing techniques, it is now possible to use 3D FEM modeling technique. For example, Wakai et al. (1999) presented a 3D FEM analysis of laterally loaded piles in soils by modeling soil as elasto-plastic material and pile as linear elastic material. Recently, Wallace et al (2002) presented a 3D FEM analysis to simulate a lateral load test using ABAQUS where soils is modeled as with Mohr-Coulomb model. However, there is a lack of finite element study on laterally loaded drilled shafts socket in rock mass.

A 3D FEM model to simulate the response of a single drilled shaft under lateral loads in rock using ABAQUS is presented here. The yielding of rock mass is modeled using modified Drucker-Prager model (CAP model). To verify the FEM model, the lateral load test result at Dayton site is employed to compare 3D FEM model predictions. The FEM model could be used for deriving theoretical p-y curves as well as for modeling complicated drilled shaft group.

4.1.1 3-D FEM Modeling

4.1.1.1 Finite Element Meshes

Fig. 4-1 shows the meshes of a single drilled shaft-rock system generated using software package PATRAN. The drilled shaft is modeled using second order 15-node triangular prism elements C3D15, as depicted in Fig. 4-2 (a). The second order elements are found to be more appropriate for modeling the shaft than the first order elements, such as 6-node triangular prism elements (C3D6) and 8-node brick elements (C3D8), because the trial simulation with these first order elements suffered convergence problem. The rock mass is modeled using 8-node brick elements C3D8 shown in Fig. 4-2 (b). The bottom of rock mass is fixed. The outer boundary of rock mass are modeled using 8-node infinite boundary elements CIN3D8, which is depicted in Fig. 4-2 (c). Because the lateral response of a drilled shaft is mainly dependent on the rock near the top of the shaft, it is preferred to use a fine mesh for the top layer of rock mass, as shown in Fig. 4-1.

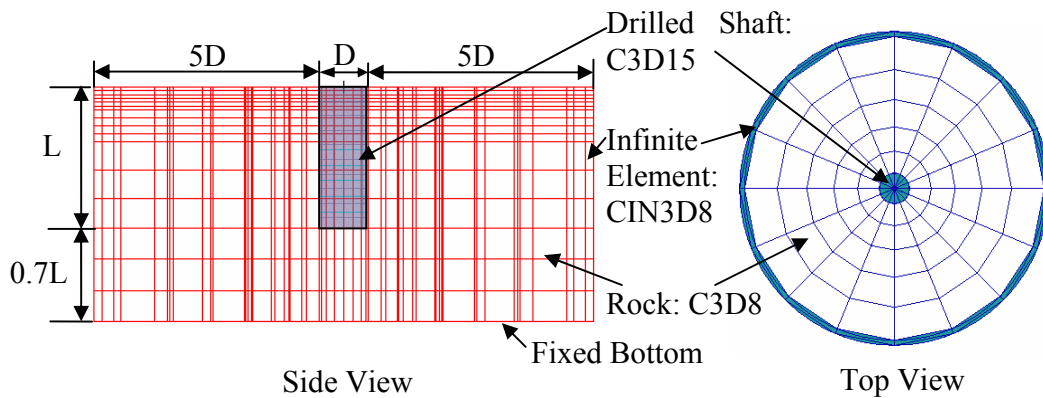


Figure 4-1 Finite element meshes of a drilled shaft-rock system

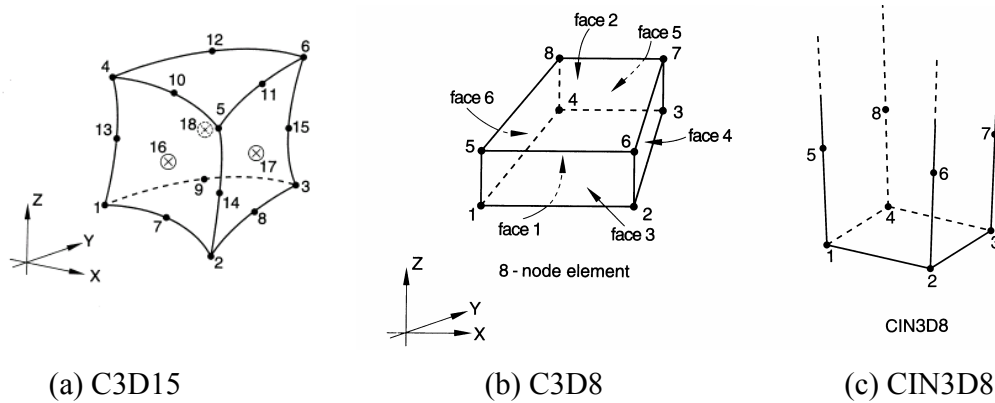


Figure 4-2 Finite elements for (a) drilled shaft, (b) surrounding rock, and (c) outside boundary of rock

Wallace et al. (2002) found that, by studying the effect of different mesh sizes on the shaft-soil contact pressure, $11D$ (D is diameter of drilled shaft) could be used to define the dimension of the diameter of the entire mesh. The depth of rock mass beneath the drilled shaft tip is $0.7 L$, where L is embedment length of the drilled shaft. This is based on findings from Trochanis et al. (1988).

4.1.1.2 Constitutive Models

The drilled shaft is modeled as a cylinder with linear elastic material property. ABAQUS built-in concrete model with embedded rebars was used initially in an effort to simulate the nonlinearity of reinforced concrete drilled shafts; however, the various numerical convergence problems are prevalent. The modified Drucker-Prager model (CAP model) was employed to model the rock mass. The ABAQUS built-in CAP model is intended to model cohesive geological materials that exhibit pressure-dependent yield, such as soils and rocks. It is based on the addition of a cap yield surface to the Drucker-Prager plasticity model, which provides an inelastic hardening mechanism to account for

plastic compaction and helps control volume dilatancy when the material yields in shear (ABAQUS, 1998).

According to ABAQUS User's Manual (1998), the yield surface of the CAP model is defined in two principal segments: a pressure-dependent Drucker-Prager shear failure segment and a compression cap segment, as shown in Fig. 4-3. The Drucker-Prager failure segment is a perfectly plastic yield surface (no hardening). A nonassociated plastic flow is used for the Drucker-Prager yield segment; and an associated plastic flow is used for the CAP segment. The deviatoric stress measure t is defined as

$$t = \frac{1}{2} q \left[1 + \frac{1}{K} - \left(1 - \frac{1}{K} \right) \left(\frac{r}{q} \right)^3 \right] \quad (4-1)$$

where

$$p = -\frac{1}{3} \text{trace}(\boldsymbol{\sigma}) \quad (4-2)$$

$$q = (3/2 \mathbf{S} : \mathbf{S})^{0.5} \quad (4-3)$$

$$r = (9/2 \mathbf{S} : \mathbf{S} \cdot \mathbf{S})^{1/3} \quad (4-4)$$

$$\mathbf{S} = \boldsymbol{\sigma} + p \mathbf{I} \quad (4-5)$$

K is a material parameter that controls the dependence of the yield surface on the value of the intermediate principal stress, and $0.778 \leq K \leq 1.0$. The default value of K is 1.0.

The main input parameters for a CAP model are E_m (elastic modulus of rock mass), d (material cohesion in p - t plane), β (material friction angle in p - t plane), and a cap hardening curve which is obtained from a hydrostatic compression test. The values of d and β can be calibrated from two uniaxial or triaxial compression tests. Alternatively, they can be calibrated from traditional Mohr-Coulomb cohesion, c , and friction angle, ϕ using the following equations.

$$d = 2c \frac{\cos \varphi}{1 - \sin \varphi} \quad (4-6)$$

$$\beta = \arctan\left(\frac{6 \sin \varphi}{3 - \sin \varphi}\right) \quad (4-7)$$

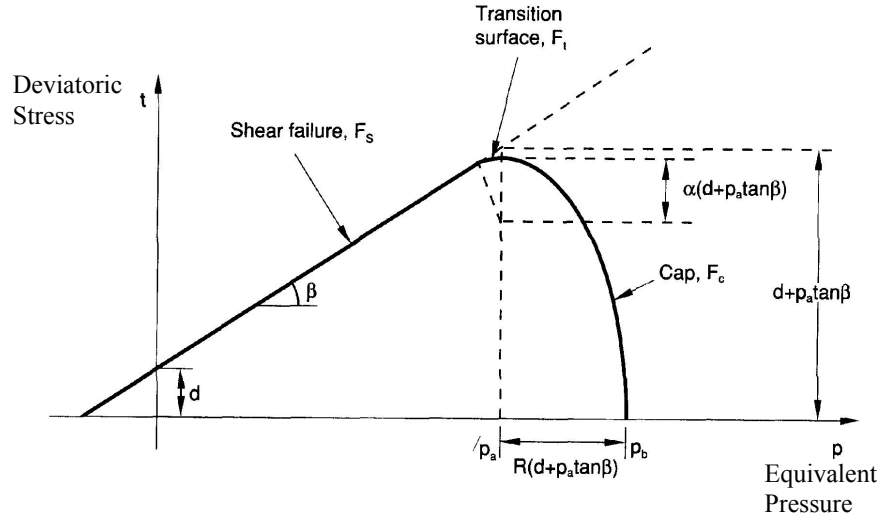


Figure 4-3 Cap model: yield surface in the p-t plane (ABAQUS, 1998)

4.1.1.3 Shaft-Rock Interaction and Loading

The interaction between drilled shaft and rock mass is modeled using a surface based contact. The shaft surface is treated as master surface, while the rock surface is taken as slave surface. In tangential direction of the shaft-rock interface, the frictional interaction is simulated using linear Coulomb friction theory, which needs an input of a coefficient of friction. In normal direction, the contact surfaces transmit no contact pressure unless the nodes of the slave surface are in contact with the master surface. There is no limit to the magnitude of contact pressure that can be transmitted when the surfaces are in contact (ABAQUS, 1998). The lateral loads are applied step by step after the gravity weight of the shaft-rock system is activated.

4.1.2 Validation of the 3D FEM Model

4.1.2.1 Load Test and Input Parameters

The field lateral load test results from Dayton test is used to validate the above 3D FEM modeling technique. The test drilled shaft is 6 feet in diameter and 18 feet in rock socket length. The elastic modulus and Poisson's ratio of the drilled shaft are 3800 ksi and 0.15, respectively. The rock mass at the test site is gray shale interbedded with limestone. The details of the test shaft dimensions and rock properties are presented in Fig. 4-4. An unconfined compression test on an intact rock sample provided q_u (unconfined compressive strength) of 5668 psi and E_i (elastic modulus of intact rock) of 590 ksi. The GSI and RMR values are also summarized.

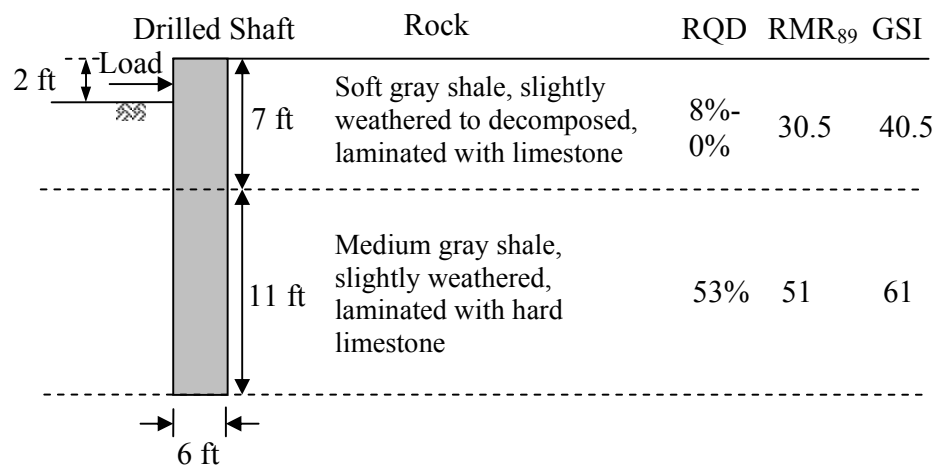


Figure 4-4 Drilled shaft dimension and rock profiles of the load test at Dayton

Based on the unconfined compression test, Mohr-Coulomb cohesion and friction angle of the rock mass, including the effects of joints, fillings, cracks, and other secondary structures of rock, can be correlated with Hoek-Brown (Hoek, et al., 2002) rock strength criterion using q_u , E_i , and GSI. By using free software RocLab (Rocscience, 2002), Mohr-Coulomb cohesion, c , and friction angle, ϕ , of the two layers of rock mass

were determined and are summarized in Table 4-1. The Drucker-Prager cohesion, d , and friction angle, β are estimated using Eqs. (4-6) and (4-7). The elastic modulus of rock mass E_m is also obtained using RocLab, which employs Hoek et al. (2002) empirical correlation equation based on q_u and GSI.

The Poisson's ratio of the rock mass is assumed to be 0.3. Due to the lack of hydrostatic tests on rock mass samples, the stress-strain curve of the unconfined compression test is used to represent isotropic hardening curve. The input pairs of the hydrostatic compression yield stress (p_b , in psi) and volumetric inelastic strain (ϵ_{in}) for the hardening curve are as follow: (1000, 0), (1500, 0.004), and (1900, 0.01). To simplify the contact interaction, the entire side interface between the drilled shaft and rock mass is simulated using one contact modeling; and a second contact modeling is used to simulate the interaction between shaft tip surface and rock mass. A coefficient of friction of 0.5 is used based on the Mohr-Coulomb friction angle of 27° of the bottom rock layer. The water table was above the surface of rock mass; therefore, the effective unit weight of 0.034 pci is used in analysis.

Table 4-1 Rock Mass Properties

Rock Layer	Mohr-Coulomb		Drucker-Prager		E_M (ksi)
	c (psi)	ϕ ($^\circ$)	d (psi)	β ($^\circ$)	
Top layer	154	20	440	38	241
Bottom layer	251	27	819	47	590

4.1.2.2 Simulation and the Results

The mesh sensitivity is studied by comparing FEM results based on varying the number of elements. It is found that the mesh with 1885 elements provides almost the same results on lateral deflections of the drilled shaft under lateral loads as the mesh with

2765 elements, as shown in Fig. 4-5. Therefore, it is believed that FEM simulation results are not sensitive to mesh density.

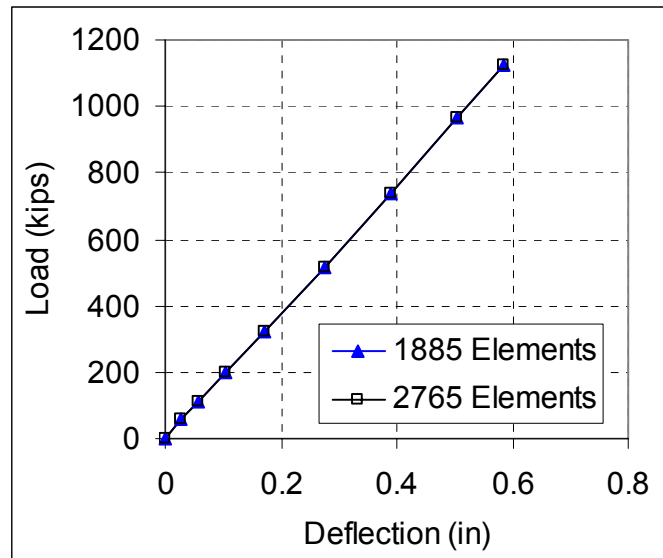


Figure 4-5 Mesh convergence

With the constitutive model parameters described previously, the FEM predicted load-deflection curve at the shaft head is compared with the measured one, as shown in Fig. 4-6. It can be seen that the predicted load-deflection curve is comparable to the measured. A good match of the deflection profiles along depth between the FEM predicted values and the inclinometer measured values is also evident, as shown in Fig. 4-7. Although, in general, the 3D FEM model predicted the deflection response of drilled shafts in rock under lateral loads, the early portion of nonlinear lateral response was not captured. This was attributed to the lack of a hydrostatic compression test to determine an accurate hardening curve for the rock mass. A back analysis is performed to match the entire range of lateral deflection response of the drilled shaft. With improved hardening curves, a good match of the load-deflection curve at the head of the shaft is obtained, as

shown in Fig. 4-6. The hardening curve of the top rock layer is adjusted to the following p_b (in psi) and ϵ_{in} pairs: (120, 0), (260, 0.01), and (400, 0.02). The cohesion of the top rock layer is reduced to 100 psi.

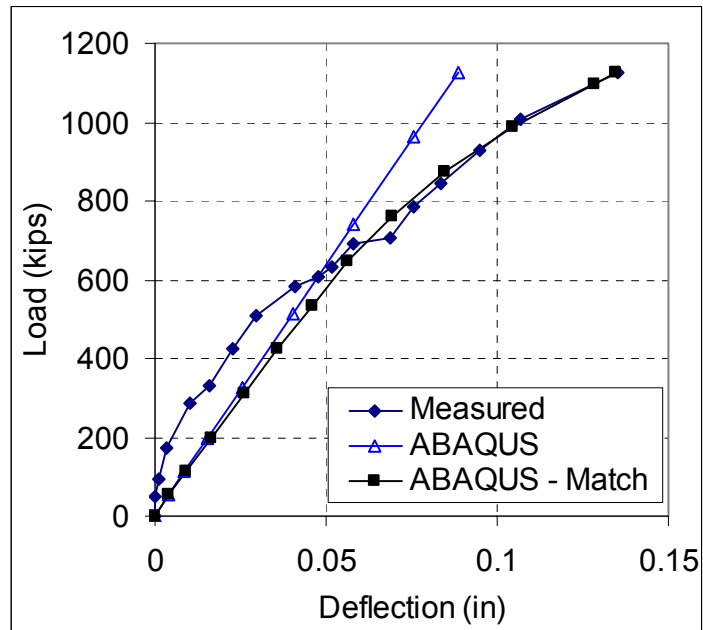
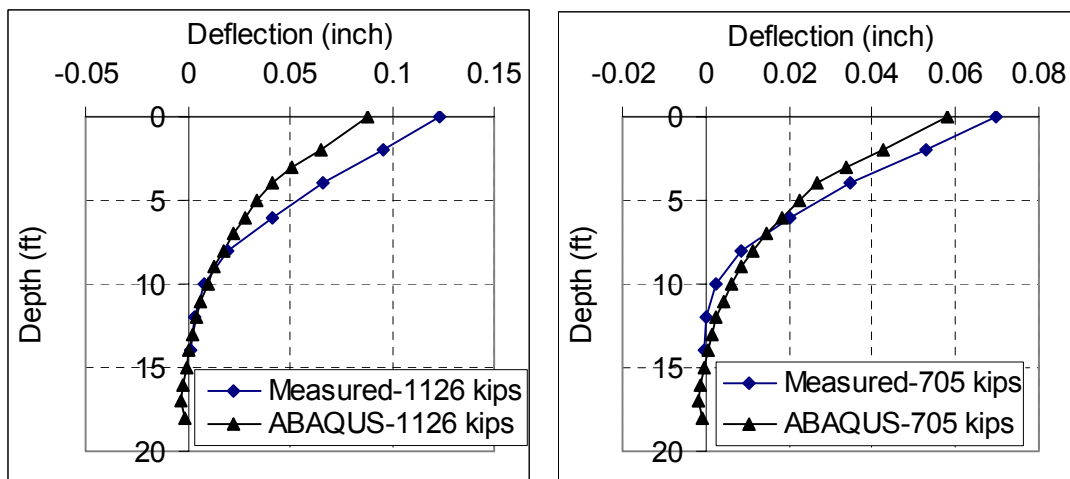


Figure 4-6 Comparison of load-deflection curves at shaft head



(a) Load at 1126 kips

(b) Load at 705 kips

Figure 4-7 Comparison of deflection profiles at the load of (a) 1126 kips and (b) 705 kip

4.2 Failure Modes of Rock Subjected to Loading from Laterally Loaded Drilled Shafts

Very few research has been focused on the failure modes of rock mass surrounding the drilled shafts under lateral loads. Generally, rock-socketed drilled shafts under lateral loads may fail either due to structural failure of shaft or strength failure of rock. Attention here is given to the later type of failure.

Carter and Kulhawy (1992) assumed that compressive failure will occur for rocks in front of shaft and shear failure will occur for interface between shaft and rock. Zhang et al. (2000) adopted Carter and Kulhawy (1992)'s assumption in their relevant theoretical work. However, Reese (1997) assumed compressive failure of rock, but ignored shear failure between shaft and rock. For jointed rock mass, To et al. (2003) proposed a wedge type failure.

Two types of rock will be investigated in FEM simulation of rock failure modes: one is intact rock or highly weathered rock that can be modeled as isotropic and homogeneous rock, and the other one is jointed rock with a set of parallel weak planes. For each type of rock, two conditions are considered: one is that the drilled shaft is fully socketed into rock, the other one is that the drilled shaft socketed into rock with overburden soils.

4.2.1 Failure of Isotropic and Homogeneous Rock without Overburden Soils

4.2.1.1 Finite Element Modeling

A drilled shaft with 30 in. diameter and 15 feet socket length is modeled using linear elasticity with elastic modulus of 4000 ksi. The Modified Drucker-Prager Model (CAP Model) is utilized to model the isotropic and homogeneous rock. The elasticity modulus of rock is assumed to be 2000 ksi; and the Mohr-Coulomb cohesion and friction angle are

assumed to be 1 ksi and 27 degree, respectively. The element type C3D15 and C3D8 are used to model drilled shafts and rock, respectively. The load applied to the top of shaft is increased from 300 kips to 3000 kips, at which time computer analysis failed to converge. Therefore, the analysis results at 3000 kips of loading level, are used to examine the failure conditions in the rock.

4.2.1.2 Failure at the Top Layer of the Rock

At the failure load of 3000 kips, the rock in front of the shaft shows a forward and upward movement according to the deformed and undeformed rock mass shown in Fig. 4-8.

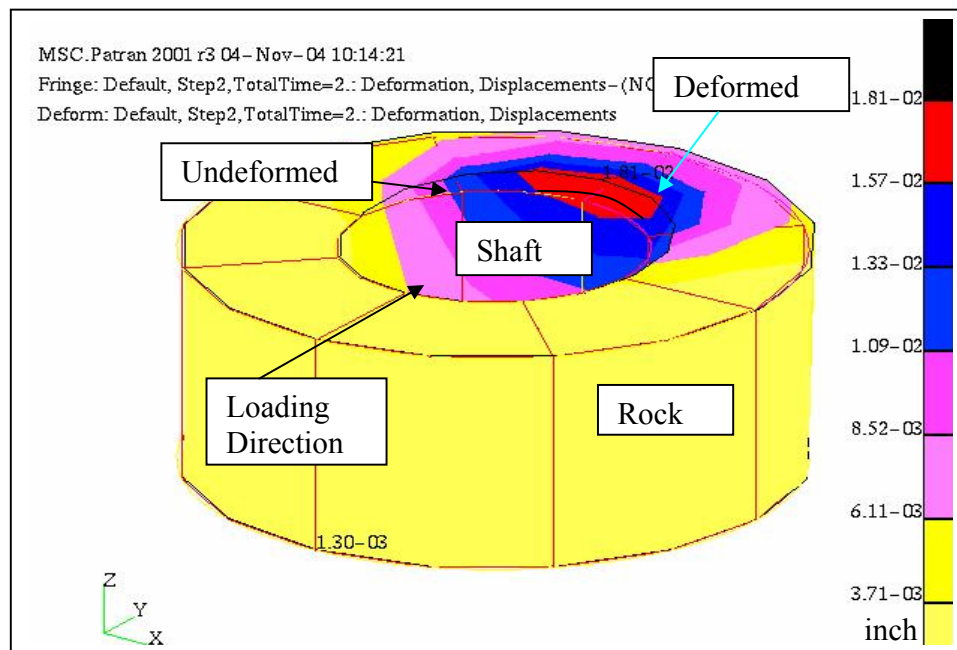


Figure 4-8 The forward movement of rock mass

Apparently, it is highly likely that without overburden soil layer on top of rock, the rock in front of the shaft will move forward under the lateral loads. Fig. 4-9 shows the

front view of the upward movement of rock mass, in which the movement is scaled up to 150 times of the original magnitude of movement.

From Figs. 4-8 and Fig. 4-9, it can be seen that a wedge type of rock mass has the tendency to move away from its original position. However, for this to happen, the rock in vertical xz plane, shown in Fig. 4-8, has to reach tensile failure; and the inclined planes of the wedge have to reach shear failure. In order to check whether the rock in xz plane surrounding the shaft can reach tensile failure, the stress distribution in rock is shown in Fig. 4-10. It can be seen that the tensile stress is developed. The magnitude of the maximum tensile stress is 2763 psi which is about half of the maximum compressive stress 5830 psi in front of the shaft. Usually, the uniaxial tensile strength of rock is about one tenth of the uniaxial unconfined compressive strength of rock. Therefore, in this case, the tensile failure is more likely to appear before the onset of compressive failure.

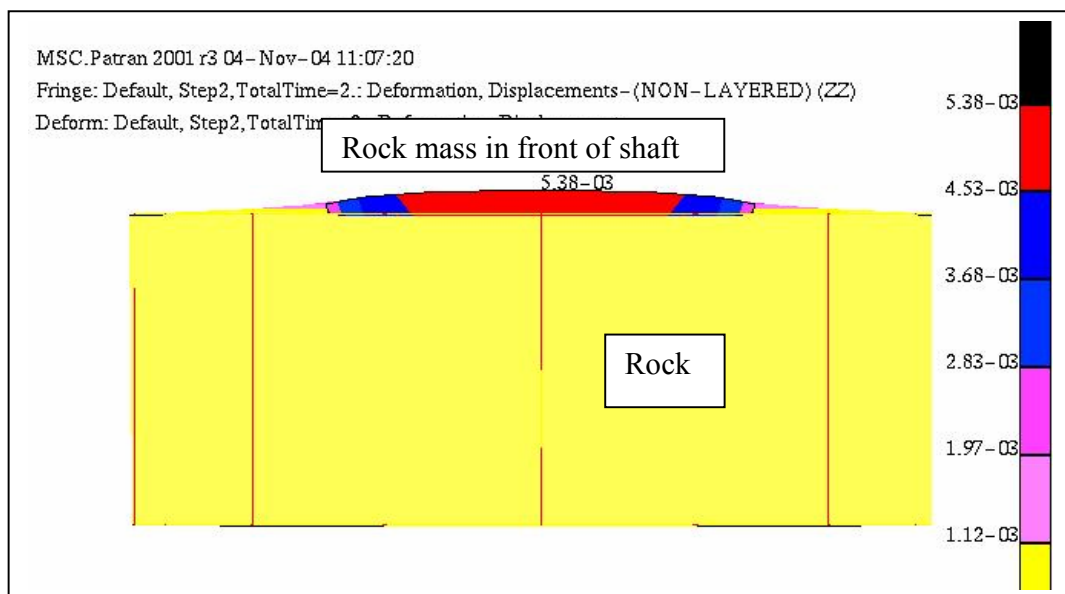


Figure 4-9 Front view of upward movement of rock mass

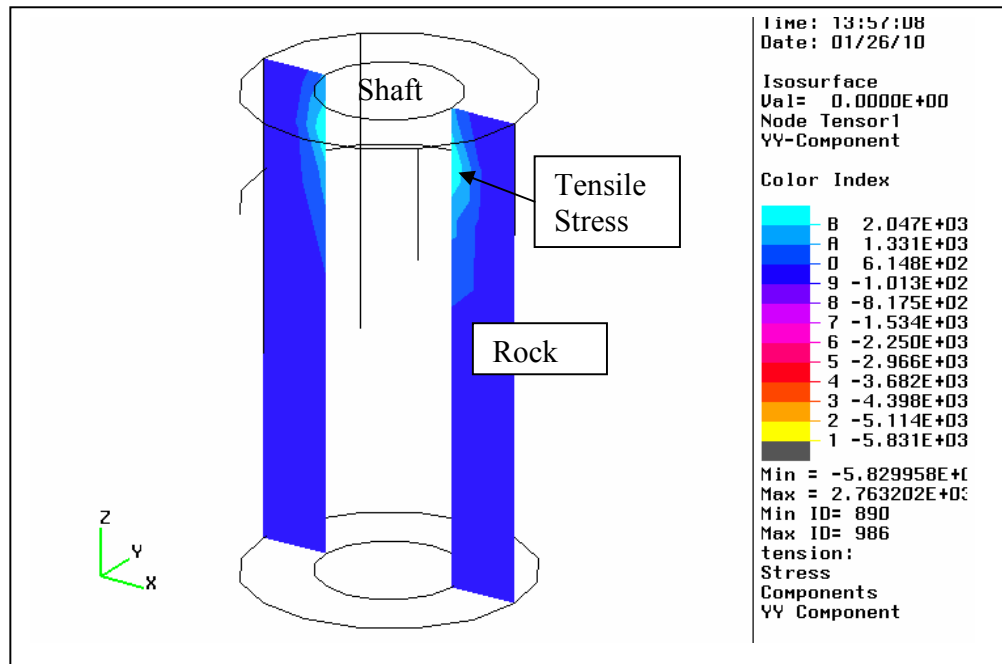


Figure 4-10 Y direction stress distribution in xz plane

Additionally, in order to confirm the proposed wedge type failure, one needs to check if the shear stress is concentrated on shear planes. Fig. 4-11 shows the maximum shear stress distribution on yz plane. It can be seen that the distributions of shear stresses at three planes are similar, which means that the bottom surface of the wedge is likely to be a plane rather than a curved surface. Although, it can not be concluded from Fig. 4-11 that the rock will be sheared out, the upward and forward movements of this portion of rock, together with the depicted shear distribution, implies a possible failure mode shown in Fig. 4-12.

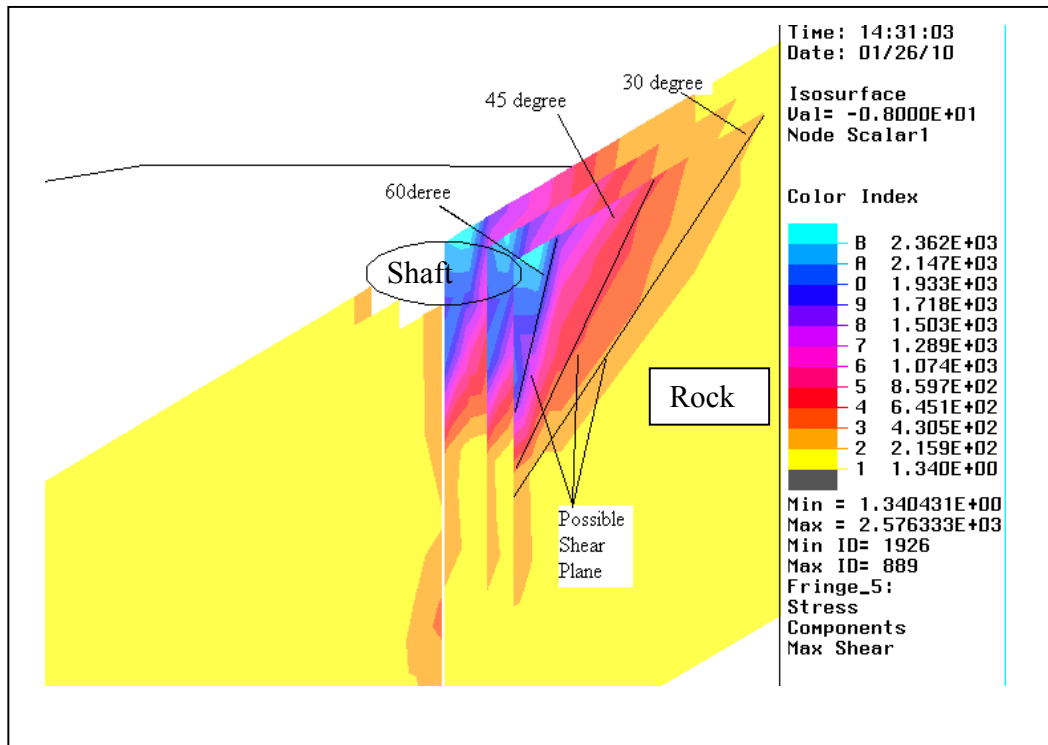


Figure 4-11 Maximum shear stress distribution on yz plane

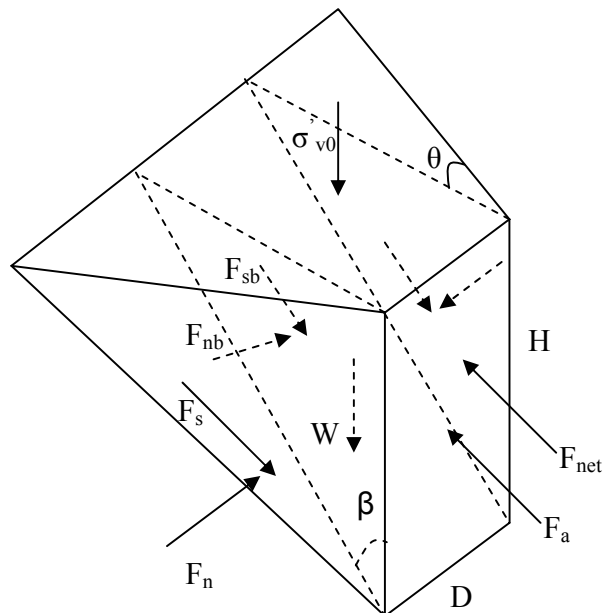


Figure 4-12 Proposed wedge type failure model for the top layer of rock

4.2.1.3 Failure of Rock at Great Depth

Generally, the wedge type of failure is unlikely to occur in rock at great depth due to overburden pressure from top layers of rock. Possible failures of in-depth rock can be tensile failure, compressive failure, or both. A separate FEM model was established in order to realize material failure of rocks.

A 5 feet long drilled shaft segment with 30 inch diameter is embedded in isotropic rock mass with the same properties as the rock used in the previous model. The lateral load of 2000 kips, considered large enough to induce failure tensile stress in rock mass, is applied at the top of the shaft segment. The in-situ vertical pressure, which is equivalent to vertical pressure at 6 ft deep in rock mass, plus self weight of shaft and rock, is applied at the top surface of the shaft and rock.

As can be seen in Fig. 4-13, the maximum tensile stress in rock surrounding the shaft is about 42% of the maximum compressive stress. The magnitude of the maximum tensile stress is 1610 psi, which is considered large enough to produce crack since the tensile strength of most rocks ranges from 725 psi to 2900 psi (Afrouz, 1992). However, the compressive strength is usually one order of magnitude higher than the tensile strength. Therefore, the tensile failure of the rock mass will occur first for in-depth rock layers.

Even with initiation and propagation of cracks in rock; the rock mass in front of shaft is still able to sustain loads. In order to identify the stress redistribution after the crack appears, the FEA model is modified to simulate a 10 inch long crack at the tensile failure areas. Fig. 4-14 shows the predefined cracks after applying 2000 kips of lateral loading. The stress in loading direction is redistributed as shown in Fig. 4-15, from which

it can be seen that the maximum tensile stress is decreased from 1610 psi to 540 psi. Because the tensile stress of 540 psi will be less than the tensile strength of the rock, the cracks would stop to propagate and the loads is redistributed to the rock in front of shaft. Actually, the maximum compressive stress is increased from 3780 psi to 3850 psi and the maximum deflection increased from 0.0553 in. to 0.0581 in.

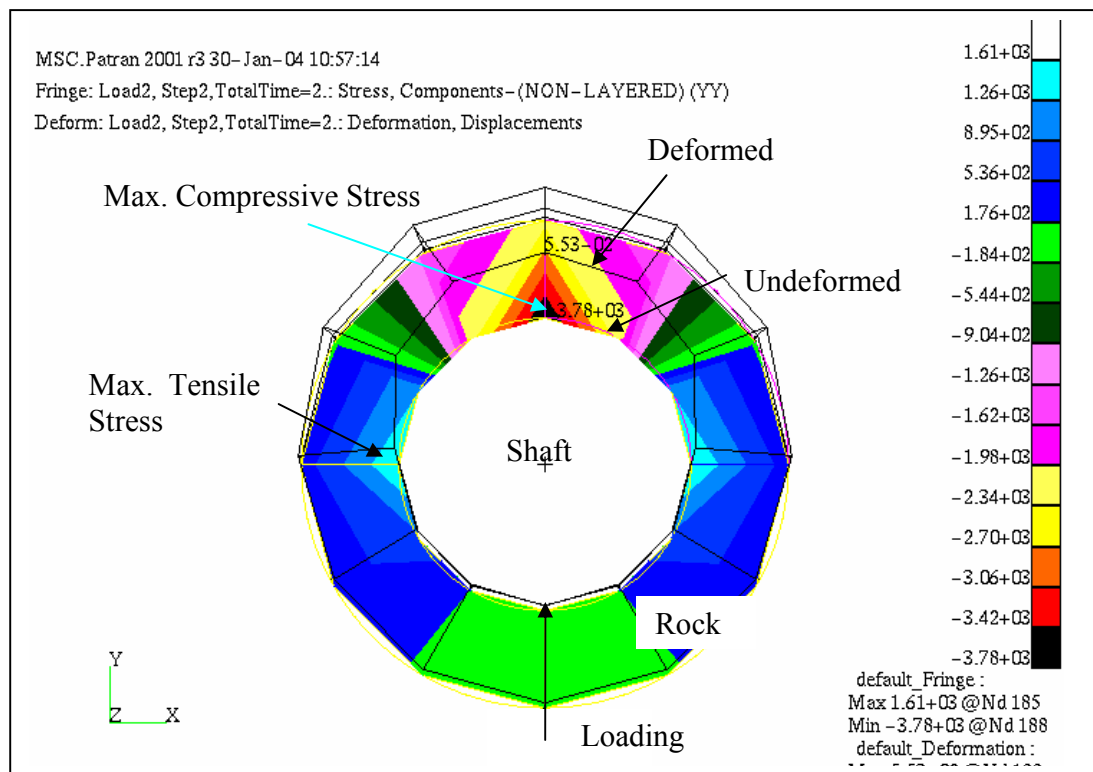


Figure 4-13 Stress distribution at Y direction of in-depth rock layer

Other than the tensile stress and compressive stress, the friction between shaft and surrounding rock mass is also developed during loading, as shown in Fig. 4-16. Although the maximum relative movement between shaft and rock is at point A, shown in Fig. 4-16, the maximum shear stress is developed at point B. Due to the applied lateral load, the normal pressure on point A is smaller than that at other positions in the interface surface.

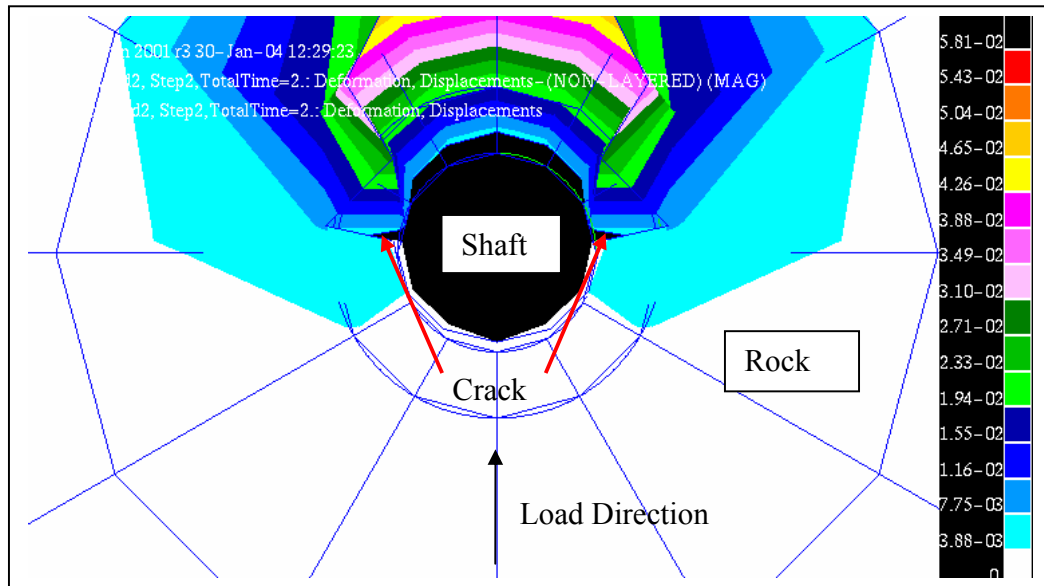


Figure 4-14 The predefined cracks

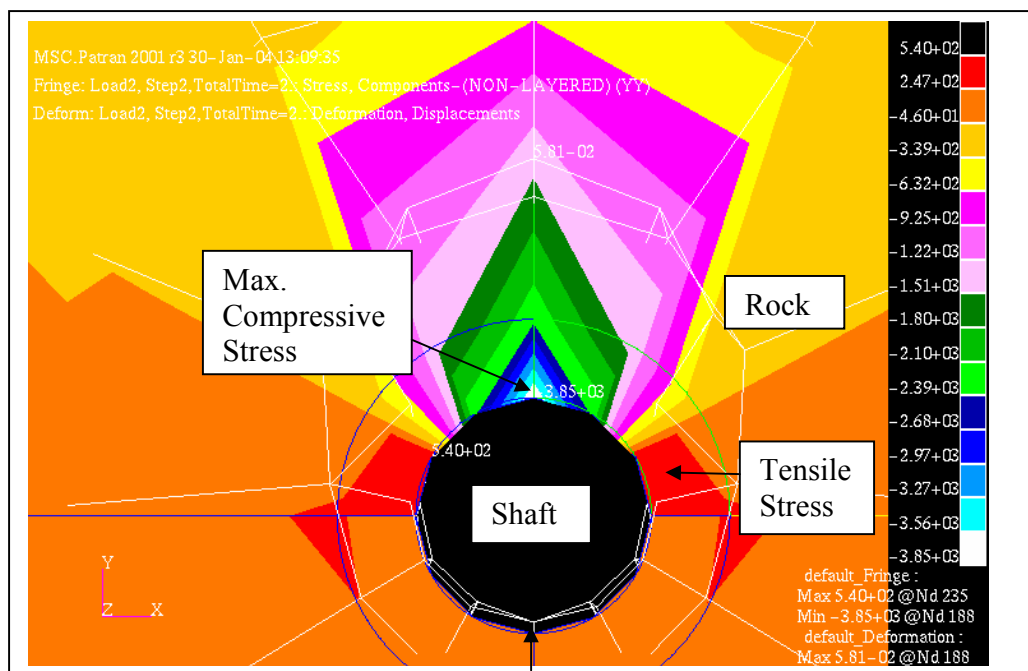


Figure 4-15 The stress redistribution at Y direction of in-depth rock layer after crack

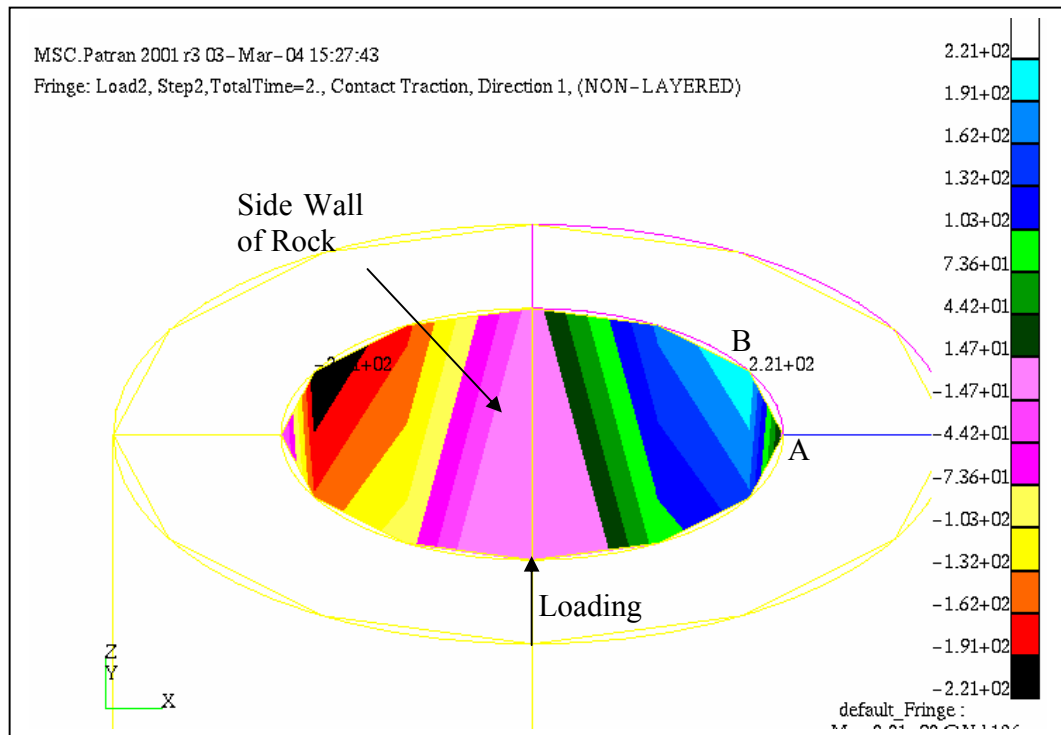


Figure 4-16 Friction distribution on the shaft-rock interface

4.2.1.4 Suggested Failure Mode for In-depth Layer of Isotropic Rock

Based on the above FEA analysis results, it is concluded that tensile failure of rock would occur first. Then the maximum friction between shaft and rock would be reached. Finally, the maximum compressive stress would reach the compressive strength of rock. Therefore, the ultimate capacity of in-depth rock mass in resisting lateral loaded shaft can be credited to compressive strength and friction between shaft and rock. This is in conformance with the assumption made by Carter and Kulhawy (1992). Based on the distributions of compressive stress shown in Fig. 4-13 and friction shown in Fig. 4-16, the normal and shear stress distribution at failure is proposed as that shown in Fig. 4-17.

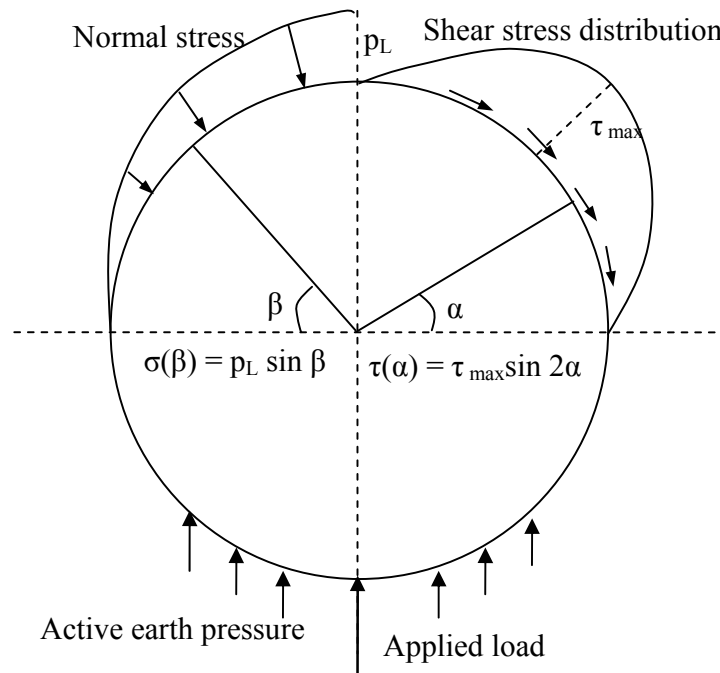


Figure 4-17 Suggested stress distribution at failure at great depth

4.2.2 Failure of Jointed Rock without Overburden Soils

4.2.2.1 Jointed Material Model in ABAQUS

The jointed material model in ABAQUS is intended to provide a simple continuum model for a material containing a high density of parallel joint surfaces where each system of parallel joints is associated with a particular orientation, such as sedimentary rock. The jointed material model assumes that the spacing of the joints of a particular orientation is sufficiently close compared to characteristic dimensions in the domain of the model such that the joints can be smeared into a continuum of slip systems.

The model is intended primarily for applications where the stresses are mainly compressive. A joint will be open when the stress normal to the joint tries to become tensile. Once a joint opens, the retained shear modulus on the joint is governed by the shear retention parameter, f_{sr} . If $f_{sr} = 0$, it means that no shear stiffness is associated with

open joints, on the other hand, when $f_{sr} = 1.0$, it corresponds to elastic shear stiffness in open joints.

The failure surface for sliding on joint system a is defined by:

$$f_a = \tau_a - p_a \tan \beta_a - d_a = 0 \quad (4-8)$$

where τ_a = the shear stress on the joint surface; p_a = the normal pressure across the joint; β_a = the friction angle for system a, and d_a = the cohesion for system a.

In addition to the joint systems described in the above, the jointed material model includes a bulk material failure mechanism, which is based on the Drucker-Prager failure criterion. The friction angle, dilation angle, and cohesion for the bulk material constitute the required input parameters.

4.2.2.2 The Modeling of Drilled Shafts in Jointed Rock Mass

The same physical model used in the previous section for drilled shaft in isotropic rock mass is used for this study. On notable change, however, is that the rock mass model is changed from CAP Model to Jointed Material model. For jointed material model, the bulk failure, joint surface failure, and shear retention are the required input parameters. In this study, one horizontal bedded joint system is assumed. For the bulk failure, the cohesion is 2 ksi and friction angle is 27 degree. For joint surface failure, same friction angle and 50% of cohesion of the input for bulk failure are assumed.

When the shear retention factor was assumed to be 0.8, the model can only be converged for the applied lateral load up to 57 kips. This is a small load for a 3 ft diameter and 15 ft long drilled shaft socketed into rock. Considering that the weak surface of jointed rock mass has been characterized by joint surface failure criterion, the shear retention is set to be 1.0 so that no shear stiffness is reduced when tensile stress is

developed across the joint surface. This change in modeling technique allows the applied load to be up to 1000 kips.

4.2.2.3 Failure at Top Layer of Jointed Rock Mass

As it can be expected, the top layer of rock mass in front of drilled shaft experiences the forward movement. Similar to the case of isotropic rock, the rock mass, which is mobilized to move forward, exhibits upward movement beyond the ground level. The mobilized maximum upward movement is 0.01 inch under 1000 kips of lateral loading. This is much larger than the upward movement of 0.0076 inch for the shaft in isotropic rock mass under 3000 kips loading. One could infer that the joint plane significantly increases the displacement of rock mass under lateral loads.

Similar to the situation of isotropic case, it is reasonable to guess a wedge type of rock mass that has the tendency to move out from its original position. In order to have a wedge to be sheared out, the shear surface has to be formed and the backside of the wedge has to be in tensile failure. Fig. 4-18 presents the tensile stress developed at the backside of the wedge. It can be seen that the maximum tensile stress is around 1181 psi, which is about 31% of the maximum compressive stress of 3858 psi developed in front of the shaft. The tensile failure of the backside of the wedge, therefore, is more likely to occur before the compressive failure of the rock in front of the shaft can materialize. This is simply due to the fact that the uniaxial tensile strength of rock is usually one tenth of the uniaxial unconfined compressive strength of rock.

It should be noted that the shear plane of the wedge has to be developed in order to form a wedge type of failure. Fig. 4-19 shows the contours of maximum shear stress concentration. It can be seen that the possible shear plane can be 45° to 60° . The upward

movement, forward movement, possible tensile failure of rock on xz plane, and the maximum shear concentration all support the notion of the development of a wedge type of failure.

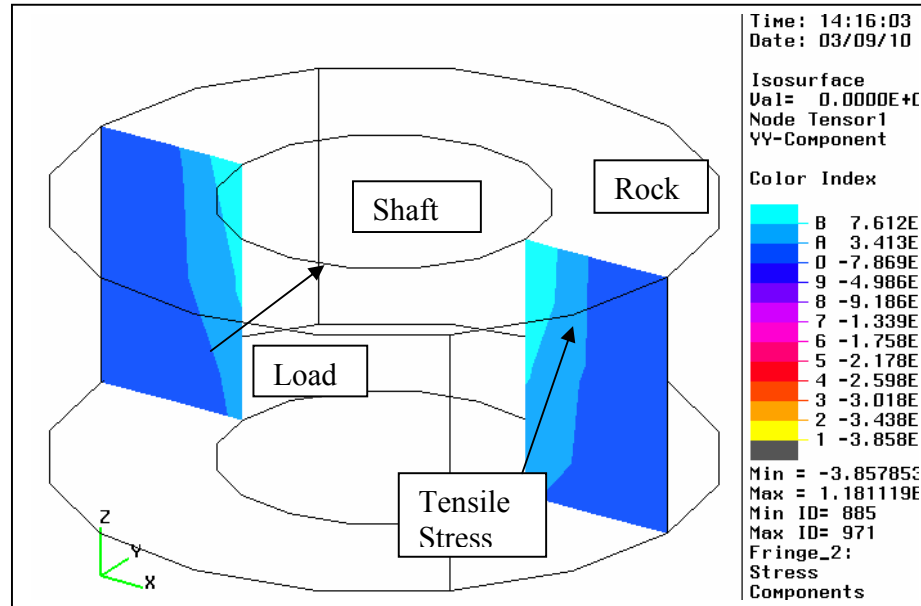


Figure 4-18 Tensile stress on xz plane for jointed rock mass case

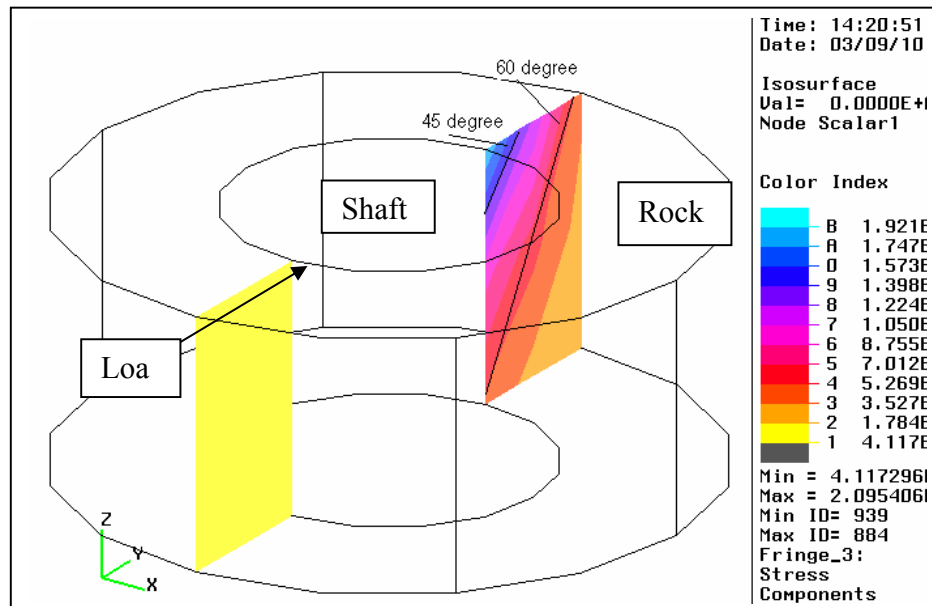


Figure 4-19 Maximum shear stress concentrations for jointed rock mass case

4.2.2.4 Suggested Failure Mode for Jointed Rock Mass

Based on the above analysis results of drilled shaft in horizontally jointed rock mass, the wedge type of failure is suggested for the top rock failure under lateral loads. For jointed rock mass with non-horizontal joints, several similar 3D FEA analyses were carried out, unfortunately, similar analysis results as the one of horizontally jointed rock mass were obtained. It appears that the FEA modeling technique is not capable of identifying the effects of joint direction. At this stage, the suggested failure mode for horizontally jointed rock could be applied to rock mass with different joint directions with a great caution.

4.2.2.5 The In-depth Failure of Jointed Rock Mass

Similar to the analysis for in-depth failure of isotropic rock mass, a shaft cylinder with 5 feet length and 30 inch diameter embedded in jointed rock mass is created to simulate the in-depth situation. The overburden pressure, which is equivalent to the pressure at 6 feet deep in the jointed rock mass, is applied to the top of rock-shaft system together with the selfweight of the rock and shaft. The stress distribution at loading direction is similar to the case of isotropic rock, as shown in Fig. 4-13. The computed maximum tensile stress surrounding shaft was 33% of the maximum compressive stress. The magnitude of tensile stress of 870 psi is believed to be able to produce cracks, as the uniaxial tensile strength of most rocks ranges from 725 psi to 2900 psi (Afrouz, 1992). Cracks and even tensile failure, therefore, are likely to appear earlier than other types of failure for in-depth jointed rock mass.

When the cracks start to propagate, the rock mass in front of the shaft would still be able to sustain the applied load. In order to identify the stress redistribution after the crack

propagates, the FEA model is modified to simulate a 10 inch long crack at the tensile failure areas. Similar to the case of isotropic rock, the maximum tensile stress is decreased from 870 psi to 326 psi, which is less than the tensile strength of most rock. On the other hand, the maximum compressive stress is increased from 2620 psi to 2790 psi.

Other than the tensile stress and compressive stress, the friction between shaft and surrounding rock mass is also developed during loading. Similar to the situation of isotropic rock, the maximum shear stress is developed at point B rather than at point A, as shown in Fig. 4-16.

4.2.2.6 Suggested Failure Mode for In-depth Jointed Rock Mass

Based on the above FEA analysis results, one can conclude that failure mode for isotropic rock shown in Fig. 4-17, could be used for horizontally jointed rock mass. For those jointed rock with non-horizontal joints, the suggested in-depth failure mode for horizontally jointed rock may be used with caution.

4.2.3 Failure of Isotropic and Jointed Rock with Overburden Soils

For drilled shafts socketed into isotropic or jointed rock with overburden soils, the in-depth failure must be same as the condition of without overburden soils. The top rock layer, however, may experience in-depth failure due to the overburden pressure. Therefore, both top layer failure and in-depth failure, shown in Figs. 4-12 and 4-17, should be checked for the top layer rock mass; and the smaller value should be adopted.

4.3 Rock Strength Criteria

Several rock strength criteria have been developed in the past. Table 4-2 provides a summary of more prevalent rock strength criteria cited in literature. Among them, Hoek-

Brown criterion appears to be widely accepted since it has been revised many times and correlated with field data from its inception in 1980 (Hoek and Brown, 1980). Ramamurthy et al. (1985) criterion is particularly suitable for jointed rock mass; however, it requires conducting well-organized lab tests on samples with weak planes.

Table 4-2 Summary of Rock Strength Criteria

Criteria	Applications	Advantages	Limitations
Hoek-Brown (Hoek et al. 2002)	Intact rock and highly fractured rock mass	Improved several times; widely referred; calibrated with numerous data	Not applicable for anisotropic rocks
Ramamurthy et al. (1985)	Intact rock, rock mass, and jointed rock	Applicable for anisotropic rocks	Needs lab test on jointed rock samples
Johnston (1985)	Intact rock, rock mass	Only uniaxial strength of intact rock is required	Discontinuities are not well considered; not applicable for anisotropic rocks

4.3.1 Hoek-Brown Criterion

Hoek-Brown criterion has been developed and improved several times since its first version published in 1980. In 2002, Hoek et al. consolidated previous revisions on the criterion and proposed the following general form of Hoek-Brown criterion.

$$\sigma'_1 = \sigma'_3 + \sigma_{ci} \left(m_b \frac{\sigma'_3}{\sigma_{ci}} + s \right)^a \quad (4-9)$$

where σ'_1 = the major principal stress at failure; σ'_3 = the minor principal stress or confining pressure; σ_{ci} = the uniaxial unconfined compressive strength of the intact rock; m_b , s and a = material constants that depend on the characteristics of rock mass and can be estimated as follows (Hoek, et al., 2002).

$$m_b = \exp \left(\frac{GSI - 100}{28 - 14D_r} \right) m_i \quad (4-10)$$

$$s = \exp\left(\frac{GSI - 100}{9 - 3D_r}\right) \quad (4-11)$$

$$a = \frac{1}{2} + \frac{1}{6}(e^{-GSI/15} - e^{-20/3}) \quad (4-12)$$

where D_r is a factor depending upon the degree of disturbance to which the rock mass has been subjected due to blast damage and stress relaxation. It varies from 0 for undisturbed in situ rock masses to 1 for very disturbed rock masses. For deep foundation analysis, although the excavation releases the horizontal earth pressure on rock masses, the pouring of concrete restores the pressure. Therefore, the value of D_r is selected as 0 for applications in deep foundation analysis.

The material constant m_i used in Eq. 4-10 can be determined from triaxial tests (Hoek and Brown, 1997). When no laboratory test data are available, it can also be estimated from Table 4-3. The values shown in Table 4-3 can be varied ± 2 .

Table 4-3 Values of Constant m_i for Intact Rock (After Marinos and Hoek, 2000)

Sedimentary Rocks							
Anhydrite	12	Breccias	20	Chalk	7	Claystones	4
Conglomerates	21	Dolomites	9	Greywackes	18	Gypsum	10
Marls	7	Sandstones	17	Siltstones	7	Shales	6
Crystalline Limestones	12	Micritic Limestones	8	Sparitic Limestones	10		
Metamorphic Rocks							
Amphibolites	26	Gneiss	28	Hornfels	19	Marble	9
Metasandstone	19	Migmatite	29	Phyllites	7	Quartzites	20
Schists	10	Slates	7				
Igneous Rocks							
Agglomerate	19	Andesite	25	Basalt	25	Breccia	19
Dacite	25	Diabase	15	Diorite	25	Dolerite	16
Gabbro	27	Granite	32	Granodiorite	29	Norite	20
Obsidian	19	Peridotite	25	Porphyries	20	Rhyolite	25
Tuff	13						

4.3.2 Converting Hoek-Brown Criterion to Mohr-Coulomb Criterion

Mohr-Coulomb criterion expressed in terms of shear strength and normal stress is commonly used in geotechnical engineering disciplines. The Hoek-Brown criterion could be converted to equivalent Mohr-Coulomb criterion, as suggested by a method proposed by Hoek (1990).

$$\phi' = 90 - \arcsin\left(\frac{2\tau}{\sigma'_1 - \sigma'_3}\right) \quad (4-13)$$

$$c' = \tau - \sigma'_n \tan \phi' \quad (4-14)$$

where σ'_1 is in-situ vertical effective stress; σ'_1 can be obtained using Eq. (4-9); and

$$\sigma'_n = \sigma'_3 + \frac{(\sigma'_1 - \sigma'_3)^2}{2(\sigma'_1 - \sigma'_3) + 0.5m_b\sigma'_{ci}} \quad (4-15)$$

$$\tau = (\sigma'_n - \sigma'_3) \sqrt{1 + \frac{m_b\sigma'_{ci}}{2(\sigma'_1 - \sigma'_3)}} \quad (4-16)$$

4.4 Side Shear Resistance

According to the identified failure mode for in-depth rock mass layer, the side shear resistance between rock and shaft will contribute to some portion of the ultimate resistance of rock. However, there are very few published methods for predicting the horizontal side shearing resistance in the rock/shaft interface. Briaud and Smith (1983) measured the side shearing resistance by means of mounting pressure cells in the leading front of drilled shaft embedded in the soil. However, there was no available analysis method to account for side shear resistance of drilled shafts in rocks in the horizontal direction.

Fortunately, there are a lot of empirical methods and a few theoretical analysis methods available for estimating the side resistance of axially loaded drilled shafts. Johnston and Lam (1989a) proposed a theoretical procedure to estimate the side shear strength based on energy theory. An equivalent 2D model is used represent 3 dimensional interaction between rock and shaft, as shown in Fig. 4-20. In this model, the upper half can move only in a vertical direction against a spring which provides the constant normal stiffness to the system. The stiffness of the spring is selected to match the rock mass modulus and the socket geometry for a given drilled shaft problem, that is $K = \frac{E_m}{(1 + \nu_m)} \frac{1}{r}$. Where r is radius of shaft; E_m and ν_m are Young's modulus and Poisson's ratio of rock mass, respectively. Based on Mohr-Coulomb strength criterion and dilation energy theory, a series of formulas were developed to calculate side shear strength by Johnston and Lam (1989a).

In this method, a lot of parameters of rock mass were required as follows. This make the application of Johnston and Lam (1989a)'s method difficult.

q_u = Uniaxial compressive strength;

c_{sl} = Cohesion from triaxial test;

ϕ_{sl}^p = Peak angle of friction from triaxial test;

c_{sh} = Cohesion from direct shear test;

ϕ_{sl}^r = Residual angle of friction from triaxial test;

ϕ_{sh}^p = Peak angle of friction from direct shear test;

ϕ_{sh}^r = Residual angle of friction from direct shear test;

i = Asperity angle;

K = Normal stiffness of rock mass;

σ_{n0} = Initial normal stress.

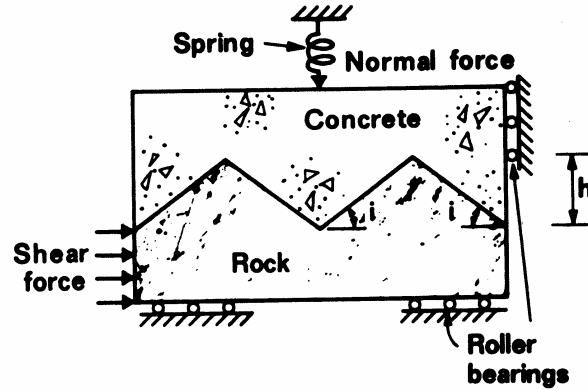


Figure 4-20 Concrete and rock joint

Comparing with complicated theoretical method proposed by Johnston and Lam (1989a), a lot of simple empirical equations have been proposed.

4.4.1 Empirical Equations for Axially Loaded Drilled Shaft in Rock

There exist several empirical relations between the ultimate vertical side shear strength, τ_{\max} , and unconfined compressive strength, σ_{ci} , of the intact rock. The relation could be expressed as $\tau_{\max} = \alpha \sigma_{ci}$, where $\alpha = 0.25$, according to Toh et al. (1987).

The power-curve relationships have also been proposed. Such as, $\tau_{\max} = 0.375\sigma_{ci}^{0.515}$ (Rosenberg and Journeaux, 1976) and $\tau_{\max} = 0.22\sigma_{ci}^{0.6}$ (Meigh and Wolshi, 1979), where τ_{\max} and σ_{ci} are in MPa.

Roughness of the wall of the excavated drill hole is an important factor controlling the development of vertical side shear resistance. Researches by Pell et al (1980) and Johnston and Lam (1989a and 1989b) have shown that the increase in side resistance could be significant from increase in roughness of the wall of excavated hole. From the

study of rock socket in mudstone and sandstone, Williams et al. (1980) found that smooth-sided sockets exhibit a brittle type of failure, whereas sockets having an adequate roughness exhibit ductile failure. Williams and Pells (1981) suggested that rough socket generates a locked-in normal stress such that there is practically no distinguishing difference between residual and peak resistance.

Pells et al. (1980) have used the size and frequency of grooves in a socket wall to classify wall roughness as R1, R2, R3, and R4, as defined in Table 4-4.

Table 4-4 Roughness Classes (After Pells et al., 1980)

Roughness Class	Description
R1	Straight, smooth-sided socket, grooves or indentation less 1.00 mm deep
R2	Grooves of depth 1-4 mm, width greater than 2 mm, at spacing 50 to 200 mm
R3	Grooves of depth 4-10 mm, width greater than 5 mm, at spacing 50 to 200 mm
R4	Grooves or undulations of depth greater than 10 mm, width greater than 10 mm, at spacing 50 to 200 mm

Kulhawy and Phoon (1993) developed a relatively extensive load test database for drilled shafts in soil and rock and presented their data both for individual shaft load tests and as site-averaged data. They concluded that the power curve relationship is closer to the real cases. On the basis of site-averaged data, the following equations for axially loaded drilled shafts in rock was proposed (τ_{\max} and σ_{ci} are in MPa).

$$\tau_{\max} = 0.45\sigma_{ci}^{0.5} \text{ for mean behavior} \quad (4-17)$$

$$\tau_{\max} = 0.67\sigma_{ci}^{0.5} \text{ for upper bound} \quad (4-18)$$

$$\tau_{\max} = 0.23\sigma_{ci}^{0.5} \text{ for lower bound} \quad (4-19)$$

Based on Kulhawy and Phoon (1993)'s database, Zhang (1997) suggested the following relation for smooth and rough socket conditions by using individual shaft load test data rather than the site-averaged data.

$$\tau_{\max} = 0.20\sigma_{ci}^{0.5} \text{ Smooth socket (R1, R2 or R3)} \quad (4-20)$$

$$\tau_{\max} = 0.80\sigma_{ci}^{0.5} \text{ Rough socket (R4)} \quad (4-21)$$

4.4.2 Suggested Empirical Equation for Side Resistance in Horizontal Direction

As described above, empirical correlations between uniaxial compressive strength of intact rock and unit shaft resistance of rock socketed drilled shafts measured in load tests could be expressed in a general equation as follow.

$$\tau_{\max} = \alpha\sigma_{ci}^{\beta} \text{ units in MPa} \quad (4-22)$$

For axially loaded drilled shafts in rock, the mobilization of side shear resistance is depicted in Fig. 4-21. On application of an axial load to the shaft, the shaft and rock mass will deform elastically until the shear stress at the interface causes slip. Fig. 4-21 also shows a drilled shaft section after a slip of the shaft relative to the rock takes place. Geometrical constraints require that this relative sliding to generate dilation at interface, and subsequent increase in socket diameter. This dilation occurs against a surrounding rock mass that must deform to compensate for enlargement of the socket diameter; therefore, resulting in an increase in normal stress at the shaft/rock interface (Johnston and Lam, 1989a), which significantly enhances the vertical side shear resistance. Additionally, to overcome the roughness of the socketed wall, the side shear resistance increases as the wall become rougher.

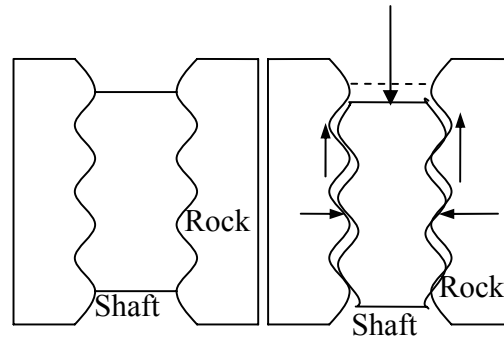


Figure 4-21 Displacement behavior of drilled shafts in rock (Johnston and Lam, 1989a)

For laterally loaded drilled shafts in rock, the relative displacement between the shaft and rock socket wall is in general parallel to the groove direction. There would be no or very small dilation taking place at the interface; therefore, roughness does not contribute much to side resistance in horizontal direction. However, the normal stress at the leading frontal side of drilled shafts will be increased because of the applied lateral loads, as shown schematically in Fig. 4-22. Therefore, the following empirical equation for predicting side shear resistance, τ_{\max} (psi), by Kulhawy and Phoon (1993), for mean behavior of rock is adopted.

$$\tau_{\max} = 5.42\sigma_{ci}^{0.5} \quad \text{where the units are in psi} \quad (4-23)$$

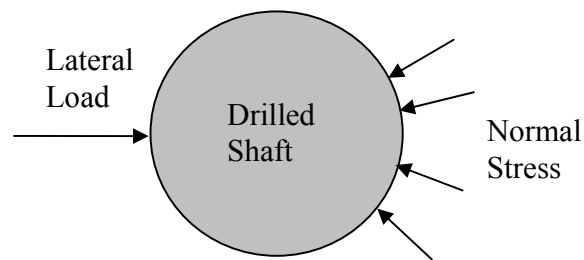


Figure 4-22 Increased normal stress due to lateral load

4.5 Ultimate Resistance of Rock Mass

4.5.1 Ultimate Resistance of Rock Near Surface

For highly fractured rock mass and competent rock, wedge type failure model for top rock layer was identified earlier in Fig. 4-12. In the figure, F_{net} is the total net rock resistance; D is the diameter of the drilled shaft; H is the height of the wedge; F_a is the active earth force exerted on the drilled shaft; F_s is the friction force on the sides of the wedge; F_n is the normal force applied to the sides of the wedge and is assumed to be equal to the at-rest earth force; F_{sb} is the friction force on the bottom face of the wedge; F_{nb} is the normal force on the bottom face of the wedge which is to be determined through force equilibrium on vertical direction; W is the weight of the wedge; σ'_{v0} is effective vertical soil pressure due to overburden soil on the top of rock and it is equal to zero if no overlying soils are present. According to force equilibrium in the loading direction, the net rock reaction can be determined as follows:

$$F_{\text{net}} = 2F_s \cos \theta \sin \beta + F_{sb} \sin \beta + F_{nb} \cos \beta - 2F_n \sin \theta - F_a \quad (4-24)$$

$$F_a = \frac{1}{2} K_a \gamma' D (H - z_0)^2 \quad (4-25)$$

$$F_n = K_0 \sigma'_{v0} A_s + \frac{1}{6} K_0 \gamma' H^3 \tan \beta \sec \theta \quad (4-26)$$

$$F_s = c' A_s + K_0 \sigma'_{v0} \tan \phi' A_s + \frac{1}{6} H^3 K_0 \gamma' \tan \phi' \tan \beta \sec \theta \quad (4-27)$$

$$F_{nb} = \frac{\sigma'_{v0} A_t + W + 2F_s \cos \theta \cos \beta + c' A_b \cos \beta}{\sin \beta - \tan \phi' \cos \beta} \quad (4-28)$$

$$F_{sb} = c' A_b + F_{nb} \tan \phi' \quad (4-29)$$

in which γ' is the effective unit weight of the rock mass; and

$$K_a = \tan^2(45 - \phi'/2) \quad (4-30)$$

$$K_0 = 1 - \sin \phi' \quad (4-31)$$

$$z_0 = \frac{2c'}{\gamma' \sqrt{K_a}} - \frac{\sigma'_{v0}}{\gamma'} \quad (4-32)$$

$$A_s = \frac{1}{2} H^2 \tan \beta \sec \theta \quad (4-33)$$

$$A_b = (D + H \tan \beta \tan \theta) H \sec \beta \quad (4-34)$$

$$A_t = (D + H \tan \beta \tan \theta) H \tan \beta \quad (4-35)$$

$$W = \gamma' \left(\frac{1}{3} H^3 \tan^2 \beta \tan \theta + \frac{1}{2} H^2 D \tan \beta \right) \quad (4-36)$$

The value of β was approximated as $45 + \phi'/2$ by Reese et al. (1974) for their wedge type of failure in sand. Hoek (1983) pointed out that the failure plane of rock is $45 + \phi'/2$ because rock mass also follows Mohr-Coulomb failure criterion. Bowman (1958) suggested values of θ from $\phi'/3$ to $\phi'/2$ for loose sand and up to ϕ' for dense sand for a similar wedge type of failure in soils. However, herein the value of θ is taken as $\phi'/2$ based on the case studies (to be discussed in detail in Chapter VI) of actual field test results. The values of ϕ' and c' can be obtained from Eqs. (4-13) and (4-14) by taking the value of σ'_3 to be the effective overburden pressure at the depth of $1/3H$, since the side surface is triangular in shape. In this study, the following equations are adopted for θ and β .

$$\theta = \frac{\phi'}{2} \quad (4-37)$$

$$\beta = 45 + \frac{\phi'}{2} \quad (4-38)$$

The ultimate resistance of rock mass per unit shaft length p_u (F/L) based on the wedge failure mode identified herein can be calculated as:

$$p_u = \frac{dF_{net}}{dH} = 2 \cos \theta \sin \beta \frac{dF_s}{dH} + \sin \beta \frac{dF_{sb}}{dH} + \cos \beta \frac{dF_{nb}}{dH} - 2 \sin \theta \frac{dF_n}{dH} - \frac{dF_a}{dH} \quad (4-39)$$

where

$$\frac{dF_a}{dH} = \gamma' K_a (H - z_0) D \quad (dF_a/dH \geq 0) \quad (4-40)$$

$$\frac{dF_n}{dH} = K_0 H \tan \beta \sec \theta (\sigma'_{v0} + \frac{1}{2} \gamma' H) \quad (4-41)$$

$$\frac{dF_s}{dH} = H \tan \beta \sec \theta (c' + K_0 \sigma'_{v0} \tan \phi' + \frac{H}{2} K_0 \gamma' \tan \phi') \quad (4-42)$$

$$\frac{dF_{nb}}{dH} = \frac{D \tan \beta (\sigma'_{v0} + H \gamma') + H \tan^2 \beta \tan \theta (2 \sigma'_{v0} + H \gamma') + c' (D + 2H \tan \beta \tan \theta) + 2 \cos \beta \cos \theta \frac{dF_s}{dH}}{\sin \beta - \tan \phi' \cos \beta} \quad (4-43)$$

$$\frac{dF_{sb}}{dH} = \tan \phi' \frac{dF_{nb}}{dH} + c' (D \sec \beta + 2H \tan \beta \sec \beta \tan \theta) \quad (4-44)$$

4.5.2 Ultimate Rock Resistance at Great Depth

For in-depth jointed rock with a set of parallel weak planes, heavily fractured rock mass and competent rock, the failure model shown in Fig. 4-17 is adopted. It is assumed that the ultimate resistance of rock is reached when both the maximum shear resistance between the drilled shaft and rock mass, τ_{max} , and the normal limit pressures of rock mass, p_L are reached. Therefore, the ultimate rock resistance per unit length, p_u , for in-depth rock can be computed as follows.

$$p_u = 2 \int_0^{\pi/2} p_L D / 2 \sin^2 \beta d\beta + 2 \int_0^{\pi/2} \tau_{max} D / 2 \sin(2\alpha) \cos \alpha d\alpha - p_a D \quad (4-45)$$

$$p_u = \frac{\pi}{4} D p_L + \frac{2}{3} D \tau_{max} - p_a D \quad (4-46)$$

where D = the diameter of a drilled shaft; p_a = the active horizontal earth pressure; Rankine's earth pressure theory can be used to obtain p_a as follows.

$$p_a = K_a \sigma'_v - 2c' \sqrt{K_a} \quad (4-47)$$

$$K_a = \tan^2 (45 - \Phi'/2) \quad (4-48)$$

where σ'_v = effective overburden earth pressure including the pressure induced by possible overlying soils. The normal limit pressure of rock mass, p_L , is the major principal stress at failure, σ'_1 , which can be calculated using Eq. (4-9) in which σ'_3 is equal to σ'_v . The ultimate shaft-rock interface friction in horizontal direction, τ_{\max} , can be estimated from Eq. (4-23). The effective cohesion c' needed in Eq. (4-47) can be calculated using Eq. (4-14) by taking σ'_3 equal to σ'_v .

Because the ultimate capacity calculated based on the presented in-depth failure model could be smaller than the one calculated based on wedge failure model; therefore, for the top layer of rock mass with or without overlying soils, the ultimate resistance of rock resistance per unit shaft length is determined as the smaller one of the values calculated from Eqs. (4-39) and (4-46).

4.5.3 Ultimate Resistance of Jointed Rock

For jointed rock with a set of parallel weak planes which dominate the behavior of rock mass under lateral loads, the above equations for p_u can still be used as long as the following modifications are made. For failure of rock mass at a great depth, the high overburden pressure will prohibit possible sliding failure on the weak planes. Eq. (4-46) for in-depth rock mass therefore would still work for jointed rock.

For rocks to follow the wedge type failure, the bottom plane of the failure wedge could be either within the rock mass or on a weak plane. It is suggested to calculate p_u for

both possible failure modes and choose the smaller value as the final p_u . For failure due to shearing through rock mass, Eq. (4-39) can be directly used. For failure shearing through a weak plane, the same wedge failure model shown in Fig. 4-12 can be used. Eq. (4-39) is still valid to calculate p_u , except angle β should become the inclination of the weak plane and the values of c' and ϕ' for the bottom face of the failure wedge should be those pertaining to properties of the weak planes. Specifically, those c' and ϕ' needed for Eqs. (4-43) and (4-44) should be the results of lab test on samples with a weak plane. However, those c' and ϕ' in Eq. (4-42) needed for the two sides of the failure wedge can be obtained using instantaneous cohesion and friction angle determined from correlations with Hoek-Brown strength criterion.

4.6 New Method for Predicting Lateral Capacity of Drilled Shafts in Rock

4.6.1 Free Head Boundary

To estimate the ultimate lateral resistance of a drilled shaft in rock with free head boundary condition, a numerical solution that is based on discretization technique is developed. The rock mass is modeled as n horizontal layers of rock with height h_i for each layer, as shown in Fig. 4-23. The ultimate resistance per unit thickness of each layer of rock p_i (F/L) can be calculated using Eqs. (4-39) and (4-46). The total resistance of each layer, Q_i , is equal to $p_i h_i$. If the drilled shaft is structurally in a yield condition under the applied lateral load, then the shaft is treated as a long or flexible shaft; otherwise, the shaft is considered as a short or rigid one. The procedure of the proposed method is presented as follows.

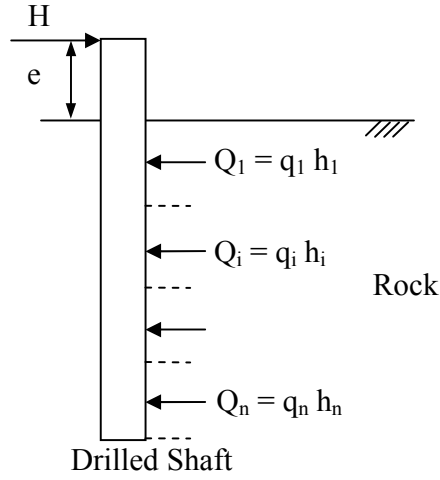


Figure 4-23 The Rock-Shaft Model

The first step is to assume the drilled shaft to be a short (rigid) one and find the ultimate capacity. Based on our observations from 3D FEA analysis and the lateral load test at Dayton, the drilled shaft rotates around some point (pivot) close to the bottom of the shaft, as shown in Fig. 4-24 (a). To calculate the lateral capacity of drilled shafts, the pivot point needs to be found. By taking the moment balance at the loading point, the pivot point can be easily determined as given in Eq. (4-49). The lateral capacity H_u can then be determined according to force balance equation given in Eq. (4-50).

$$\sum M = 0 \Rightarrow \sum_{i=1}^m Q_i L_i = \sum_{j=m+1}^n Q_j L_j \quad (4-49)$$

$$\sum Q = 0 \Rightarrow H = \sum_{i=1}^m Q_i - \sum_{j=m+1}^n Q_j \quad (4-50)$$

where e is the distance between the load point and ground surface; x_r is the depth of pivot point; and L_i is the distance between the loading point and concentration point of force Q_i ; m is the layer number of rock layer where the pivot point is located; n is the total number of rock layers.

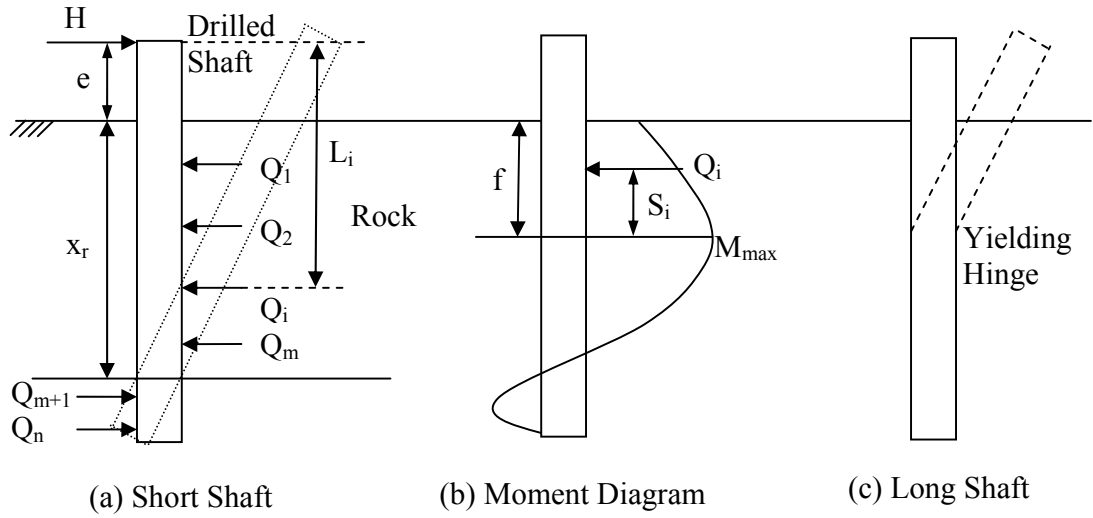


Figure 4-24 Lateral capacity calculation models for drilled shafts in rocks

The second step is to check whether the maximum moment of the drilled shaft exceeds the yielding moment of the shaft. If it does not, then the assumption of a short shaft is valid and the calculated H_u is the final estimate of capacity. Otherwise, the assumption of short shaft is not valid and a third step follows to obtain the capacity of the long drilled shaft.

The maximum moment of the drilled shaft is located at the section where shear force is zero, as shown in Fig. 4-24 (b). The depth f where shear force in the shaft is zero is located using the following equation:

$$H_u = \sum_{i=1}^o Q_i \quad (4-51)$$

where H_u is the calculated capacity in step one assuming the shaft is a rigid one; o is the layer number of the rock layer where f is located. A trial and error process can be used to solve Eq. (4-51). Then the maximum moment M_{max} is given by:

$$M_{\max} = H_u (e + f) - \sum_1^o Q_i S_i \quad (4-52)$$

where S_i is the distance between the concentration point of Q_i and the position of shaft where shear force is zero.

Step three is to calculate the lateral capacity for a long drilled shaft in which a plastic hinge appears at the location of maximum moment, as shown in Fig. 4-24 (c). An iterative process is used to find the capacity so that the computed maximum moment in shaft is equal to the yielding moment of the shaft, M_y . A new value of H_u which is less than that calculated in first step is assumed. Then step two is used to find the maximum moment corresponding to the new H_u . The final H_u for a long (flexible) drilled shaft is obtained when convergence is achieved (i.e., the calculated maximum moment is equal to the yielding moment of the drilled shaft).

4.6.2 Fixed Head Boundary

For the case of fixed head boundary condition, the following procedure can be used to determine ultimate lateral capacity. As before, the rock mass is modeled as n horizontal layers of rock with height h_i for each layer. The ultimate resistance per unit thickness of each layer of rock p_i (F/L) can be calculated using Eqs. (4-39) and (4-46). Then, the total resistance of each layer Q_i is equal to $p_i h_i$.

The first step is to assume the drilled shaft behaves as a rigid pile, as shown in Fig. 4-25. It is assumed that the drilled shaft will move rigidly in loading direction. The following two equations can be used to calculate the lateral capacity H_u and the maximum moment at the ground surface level. The value of M_{\max} needs to be less than

the yielding moment of the drilled shaft, otherwise the second step needs to be followed to calculate H_u .

$$H_u = \sum_{i=1}^n Q_i \quad (4-53)$$

$$M_{\max} = \sum_{i=1}^n Q_i L_i \quad (4-54)$$

where L_i is the distance between the ground surface and the loading point of Q_i .

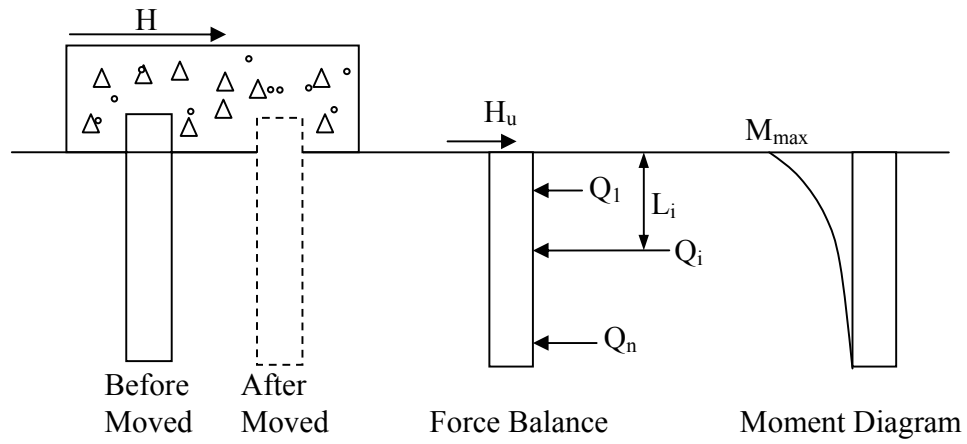


Figure 4-25 Capacity of rigid drilled shaft at fixed head boundary

In step 2, the drilled shaft is assumed to behave as shown in Fig. 4-26, where the drilled shaft rotates around a pivot point and the moment of shaft at the point right beneath the cap reaches the yielding moment. By taking moment balance at the loading point (the point beneath the cap), the rotation point can be easily determined as given by Eq. (4-55). The lateral capacity can be determined using Eq. (4-56). Additionally, the maximum moment M_{\max} shown in Fig. 4-26 needs to be less than the yielding moment M_y . The maximum moment of the drilled shaft is located at the section where shear force is zero. After the location of M_{\max} is found using Eq. (4-51), the value of M_{\max} can be

easily determined using Eq. (4-57). If the maximum moment is greater than the yielding moment, the third step needs to be followed.

$$\sum M = 0 \Rightarrow M_y + \sum_{m+1}^n Q_i L_i = \sum_1^m Q_i L_i \quad (4-55)$$

$$H_u = \sum_1^m Q_i - \sum_{m+1}^n Q_i \quad (4-56)$$

$$M_{\max} = H_u \cdot f - \sum_1^0 Q_i S_i - M_y \quad (4-57)$$

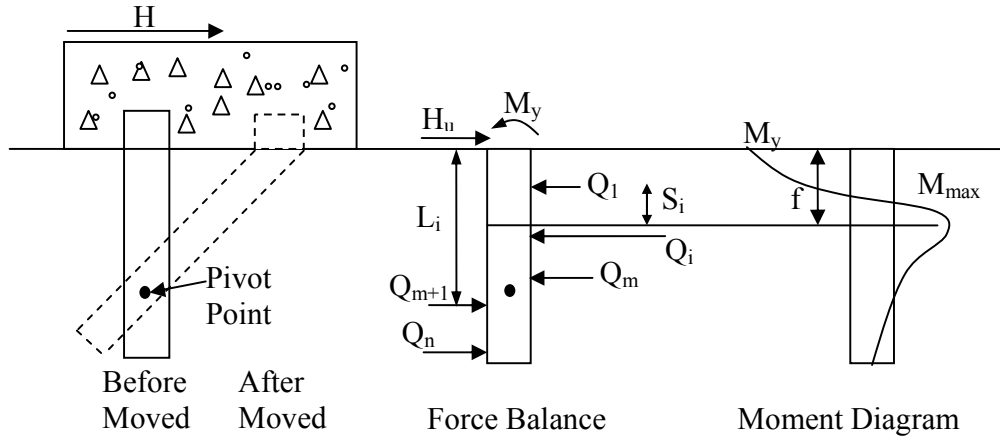


Figure 4-26 Capacity of intermediate length drilled shaft at fixed head boundary

Step 3 assumes the drilled shaft behave as a long pile, as shown in Fig. 4-27. The drilled shaft will have two yielding points: one is located at the top of the drilled shaft or the loading point; the other one is located at certain depth where shear force is zero. Assume a value of H_u which is less than the value of H_u calculated in Step 2. Next, find the location where shear force is zero and the corresponding maximum moment at that location using Eqs. (4-51) and Eq. (4-57). Repeat this procedure until the calculated maximum moment is equal to the yielding moment. The final value of lateral capacity H_u is then obtained after the iteration is converged.

The proposed method is not only suitable for drilled shafts entirely socketed in rock, but can also be used for drilled shafts in rock layers with overlying soils. Although the developed method is somewhat time consuming for hand calculation, a spreadsheet or computer program can be easily developed to facilitate calculation.

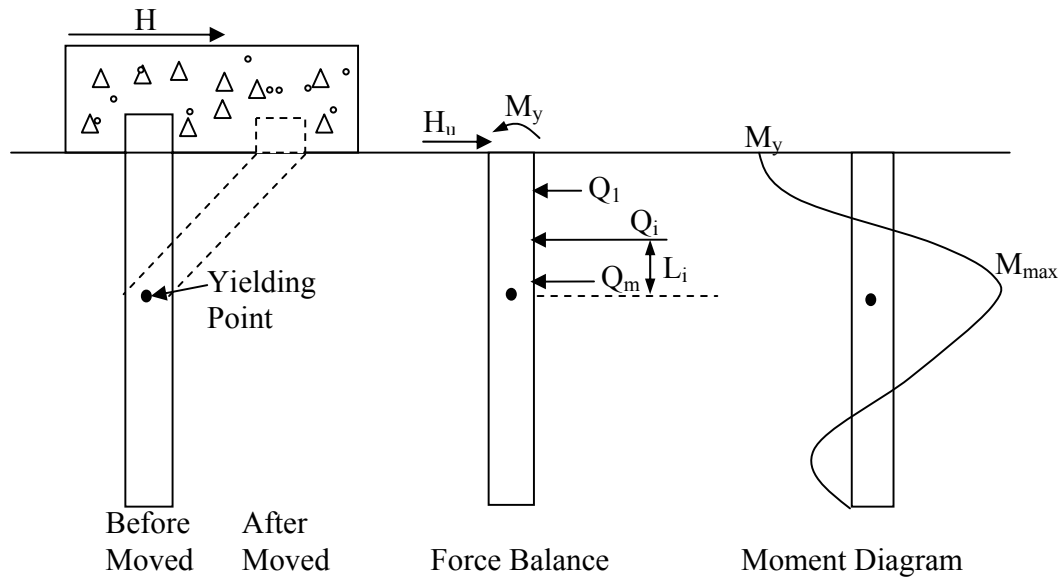


Figure 4-27 Capacity of long drilled shaft at fixed head boundary

4.7 Ultimate Reaction of Soils

To make the lateral capacity prediction method presented above to be applicable to soils, the following sections describe the methods for estimating the ultimate reaction of clay, sand, and $c-\phi$ soils.

4.7.1 Ultimate Resistance of Clay

Baguelin et al. (1977) examined the mechanism of the lateral reaction of piles in an elasto-plastic medium. It was found that the soil resistance is composed of the resistances from both normal and tangential directions, as shown in Fig. 4-28.

By integrating the stress distribution as shown in Fig. 4-28, the total ultimate soil resistance per unit shaft length, p_u , can be calculated as:

$$p_u = \frac{\pi}{4} D(p_L + \tau_{\max}) \quad (4-58)$$

where p_L = ultimate normal resistance of soil; τ_{\max} = ultimate shear resistance of soil.

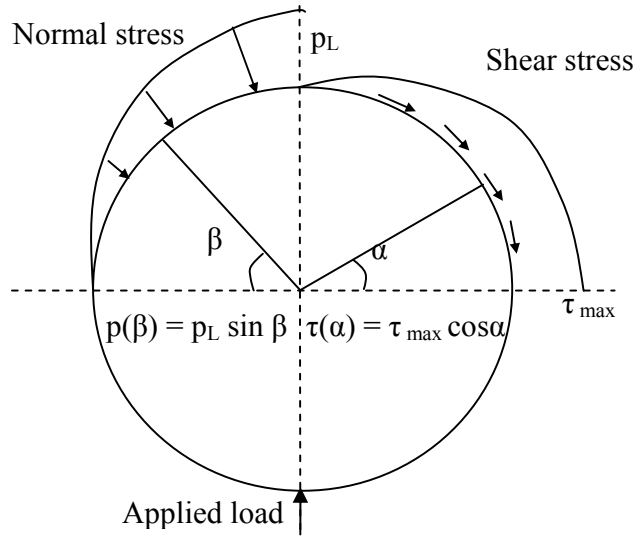


Figure 4-28 Distribution of lateral reaction stresses

The theoretical equation for calculating ultimate soil normal resistance by Reese et al. (1975) is used herein. Based on the wedge failure mode, the limit resistance of top soil layer, p_{Lt} , is given by:

$$p_{Lt} = 2S_u + \gamma'z + \frac{2.83S_u z}{D} \quad (4-59)$$

where S_u is undrained shear strength of clay; and z is the depth under consideration. Based on the flow-around type failure for clay exists at a great depth, the limit resistance of in-depth clay, p_{Ld} , is given by:

$$p_{Ld} = 11S_u \quad (4-60)$$

The final value of p_L is selected as the smaller value of p_{Lt} and p_{Ld} , using Eqs. (4-59) and (4-60).

The ultimate side shear resistance of clay can be calculated using α method given by.

$$\tau_{\max} = \alpha S_u \quad (4-61)$$

where α is adhesion factor which can be found in O'Neill and Reese (1999) as follows.

$\alpha = 0.55$ for $S_u/p_a \leq 1.5$; and

$$\alpha = 0.55 - 0.1(S_u/p_a - 1.5) \text{ for } S_u/p_a > 1.5 \quad (4-62)$$

in which p_a is the atmospheric pressure (14.65 psi).

4.7.2 Ultimate Resistance of Sand

The following procedure for calculating the ultimate resistance of sand was suggested by Zhang et al. (2005). That is, the ultimate resistance per unit length of drilled shaft can be calculated as

$$p_u = (0.8p_L + \tau_{\max})D \quad (4-63)$$

The limit normal stress of sand, p_L , according to Fleming et al. (1992), can be calculated as

$$p_L = K_p^2 \gamma' z \quad (4-64)$$

where $K_p = \tan^2(45 + \phi'/2)$ = passive earth pressure coefficient.

The ultimate τ_{\max} in horizontal direction is assumed to be the same as the ultimate vertical shear resistance estimated with the following equation from API (1991)

$$\tau_{\max} = K \gamma' z \tan \delta \quad (4-65)$$

where K = lateral earth pressure coefficient; and δ = interface friction angle between the drilled shaft and the soil. Tables 4-5 and 4-6 taken from Kulhawy et al. (1983) and Kulhawy (1991) can be used to estimate appropriate values for K and δ .

Table 4-5 Recommended Values of K by Kulhawy et al. (1983) and Kulhawy (1991)

Pile type and method of construction	K
Pile-jettied	(0.5-0.7) K_0
Pile-small displacement, driven	(0.7-1.2) K_0
Pile-large displacement, driven	(1.0-2.0) K_0
Drilled shaft-build using dry method with minimal sidewall disturbance and prompt concreting	(0.9-1.0) K_0
Drilled shaft-slurry construction with good workmanship	(0.9-1.0) K_0
Drilled shaft-slurry construction with poor workmanship	(0.6-0.7) K_0
Drilled shaft-casing method blow water table	(0.7-0.9) K_0

Note: K_0 = coefficient of lateral earth pressure at rest

Table 4-6 Recommended Values of δ by Kulhawy et al. (1983) and Kulhawy (1991)

Pile type	δ
Rough concrete	1.0 ϕ'
Smooth concrete (i.e., precast pile)	(0.8-1.0) ϕ'
Rough steel (i.e., step-taper pile)	(0.7-0.9) ϕ'
Smooth steel (i.e., pipe pile or H pile)	(0.5-0.7) ϕ'
Wood (i.e., timber pile)	(0.8-0.9) ϕ'
Drilled shaft built using dry method or with temporary casing and good construction techniques	1.0 ϕ'
Drilled shaft built with slurry method (higher values correspond to more careful construction methods)	(0.8-1.0) ϕ'

4.7.3 Ultimate Resistance of c- ϕ Soils

Brinch Hansen's (1961) theory can be used to calculate p_u of c- ϕ soils. An empirical modification factor M was later suggested by Mokwa et al. (2000) to modify Brinch Hansen's equation as follow:

$$p_u = M(\gamma'zK_q + c'K_c)D \quad (4-66)$$

where M = an empirical modification factor = 0.85; K_q = a coefficient for the frictional component of net soil resistance under 3D condition; and K_c = a coefficient for the cohesive component of net soil resistance under 3D condition. The values of K_q and K_c can be calculated as follows:

$$K_q = \frac{K_q^0 + K_q^\infty \alpha_q Z/D}{1 + \alpha_q Z/D} \quad (4-67)$$

$$K_c = \frac{K_c^0 + K_c^\infty \alpha_c Z/D}{1 + \alpha_c Z/D} \quad (4-68)$$

$$\alpha_q = \frac{K_q^0}{K_q^\infty - K_q^0} \frac{K_0 \sin \phi'}{\sin(45^\circ + 0.5\phi')} \quad (4-69)$$

$$\alpha_c = \frac{K_c^0}{K_c^\infty - K_c^0} \cdot 2 \sin(45^\circ + 0.5\phi') \quad (4-70)$$

$$K_q^0 = e^{(\pi/2 + \phi') \tan \phi'} \cos \phi' \tan(45^\circ + \phi'/2) - e^{-(\pi/2 - \phi') \tan \phi'} \cos \phi' \tan(45^\circ - \phi'/2) \quad (4-71)$$

$$K_c^0 = [e^{(\pi/2 + \phi') \tan \phi'} \cos \phi' \tan(45^\circ + \phi'/2) - 1] \cot \phi' \quad (4-72)$$

$$K_q^\infty = N_c d_c^\infty K_0 \tan \phi' \quad (4-73)$$

$$K_c^\infty = N_c d_c^\infty \quad (4-74)$$

$$N_c = [e^{\pi \tan \phi'} \tan^2(45^\circ + \phi'/2) - 1] \cot \phi' \quad (4-75)$$

$$d_c^\infty = 1.58 + 4.09 \tan^4 \phi' \quad (4-76)$$

$$K_0 = 1 - \sin \phi' \quad (4-77)$$

4.8 Validation of the Derived Capacity Prediction Method

Four field lateral load tests results are employed herein to evaluate the derived lateral capacity prediction method. Shaft #4 of Dayton load test and shaft #2 of Pomeroy-Mason load test are selected. Additionally, the load test results reported by Hall and Wang (2000) and the short shaft of I-85 load test reported by Gabr et al. (2002) are used. The dimensions and strength parameters of the test drilled shafts of the three load tests are summarized in Table 4-7, in which total length reflects the distance between the

loading point and the tip of the drilled shaft. The yielding moments of the drilled shafts are obtained from LPILE computer analysis by inputting reinforcement and physical dimensions of the drilled shafts. The soil and rock properties required for calculation are summarized in Table 4.8. The depth is measured from the ground surface down.

Table 4-7 Test Drilled Shaft Information

Test	Diameter (ft)	Total Length (ft)	Loading Eccentricity (ft)	Reinforcement	Concrete Strength (psi)	Yielding Moment (kip-ft)
Dayton	6	18	0	34#11	4500	8008
Pomeroy-Mason	8	112.9	53.1	28#18 plus 1 inch casing	5115	21640
Hall & Wang (2000)	5	32	1	12#18	4000	5488
Gabr et al. (2002)	2.5	10.2	1	12#10 plus 0.5 inch casing	5000	2819

Table 4-8 Input rock mass parameters of the load tests

Tests	Depth (ft)	γ' (pci)	q_u (psi)	GSI	m_i	Rock
Dayton Shaft #4	0-7	0.038	5668	40	6	Shale
	7-18	0.038	5668	61	6	Shale
Pomeroy-Mason Shaft #2	0-21.9	0.059	3797	42	6	Shale
	21.9-29.4	0.060	9073	45	17	Sandstone
	29.4-37.3	0.049	19	38	4	Claystone
	37.3-48	0.047	44.3	28	4	Claystone
	48-56.8	0.055	826.2	44	4	Claystone
Hall & Wang (2000)	0-14.5	0.036	-	-	-	Sand ($\phi = 34^\circ$)
	14.5-18	0.057	700	34	6	Clayshale
	18-20	0.057	1200	35	6	Clayshale
	20-25	0.057	1750	57	6	Clayshale
	25-31	0.059	1750	57	7	Siltstone
Gabr et al. (2002)	0-3.9	0.055	4220	59	9	Siltstone
	3.9-6.2	0.055	3596	59	9	Siltstone
	6.2-9.2	0.055	6598	59	9	Siltstone

The four load tests did not reach either structural yielding or rock mass failure during actual load tests. Therefore, Kulhawy and Chen (1995)'s hyperbolic curve fit technique is used to simulate the non-linear load-deflection behavior to the ultimate load, from which the ultimate capacity of piles (drilled shafts) is determined. The hyperbolic equation in terms of the lateral load (H) and the lateral deflection at the loading point (δ) can be expressed as follows:

$$H = \frac{\delta}{a + b\delta} \quad (4-78)$$

where a and b are two curve fitting constants. The ultimate lateral load capacity is defined as the deflection δ becomes infinite large and is calculated as $1/b$.

A computer program LCPILE (lateral capacity of piles) using VC++ is developed in this study to facilitate computation of the developed method. The calculated capacities and the measured values from hyperbolic curve fitting technique of actual load tests data are summarized in Table 4.9. The prediction errors defined as the difference of capacities divided by the measured capacities from load tests are given in Table 4.9 as well. The capacity prediction error of Dayton site is relatively higher than the other two cases. This may be due to extremely small shaft head deflection of 0.135 inch at maximum applied lateral load of 1126 kips. Nevertheless, the developed method can yield reasonable predictions of the lateral capacities of drilled shafts socketed in rock mass.

Table 4-9 Comparison of Lateral Capacities of Test Drilled Shafts

Test	Predicted (kips)	Measured (kips)	Error (%)
Dayton	2447	1612	52
Pomeroy-Mason	405	431	-6
Hall and Wang (2000)	500	589	-15
Gabr et al. (2002)	718	677	5.7

4.9 Summary and Conclusions

The work presented in this chapter can be summarized as follows:

1. A 3-D FEM model for simulating a laterally loaded drilled shaft in rock is developed and validated against the lateral load test results at Dayton site.
2. A wedge failure mode for rock mass at or near ground surface is identified using 3D FEM analysis techniques. Strength controlled failure mode for rock at great depth is identified as well.
3. The effect of secondary structures of rock mass, such as joints and fillings is taken into consideration through adoption of a rock classification system GSI. Additionally, equations by Hoek (1990) for instantaneous cohesion and friction angle of rock mass are used in this study.
4. Empirical equation for estimating the axial side shear resistance of the rock-shaft interface by Kulhawy and Phoon (1993) is adopted herein to compute the side shear resistance of the interface in horizontal direction.
5. Based on the suggested failure modes, theoretical equations for calculating the ultimate resistance of rock mass per unit shaft length, p_u , are derived for top layer rock mass and rock at great depth. The adoption of Hoek-Brown rock strength criterion and the empirical equation for side shear resistance ensures that the derived theoretical equations incorporate secondary structure effects.
6. A new method for predicting the ultimate lateral capacity of a drilled shaft socketed in rock mass is proposed. The method is also extended for use of a drilled shaft in various types of soils.

7. Finally, evaluation of the developed method for determining ultimate lateral capacity of a rock-socketed drilled shaft against load test results validate the accuracy of the method.

Based on above work, the following conclusions can be drawn.

1. The 3D FEM model can be used to simulate the lateral response of drilled shafts in rock. This modeling technique can help verify a drilled shaft foundation design to avoid an expensive lateral load test.
2. The identified rock mass failure modes due to laterally loaded drilled shaft are useful for deriving theoretical equations for estimating the ultimate resistance of rock mass.
3. The secondary structures of rock mass were considered in the developed theoretical equations for calculating p_u . The accuracy of the theoretical equations for calculating p_u is acceptable based on evaluation against three field load test results.
4. Hyperbola extrapolation technique originally developed by Kulhawy and Chen (1995) may under estimate the lateral capacity of drilled shafts in rock if the deflection is small at the maximum applied load during lateral load tests.
5. The proposed method for estimating lateral capacity of drilled shafts in rock can provide reasonable predictions according to the evaluation using field test data. The average prediction error is about 21% which is adequate for practice considering the measured capacity may be under estimated.
6. The proposed capacity prediction method is versatile. It can be used for estimating the lateral capacity of drilled shafts in clay, sand, silts, and rock. The soil or rock can be layered. Both short and long drilled shafts can be considered. The boundary condition can free head or fixed head.

CHAPTER V

ELASTIC SOLUTION OF LATERALLY LOADED DRILLED SHAFTS IN ROCK

Although nonlinear p-y analysis is the most widely used method for analysis of laterally loaded piles, an elastic subgrade reaction solution nevertheless is an important alternative method for solving the problem in linear elastic range due to its simplicity and easy to use. Subgrade reaction method models soils as Winkler springs and the pile as a beam. In order to develop an elastic subgrade reaction solution for drilled shafts in rock, a methodology for determining deformation modulus of rock mass and an empirical equation for estimating the modulus of subgrade reaction of rock are developed in this chapter.

5.1 Determination of Rock Mass Deformability

5.1.1 Introduction

The fact that jointed rock masses do not behave elastically has prompted the usage of the term modulus of deformation rather than modulus of elasticity or Young's modulus. The Commission of Terminology of International Society for Rock Mechanics (ISRM) published the definitions: Modulus of deformation - the ratio of stress to corresponding strain during loading of a rock mass including elastic and inelastic behavior; Modulus of

elasticity – the ratio of stress to corresponding strain below the proportionality limit of a material (Bieniawski, 1978).

There are two categories of approaches, in-situ testing and empirical equations, for determining the deformation modulus of rock mass (E_m). The existing in-situ testing for determination of E_m includes plate loading, pressuremeter/dilatometer testing, Goodman Jack test. Although all of the in-situ testing methods have their limitations in measuring the actual deformation modulus, they are still the most desirable approach. To reach rocks at depth such as for deep foundation applications, pressuremeter/dilatometer test and Goodman Jack test are most appropriate. The Goodman Jack test will be introduced in this chapter. However, the details of pressuremeter/dilatometer test will be presented in Chapter VII.

5.1.2 Goodman Jack Test

5.1.2.1 Description of Goodman Jack

The NX borehole jack device, also called Goodman Jack, was introduced in 1966 by Goodman et al. (1972). The Goodman Jack test is designed to be used in 3" boreholes. The schematic of loading mechanism of Goodman Jack is shown in Fig. 5-1 (Heuze 1984). The device consists of two steel plates forced apart by 12 racetrack-shaped pistons. The shape of these pistons was selected to give maximum hydraulic efficiency. The jack is attached to drill rod and inserted into the borehole. A hand pump is used to create hydraulic pressure in the lines connected to the jack, which in turn activates the pistons and produces a uniform and unidirectional stress field at the bearing plate. The applied hydraulic pressure is measured with a pressure gauge. The deformation of the rock is measured by two linear variable differential transformers (LVDT) and data are displayed

by the indicator at the ground surface. Two return pistons close the instrument to a thickness of 2¾ in., affording ¼ in. clearance for positioning in an NX borehole. The total piston travel is 0.5 inch; the LVDTs have a linear range of 0.2 inch and are adjusted to begin their linear travel when the plates are about to contact the rock.

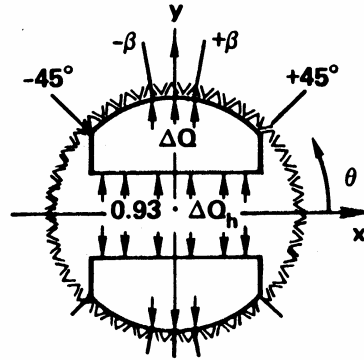


Figure 5-1 The schematic of loading of Goodman Jack (Heuze, 1984)

5.1.2.2 Test Data Interpretation

Goodman Jack test data was interpreted through theory of elasticity to derive the deformation modulus of rock. Goodman et al. (1972) studied the effect of Poisson's ratio and the finite length of platens since the theoretical analysis of jack test assumes infinite length of the platens. The effect of Poisson's ratio ν is small, because a 50% overestimation in ν , from 0.2 to 0.3, would lead to a 3.25% underestimate of modulus of rock. The effect of finite test length was investigated by using a 3D finite element analysis and taken into account by reducing 14% values of calculated modulus of rock.

By considering the effect of limited length and the hydraulic efficiency, the equation for interpretation of test data is given by (Goodman et al., 1972)

$$E = (0.86)(0.93)[K(\nu, \beta)] \frac{\Delta Q_h}{\Delta u_d / d} \quad (5-1)$$

where, constant 0.86 is for considering 3-D effect, constant 0.93 is for considering hydraulic efficiency, ΔQ_h is change of hydraulic pressure on platens, Δu_d is increment of diametral displacement, d is diameter of borehole, and $K(v, \beta)$ is a constant defined in Table 5-1.

Table 5-1 Values of Constant $K(v)$ for $\beta=45^\circ$

v	0	0.05	0.1	0.15	0.2	0.25	0.3	0.35	0.4	0.45	0.5
$K(v)$	1.38	1.29	1.29	1.28	1.27	1.25	1.23	1.20	1.17	1.13	1.09

Goodman et al. (1972) also investigated the influence of crack generated by jacking or a nature joint located along the borehole by using finite element analysis. For a crack extending a half radius away from the hole, the rock mass modulus would be calculated as 13% lower than the modulus calculated without cracking.

Since introduction of the Goodman Jack, several researchers have evaluated various data interpretation methods, such as Meyer and McVey (1974), Hustrulid (1976), Heuze and Salem (1976), Shuri (1981) and Heuze and Amadei (1985). Meyer and McVey (1974) conducted a jack test in a block of 5052 aluminum alloy measured $18 \times 18 \times 20$ inch with a 3 inch central hole. The calculated modulus using Eq. (5-1) was 2.93×10^6 psi, which is much less than the known elastic modulus of aluminum alloy of 10.08×10^6 psi. Meyer and McVey (1974)'s carefully conducted tests showed that the calculated modulus could be very different from the true modulus. Subsequent to this research, Hustrulid (1976) re-derived the $K(v, \beta)$ function in Eq. (5-1). A new expression T^* was proposed for K . For $\beta = 45^\circ$, where the definition of β is shown in Fig. 5-1, the formula for modulus calculation is given as:

$$E_{\text{calc}} = (0.93)(3)(T^*) \frac{\Delta Q_h}{\Delta u_d} \quad (5-2)$$

It should be noted that Eq. (5-2) was based on two-dimensional analysis. Hustrulid (1976) also discussed the effect of oversized holes on the calculation of modulus. Heuze and Salem (1976) performed both two-dimensional and 3-dimensional analysis and found that the ratio of plate modulus to rock modulus, the rock anisotropy, and the plate geometry would influence the deformations during jack test. Shuri (1981) re-evaluated the radius mismatch problem first discussed by Hustrulid (1976). Shuri analyzed both the undersize and oversize cases relative to 3 in. borehole diameter and the modulus reduction factors are shown in Fig. 5-2, in which E_{app} is calculated modulus of rock E_{calc} without considering the undersize or oversize effect; and E_{act} is the modulus considering the effect of undersize and oversize. Shuri ignored the plate bending problem. Therefore, what Shuri refers to as the E_{act} (E_{actual}) is in fact the modulus without considering the plate bending effect. It is however essential to apply the plate bending correction to yield the true rock modulus.

Heuze and Amadei (1985) integrated all the advances made in understanding the jack behavior prior 1985. Shuri (1981)'s work on oversize and undersize borehole was re-evaluated. The Shuri approach for oversize holes was found to be correct. However, the derivation by Shuri for undersize holes was found to be incorrect and was corrected by including the new value of T^* from Heuze and Amadei (1985). Additionally, the original correction from E_{calc} to E_{true} obtained by Heuze and Salem (1976) via 3-D finite element analysis for the plate bending, was recalculated with the T^* of Heuze and Amadei (1985).

The current version of test data interpretation follows the following steps. Step 1: calculate the E_{calc} by using the following equation for full contact condition:

$$E_{calc} = (0.86)(0.93)(d) \frac{\Delta Q_h}{\Delta u_d} (T^*) \quad (5-3)$$

The values of T^* are provided in Table 5-2. Step 2: the E_{calc} calculated from Step 1 is corrected using Fig. 5-2 to account for the undersize and oversize effect. Finally, the corrected modulus from Step 2 is further corrected using Fig. 5-3 to account for the platen bending effect.

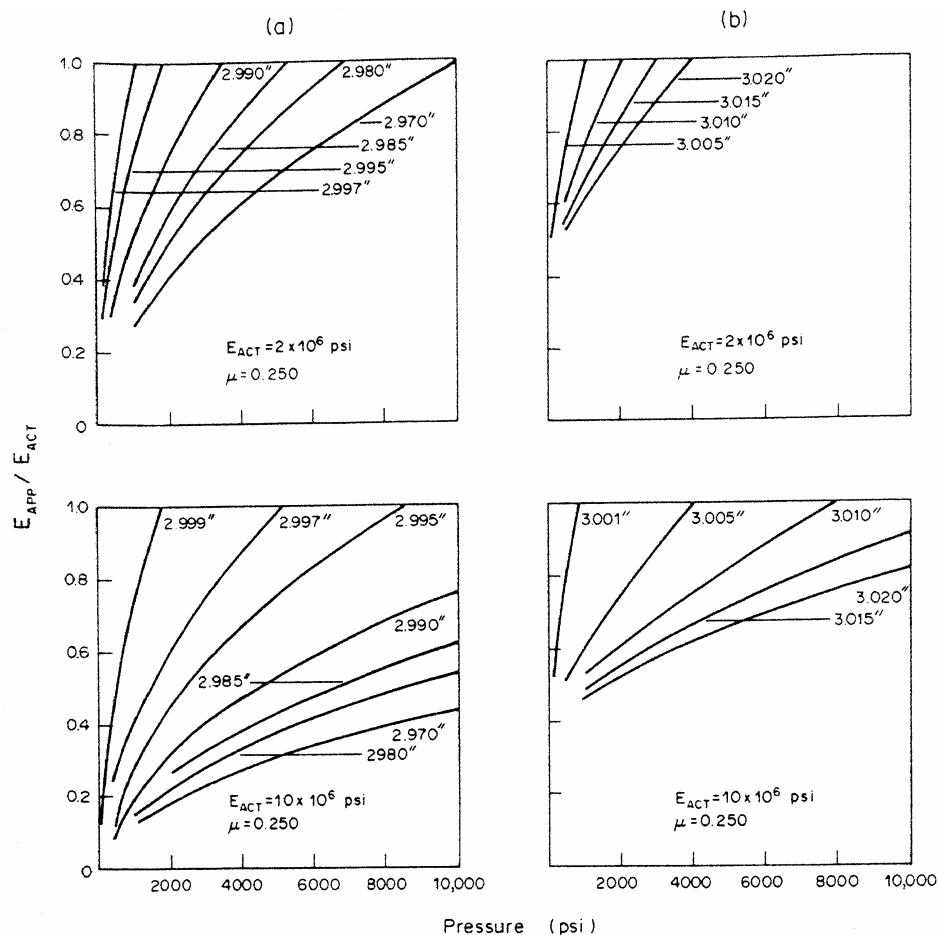


Figure 5-2 Modulus reduction vs. hydraulic pressure for various borehole diameters (a) undersize – the pressure must be decreased by about 14% for a given E_{app}/E_{act} as recalculated by Heuze et al.(1985). (b) oversize holes

Table 5-2 Values of T^* (Heuze and Amadei, 1985)

ν	0.1	0.2	0.25	0.3	0.33	0.4	0.5
T^*	1.519	1.474	1.438	1.397	1.366	1.289	1.151

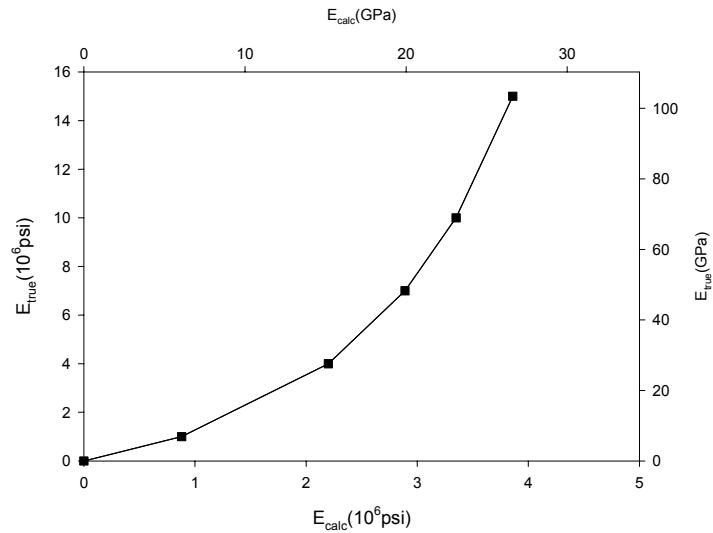


Figure 5-3 Correction for platen bending of the jack (after Heuze and Amadei, 1985)

5.1.3 Selection of In-Situ Test Method

From fundamental point of view, both dilatometer and Goodman Jack involve similar assumptions and theoretical derivations for test data interpretation. Both of them assume that the test chamber or platen is infinite long and that the rock is isotropic, homogeneous, and linearly elastic. The difference between the two devices is the method to apply the pressure to the borehole walls. Dilatometer can apply uniform pressure to the whole borehole wall; but the Goodman Jack applies unidirectional pressure to the borehole wall.

The disadvantage of dilatometer is the limit of applied pressure, which usually is less than 4,350 psi (30 MPa). In fact, this is a satisfactory upper limit of pressure for

many rock types and it exceeds the actual stress level experienced by rock in most of civil engineering works (Goodman et al., 1972). The disadvantage of Goodman Jack is the less precisely known pressure condition under the load comparing with dilatometer. However, the Goodman Jack can reach 10,075 psi (69MPa) pressure limit. Further, the ability to generate higher pressures allows the test to be carried beyond the elastic region of many rock types.

The current practice of dilatometer and Goodman Jack in determining the deformation modulus of rock mass has shown both successful and unsuccessful cases (Rocha et al., 1970; Bukovansky, 1970; Georgiadis and Michalopoulos, 1986; Reese, 1997; and Littlechild, 2000). Rocha et al. (1970) pointed out that the dilatometer test results are reliable based on their 387 dilatometer tests carried out in 9 test programs. Georgiadis and Michalopoulos (1986) investigated the application of dilatometer test to design grouted pile in rock. A total number of 20 dilatometer tests were performed in seven boreholes, mainly in jointed weak mudstone. The dilatometer test results were utilized in conjunction with laboratory test results to design laterally loaded steel-pipe piles drilled and grouted in mudstone. Reese (1997) utilized dilatometer test results to correlate the initial slope of his interim p-y criterion for weak rock.

However, in contrary to the preceding successfully application of dilatometer, Bukovansky (1970) found that the deformation modulus determined from test results of dilatometer were surprisingly low comparing that from plate-load, Flatjack, and radial jacking tests. Littlechild et al. (2000) investigated the use of high pressure dilatometer, self-boring pressuremeter and Goodman Jack tests in Hong Kong. It was found that the dilatometer tests were not necessarily successful. In highly fractured rocks, such as

granodiorite, dilatometer membrane tended to fail (puncture) frequently. It was shown that Goodman Jack test can be easily carried out in more uniform and competent rocks that exhibit little fracturing or weathering. However, for weak rock, Goodman Jack tests require careful consideration of the maximum pressure that will be applied so that the device can be retracted from the bore hole (Littlechild et al., 2000).

Based on review provided in the above sections, it can be concluded that dilatometer test is suitable for the determination of weak rock mass modulus, except for highly fractured rock, while Goodman Jack test is applicable to hard rock mass. The purchasing price for either of the test devices is around \$30,000 in 2003.

5.1.4 Existing Empirical Equations

Several empirical equations are available for the determination of deformation modulus of rock mass using empirical correlations with rock properties. Bieniawski (1978) could be credited for the development of earlier empirical equations. Other empirical equations found in literature are summarized in Table 5-3. The parameters used for correlations and perceived limitations of these empirical equations are provided in Table 5-3, in which RMR = Bieniawski (1976)'s Rock Mass Rating, E_m = the deformation modulus of rock mass, E_i = the modulus of intact rock, GSI = Geological Strength Index, $UCS = \sigma_{ci}$ = unconfined compressive strength of intact rock; RQD = Rock Quality Designation; WD = weathering degree.

Gokceoglu et al. (2003) evaluated existing empirical equations by utilizing a database consisting of 115 in-situ test data points. The database was obtained from two dam sites with quartzdiorite and limestone, and another construction site with heavily jointed marly rock mass. The measured deformation modulus of rock mass was obtained

using in-situ plate load test and dilatometer test. However, the data for weak rocks in this database was limited.

Table 5-3 Empirical Equations for Estimating the Deformation Modulus of Rock Mass

Empirical Equation	Required Parameters	Limitation	Equation
Bieniawski (1978)	RMR	$RMR > 50$	$E_m = 2RMR - 100$ (GPa)
Serafim and Pereira (1983)	RMR	$RMR \leq 50$	$E_m = 10^{(RMR-10)/40}$ (GPa)
Nicholson & Bieniawski (1990)	E_i and RMR	-	$E_m = E_i [0.0028RMR^2 + 0.9 \exp(RMR/22.82)] / 100$
Hoek and Brown (1997) & Hoek et al. (2002)	GSI, σ_{ci} and D_r which is disturbance factor	-	$E_m = (1 - D_r / 2) \sqrt{\frac{\sigma_{ci}}{100}} 10^{(GSI-10)/40} \quad (\text{GPa})$ for $\sigma_{ci} \leq 100 \text{ MPa}$; $E_m = (1 - D_r / 2) 10^{(GSI-10)/40} \quad (\text{GPa}) \quad \text{for}$ $\sigma_{ci} > 100 \text{ MPa}$
Kayabasi et al. (2003)	E_i , RQD and WD	-	$E_m = 0.135 \left[\frac{E_i (1 + RQD / 100)}{WD} \right]^{1.1811}, E_m \text{ and}$ $E_i \text{ in GPa}$
Gokceoglu et al. (2003)	E_i , RQD, UCS and WD	-	$E_m = 0.001 \left[\frac{(E_i / \text{UCS})(1 + RQD / 100)}{WD} \right]^{1.5528}$ (GPa)

The root mean square errors (RMSE) were calculated to evaluate the performance of the existing empirical correlation equations. The evaluation results show that Hoek and Brown (1997)'s equation gave the best results for a weak marly rock mass, having a mean uniaxial compressive strength of 2697 psi. Kayabasi et al. (2003)'s equation exhibited a high predictive capability with the value of RMSE equal to 0.99 for dilatometer data including the weak marly rock mass results. However, Kayabasi et al. (2003)'s equation was developed with half of the data points in the entire database.

Nicholson and Bieniawski (1990)'s equation, which was developed from the test data of Bieniawski (1978) and Serafim and Pereira (1983), exhibited good results based on the RMSE values calculated using all the data in Gokceoglu et al. (2003)'s database. Contrary to these, the equations proposed by Bieniawski (1978) yielded the most scattered results.

Based on Gokceoglu et al. (2003)'s evaluation discussed previously, it appears that Nicholson and Bieniawski (1990)'s equation could be adopted. Although the equation proposed by Gokceoglu et al. (2003) yields good prediction for his database, it nevertheless needs to be further evaluated with other database. Hoek and Brown (1997)'s equation provides good estimate on modulus for weak rock; however, Littlechild et al. (2000) found that this equation was not appropriate for foundation design on weathered rock according to their field test results in Hong Kong for igneous, volcanic and metamorphosed sedimentary rocks.

5.1.5 Parameters for Determination of E_m

Based on literature review in the previous sections, in general, rock properties such as RMR, q_u , E_i , and RQD have been selected to correlate with deformation modulus of rock masses.

Kayabasi et al. (2003) employed cosine amplitude method to investigate the strength of correlations between E_m and the intact rock and discontinuity properties of rock masses based on 57 test data points. The statistical analysis results are summarized in Table 5-4. It can be seen that modulus of intact rock correlates best with E_m . All the parameters associated with secondary structures (such as RQD, weathering) show high correlations with E_m than that of the unconfined compressive strength of intact rock.

Table 5-4 The Strength of the Relation between E_M and Parameters (Kayabasi et al. 2003)

Parameter	Strength Value
Modulus of elasticity of intact rock	0.878
RQD	0.873
Weathering of the discontinuities	0.865
Roughness of the discontinuities	0.851
Aperture of the discontinuities	0.832
Continuity of the discontinuities	0.768
Infilling	0.761
Spacing of the discontinuities	0.750
Uniaxial compressive strength of intact rock	0.720

Although Kayabasi et al. (2003) selected the first three factors in Table 5-4 (E_i , RQD and weathering degree) for their correlation equation. This research adopts the modulus of intact rock and a rating system (such as RMR and GSI) that represents the effects of all secondary structures. The good prediction results on E_m from Nicholson and Bieniawski (1990)'s equation based on Gokceoglu et al. (2003)'s database and the unsatisfactory predictions from Hoek and Brown (1997)'s equation based on Littlechild et al. (2000)'s test data support this conclusion.

A set of dilatometer test data in Ironton-Russell (Paul and Martin 2004) is compiled in Table 5-5 for independent check on various correlation equations.

Table 5-5 Properties of Rock Masses in Ironton-Russell

No.	RQD	q_u (psi)	E_i (psi)	E_M , mea. (psi)	GSI	RMR	WD
1	75	8406	1689.7	667.1	74	64	0.400
2	98	9544	1751.5	586.4	77	67	0.400
3	78	9559	1809.4	625.5	74	64	0.400
4	100	9005	1569.1	636.8	77	67	0.400
5	100	8002	1343.4	439.4	77	67	0.400
6	98	9137	1763.3	525.6	77	67	0.400
7	98	8578	1774.5	504.3	77	67	0.400

Table 5-6 provides the predictions of E_m and the ratio of predicted over measured deformation modulus of rock masses using Nicholson and Bieniawski (1990)'s equation, Hoek and Brown (1997)'s equation, and Kayabasi et al. (2003)'s equation. Nicholson and Bieniawski (1990)'s equation which employs E_i and RMR as the parameters provides the best estimate on E_m , while the other two methods over-predict E_m . Therefore, E_i and rock rating system (such as RMR and GSI) are the most important parameters for correlating with modulus of rock masses.

Table 5-6 Predictions and Ratios of Predicted over Measured Modulus of Rock Masses

No.	Nicholson and Bieniawski (1990)		Hoek and Brown (1997)		Kayabasi et al. (2003)		Serafim and Pereira (1983)	
	Prediction	Ratio	Prediction	Ratio	Prediction	Ratio	Prediction	Ratio
1	445.0	0.67	4395.2	6.6	2033.9	3.05	2434	3.6
2	517.1	0.88	5566.1	9.5	2455.3	4.19	2893	4.9
3	476.5	0.76	4686.9	7.5	2249.9	3.60	2434	3.9
4	463.3	0.73	5406.6	8.5	2182.0	3.43	2893	4.5
5	396.7	0.90	5096.6	11.6	1816.3	4.13	2893	6.6
6	520.6	0.99	5446.1	10.4	2474.8	4.71	2893	5.5
7	523.9	1.04	5276.9	10.5	2493.4	4.94	2893	5.7

5.1.6 Proposed Empirical Equation

Although Nicholson and Bieniawski (1990)'s equation is the most promising empirical equation for estimating deformation modulus of rock masses, the use of RMR makes it suffer some inherent drawbacks. The RMR value is difficult to estimate for very poor rock, especially for borehole cores in which relatively few intact core pieces longer than 4 inch can be recovered (Hoek and Brown, 1997). In these circumstances, the physical appearance of material recovered in the core can be used to estimate a GSI value. Therefore, the GSI system is proposed as an alternative to the RMR system for estimating deformation modulus of rock masses.

To preserve the merit of Nicholson and Bieniawski (1990)'s equation, the test data (Bieniawski, 1978 and Serafin and Pereira, 1983) used to develop their equation is used to develop a new empirical equation. According to Hoek and Brown (1997), GSI equals to RMR (Bieniawski, 1976), with the ground water rating set to 10 and the adjustment for joint orientation set to 0. Due to the lack of details of estimating RMR of these data, it was assumed that the ground water rating was set to an average value of 5. Therefore, GSI values of these test data are estimated by adding original RMR with 5. Additionally, the new data from Iron-ton-Russell is included. A regression analysis is carried out and the results are plotted in Fig. 5-4. The following equation is proposed to estimate deformation modulus of rock masses using modulus of intact rock and GSI.

$$E_m = \frac{E_i}{100} (e^{GSI/21.7}) \quad (5-4)$$

5.1.7 Recommended Methodology for Determination of Deformation Modulus of Rock

In-situ tests usually provide more reliable values for the deformation modulus of rock mass than empirical equations. For weak rock, dilatometer test is recommended since this test has been widely and successfully used in geotechnical engineering applications. However, for hard and competent rock, Goodman Jack test is recommended since it can provide higher pressure than dilatometer. For preliminary design or where in-situ tests are not available, the derived Eq. 5-4 is recommended to estimate the deformation modulus of rock mass.

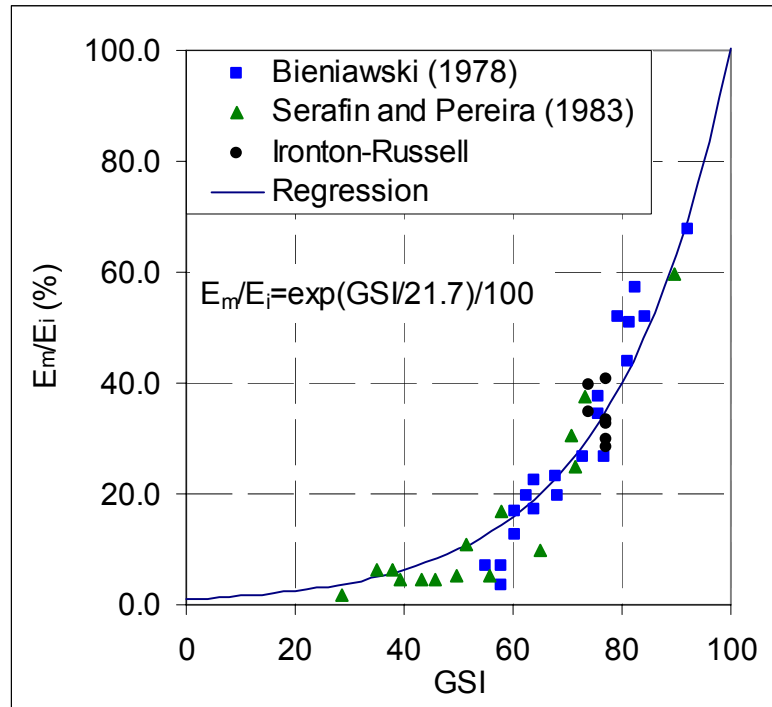


Figure 5-4 Proposed empirical equation using GSI

5.2 Initial Modulus of Subgrade Reaction of Rock Mass

5.2.1 Introduction

The term initial modulus of subgrade reaction refers to the initial slope of a p-y curve. In literature, few studies and discussions are available regarding the determination of modulus of subgrade reaction, especially for rock masses. By fitting the subgrade reaction solution with continuum elastic solution for beam on elastic foundation, Vesic (1961) provided an elastic solution for the modulus of subgrade reaction, K (F/L^2) as follows.

$$K = \frac{0.65E}{1 - \nu^2} \left[\frac{ED^4}{E_p I_p} \right]^{1/12} \quad (5-5)$$

where E = modulus of elastic materials; ν = Poisson's ratio; D = beam width; and $E_p I_p$ = flexural rigidity of beam.

Bowles (1988) suggested to double the value of K in Eq. (5-5) for piles under lateral loading since the pile would have contact with soils on both sides. However, in reality, soils are not in full contact with the piles when the lateral loads are applied. Based on field test data, Carter (1984) modified Vesic's equation as follows that would account for the effect of pile diameter.

$$K = \frac{1.0ED}{(1 - \nu^2)D_{\text{ref}}} \left[\frac{ED^4}{E_p I_p} \right]^{1/12} \quad (5-6)$$

where the reference pile diameter, $D_{\text{ref}} = 1.0$ m, $E_p I_p$ = flexural rigidity of piles or drilled shafts.

Guo (2001) proposed an expression for K based on a closed form elastic solution for laterally loaded piles. The subgrade reaction modulus was given by:

$$K = \frac{3\pi G_s}{2} \left(2\eta \frac{K_1(\eta)}{K_0(\eta)} - \eta^2 \left(\left(\frac{K_1(\eta)}{K_0(\eta)} \right)^2 - 1 \right) \right) \quad (5-7)$$

where G_s = shear modulus of soils; η = a load transfer factor (Guo, 2001); and K_0 and K_1 = Bessel functions.

The above discussions were focused on piles in soils or a linear elastic media. For drilled shafts in rock masses, Reese (1997) proposed an interim p-y curve criterion for weak rock. In this criterion, the initial slope of p-y curves (initial modulus of subgrade reaction), K_i , was given by:

$$K_i \approx k_i E_m \quad (5-8)$$

where E_m = modulus of rock mass; and k_i = dimensionless constant. From experimental data, empirical equations for determining k_i are given as:

$$k_i = (100 + 400z/(3D)); \quad 0 \leq z \leq 3D \quad (5-9)$$

$$k_i = 500; \quad z > 3D \quad (5-10)$$

where D = the diameter of drilled shafts; and z = depth.

Vesic (1961) elastic solution for beam-on-Winkler foundation is directly applicable to laterally loaded drilled shafts in soils or rock. Guo (2001) solution is complex for practical use and requires further verification with actual test data. The equation proposed by Reese (1997) is empirical in nature and only based on two load tests results. An empirical model for initial subgrade reaction modulus of rock masses is proposed in this study. A parametric study using the 3D FEM model presented in Chapter IV is carried out to obtain an empirical equation for estimating initial subgrade reaction modulus. Finally, the validation using field test data shows that the proposed empirical equation would provide good prediction on initial subgrade reaction modulus of rock mass.

5.2.2 FEM Model and Parametric Study

5.2.2.1 FEM Modeling

The 3D FEM model developed in Chapter IV is used to simulate the response of a laterally loaded drilled shaft in rock. The drilled shaft is modeled as a cylinder with elastic material properties. The Modified Drucker-Prager Model (CAP Model) is utilized to represent isotropic, homogeneous rock masses. The solid elements C3D15 and C3D8 are used to develop mesh representation for drilled shaft and rock, respectively. Surface interface technique is employed to simulate the rock-shaft interface. Since the

determination of initial subgrade reaction modulus is the primary objective of this study, only the elastic response of rock will be the concern of this parametric study.

The rock mass surrounding the shaft will be modeled as multiple horizontal layers with 12 inch thickness for each layer. The force applied to rock mass per unit thickness surrounding the shaft is obtained directly from the output of FEM analysis. The rock resistance per unit shaft length p is then calculated by dividing the force with the rock layer thickness of 12 inch for each loading level. By extracting the deflections of the shaft under various load levels at the corresponding depth of the rock layer, p - y curves of the rock layer can be obtained. The initial subgrade reaction modulus K_i is obtained as the initial tangent to the p - y curves. Hyperbolic curve fitting technique is employed to fit the p - y curves so that a unique value of initial slope of the p - y curves is obtained. Various factors, such as shaft diameter (D), shaft-rock relative stiffness ($E_p I_p / (E_m D^4)$), shaft-rock interface properties, Poisson's ratio (ν), and deformation modulus of rock mass (E_m), are studied. The diameter of shaft used for parametric study varies from 2 feet to 10 feet. A total of 30 cases of FEM analysis were carried out.

5.2.2.2 Effect of Rock Mass Modulus E_m

The effect of deformation modulus of rock mass, E_m , is studied. The range of modulus was ranged from 100 to 2000 ksi for weak rock. Other pertinent parameters are kept constant: $D = 72$ inch, $L = 216$ inch, $E_p = 4000$ ksi, $\nu = 0.3$. P - y curve is generated at a depth of 18 inch. It is found that it has a linear relationship with initial modulus of subgrade reaction modulus K_i , as shown in Fig. 5-5.

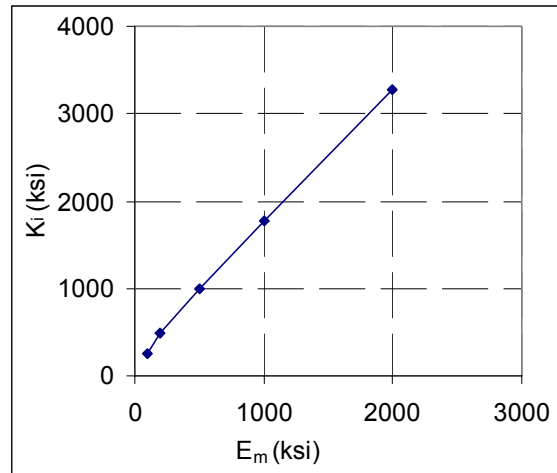


Figure 5-5 Initial modulus of subgrade reaction for various moduli of rock

5.2.2.3 Effect of Poisson's Ratio ν

The Poisson's ratio for rocks is varied from 0.1 to 0.4, while maintaining other pertinent parameters constant as follows: $D = 72$ inch, $L = 216$ inch, $E_p = 4000$ ksi, $E_m = 200$ and 500 ksi. Again, p - y curve is generated at a depth of 18 inch. Fig. 5-6 shows an exponential relationship between K_i and Poisson's ratio ν . The variation of modulus of rock mass does not change the relationship between K_i and ν , as shown in Fig. 5-6.

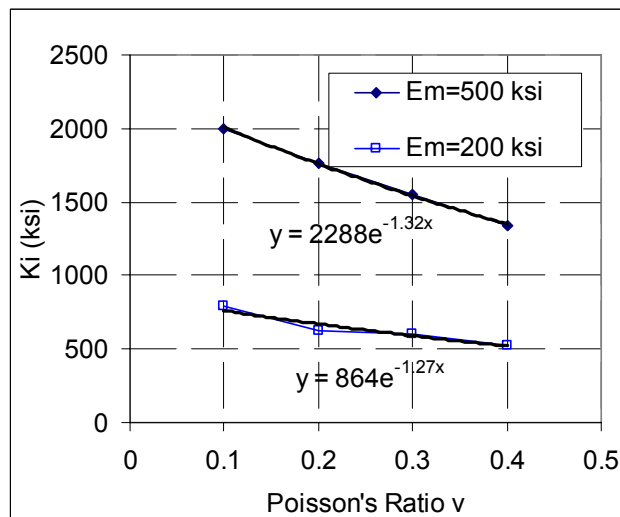


Figure 5-6 Initial modulus of subgrade reaction for various Poisson's ratio

5.2.2.4 Effect of Depth

The relationship between initial subgrade reaction modulus and depth is also investigated using the same set of rock properties as discussed in previous section. The rock properties were set to be same along the depth. It is found that K_i (the tangent to p-y curve) decreases along depth, while the ultimate resistance of rock mass increases with depth, as shown in Fig. 5-7. Because the rock modulus is constant along depth, supposedly the deformability of rock should be same along depth. The difference of K_i along depths is very small; therefore, it could be attributed to the numerical integration for calculating p.

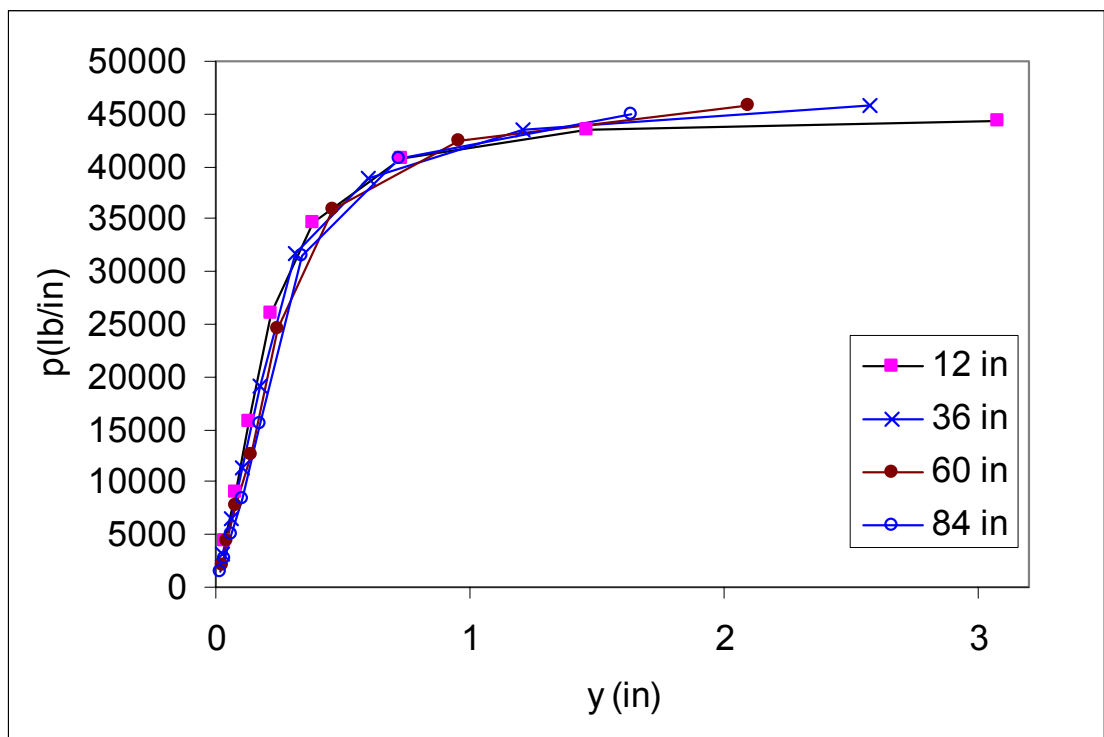


Figure 5-7 P-y curves along with depth

5.2.2.5 Effect of Interface Properties

The interface between shaft and rock was modeled by a surface based interface technique in the ABAQUS software. The coefficient of friction of the interface is the main controlling parameter of the shaft-rock interface. The computational results shown in Fig. 5-8 clearly indicate that the interface frictions exert no effect on the initial modulus of subgrade.

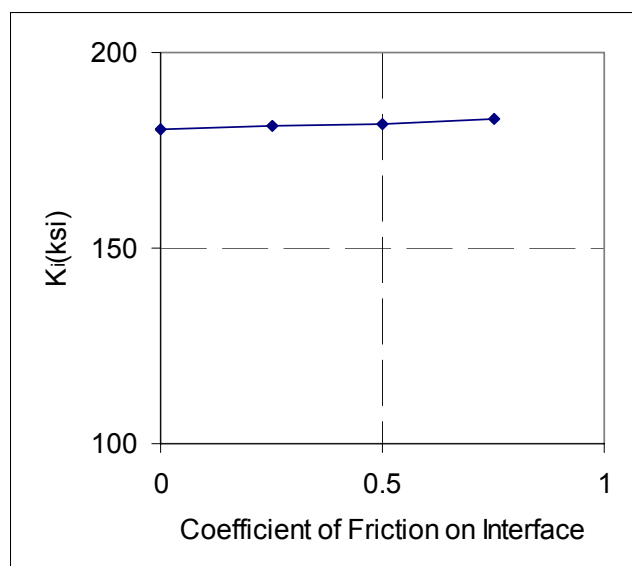


Figure 5-8 Initial modulus of subgrade reaction for various rock-shaft interface frictions

5.2.2.6 Effect of Diameter

There has been a long history of debate regarding the effect of diameter on the modulus of subgrade reaction. Terzaghi (1955) and Vesic (1961) concluded that the diameter of piles has no effect. Additionally, Ashford and Juirnarongrit (2003) indirectly verified that the modulus of subgrade reaction is independent of pile diameter when examining full-scale vibration tests results on cast-in-drilled-hole piles in a sand deposit.

However, Carter (1984) found from his own field test data that the diameter of piles has exerted significant effect on modulus of subgrade reaction.

In this study, the effect of diameter is investigated using the following input parameters: D ranges from 24 inch to 120 inch, $E_p = 4000$ ksi, $E_m = 500$ ksi, $\nu = 0.3$. P-y curve is generated at a depth of 18 inch. The FEM computed relationship between the shaft diameter and initial modulus of subgrade reaction of rock mass is presented in Fig. 5-9. It can be seen that K_i increases with diameter linearly. The shaft diameter is normalized with a reference diameter of 1 foot.

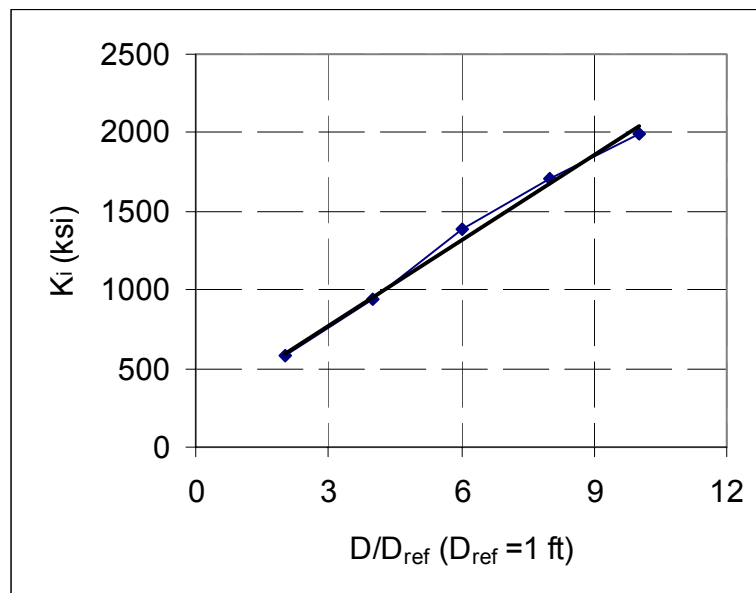


Figure 5-9 K_i varies with shaft diameter

5.2.2.7 Effect of Shaft-Rock Relative Stiffness

The effect of shaft-rock relative stiffness, $E_p I_p / (E_m D^4)$, is also investigated herein. The input parameters are: $D = 72$ inch, $L = 216$ inch, $\nu = 0.3$, E_p varies from 3500 to 4500 ksi, E_m varies from 100 to 2000 ksi. Again, the p-y curve is generated for a depth of 18 inch. It is found that a power law can be used to describe the relationship between K_i

and shaft-rock relative stiffness, as shown in Fig. 5-10. Similar results concerning the effect of relative stiffness on K_i were found previously by Guo (2001) in his numerical study.

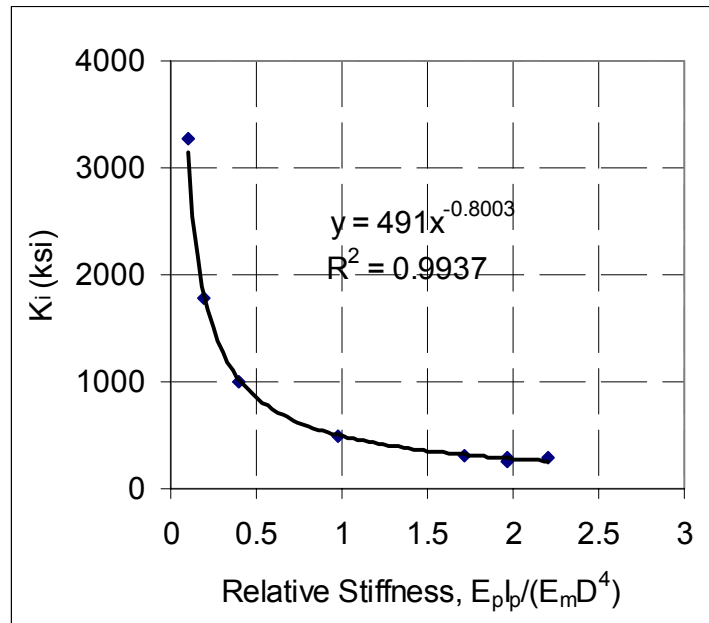


Figure 5-10 Initial modulus of subgrade reaction for various shaft-rock relative stiffness

5.2.3 Suggested Empirical Equation

Based on the parametric study presented in the previous sections, the following conclusions may be drawn:

- Both the modulus of rock masses and shaft diameter exhibit a linear relationship with K_i ;
- K_i exponentially decreases with increasing Poisson's ratio of rock mass;
- Rock-shaft interface friction exerts no effect on K_i ;
- The relative stiffness of the pile and rock has shown a power relationship with K_i .

A regression analysis on data from the FEM parametric study is carried out. An equation for predicting initial modulus of subgrade reaction is fitted to match K_i values

obtained from FEM parametric study. As shown in Fig. 5-11, the empirical equation can be derived as

$$K_i = E_m (D / D_{ref}) e^{-2\nu} \left(\frac{E_p I_p}{E_m D^4} \right)^{0.284} \quad (5-11)$$

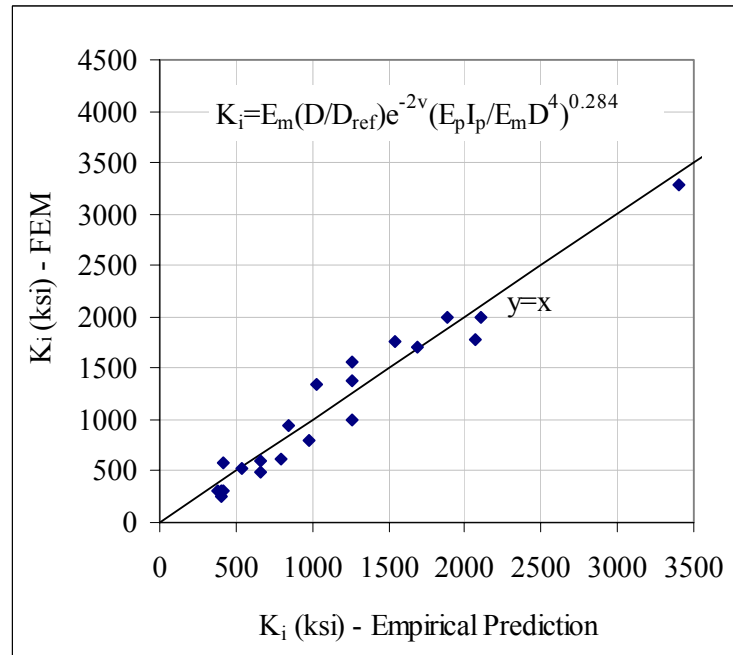


Figure 5-11 Comparison of FEM computed and predicted subgrade reaction modulus

5.2.4 Validation of the Empirical Equation

5.2.4.1 Field Tests

Three lateral load tests in rock (i.e., Dayton, Pomeroy-Mason, and North Carolina by Cho, et al., 2000), are employed to verify the developed empirical equation for predicting initial modulus of subgrade reaction of rock mass. The Dayton and Pomeroy-Mason load tests were previously presented in Chapter III; and the load test in North Carolina is collected from open literature. A summary of the properties of the test drilled shafts for three cases is provided in Table 5-7.

Table 5-7 Summary of Lateral Load Test Drilled Shafts

Drilled Shafts	Diameter (in)	Length (ft)	Socket Length (ft)	Overlying Soils (ft)
Dayton Shaft #4	72	18	18	0
Pomeroy-Mason Shaft #2	96 (socketed)	112.9	56.8	0
North Carolina Long Shaft	30	16	9.8	4.2

For the lateral load tests in North Carolina, the experimental p-y curves were derived and presented by the authors. Although the accuracy of the experimental p-y curves was verified by the authors, an independent verification of the experimental p-y curves is carried out. The experimental p-y curves are used as input in COM624P analysis. The predicted load-deflection curve at the shaft head is compared with the measured curve in Fig. 5-12. It can be seen that a good agreement between the predicted and measured load-deflection curves at the shaft head is achieved, thus indirectly verifying the representativeness of the experimental p-y curves.

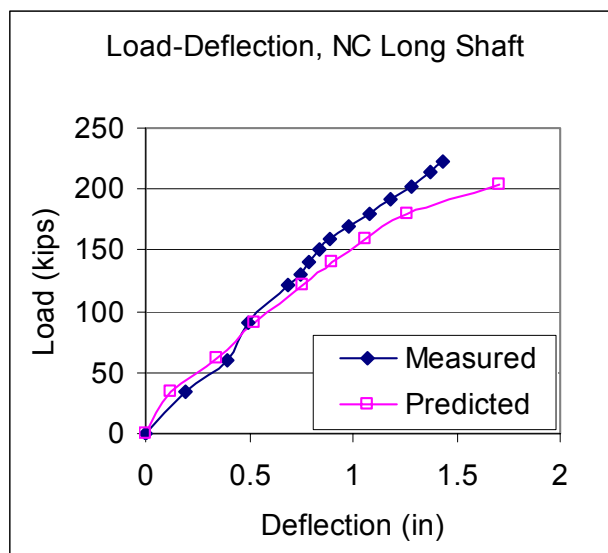


Figure 5-12 Comparison of load-deflection curves of North Carolina load test

The experimental p-y curves of rock masses for Dayton and Pomeroy-Mason Load tests were derived using piecewise polynomial curve fitting. The accuracy of the experimental p-y curves of the two tests have been verified in Chapter III.

The modulus of rock masses at North Carolina test site was determined from pressuremeter test results. The other two load tests only have information on the lab test data of modulus of intact rock. Thus, the rock mass modulus is estimated using the proposed empirical equation, Eq. (5-4). The mean GSI values determined in previous sections 3.1.1 and 3.2.1 are used.

The initial linear portion of the pressuremeter test curves of the North Carolina test was used to determine the modulus of rock masses. The calculated values of E_m for the two drilled shafts in the North Carolina lateral load test is provided in Table 5-8. The values of rock mass modulus for Dayton and Pomeroy-Mason test sites are estimated using the proposed empirical equation and they are summarized in Table 5-9.

Table 5-8 Modulus of Rock Masses Based on Pressuremeter Test

Drilled Shaft	Depth (in)	E_m (psi)	$E_p I_p$ (lb-in ²)
NC Long Shaft	102	25252	1.43E+11
NC Long Shaft	141	40060	1.43E+11
NC Long Shaft	180	54998	1.43E+11

Table 5-9 Modulus of Rock Masses Based on Empirical Equation

Test	Depth (in)	GSI	E_i (ksi)	E_m (ksi)	$E_p I_p$ (lb-in ²)
Dayton Shaft #4	36	40.5	590	38.1	5.23E+12
Dayton Shaft #4	60	40.5	590	38.1	5.23E+12
Dayton Shaft #4	96	61	590	98.1	5.23E+12
Dayton Shaft #4	132	61	590	98.1	5.23E+12
Dayton Shaft #4	156	61	590	98.1	5.23E+12
Pomeroy-Mason Shaft #2	6	42	345	23.9	1.77E+13
Pomeroy-Mason Shaft #2	66	42	345	23.9	1.77E+13

5.2.4.2 Verification of the Empirical Equation

The above field test data are used to verify the empirical equation for predicting initial modulus of subgrade reaction of rock mass. The Poisson's ratio is assumed to be 0.3 for these tests. The shaft stiffness of test drilled shafts is computed based on reinforcement and dimension and shown in Tables 5-7 and 5-8. The measured initial subgrade reaction modulus of rock masses obtained from the experimental p-y curves for rocks at various depths are provided in Table 5-10.

The predicted K_i using the proposed equation and the ratio of the predicted values over the measured values are provided in Table 5-10. The predicted K_i and measured K_i are plotted in Fig. 5-13. It can be seen that the predicted values are smaller than the measured values for most of cases. In general, the empirical equation will provide conservative predictions on the initial modulus of subgrade reaction.

Table 5-10 Measured and Predicted Initial Modulus of Subgrade Reaction

Test	Depth (in)	K_i (psi), Measured	K_i (psi), Predicted	Pred./Mea.
Dayton Shaft #4	36	407787	199467	0.49
Dayton Shaft #4	60	355468	199467	0.56
Dayton Shaft #4	96	454901	392310	0.86
Dayton Shaft #4	132	1016462	392310	0.39
Dayton Shaft #4	156	1557558	392310	0.25
Pomeroy-Mason Shaft #2	6	350938	194066	0.55
Pomeroy-Mason Shaft #2	66	383584	194066	0.51
NC Long Shaft	102	48112	60229	1.25
NC Long Shaft	141	144581	83811	0.58
NC Long Shaft	180	216130	105159	0.49

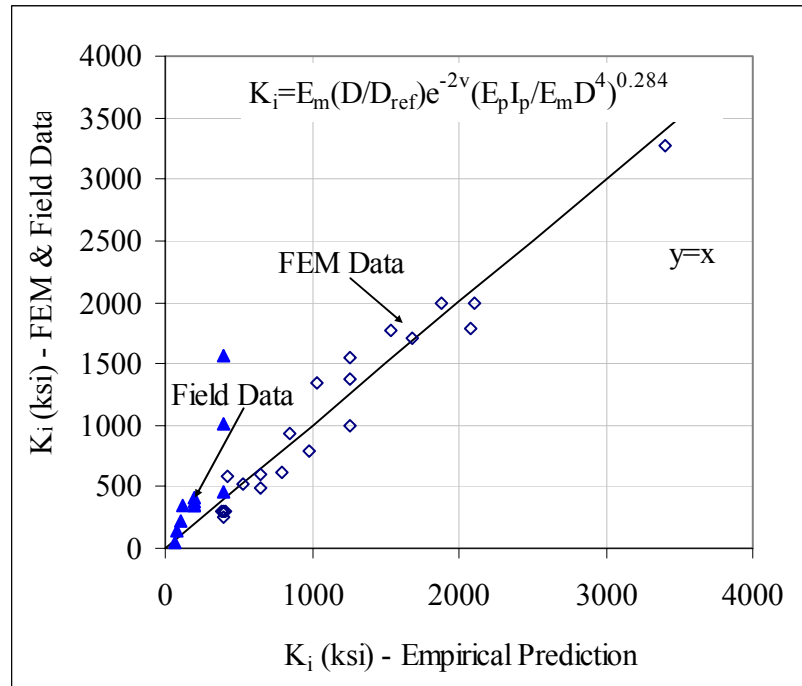


Figure 5-13 Validation of empirical equation using field test data

5.3 Numerical Solution for Laterally Loaded Piles in A Two Layer Soil Profile

5.3.1 Introduction

Although nonlinear p-y analysis is the most widely used method for design of laterally loaded piles, an elastic subgrade reaction solution is a good alternative for piles under small working loads because of its simplicity and easy for use. Subgrade reaction method models soils as Winkler springs and pile as a beam. A closed form solution for laterally loaded piles in one layer soil with constant subgrade reaction modulus was given by Hetenyi (1946). A non-dimensional solution for soil stiffness linearly varying with depth was also presented by Reese and Matlock (1956) for piles in one layer soil. In reality, however, piles are often embedded in layered soils, such as clay overlying on

rock mass. The stiffness of soil could be varying with depth (such as sand and sedimentary rock) or keeping constant along depth (such as clay).

For piles in layered soils under small working loads, although the solutions proposed by Davisson and Gill (1963) and Pise (1982) can be used, they require the soil stiffness to be constant along depth for each layer. This may not represent the actual soil profiles, especially when soil stiffness is varying with depth. In this paper, a variational approach, which has been successfully used by Shen and Teh (2004) for a laterally loaded single pile in one layer soil, is employed to numerically solve the problem of a laterally loaded pile in a two-layer soil system using subgrade reaction theory. The soil stiffness, which is represented by modulus of subgrade reaction of soils, can be either constant along depth or linearly varying with depth. The proposed solution is then able to be used for layered soil condition with variation of stiffness, especially for piles socketed in rock with overburden sands. Realistic soil stiffness distribution along depth can be more accurately modelled comparing with existing solutions for a layered soil system.

The general computational software Mathematica is used to carry out the numerical calculation, which makes the solution easy and efficient for use. The numerical solution is validated against a non-dimensional solution (Reese and Matlock, 1956) for linearly varying soil stiffness and against Davisson and Gill (1963) non-dimensional charts for a two-layer soil system with constant soil stiffness. For practical use, methods for determining modulus of subgrade reaction are provided. Two case studies using the numerical solution for field lateral load tests are performed to further validate the practical applicability of the numerical solution. Finally, discussions on the applications

of the proposed method show that the lateral deflection of a pile may be under estimated by a factor of 2.3 if constant soil stiffness is used for the whole soil layer.

5.3.2 Definition of the Problem

It is very common for piles embedded in layered soils. The soil stiffness can be treated as constant along depth for overconsolidated clay and igneous rocks. However, it is reasonable to assume linearly varying soil stiffness along depth for sands and sedimentary rocks. To make this Chapter easier to follow, the definitions of various terms related with subgrade reaction theory are summarized in Table 5-11. Four possible soil layer combinations are shown in Fig. 5-14, in which K_{s0} , K_{r0} = the initial modulus of subgrade reaction of layer 1 and layer 2, respectively; n_{hs} , n_{hr} = the constant of subgrade reaction of layer 1 and layer 2, respectively; L_s = the thickness of layer 1; L = the total thickness of the two layers. The four layered cases can be represented by case (a) shown in Fig. 5-14, by choosing a zero or non-zero value for the two constants of subgrade reaction.

Table 5-11 Summary of Definitions Related to Subgrade Reaction Theory

Description	Symbol	Definition	Dimension
Soil resistance per unit length	p	Pressure times diameter	F/L
Pile deflection	y		L
Pile diameter	D		L
Depth	z		L
Modulus of subgrade reaction	K	$K=p/y$	F/L^2
Coefficient of subgrade reaction	k	$k=K/D$	F/L^3
Constant of subgrade reaction	n_h	$n_h = K/z$; $n_h = kD/z$	F/L^3

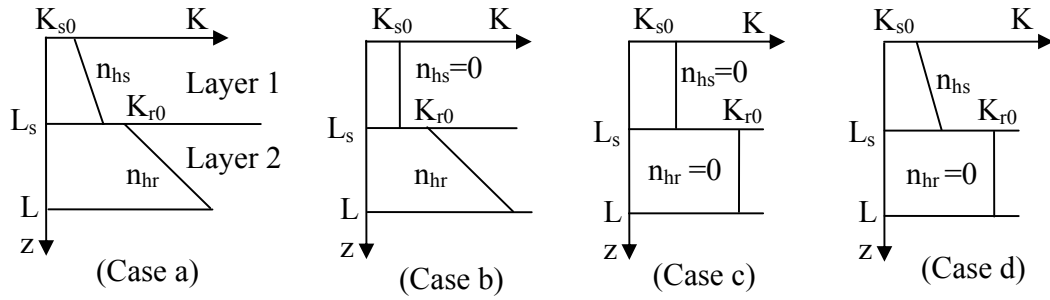


Figure 5-14 Two-layer soil profile with four possible variations

5.3.3 Variational Solution

Shen and Teh (2002) proposed a numerical solution for pile groups under lateral loads using a variational approach. After that, Shen and Teh (2004) presented a variational solution for soil with stiffness increasing with depth. This study is a further development of the variational approach to the layered soil conditions. The solution for piles embedded in soils having the soil stiffness shown in case (a) of Fig. 5-14 will be presented. By changing the values of the two constants of subgrade reaction, the response of piles in the other three layered conditions can be obtained. The soil-pile system is schematically shown in Fig. 5-15. Here H_t and M_t are the applied lateral load and moment at the top of the pile; p_z is the soil resistance per unit pile length at depth z ; K_1 and K_2 are the modulus of subgrade reaction of layer 1 and 2; and L and D are the length and diameter of the pile, respectively.

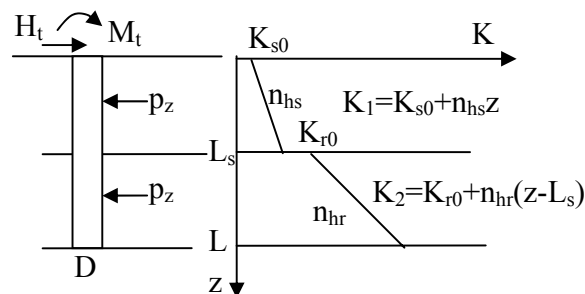


Figure 5-15 Soil-pile system

5.3.3.1 Potential Energy

The total potential energy of the pile under lateral loads, as illustrated in Fig. 5-15, can be expressed as

$$\pi_p = U_p + \frac{1}{2} \int_0^{L_s} K_1 y_z^2 dz + \frac{1}{2} \int_{L_s}^L K_2 y_z^2 dz - H_t y_t - \frac{\partial y_t}{\partial z} M_t \quad (5-12)$$

$$\text{where } U_p = \frac{1}{2} \int_0^L E_p I_p \left(\frac{d^2 y_z}{dz^2} \right)^2 dz \quad (5-13)$$

U_p is the elastic strain energy of the pile, where E_p is the pile Young's modulus; I_p is the moment of the inertia of the pile section; and y_z is the deflection of the pile at depth z . The second and third terms on the right side of Eq. (5-12) are the energy consumed by the soil resistance of the first and second soil layers, respectively. The fourth and fifth terms are the input work done by the lateral load H_t and the moment M_t acting at the pile head, where y_t is the deflection of the pile at the pile head.

5.3.3.2 Deflection Series

Shen and Teh (2002) employed two finite series to model the deflections of a pile subjected to lateral loads and moments at the pile head respectively. In this study, the two finite series is also employed to closely match the pile deflections under lateral loads and moments. The deflections of a pile subjected to a lateral load at the pile head can be approximately described in matrix form by

$$y_{zh} = \{Z_h\}^T \{\delta_h\} \quad (5-14)$$

where

$$\{Z_h\} = \left\{ 1, \frac{z}{L}, \sin \frac{\pi z}{L}, \sin \frac{2\pi z}{L} \dots \sin \frac{n\pi z}{L} \right\}^T \quad (5-15)$$

$$\{\delta_h\} = \{a_h, b_h, \beta_{h1}, \beta_{h2} \dots \beta_{hn}\}^T \quad (5-16)$$

The deflections of a pile subjected to a moment at the pile head can be approximately represented in matrix form by

$$y_{zm} = \{Z_m\}^T \{\delta_m\} \quad (5-17)$$

where

$$\{Z_m\} = \{1, \frac{z}{L}, \cos \frac{\pi z}{2L}, \cos \frac{3\pi z}{2L} \dots \cos \frac{(2n-1)\pi z}{2L}\}^T \quad (5-18)$$

$$\{\delta_m\} = \{a_m, b_m, \beta_{m1}, \beta_{m2} \dots \beta_{mn}\}^T \quad (5-19)$$

In above equations, a_h and a_m are the unknown constants to represent the rigid body movement of the pile under lateral loads and moments, respectively; b_h and b_m are the unknown constants to capture the deflections due to the rotation of the pile; and β_{hi} and β_{mi} are the unknown constants to capture the nonlinear mode of the deflected pile; and n is the number of terms used in the trigonometric function. The above expressions for pile deflections are validated in the subsequent section by the comparisons with the non-dimensional solutions by Reese and Matlock (1956) and Davisson and Gill (1963). The total deflection (y_z) of the pile subjected to lateral loads and moments is the summation of y_{zh} and y_{zm} .

5.3.3.3 Minimization of Potential Energy

The principle of minimum potential energy requires that π_p be an extremum with respect to the admissible deflection field characterized by the undetermined coefficients in Eqs. (5-14) and (5-17). This leads to:

$$\frac{\partial \pi_p}{\partial \delta_i} = 0 \quad (i = 1, 2 \dots n + 2) \quad (5-20)$$

where δ_i denotes the undetermined coefficients in Eq. (5-16) for the lateral load case and in Eq. (5-19) for the moment case, respectively. By using Eq. (5-16), the potential energy can then be reduced to:

$$\frac{\partial U_p}{\partial \delta_i} + \int_0^{L_s} K_1 y_z \frac{\partial y_z}{\partial \delta_i} dz + \int_{L_s}^L K_2 y_z \frac{\partial y_z}{\partial \delta_i} dz = H_t \frac{\partial y_t}{\partial \delta_i} + M_t \frac{\partial}{\partial z} \left(\frac{\partial y_t}{\partial z} \right) / \partial \delta_i \quad (5-21)$$

Eq. (5-21) is the governing variational formulation that a single pile in two layers soil/rock needs to follow.

5.3.3.4 Numerical Solution

The Eq. (5-21) will be solved by separating the effects of lateral loads and moments on pile deflections. For the case of piles under a lateral load, by substituting Eqs. (5-13) and (5-14) into Eq. (5-21), we have:

$$\left[\int_0^L E_p I_p \frac{\partial^2 \left(\frac{\partial^2 y_{zh}}{\partial z^2} \right)}{\partial \delta_{hi}^2} \frac{\partial^2 \{Z_h\}^T}{\partial z^2} dz + \int_0^{L_s} K_1 \frac{\partial y_{zh}}{\partial \delta_{hi}} \{Z_h\}^T dz + \int_{L_s}^L K_2 \frac{\partial y_{zh}}{\partial \delta_{hi}} \{Z_h\}^T dz \right] \{\delta_h\} = H_t \frac{\partial y_{ht}}{\partial \delta_{hi}} \quad (5-22)$$

For the case of piles under moment, by substituting Eqs. (5-13) and (5-17) into Eq. (5-21), we have:

$$\left[\int_0^L E_p I_p \frac{\partial^2 \left(\frac{\partial^2 y_{zm}}{\partial z^2} \right)}{\partial \delta_{mi}^2} \frac{\partial^2 \{Z_m\}^T}{\partial z^2} dz + \int_0^{L_s} K_1 \frac{\partial y_{zm}}{\partial \delta_{mi}} \{Z_m\}^T dz + \int_{L_s}^L K_2 \frac{\partial y_{zm}}{\partial \delta_{mi}} \{Z_m\}^T dz \right] \{\delta_m\} = M_t \frac{\partial \left(\frac{\partial y_{mt}}{\partial z} \right)}{\partial \delta_{mi}} \quad (5-23)$$

where δ_{hi} and δ_{mi} are the constants in the vectors $\{\delta_h\}$ and $\{\delta_m\}$ respectively; y_{ht} and y_{mt} are the deflections of the pile at the pile head under the applied lateral load and moment respectively.

The above two equations can be reduced to matrix forms as:

$$[K_H] \{\delta_h\} = \{H\} \quad (5-24)$$

$$[K_M] \{\delta_m\} = \{M\} \quad (5-25)$$

where $[K_H]$ and $[K_M]$ are the matrices reflecting the pile-soil stiffness under a lateral load and a moment, respectively; $\{H\}$ and $\{M\}$ are the vectors reflecting the lateral load and moment applied at the pile head, respectively.

After the two matrices $[K_H]$ and $[K_M]$ are obtained according to Eqs. (5-22) and (5-23), then the vectors $\{\delta_h\}$ and $\{\delta_m\}$ can be calculated. Correspondingly, the deflections of a pile under a lateral load and a moment can be calculated using Eq. (5-14) and (5-17), respectively. By superposing y_{zh} and y_{zm} , the deflection of a pile, y_z , can be obtained. The moment of the pile at any depth can be calculated by double differentiating y_z .

The above described procedure is for free-head pile condition. For a fixed-head pile under a lateral load, the moment developed at the pile head due to the fixity can be obtained based on the zero-rotation condition at the pile head. A try-and-error procedure can be used to find out the value of the generated moment by ensuring the zero rotation of the pile at the pile head.

5.3.4 Validations

The above calculation procedure is easily coded into Mathematica. It is found that a size of 10×10 for the stiffness matrices $[K_H]$ and $[K_M]$ provides sufficiently accurate results. The accuracy of the present solution is verified with a non-dimensional solution by Reese and Matlock (1956) for a single soil layer with stiffness increasing with depth. Four cases with a constant of subgrade reaction, n_h , varying from 1.6 to 152 MN/m³ are evaluated. The pile used for comparison has a diameter of 0.76 m and a length of 6 m. The pile head deflections at a lateral load of 44.5 kN and a moment of 27.1 kN-m predicted by Reese and Matlock (1956) and the proposed solution for various n_h values are presented in Fig. 5-16. Apparently, a very good match is obtained.

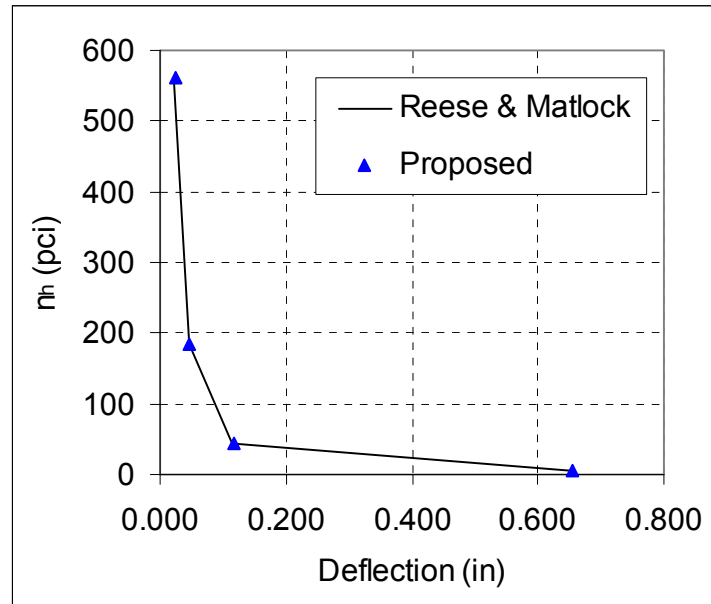
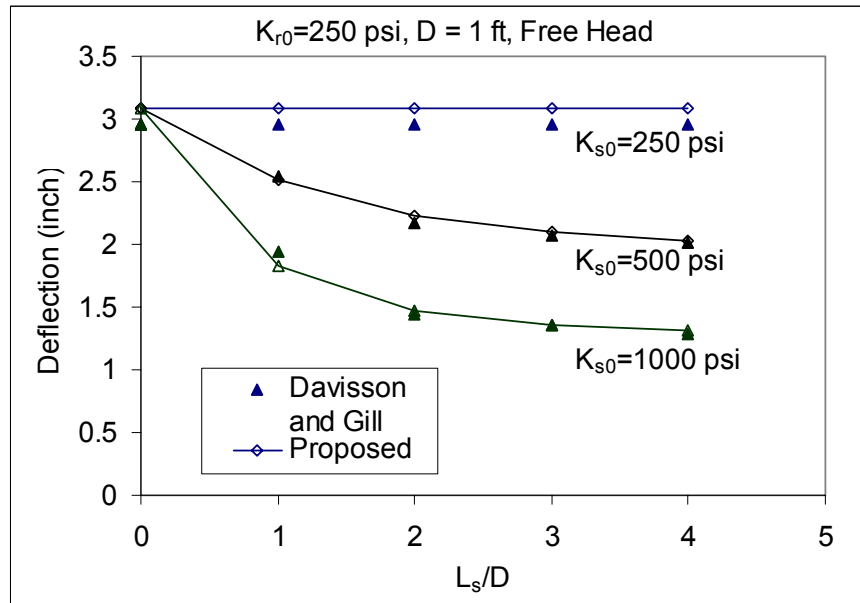


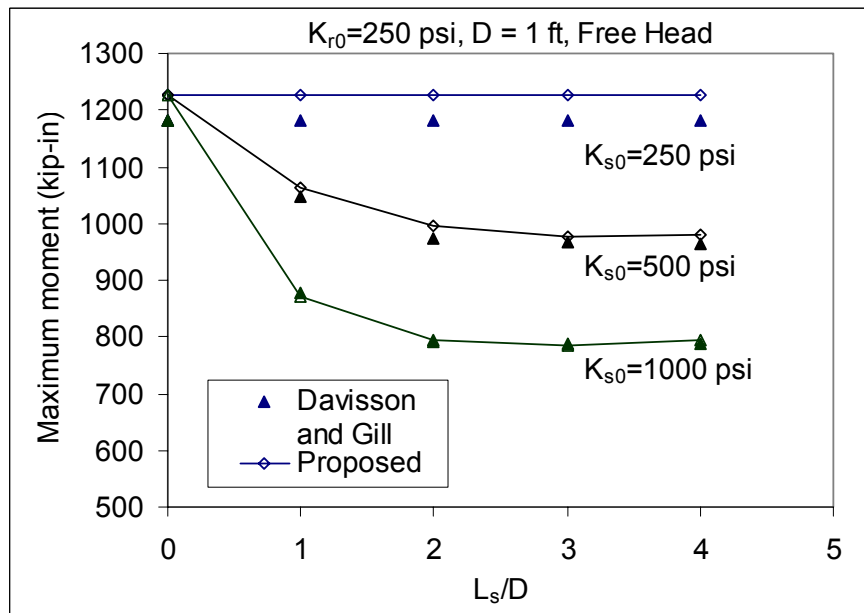
Figure 5-16 Comparison with Reese and Matlock solutions—varying soil stiffness

For layered soil condition, Davisson and Gill (1963) non-dimensional charts are employed to validate the proposed solution. Constant modulus of subgrade reaction for each layer is required by Davisson and Gill (1963) method. A hypothetical case of a 0.305 m diameter concrete pile embedded 7.32 m in a uniform soft clay. A subgrade reaction modulus, K_{r0} , of 1723.8 kPa is selected for the soft clay according to Terzaghi (1955) recommendations on K for stiff clay. The top portion of the soft clay is then replaced with 1D (diameter of pile) to 4D thick of medium and stiff clay with K_{s0} values of 3447.5 kPa and 6895 kPa, respectively. The pile has modulus of elasticity of 24.8 GPa. Both free head with a lateral load of 89 kN and a moment of 135.6 kN-m and fixed head with a lateral load of 89 kN are considered. Comparisons of deflections at the pile head and the maximum moments in the pile for cases with varying surface layer thickness L_s and varying modulus of subgrade reaction K_{s0} by Davisson and Gill non-dimensional

charts and the proposed solution are presented in Figs. 5-17 and 5-18. It can be seen that a good match for both deflection and maximum moment predictions is achieved.

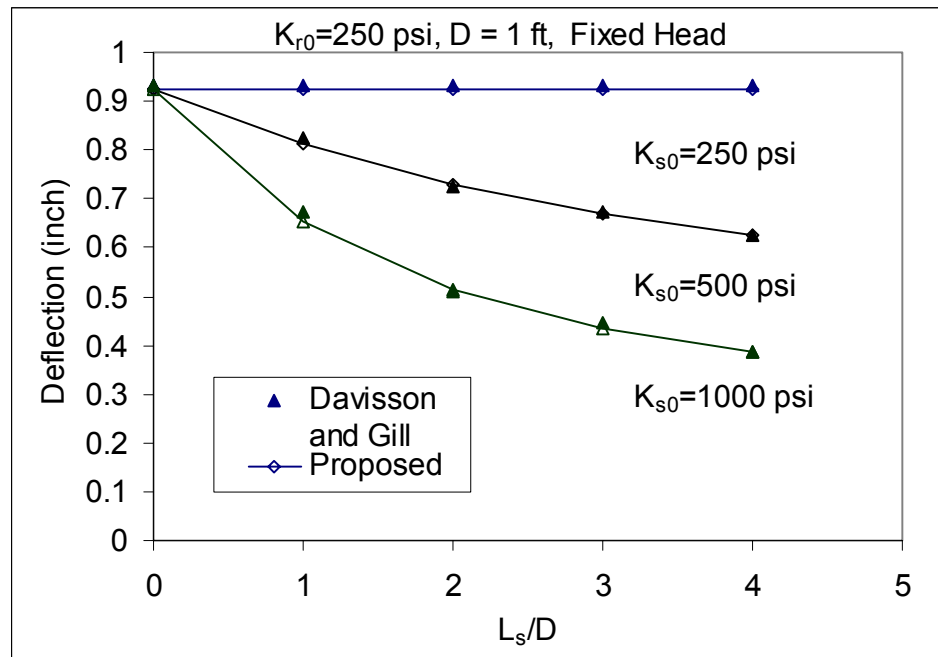


(a) Deflection

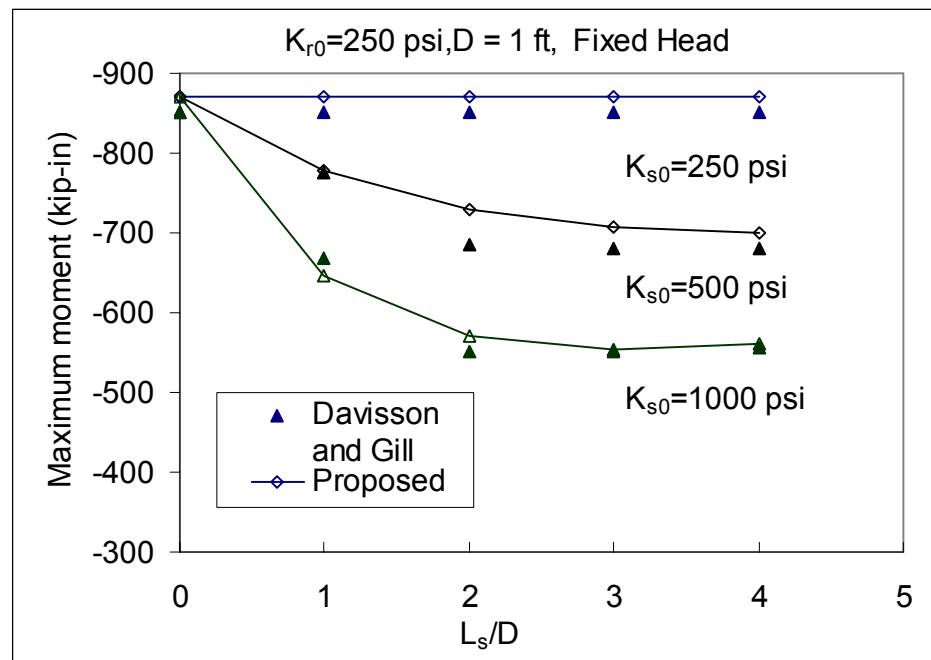


(b) Maximum moment

Figure 5-17 Comparisons with Davisson and Gill method for free head condition



(a) Deflection



(b) Maximum moment

Figure 5-18 Comparison with Davisson and Gill solution for fixed head condition

5.3.5 Methods for Determining Input Parameters

For soils, modulus of subgrade reaction can be determined using Carter (1984) equation as previously provided in Eq. (5-6). The value of n_h of soils can be determined by fitting a straight line through calculated K values along depth.

If Carter (1984) equation can not be used due to lack of soil input parameters, the following alternatives can be used. For sand, modulus of subgrade reaction is usually assumed to be linearly varying with depth. The constant of subgrade reaction n_h can be determined from Table 5-12 proposed by Liang (2002). This SPT correlation table was developed based on a sensitivity study on an extensive lateral load test database. For clay, modulus of subgrade reaction K is generally assumed to be constant with depth except the surface portion of the soil. Terzaghi (1955) recommendations on K of 7.16 MPa, 14.3 MPa, and 28.6 MPa for stiff, very stiff, and hard clay can be used for rough estimation.

For rock, the empirical equation Eq. (5-11) presented in previous section can be used to estimate modulus of subgrade reaction. The value of n_h of rock can be determined by fitting a straight line through calculated K values along depth. The following case study will demonstrate the use of these soil or rock parameter determination tables and equations.

5.3.6 Case Study

The applicability of the proposed solution for piles in layered soils, especially rock with an overlying soil layer, is validated against the results of Shaft #1 of Pomeroy-Mason lateral load test. The lateral load test was performed on a free-head drilled shaft with a diameter of 102 inch and a total embedment length of 792 inch. The shaft was embedded in rock with 312 inch of overlying sand.

The shaft and soil information are depicted in Fig. 5-19. The average SPT N value of the sand was 9.5. The modulus of rock mass for various rock depths obtained from Eq. (5-4) using modulus of intact rock core and mean GSI values are also provided in Fig. 5-19. It is assumed that the stiffness of the sand and the rock layers increasing with depth. The constant of subgrade reaction for the sand layer, n_{hs} , is taken as 38.3 pci according to the correlation table by Liang (2002).

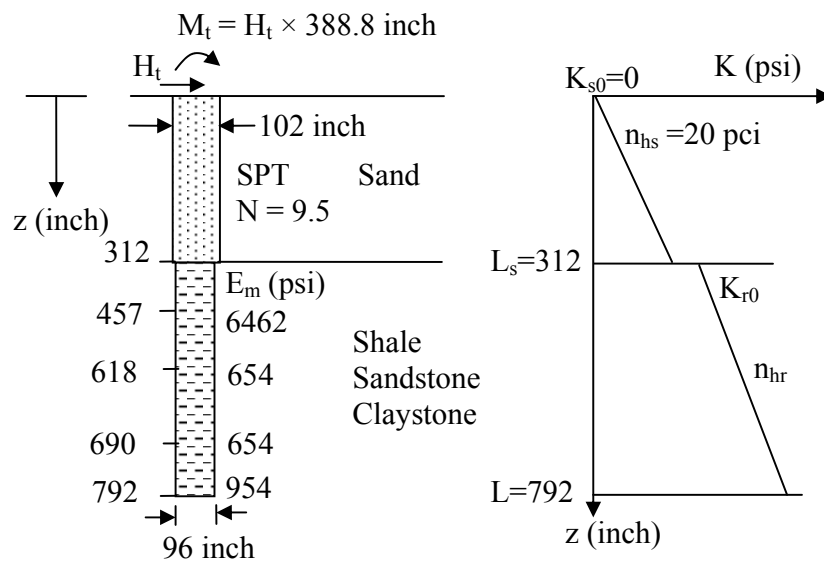


Figure 5-19 Shaft and soil profiles of the case study

Two sets values of modulus of subgrade reaction for various depths of weak rock mass are used for comparison. One set of K_{rz} is directly obtained from the experimental p-y curves derived from strain data in Chapter III, as shown in Fig. 5-20. The depth is measured from the top of rock. The trendline, which fits the data points meanwhile ensuring a positive value for K_{r0} , gives a value of 7191 psi for K_{r0} and a value of 273.5 pci for n_{hr} . The other set of K_{rz} is correlated from E_m using the proposed equation (Eq. 5-11). Based on the values of K_{rz} from the proposed empirical equation, K_{r0} and n_{hr} are obtained to be 7452.9 psi and 21.8 pci, respectively.

Other required input parameters for the code programmed in Mathematica are given as: $K_{s0} = 0$; $L_s = 312$ inch; $L = 792$ inch; $E_p = 6522$ ksi. The comparison between the measured deflections from inclinometer readings and the predicted values using the proposed solution at the soil surface is shown in Fig. 5-21. It can be seen that the proposed solution over predicts the deflections. This is desirable from view point of safety margin. Additionally, it can be seen that the predicted deflection values do not change much when the n_{hr} of the bottom rock layer is varied from 21.8 pci to 273.5 pci. This conforms to the previous conclusion that the lateral response mainly depends on properties of the surface layer. From this case study, it can be concluded that the proposed solution can provide reasonable prediction on deflections of laterally loaded drilled shafts in a two-layer soil/rock system.

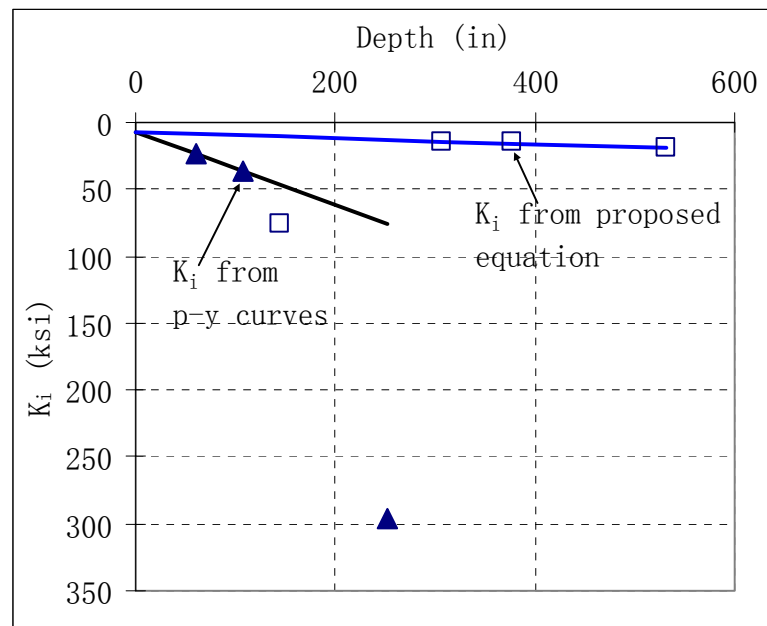


Figure 5-20 Interpretation of subgrade reaction modulus of rock

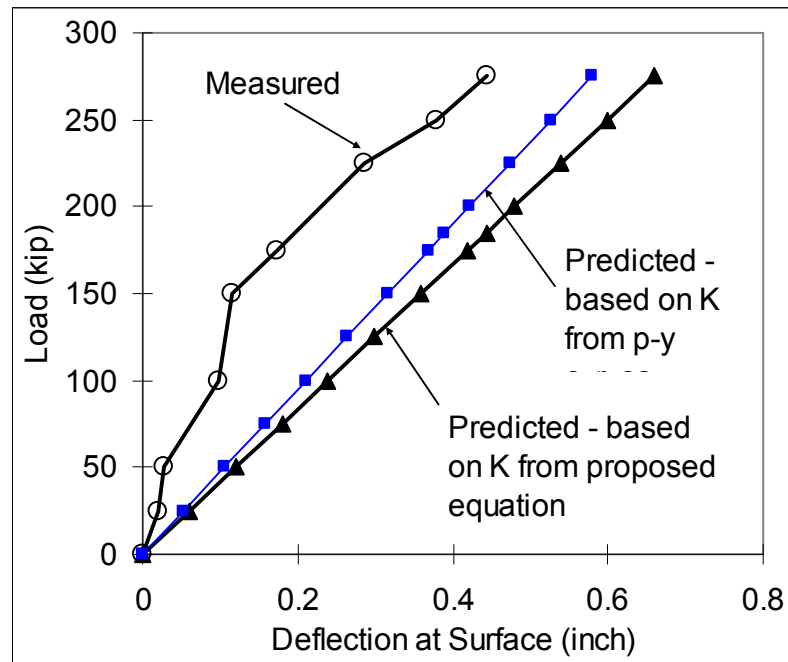


Figure 5-21 Comparison of shaft head deflections

5.4 Summary and Conclusions

In this chapter, a methodology for determining the deformation modulus of rock mass is proposed. Next, an empirical equation for estimating modulus of subgrade reaction modulus of rock mass is developed based on a parametric study using 3D FEM analysis. Finally, an elastic numerical solution based on subgrade reaction theory is proposed for a two layer soil/rock profile, especially rock mass overlying with a layer soil, using variational approach.

Based on above work, the following conclusions are drawn:

1. Dilatometer test is good for weak rock and the Goodman Jack test is good for hard and competent rock;

2. The proposed empirical equation for estimating the deformation modulus of rock mass can provide reasonable estimation on E_m according to the field data from Iron-ton-Russell;
3. The validation using field test data on the proposed empirical equation for determining the modulus of subgrade reaction K shows that it can yield reasonable and conservative results;
4. The proposed elastic numerical solution can match the results from rigorous subgrade reaction solution for an assumed one layer soil problem;
5. The validation using field lateral load test data shows that the proposed elastic numerical solution can provide reasonable results for small working loads. Therefore, the elastic solution provides an efficient way to preliminarily estimate the deflections of a drilled shaft in layered soil/rock under small working lateral loads.

CHAPTER VI

P-Y CRITERION FOR ROCK MASS

In this chapter, a hyperbolic p-y criterion is developed based on considerations of both theoretical derivations and numerical (finite element) analysis results. The methods for determining pertinent rock parameters needed for constructing the p-y curves are presented. Two full-scale lateral load tests introduced in Chapter III are used to validate the applicability of the developed hyperbolic p-y curves for rock. The comparisons between the computed shaft responses and the actual measured are fairly good for the load-deflection curves at the load point as well as the maximum bending moment in the shaft. Although some materials have been presented in previous chapters, essential information is duplicated here to make this chapter easy to read.

6.1 General Shape of P-y Curve in Rock

Two full-scale lateral load tests results of fully instrumented drilled shafts socketed into rock mass have been presented in Chapter III. Piecewise polynomial curve fitting technique was employed to deduce p-y curves from strain gage readings obtained during lateral load tests. As can be seen in Figs. 6-1 and 6-2, the general shape of these p-y curves for rocks could be fit mathematically by a hyperbolic equation given in Eq. (6-1) and illustrated schematically in Fig. 6-3.

$$p = \frac{y}{\frac{1}{K_i} + \frac{y}{p_u}} \quad (6-1)$$

where p_u is the ultimate resistance of rock mass per unit shaft length, and K_i is the initial tangent slope to the p-y curves.

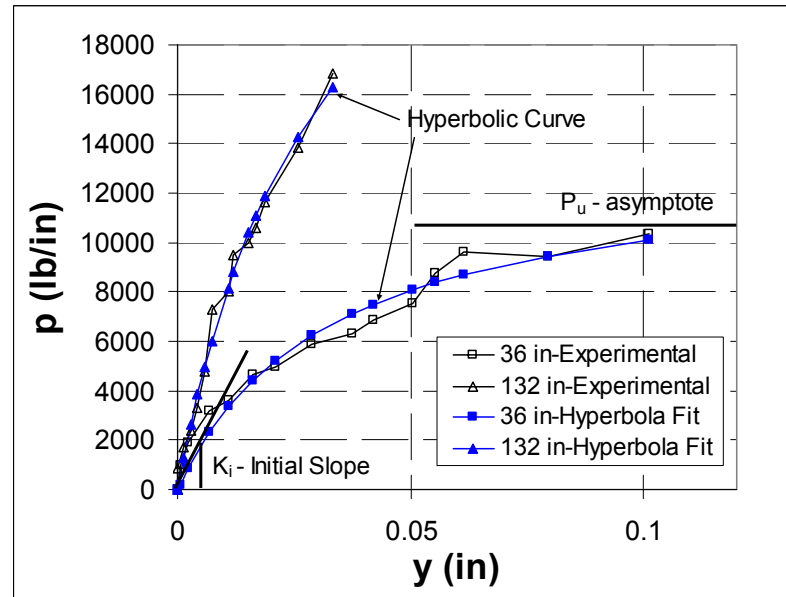


Figure 6-1 P-y curves deduced from shaft #4 of load test at Dayton

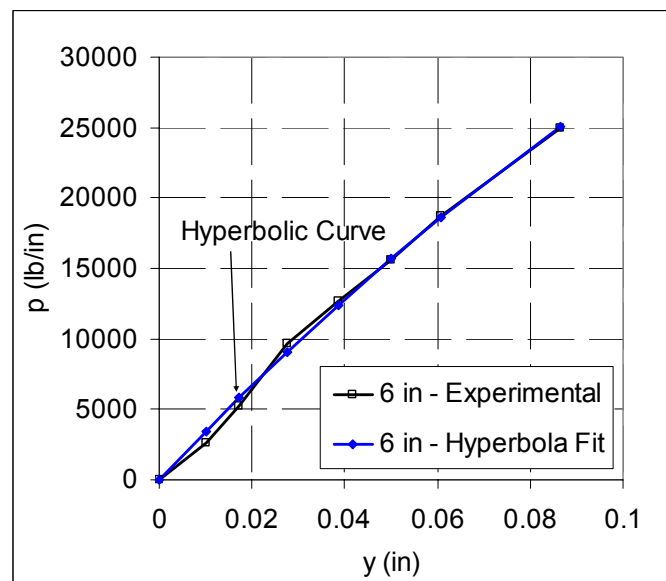


Figure 6-2 P-y curves deduced from Shaft #2 of load test at Pomeroy-Mason

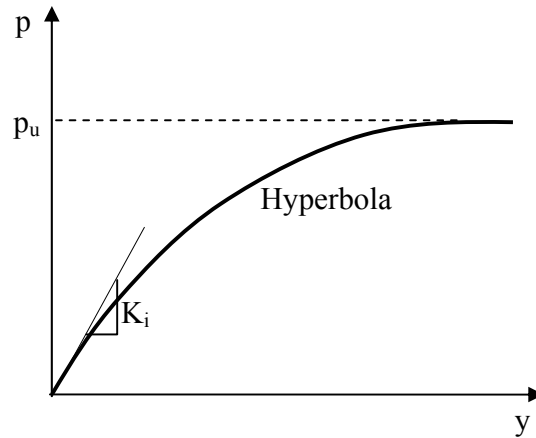


Figure 6-3 Schematics of a hyperbolic p-y curve

6.2 Determination of p_u

6.2.1 Failure Modes

A 3D finite element model (FEM) using ABAQUS was used to investigate the mobilization mechanisms of resistance of rock mass near ground surface and at great depth. Detailed investigation results have been presented previously in Chapter IV.

For rock mass existing near ground surface, the FEM simulation results show that the lateral loading of the shaft tends to fail the rock mass as a wedge as shown in Fig. 6-4, where, F_{net} is the total net rock resistance, D is the diameter of the drilled shaft, H is the height of the wedge, F_a is the active earth force exerted on the drilled shaft, F_s is the friction force on the sides of the wedge, F_n is the normal force applied to the side faces and is assumed to be equal to at-rest earth force, F_{sb} is the friction force on the bottom surface, F_{nb} is the normal force on the bottom surface determined through force equilibrium in vertical direction, W is the weight of the wedge, σ'_{v0} is effective overburden earth pressure on the top of rock and equals to zero if no overlying soil is present.

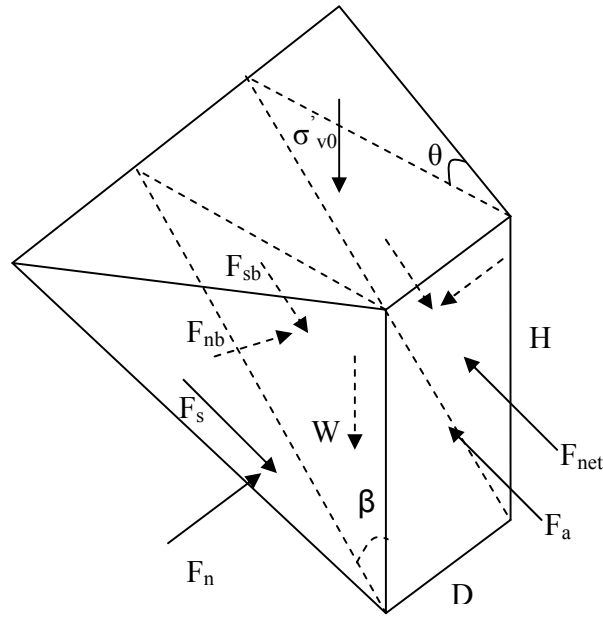


Figure 6-4 Failure mode for rock near ground surface

For rock mass at great depth, considering the possible reduction of strength of brittle rock mass after the maximum stress reaches the peak strength of rock, the ultimate state (or failure) is defined when the rock has experienced maximum compressive stress equal to compressive strength and the rock-shaft side shear strength has reached, as shown in Fig. 6-5, where τ_{\max} is the maximum side shear resistance between a drilled shaft and rock mass, and p_L is the normal limit pressure of rock mass. The patterns of normal and shear stress distribution at the ultimate state are obtained from FEM simulation results and could be described as sine functions. In particular, FEM study shows that the normal stresses are very small at points A and D in Fig. 6-5; whereas, the maximum shear stresses are observed at points C and E and negligible shear stresses are observed at points B and D.

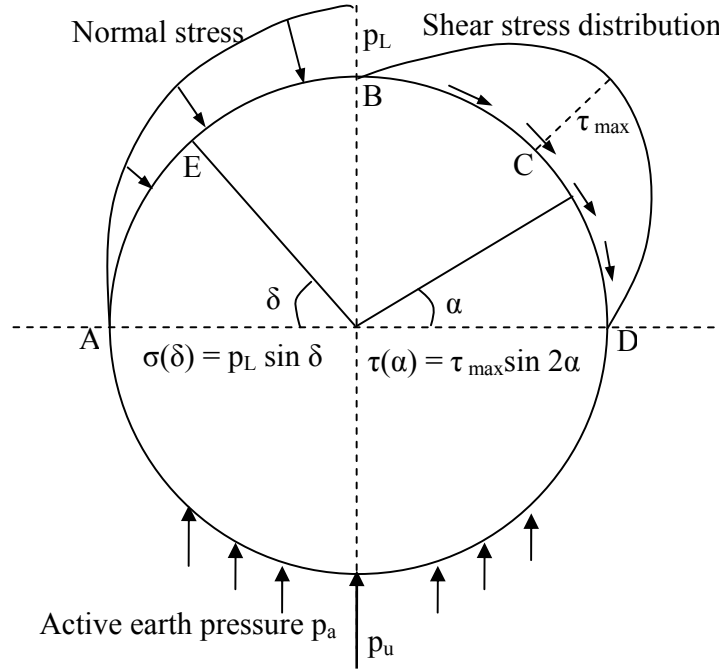


Figure 6-5 Failure mode of rock at great depth

6.2.2 P_u Near Surface

For wedge type of failure, the ultimate rock resistance per unit length, p_u (in the unit of Force/Length) of the drilled shaft at depth H is given as follows (See Section 4.5.1 for more detailed derivation).

$$p_u = 2C_1 \cos \theta \sin \beta + C_2 \sin \beta + C_3 \cos \beta - 2C_4 \sin \theta - C_5 \quad (6-2)$$

where

$$C_1 = H \tan \beta \sec \theta (c' + K_0 \sigma'_{v0} \tan \phi' + \frac{H}{2} K_0 \gamma' \tan \phi') \quad (6-3)$$

$$C_2 = C_3 \tan \phi' + c' (D \sec \beta + 2H \tan \beta \sec \beta \tan \theta) \quad (6-4)$$

$$C_3 = \frac{D \tan \beta (\sigma'_{v0} + H\gamma') + H \tan^2 \beta \tan \theta (2\sigma'_{v0} + H\gamma') + c' (D + 2H \tan \beta \tan \theta) + 2C_1 \cos \beta \cos \theta}{\sin \beta - \tan \phi' \cos \beta} \quad (6-5)$$

$$C_4 = K_0 H \tan \beta \sec \theta (\sigma'_{v0} + \frac{1}{2} \gamma' H) \quad (6-6)$$

$$C_5 = \gamma' K_a (H - z_0) D \quad (C_5 \geq 0) \quad (6-7)$$

$$K_a = \tan^2 (45 - \phi' / 2) \quad (6-8)$$

$$K_0 = 1 - \sin \phi' \quad (6-9)$$

$$z_0 = \frac{2c'}{\gamma' \sqrt{K_a}} - \frac{\sigma'_{v0}}{\gamma'} \quad (6-10)$$

$$\beta = 45 + \phi'/2 \quad (6-11)$$

$$\theta = \phi'/2 \quad (6-12)$$

in which c' is the effective cohesion of the rock mass, ϕ' is the effective friction angle of the rock mass, γ' is the effective unit weight of rock mass. Discussions of methods for determining pertinent rock mass properties will be discussed later in this Chapter.

6.2.3 P_u at Great Depth

When the existing vertical soil pressure is sufficiently high, for example, as in the case of shaft/rock interaction at great depth, then FEM simulation results reveal that the ultimate rock resistance is reached when both the maximum shear and normal pressure of rock mass have reached their limiting values τ_{\max} and p_L , respectively. The distributions of the shear and normal stresses based on FEM analysis are depicted in Fig. 6-5. As previously shown in detail in Section 4.5.2 of Chapter IV, the ultimate rock resistance, p_u , at great depth can be calculated as follows.

$$p_u = \left(\frac{\pi}{4} p_L + \frac{2}{3} \tau_{\max} - p_a \right) D \quad (6-13)$$

where p_a = active horizontal earth pressure and is given by

$$p_a = K_a \sigma'_v - 2c' \sqrt{K_a} \quad (p_a \geq 0) \quad (6-14)$$

σ'_v = effective overburden pressure at the depth under consideration including the pressure from overburden soils.

6.2.4 P_u of Jointed Rock

For jointed rock with a set of parallel weak planes which dominates the behavior of rock mass under lateral loads, the above equations for p_u can still be used after making the following adjustments. For rock mass failure at a great depth, the high overburden pressure will prohibit the possible sliding failure on the weak planes. Therefore, Eq. (6-13) for in-depth rock mass still works for jointed rock.

For rocks that follow the wedge type failure, the bottom plane of the failure wedge can either be within the rock mass or on a weak plane. It is therefore necessary to calculate p_u for both failure modes and that the smaller value is used as the final p_u . For failure mode due to shearing failure of rock mass, Eq. (6-2) can be directly used. For failure mode due to shearing failure through a weak plane, the same wedge failure model shown in Fig. 6-4 can be used. Eq. (6-2) is therefore valid for calculating p_u , except that the angle β is the inclination of the weak plane and the values of c' and ϕ' for the bottom face of the failure wedge should be obtained from laboratory tests by shearing samples along a weak plane. Specifically, the c' and ϕ' needed for Eqs. (6-4) and (6-5) should come from the results of lab tests on samples with a weak plane. However, the c' and ϕ' in Eq. (6-3) needed for the two sides of the failure wedge can still be obtained using instantaneous cohesion and friction angle correlated from Hoek-Brown strength criterion.

6.3 Initial Tangent to P-y Curve K_i

The initial tangent to a p-y curve, which has a unit of F/L^2 , was recommended previously by Reese (1997) as follows.

$$K_i \approx k_i E_m \quad (6-15)$$

where k_i = a dimensionless constant. Reese (1997) further suggested the following empirical correlations:

$$k_i = 100 + 400 z/(3D) \text{ for } 0 \leq z \leq 3D \quad (6-16)$$

$$k_i = 500 \text{ for } z > 3D \quad (6-17)$$

Although Reese's equation is simple to use, it nevertheless does not take into account other potential influencing factors, such as relative stiffness between shaft and rock, Poisson's ratio of rock, and diameter of shaft.

The parametric study presented previously in Chapter V has led to the findings that the following semi-empirical equation may work better.

$$K_i = E_m (D / D_{\text{ref}}) e^{-2v \left(\frac{E_p I_p}{E_m D^4} \right)^{0.284}} \quad (6-18)$$

where E_m = modulus of rock mass; D_{ref} = reference shaft diameter equal to one foot.

6.4 Rock Mass Properties

6.4.1 Strength Parameters

Hoek-Brown (H-B) strength criterion for rock mass (Hoek et al., 2002) possesses distinct advantages in that it considers the effect of secondary structures of rock (e.g., joint, filling, and spacing) on the rock strength. It should be noted that this strength criterion is not suitable for rock with one or two sets of dominant joints. The H-B strength criterion can be expressed as

$$\sigma'_1 = \sigma'_3 + \sigma_{ci} \left(m_b \frac{\sigma'_3}{\sigma_{ci}} + s \right)^a \quad (6-19)$$

where σ'_1 = the major principal stress at failure, σ'_3 = the minor principal stress at failure, σ_{ci} = uniaxial unconfined compressive strength of intact rock, GSI = Geological Strength Index (Marinos and Hoek, 2000), m_b , s and a = constants that depend on the characteristics of rock mass and can be estimated as follows (Hoek, et al., 2002).

$$m_b = \exp\left(\frac{GSI - 100}{28 - 14D_r}\right)m_i \quad (6-20)$$

$$s = \exp\left(\frac{GSI - 100}{9 - 3D_r}\right) \quad (6-21)$$

$$a = \frac{1}{2} + \frac{1}{6}(e^{-GSI/15} - e^{-20/3}) \quad (6-22)$$

where m_i is a material constant that can be obtained from Table 4-3 in Chapter IV, D_r is a factor that depends upon the degree of disturbance to which the rock mass has been subjected to due to blast damage and stress relaxation. For deep foundation excavation, D_r can be assumed to be zero.

Hoek (1990) further provides the method for estimating Mohr-Coulomb friction angle ϕ' and cohesion c' from Hoek-Brown strength criterion as follows.

$$\phi' = 90 - \arcsin\left(\frac{2\tau}{\sigma'_1 - \sigma'_3}\right) \quad (6-23)$$

$$c' = \tau - \sigma'_n \tan \phi' \quad (6-24)$$

where σ'_1 can be obtained using Eq. (6-19); and

$$\sigma'_n = \sigma'_3 + \frac{(\sigma'_1 - \sigma'_3)^2}{2(\sigma'_1 - \sigma'_3) + 0.5m_b\sigma'_{ci}} \quad (6-25)$$

$$\tau = (\sigma'_n - \sigma'_3)\sqrt{1 + \frac{m_b\sigma'_{ci}}{2(\sigma'_1 - \sigma'_3)}} \quad (6-26)$$

σ'_3 is computed as vertical effective stress.

6.4.2 Rock-Shaft Interface Strength

The empirical equation for estimating side shear resistance, τ_{\max} (MPa), proposed by Kulhawy and Phoon (1993) is adopted here.

$$\tau_{\max} = 5.42 \sigma_{ci}^{0.5} \quad \text{where the units are in psi} \quad (6-27)$$

6.4.3 Rock Mass Modulus E_m

The empirical equation (6-18) requires input of E_m in order to compute K_i . Ideally, it is preferred to perform dilatometer/pressuremeter tests to obtain in-situ modulus of rock mass. However, if dilatometer tests could not be performed at the site, then the following empirical equation derived in Chapter V could be used.

$$E_m = \frac{E_i}{100} (e^{GSI/21.7}) \quad (6-28)$$

where E_i is the modulus of intact rock core that could be determined from unconfined compression test on rock core samples.

6.5 Construction of P-y curves for Rock Mass

To calculate p_u according to wedge failure mode (Eq. 6-2), it should be noted that the value of σ'_3 can be taken as effective overburden pressure at the depth of $1/3H$ for estimating the values of ϕ' and c' using Eqs. (6-23) and (6-24), as the side surface is triangular. For in-depth failure mode, p_L is taken as the major principal stress at failure σ'_1 , which is calculated using Eq. (6-19) by equating σ'_3 to σ'_v . The effective cohesion c' needed in Eq. (6-14) can be calculated using Eq. (6-24) by equating σ'_3 to σ'_v .

The value of p_u is the smaller of the values calculated using Eqs. (6-2) and (6-13). The main parameters required for calculating p_u , other than the properties of a drilled shaft, are: σ_{ci} (unconfined compressive strength of intact rock core), GSI, and m_i . The value of m_i can be obtained according to Marinos and Hoek (2000). GSI values are based on the structure and the surface condition of rock mass. For cored rock, the physical appearance of the material recovered in the core can be used to estimate GSI value using the charts presented by Marinos and Hoek (2000).

Additionally, GSI can be obtained from Rock Mass Rating (RMR) (see Hoek and Brown, 1997). If Bieniawski (1976) RMR_{76} is used, the rock mass should be assumed to be completely dry and a rating of 10 could be assigned to the groundwater, and adjustment for discontinuity orientation value should be set to zero. If Bieniawski (1989) RMR_{89} is used, the value of 15 should be assigned to groundwater rating and adjustment for discontinuity value is set to zero. Consequently, the following relationship can be established.

$$GSI = RMR_{76} \quad (6-29)$$

$$GSI = RMR_{89} - 5 \quad (6-30)$$

6.6 Comparison of the Proposed P-y Criterion with That of Gabr et al. (2002)

Although the proposed p-y criterion has same mathematic expression as that of Gabr et al. (2002), the equations for calculating the modulus of rock mass and ultimate resistance of rock mass are different. Gabr et al. (2002)'s p-y criterion is mainly based on the equations of Vesic (1961) for calculating K_i and Zhang et al. (2000)'s equation for calculating p_u . As pointed out previously in Chapter II, Vesic (1961)'s equation was

developed for the case of beam on elastic foundation, while Zhang et al. (2000)'s equation was based on a pure assumption of stress distribution of shaft-rock interaction. However, the proposed p-y criterion employs 3D FEM studies to carefully identify the failure modes of rock mass under lateral loads and establish an empirical equation for estimating modulus of rock mass. The main differences of the two p-y criteria are summarized in Table 6-1.

6.7 Case Studies

The two lateral load tests reported in Chapter III and another two load tests by Gabr et al. (2002) are used for validating the developed p-y criterion. The soils above the rock at the test sites were either excavated or isolated using a casing with its diameter larger than the diameter of test drilled shafts. This was done to eliminate the influence of soils on the soil/shaft lateral interaction. The diameter of test drilled shafts ranges from 6 ft to 8 ft; and the rock-socket length ranges from 18 ft to 57 ft. The types of rock at these sites are shale, limestone, claystone, siltstone, sandstone, and mudstone. The unconfined compressive strength of rock mass ranges from 19 psi to 9073 psi. The modulus of intact rock mass ranges from 1.5 ksi to 1292 ksi.

Table 6-1 Comparison of P-y Criteria

	Proposed p-y criterion	P-y criterion by Gabr et al. (2002)
P-y expression	$p = \frac{y}{\frac{1}{K_i} + \frac{y}{p_u}}$	$p = \frac{y}{\frac{1}{K_i} + \frac{y}{p_u}}$
K _i , modulus of subgrade reaction	$K_i = E_m (D / D_{ref}) e^{-2\nu \left(\frac{E_p I_p}{E_m D^4} \right)^{0.284}}$ <p>This empirical equation is developed based on a parametric study using 3D FEM analysis which is validated against the Dayton lateral load test results. Effects of diameter of drilled shaft, modulus of rock mass, Poisson's ratio of rock, and shaft-rock relative stiffness on K_i are considered. It is validated against field test data at Dayton, Pomeroy-Mason, and North Carolina reported by Cho et al. (2001).</p>	<p>When dilatometer tests are performed to obtain E_m, the following procedure is used:</p> <p>For $z < T_0$, $K_i = \frac{0.65E}{1-\nu^2} \left[\frac{ED^4}{E_p I_p} \right]^{1/12}$ This equation was originally proposed by Vesic (1961) based on a solution for beam on elastic foundation.</p> <p>For $z > T_0$, $K_i = I_T \frac{0.65E}{1-\nu^2} \left[\frac{ED^4}{E_p I_p} \right]^{1/12}$ where T₀ is depth of point of rotation, and $T_0 = [1 + 0.18 \log(E_p I_p / E_m L^4)] L$. The value of K_i at a depth greater than T₀ is increased by an empirical factor I_T which is equal to $-28 - 383 \log (T_0 / L)$.</p>
E _m , modulus of rock mass	<p>Empirical equation $E_m = \frac{E_i}{100} (e^{GSI/21.7})$ can be used. This equation was developed based on Ironton-Russell dilatometer test data and historical data by Bieniawski (1978) and Serafin and Pereira (1983).</p>	<p>Empirical equation proposed by Hoek and Brown (1997) is used as follows.</p> $E_m = \sqrt{\frac{\sigma_{ci}}{100}} 10^{(GSI-10)/40} \text{ (GPa)}$ <p>where σ_{ci} is unconfined compressive strength of rock core sample. This equation predicted 6.6 to 10 times of the measured E_m according to the dilatometer test data from Ironton-Russell project.</p>
P _u , ultimate resistance of rock per unit length of shaft	<p>Eq. (6-2) for rock layer near surface</p> $p_u = \left(\frac{\pi}{4} p_L + \frac{2}{3} \tau_{max} - p_a \right) D \text{ for in-depth layer}$ <p>p_L is calculated using Hoek-Brown strength criterion and τ_{max} is based on Kulhawy and Phoon (1993) equation:</p> $\tau_{max} = 0.45 \sigma_{ci}^{0.5} \text{ (MPa)}.$	<p>p_u = (p_L + τ_{max}) D. This was proposed by Zhang et al. (2000).</p> <p>p_L is calculated using Hoek-Brown strength criterion and</p> $\tau_{max} = 0.2 \sigma_{ci}^{0.5} \text{ (MPa)}.$

6.7.1 Dayton Load Test

The drilled shafts tested at Dayton site are 6 feet in diameter with 18 feet rock socket in shale. The test set up and the instrumentation installed in the drilled shafts were depicted previously in Fig. 3-2. A total of 36 #11 primary rebars and #6 spirals are used to form a reinforcement cage. Details of this full-scale lateral load test were reported in Section 3.1 of Chapter III. The rock consists of soft to medium gray shale interbedded with hard gray limestone. The limestone interbeds are typically less than 1 ft thick. The gray shale is slightly weathered to decomposed, weakly calcareous, and very thinly laminated. The parameters used for generating the proposed p-y curves for rock are summarized in Table 6-2. The determination of the values of σ_{ci} , GSI and E_i has been discussed previously in Section 3.1.1. The values of m_i are obtained from Table 4-3 based on rock types previously described in section 3.1.1.

Table 6-2 Input Rock Mass Parameters of Dayton Load Test

Depth (in)	γ' (pci)	σ_{ci} (psi)	GSI	m_i	E_i (ksi)
36	0.038	5668	40.5	6	590
60	0.038	5668	40.5	6	590
96	0.038	5668	61	6	590
132	0.038	5668	61	6	590
156	0.038	5668	61	6	590

The p-y curves generated from hyperbolic criterion and tabulated rock properties are presented in Fig. 6-6. They are fed into LPILE computer program (Reese, et. al., 2004) to compute the response of the test shaft #4 under the applied lateral loads. The pertinent properties for drilled shafts are as follows: $D = 6$ ft; $E_p = 3961000$ psi; Poisson' ratio = 0.3; $I_p = 1319167$ in⁴. Non-linear shaft stiffness option in LPILE is used to take into

account of the evolution of stiffness due to concrete cracking. The modulus of rock mass is obtained by correlation using the empirical equation (6-28).

The predicted load-deflection curve at the shaft head is compared with the measured in Fig. 6-7. In general, a good agreement between the measured and the predicted can be observed. Although there is some discrepancy between the two curves at small load levels, the predicted deflections are larger than the measured values (on safe side). As shown in Fig. 6-8, a good match of the maximum moments in the drilled shaft at various lateral load levels applied at shaft head is achieved between the measured and computed. The comparison between the measured deflection-depth curves from inclinometer readings and those predicted from LPILE analysis is provided in Fig. 6-9. Fig. 6-10 shows the comparison of the measured moment-depth curves from strain gage readings and those predicted from LPILE analysis. From Figs. 6-9 and 6-10, it can be seen that the predictions are comparable with those measured values.

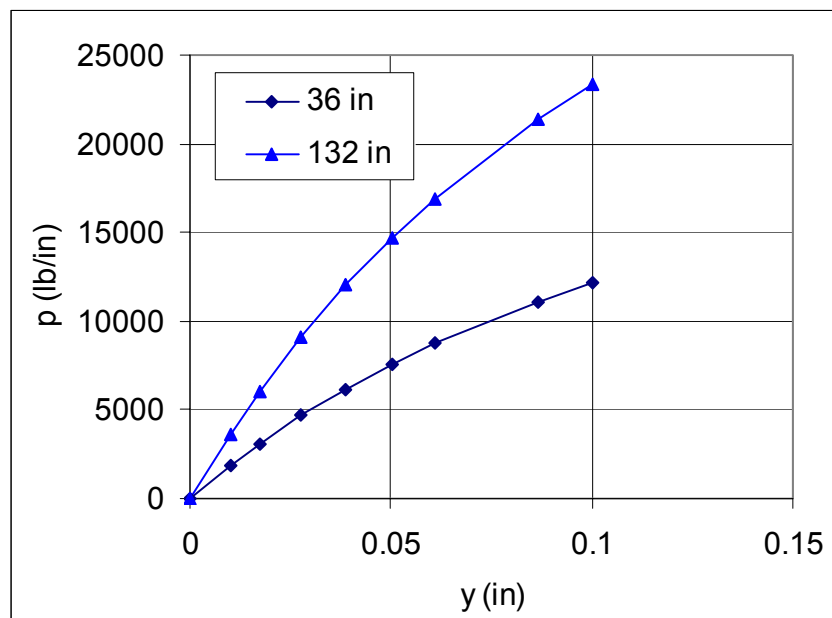


Figure 6-6 Hyperbolic p-y curves of Dayton site

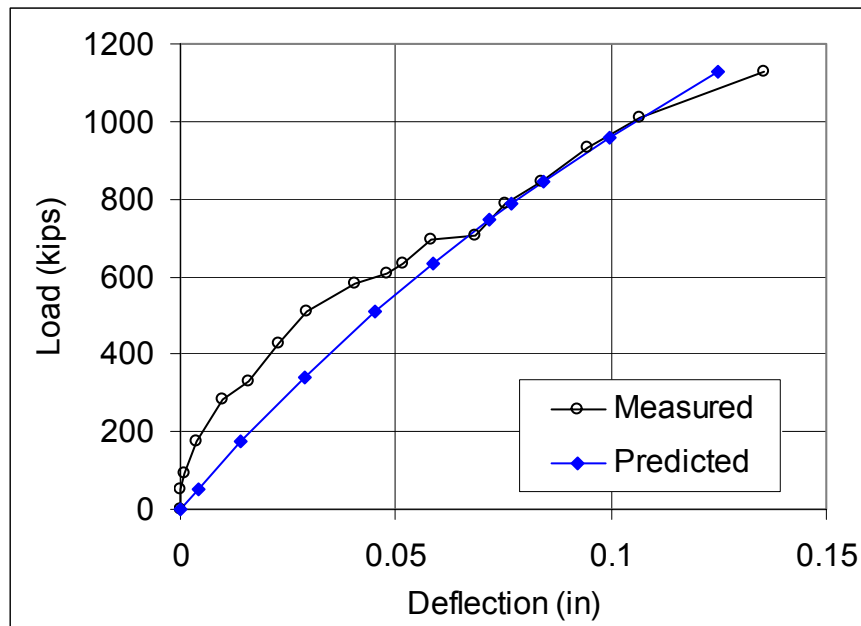


Figure 6-7 Comparison of load-deflection of test shaft #4 at Dayton load test

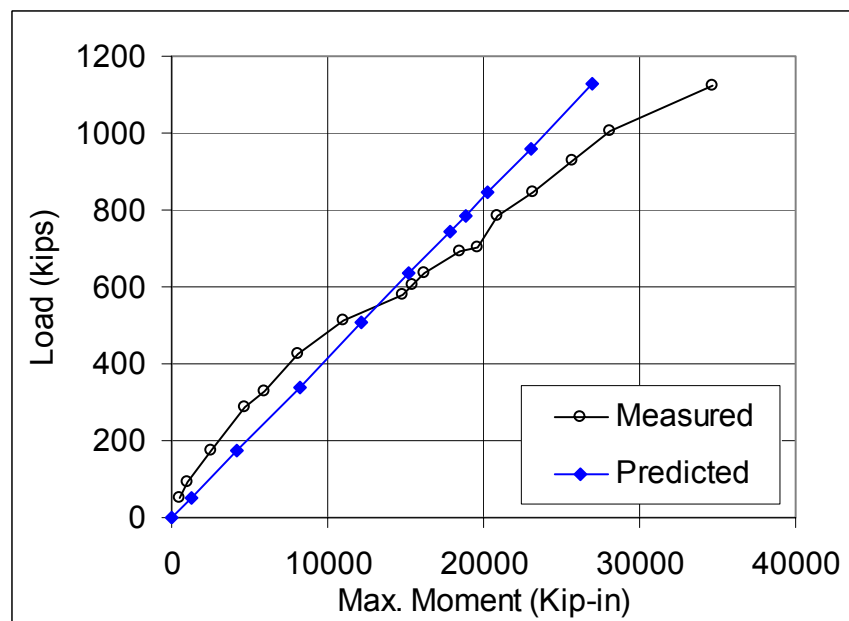


Figure 6-8 Comparison of load-Maximum moment of test shaft #4 at Dayton load test

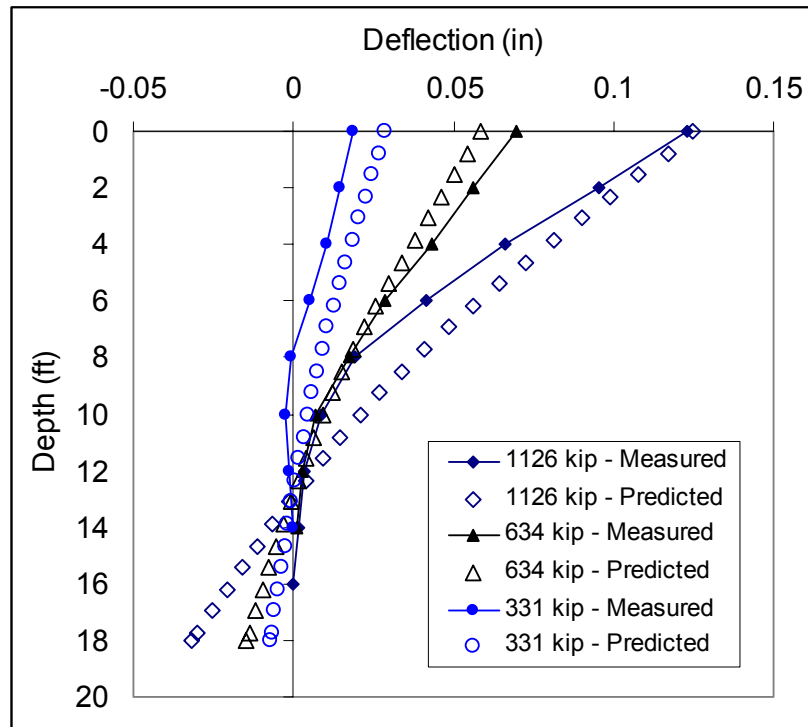


Figure 6-9 Comparisons of deflection-depth curves of shaft #4 at Dayton test

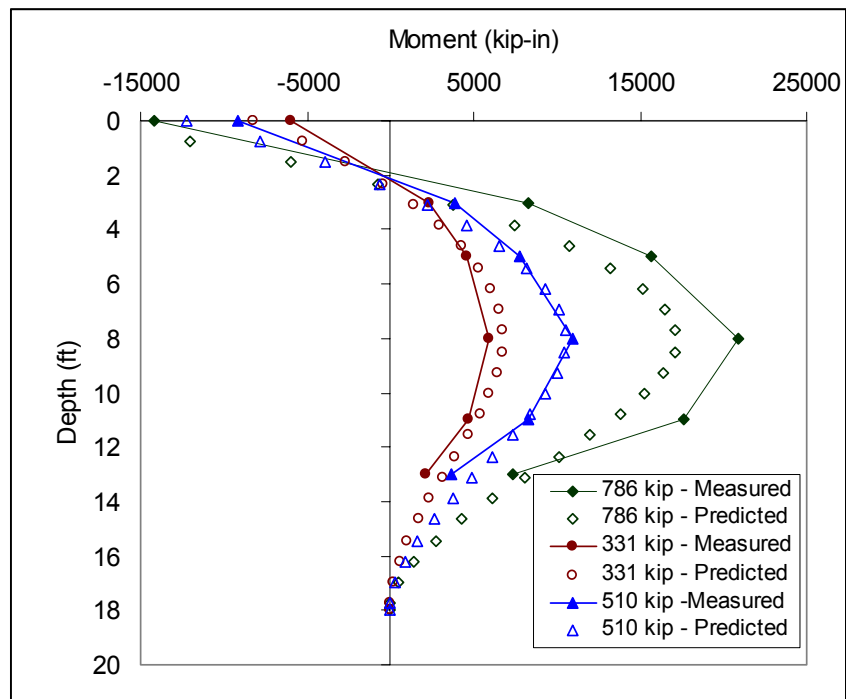


Figure 6-10 Comparisons of moment-depth curves of shaft #4 at Dayton test

6.7.2 Pomeroy-Mason Load Test

The results of a lateral load test on two drilled shafts socket in shale near Ohio River between Pomeroy, Ohio and Mason, West Virginia were reported in Section 3.2 of Chapter III. The test drilled shaft was 8.5 feet in diameter and 112.9 feet long, in which rock socket length was 56.8 feet. The diameter of the rock socket was 8 feet. A total of 28#18 bars and #6 ties at 12 inch spacing are used to form the reinforcement cage. The 28-day unconfined compressive strength of concrete was 5115 psi. To eliminate soil and shaft interaction, a 1 inch thick casing with 8.5 ft diameter and a second casing with 11 ft diameter were installed in the top 56 feet of overburden soil. The details of the load test set up and instrumentation were previously shown in Fig. 3-10.

The bedrock core recovered was described as shale with interbedded siltstone, sandstone and mudstone. The properties of rock used to generate p-y curves are summarized in Table 6-2. The depth shown in Table 6-3 is measured from the top of the bedrock. Poisson's ratio of the rock mass is assumed to be 0.3. The modulus of rock mass is determined by the empirical correlation equation (6-28). The determination of the values of γ' , σ_{ci} , GSI and E_i has been discussed previously in Section 3.1.1. The values of m_i are obtained from Table 4-3 based on rock types previously described in section 3.2.1.

Table 6-3 Input Rock Mass Parameters of Pomeroy-Mason Load Test

Depth (in)	γ' (pci)	σ_{ci} (psi)	GSI	m_i	E_i (ksi)
6	0.059	3797	42	6	344.8
66	0.059	3797	42	6	344.8
126	0.059	3797	42	6	344.8
210	0.059	3797	42	6	344.8
314	0.060	9073	45	17	1292
391	0.049	19	38	4	1.5
504	0.047	44.3	28	4	1.5
648	0.055	826.2	44	4	81

The p-y curves generated from hyperbolic criterion and tabulated rock properties are presented in Fig. 6-11. The computer program LPILE with the generated p-y curves is used to compute the response of the test shafts under the applied lateral loads. The effect of 1 inch thick casing for the drilled shaft above rock is included in the computer analysis.

The computed load-deflection curve at the loading point of the test Shaft #2 is compared with the actual measured in Figs. 6-12. It can be seen that a good match between the predicted curve and the measured curve is achieved for the initial portion of the curve. Although LPILE with the input p-y curves under-predicts the deflections at large loading levels, the error defined as the ratio of the deflection difference divided by the measured deflection, is less than 34%. A good agreement between the measured maximum moment from strain gage readings and the LPILE computed maximum moment in the shaft is achieved, as shown in Fig. 6-13. The comparison between the measured deflection-depth curves from inclinometer readings and those predicted from LPILE analysis is provided in Fig. 6-14. Fig. 6-15 shows the comparison of the measured moment-depth curves from strain gage readings and those predicted from LPILE analysis. From Figs. 6-14 and 6-15, it can be seen that the predicted values match those measured.

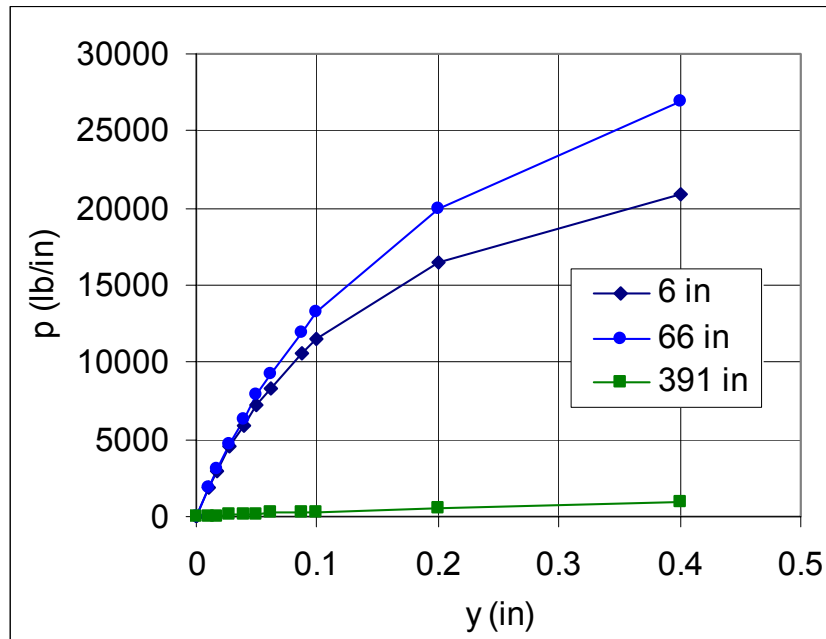


Figure 6-11 Hyperbolic p-y curves of Pomeroy-Mason site

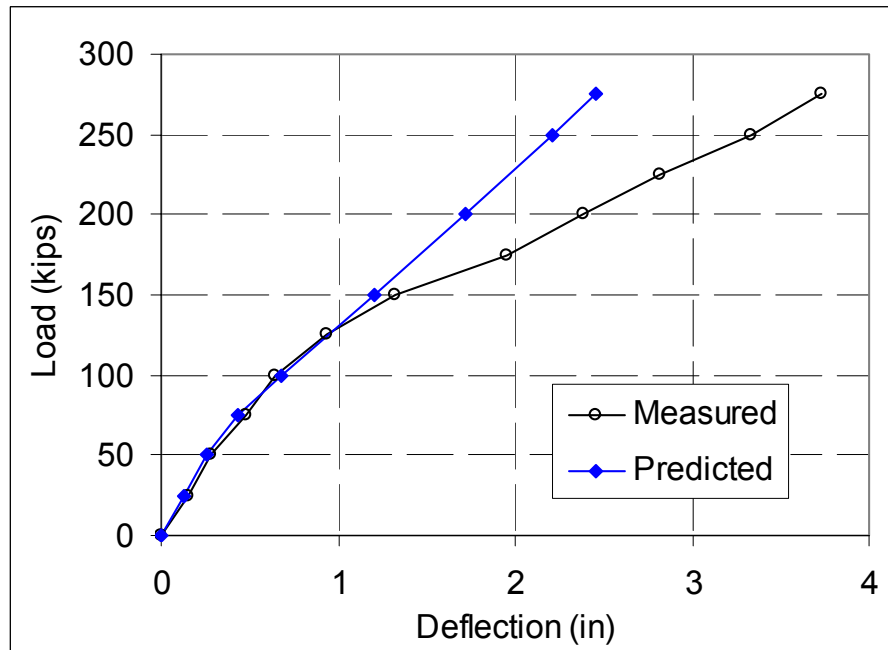


Figure 6-12 Comparison of load-deflection at the loading point for Pomeroy-Mason test

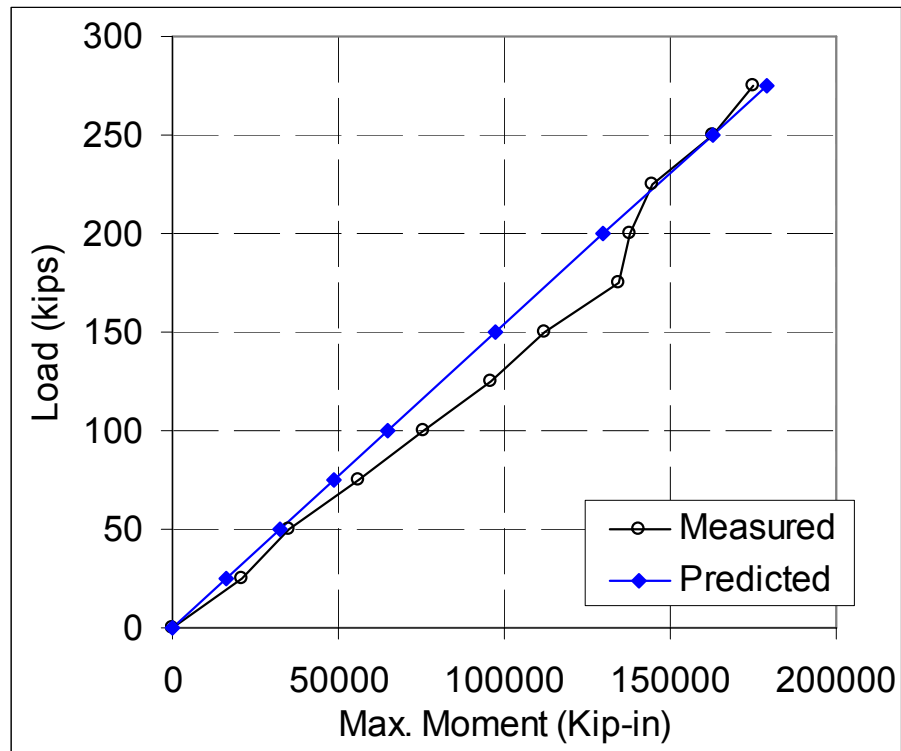


Figure 6-13 Comparison of load-Maximum moment of Pomeroy-Mason load test

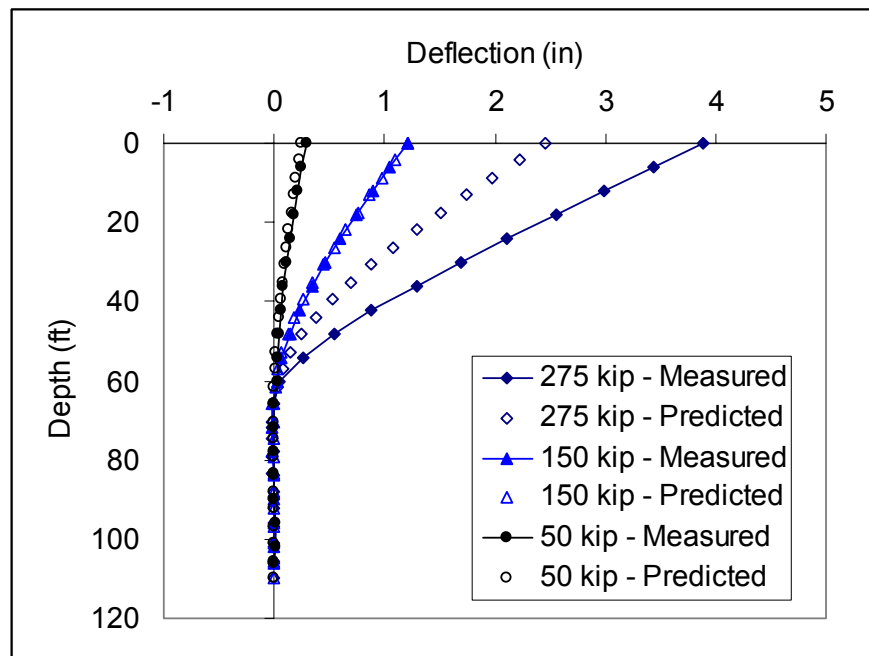


Figure 6-14 Comparisons of deflection-depth curves of shaft #2 at Pomeroy-Mason test

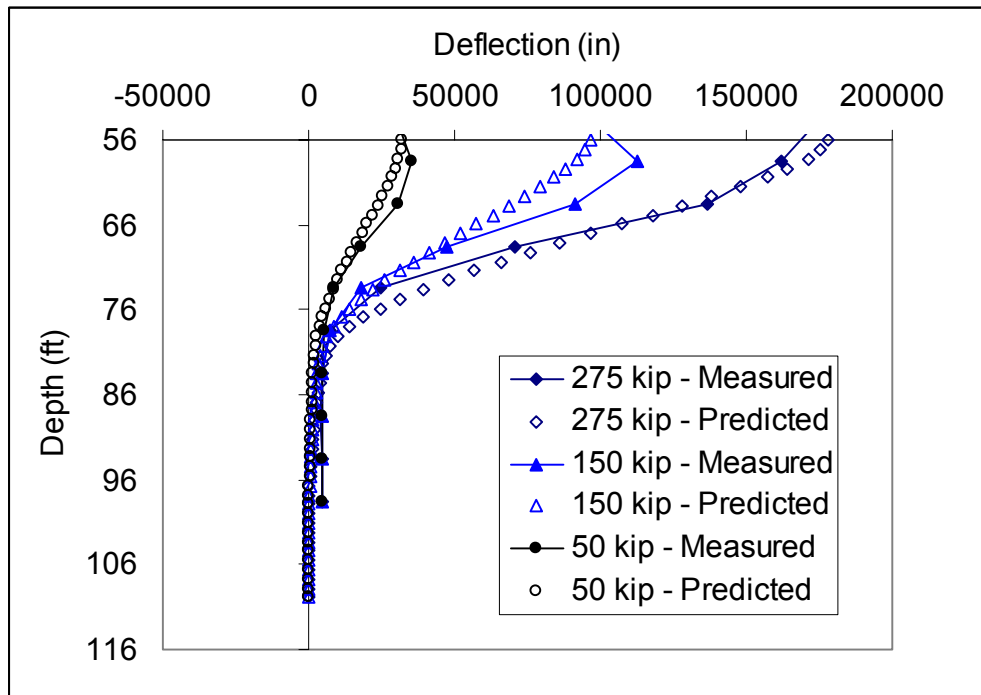


Figure 6-15 Comparisons of moment-depth curves of shaft #2 at Pomeroy-Mason test

6.7.3 Load Tests at North Carolina

Two lateral load tests at North Carolina were reported by Gabr et al. (2002). The drilled shafts are 2.5 feet in diameter with 9.15 feet to 13.8 feet rock socket in siltstone and sandstone. The test set up is depicted in Figs. 6-16 and 6-17 for the load test at I-40 and I-85, respectively. The reinforcement was 12 #10 primary rebars and a 0.5 inch thick casing. The rock consists of soft to medium hard siltstone and sandstone. The parameters used for generating the proposed p-y curves for rock are reported by Gabr et al. (2002) and summarized in Table 6-4 and Table 6-5 for load test at I-40 and I-85, respectively.

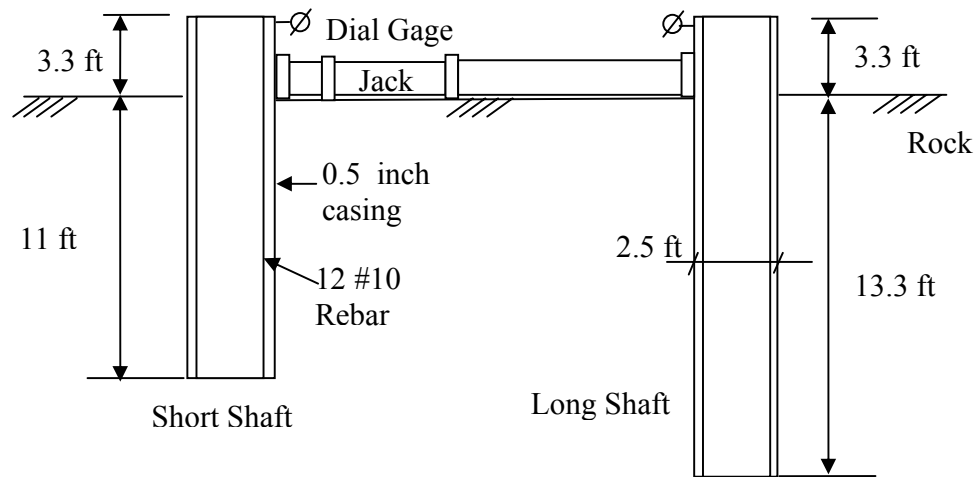


Figure 6-16 Layout of I-40 load test

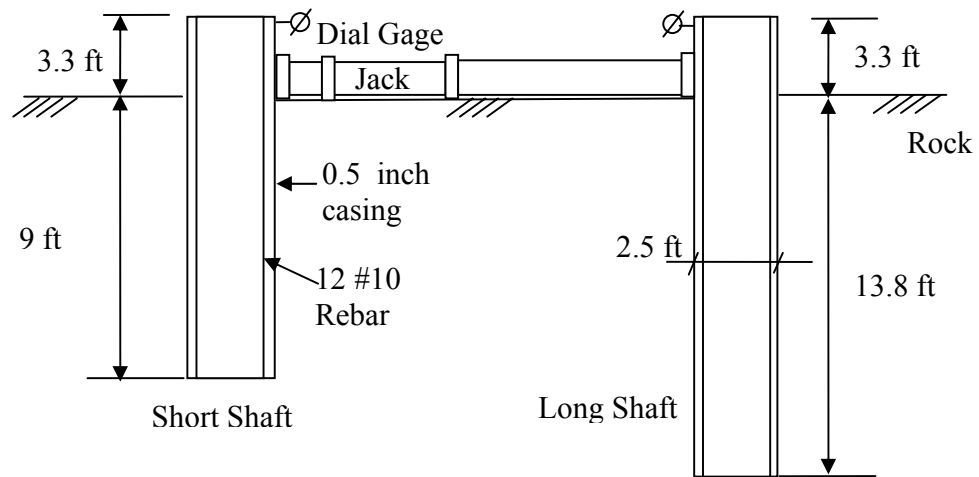


Figure 6-17 Layout of I-85 load test

Table 6-4 Input Rock Mass Parameters of I-40 Load Test

Depth (in)	γ' (pci)	σ_{ci} (psi)	GSI	m_i	E_m (psi)
Short Shaft					
35	0.092	1639	87	9	23345
90	0.092	1769	74	9	28362
121	0.092	5061	76	19	63351
Long Shaft					
24	0.092	1769	57	9	25230
75	0.092	4002	66	14	57203
122	0.046	3756	76	14	54201
150	0.046	3538	74	14	50620

Table 6-5 Input Rock Mass Parameters of I-85 Load Test

Depth (in)	γ' (pci)	σ_{ci} (psi)	GSI	m_i	E_m (psi)
Short Shaft					
23.6	0.055	4220	59	9	15646
61	0.055	3596	59	9	13340
90.2	0.055	6598	59	9	48749
Long Shaft					
29.5	0.055	3625	38	9	32509
78.7	0.055	4162	38	9	15428
112	0.055	4785	38	9	167026
145	0.055	4785	59	9	87667

The p-y curves generated from the hyperbolic criterion and tabulated rock properties are fed into LPILE computer program (Reese, et. al., 2004) to compute the response of the test shafts under the applied lateral loads. Non-linear shaft stiffness option in LPILE is used to take into account of the evolution of stiffness due to concrete cracking.

The predicted load-deflection curve at the shaft head is compared with the measured in Figs. 6-18 and 6-19 for I-40 short and long shaft, respectively. In general, a good agreement between the measured and the predicted can be observed. The prediction results of I-85 short and long shaft are presented in Figs. 6-20 and 6-21, respectively. Smaller deflections are predicted for this load test. However, the discrepancy is not very significant, especially for the case of long shaft.

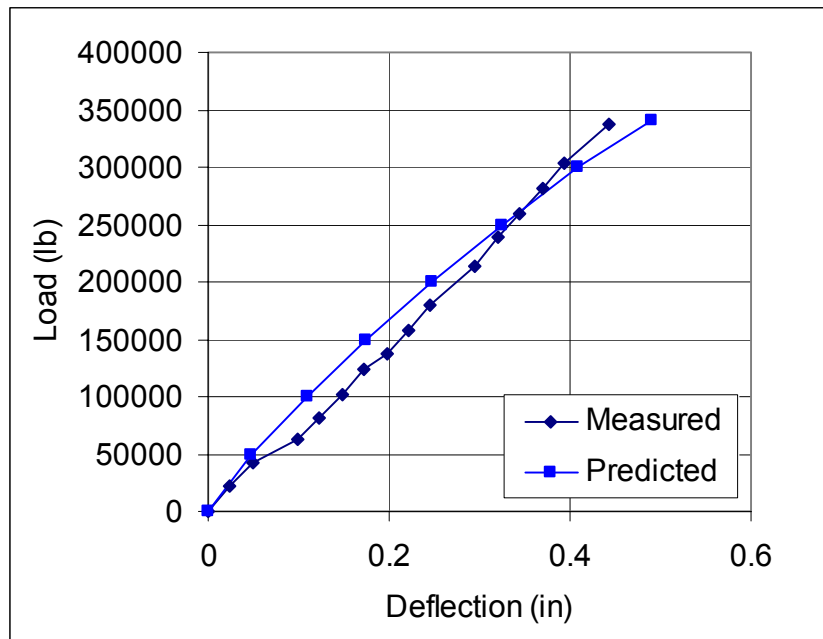


Figure 6-18 Comparison of load-deflection curves of I-40 short shaft

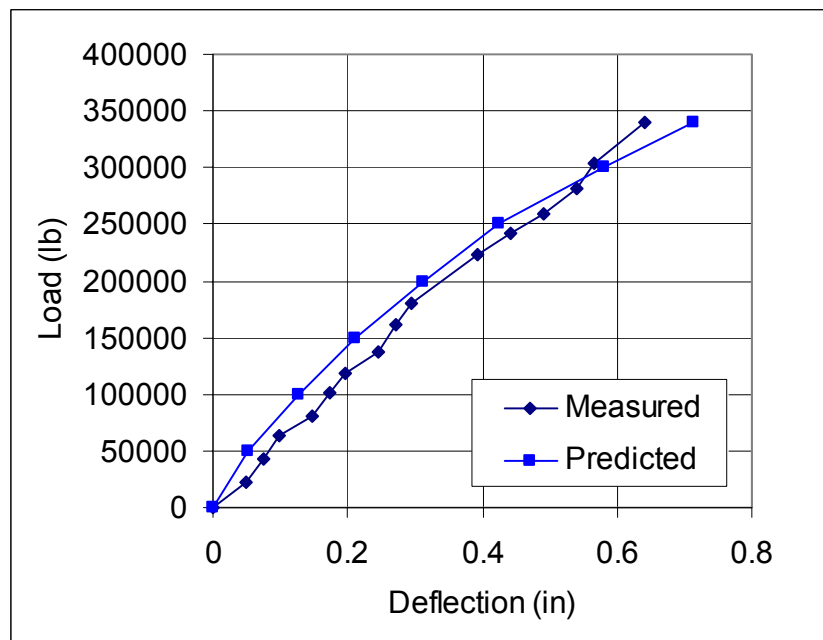


Figure 6-19 Comparison of load-deflection curves of I-40 long shaft

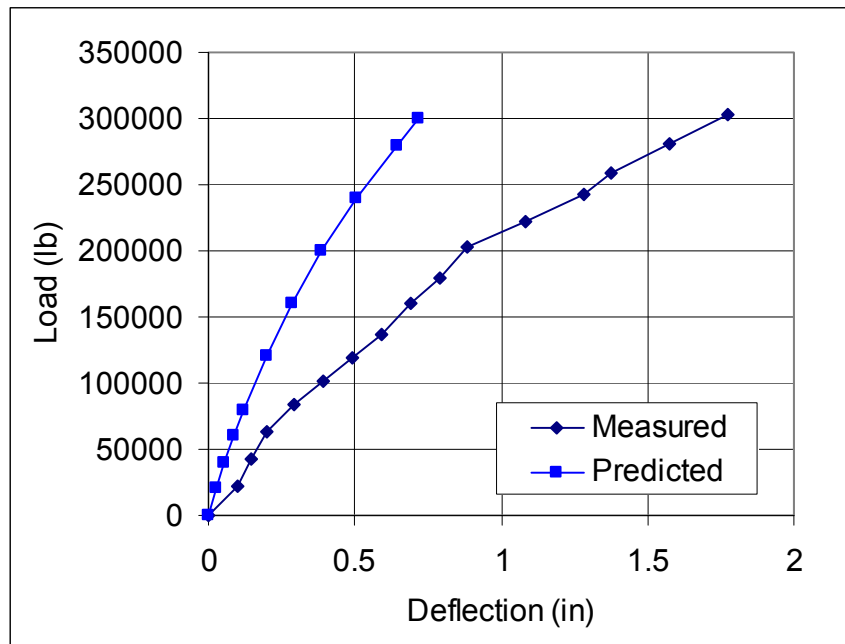


Figure 6-20 Comparison of load-deflection curves of I-85 short shaft

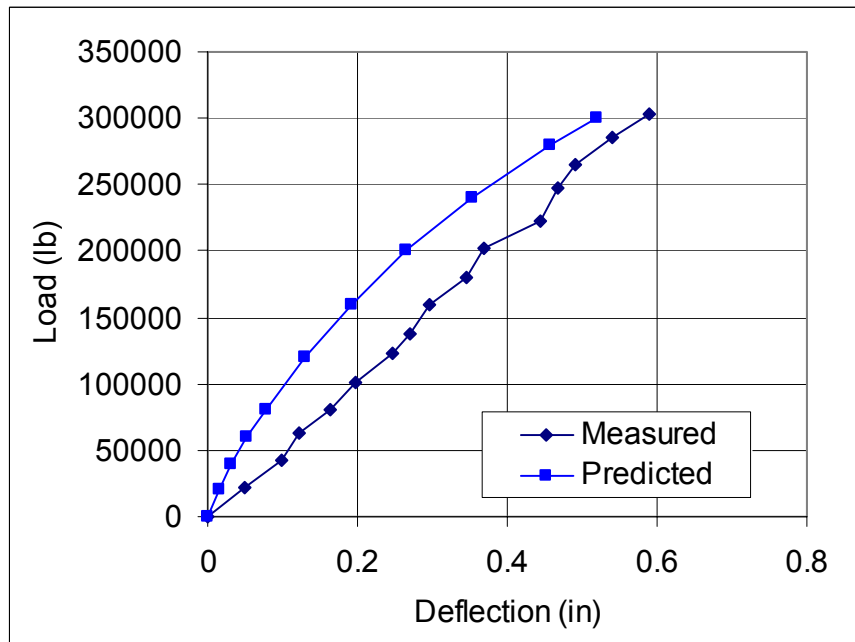


Figure 6-21 Comparison of load-deflection curves of I-85 long shaft

6.8 Conclusions

A hyperbolic p-y criterion for rock is developed in this study that can be used in conjunction with either COM624P or LIPLE computer analysis program to predict the deflection, moment, and shear responses of the shaft under the applied lateral loads. 3-D finite element simulation results have provided basic understanding of the mobilization mechanisms of lateral resistance of rock mass to the drilled shafts, from which analytical equations are derived for computing p_u . Hoek-Brown strength criterion for the rock mass as well as pertinent empirical equations for the rock/shaft interface strength have been utilized in deriving the analytical equations. Proper considerations for the effects of joints and discontinuities on the rock mass modulus and strength are discussed. Evaluations based on comparisons between the predicted and measured responses of full-scale lateral load tests on fully instrumented drilled shafts have shown the practical uses of the proposed p-y criterion and the associated methods for determining the corresponding input of rock properties.

CHAPTER VII

DERIVING P-Y CURVE FROM DILATOMETER TESTS

7.1 Pressuremeter and Dilatometer

The term pressuremeter was first used by Menard to describe his testing equipment developed in 1955. The widely recognized definition of pressuremeter is as follows: a cylindrical probe that has an expandable flexible membrane designed to apply a uniform pressure to the walls of a borehole. Pressuremeter is usually used for the testing in soils and weak rock due to the limit pressure that can be applied (10 MPa). For hard rock, the high limit pressure (30 MPa) testing device dilatometer, which shares the same testing principle as the pressuremeter, can be used. Figure 7-1 and 7-2 show respectively the pressuremeter and dilatometer manufactured by RocTest.

Usually, the raw data collected during the pressuremeter/dilatometer test consists of the pressure read on the gauge of the control unit P_R and the volume read on the volume measuring device of the control unit V_R . Two calibrations are needed to correct the raw data. The pressure calibration of the probe is performed at ground level, beside the control unit, unconfined, to establish the pressure-volume relationship of the probe itself. This is a measure of the probe inertia. The second calibration is the volume calibration of the complete system, including the probe, coaxial tubing and control unit circuitry. The probe is confined by placing it in a steel casing. The pressure-volume relationship of the

system is determined. This calibration is a measure of the intrinsic volumetric expansion of the components under pressure. The calibration of volume and pressure losses is schematically presented in Fig. 7-3.

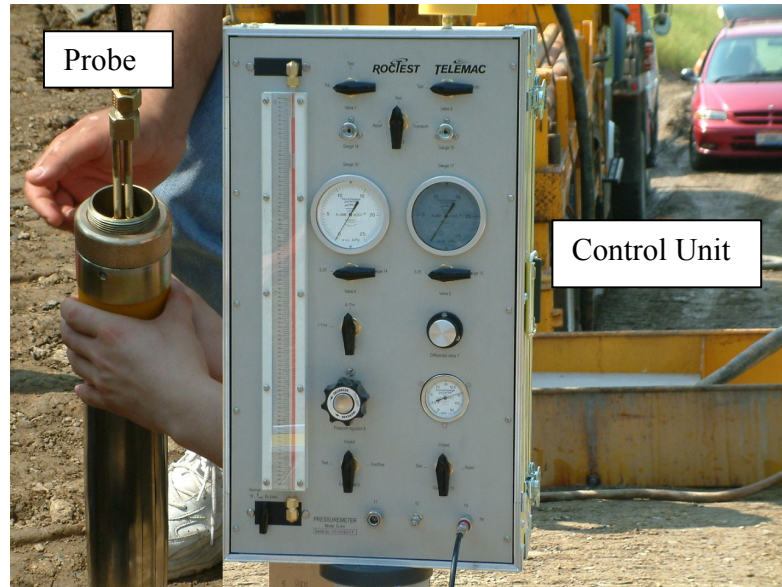


Figure 7-1 Menard G-Am pressuremeter from RocTest

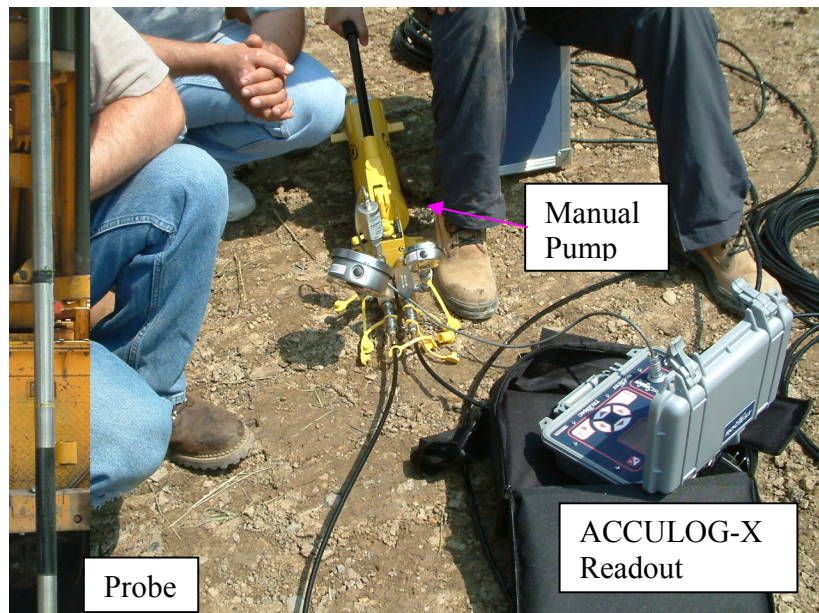


Figure 7-2 PROBEX-1 Dilatometer from RocTest

The measured pressure and volume can be corrected using the following equations per ASTM D 4719.

$$P = P_R + P_\delta - P_c \quad (7-1)$$

$$V = V_R - a(P_R + P_\delta) \quad (7-2)$$

where P is the corrected water pressure exerted by the probe on the soil,

P_R is the pressure reading on the control unit,

P_δ is the hydrostatic pressure between control unit and the probe,

P_c is the pressure correction due to stiffness of instrument at corresponding volume, determined in Fig. 7-3,

V is the corrected increase in volume of the measuring portion of the probe,

V_R is the volume reading on readout device, and

a is the slope shown in Fig. 7-3.

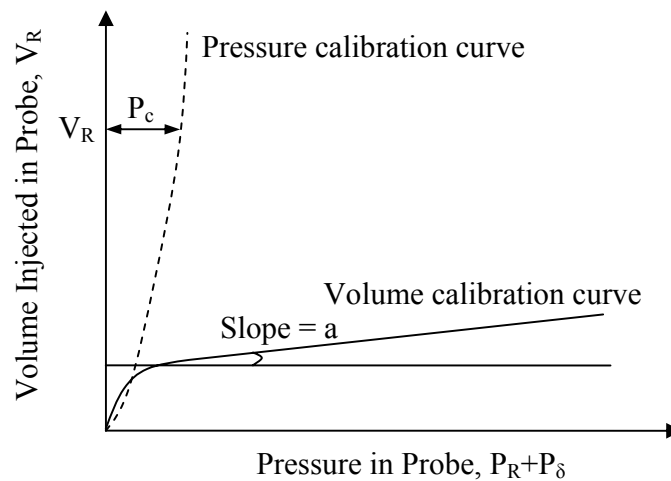


Figure 7-3 Calibration for volume and pressure losses

For dilatometer test data, the two calibration procedures are the same as those of pressuremeter. However, the equations used for correction is slightly different. Due to the

nature of dual-action oil-type hydraulic pump system, the pressure readings can be corrected using the following equation.

$$P = 0.955P_R + 8.82\Delta h \quad (7-3)$$

where Δh is the difference in elevation between the manual pump and the center of the dilatometer probe in meters.

Two deformation components contribute to the value of “a” shown in Fig. 7-3. They are the intrinsic volumetric expansion of the dilatometer system known as “c” and the small expansion undergone by the calibration tube during pressurization. The expansion of the thick wall metallic tube is determined theoretically and is expressed by the “b” parameter. Because the volume calibration of dilatometer test reaches high pressure, therefore the volume change of the steel casing needs to be considered. The following equation can be used to correct the volume readings.

$$V = V_R - cP \quad (7-4)$$

where $c = a - b$, and

$$b = \frac{2V_{\text{tube}}[r + e(1 + m)]}{E_{\text{tube}}e} \quad (7-5)$$

where V_{tube} is the volume taken by the dilatable membrane of the probe of the dilatometer when in contact with the metallic calibration tube, r is the internal radius of the calibration tube, e is the wall thickness of the calibration tube, m is the Poisson’s ratio of the calibration tube material, and E_{tube} is the modulus of elasticity of the calibration tube material. The PROBEX-1 dilatometer from RocTest is supplied with a standard, steel calibration tube. Assuming a dilatable length of the PROBEX-1 dilatometer membrane equal to 18 inch (457 mm), one obtains a “b” value of $84.57 \times 10^{-6} \text{ cm}^3/\text{kPa}$.

A typical corrected pressure-volume curve is presented in Fig. 7-4, where P_i is the corrected pressure when the probe made contact with the borehole, V_i is the corrected volume reading at the pressure of P_i , ΔP is the corrected pressure increase in the center part of the straight line portion of the pressure-volume curve, ΔV is the corrected volume increase in the center part of the straight line portion of the pressure-volume curve, corresponding to ΔP pressure increase, P_y is the yield pressure at the end of the straight line portion of the pressure-volume curve, the creep curve is pressure versus the volume difference between the volume measured at 60 seconds and 30 seconds, and V_m is the corrected volume in the center portion of the ΔV volume increase. The values of P_i and P_y can be determined from the intersections of the creep curve. With the corrected P-V curve, the soil/rock shear modulus, Young's modulus, shear strength, and p-y curve can be obtained approximately by assuming that the expansion of the pressuremeter probe is considered to be the expansion of an infinitely long cylinder in an elastic infinite mass of soil/rock.

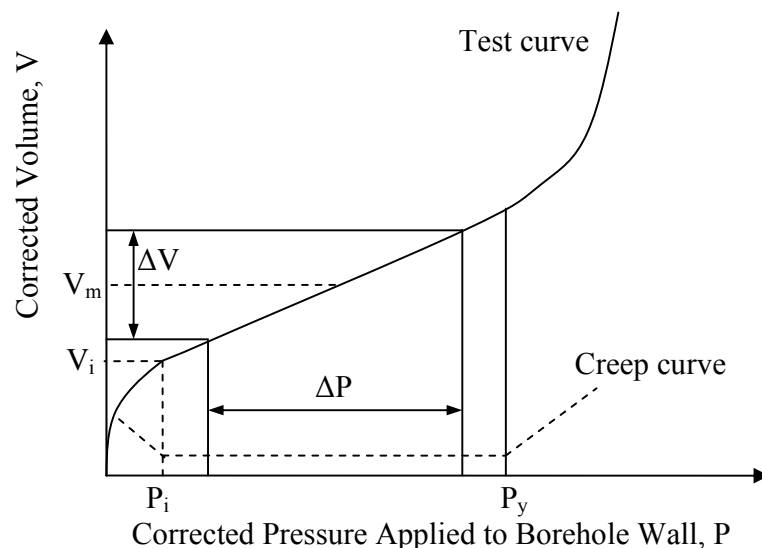


Figure 7-4 Typical pressuremeter/dilatometer test curve

7.1.1 Modulus of Rock Mass

By assuming the rock mass is an elastic media and the cavity is expended in infinitely long, the pressuremeter/dilatometer modulus E of rock mass or soils can be determined as follows (ASTM D 4719):

$$E = 2(1 + \nu)(V_0 + V_m) \frac{\Delta P}{\Delta V} \quad (7-6)$$

where ν is Poisson's ratio, and V_0 is the initial volume of the measuring portion of the uninflated probe at the ground surface.

7.1.2 Limit Pressure

According to ASTM D4719, the limit pressure (P_l) is defined as the pressure where the probe volume reaches twice the original soil/rock cavity volume, defined as the volume $V_0 + V_i$ where V_i is defined in Fig. 7-4. The volume reading at the twice of the original soil cavity volume is $(V_0 + 2V_i)$.

The limit pressure is usually not obtained by direct measurements during the test due to the limit of the probe expansion or the need for excessively high pressure. If the test was conducted to read sufficient plastic deformation, the limit pressure can be determined by a $1/V$ versus P plot, as shown in Fig. 7-5.

7.1.3 Undrained Shear Strength

The undrained shear strength S_u of cohesive soils or soft rock can be determined in various ways, including the limit pressure method (Bishop et al., 1954), empirical correlations (Menard, 1970), the yield pressure method, and the Gibson-Anderson method.

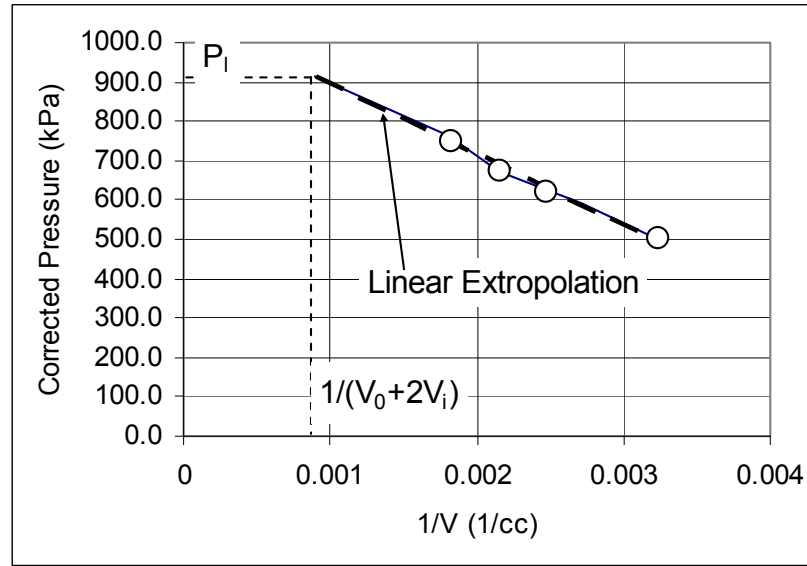


Figure 7-5 Determination of limit pressure from inverse of volume versus pressure

Bishop et al. (1945) derived a theoretical expression of the limit pressure using plasticity theory with Tresca criterion:

$$P_l = P_i + S_u \left(1 + \ln \frac{E}{2(1+\nu)S_u} \right) \quad (7-7)$$

where P_l is the limit pressure determined from Fig. 7-5, and P_i is the horizontal in-situ earth pressure at rest determined from Fig. 7-4. Equation (7-7) can be rewritten as:

$$S_u = \frac{P_l^*}{\beta} \quad (7-8)$$

where the net limit pressure P_l^* is equal to $P_l - P_i$. The value of β can range from 5.2 to 7.5 for typical ratio of E/S_u varies from 200 to 2000 for clay. Menard (1970) proposed a value of 5.5 for computing the residual strength of clay.

The yield pressure method was based on the theoretical expression of the yield pressure P_y :

$$S_u = P_y - P_i \quad (7-9)$$

Both P_y and P_i are obtained from the pressuremeter curve. This method is not recommended as it typically overestimates the undrained shear strength (Briaud, 1992).

The Gibson-Anderson (1961) method is based on the theoretical expression of the pressuremeter curve after the yield pressure:

$$P = P_y + S_u \left(\ln \frac{G}{S_u} + \ln \frac{\Delta V}{V} \right) \quad (7-10)$$

where P is the corrected pressuremeter pressure, G is the shear modulus, ΔV is the increase in cavity volume, and V is the current volume of the cavity. A plot of P versus $\ln(\Delta V/V)$ for the pressuremeter test data points past the yield (or creep) pressure leads to a straight line. The slope of the straight line is S_u .

Baguelin et al. (1978) presented an extensive comparison of undrained shear strength S_u and P_1^* based on pressuremeter tests on clay. Based on Baguelin et al. (1978) database and Briaud's own data, Briaud (1989) developed a nonlinear relationship between S_u and P_1^* by performing a regression analysis.

$$S_u = 0.25(P_1 - P_i)^{0.75} \text{ with units of ksf} \quad (7-11)$$

This equation was adopted by FHWA (Briaud, 1989) and is suggested for future use as it is based on an extensive database and is simple for use. However, it should be noted that this equation was based on test data on clay.

7.1.4 Friction Angle

There are several ways of obtaining the friction angle ϕ of a cohesionless soil from a pressuremeter test; however, none of them is very satisfactory (Briaud, 1992). These

methods include the yield pressure method (Briaud, 1992), the limit pressure method (Briaud, 1992), and the Hughes-Wroth-Windle method (Hughes, et al. 1977).

The yield pressure method employs the theoretical expression of the effective stress yield pressure P_y' :

$$P_y' = P_i' (1 + \sin \phi) \quad (7-12)$$

where P_i' is the effective horizontal pressure at rest. This method is not used because it is too difficult to determine P_y' with enough precision.

The limit pressure P_l' can also be used to theoretically obtain the friction angle.

$$P_l' = P_i' (1 + \sin \phi) \left(\frac{G}{P_i' \sin \phi} \right)^{0.5(1-K_a)} \quad (7-13)$$

where K_a is the coefficient of active earth pressure, G is shear modulus of the soil. This method is not used because of a few shortcomings as pointed out by Briaud (1992). For instances, the method assumes no volume change of soil. It is based on theory of expansion of infinitely long cavity while actual pressuremeter probe has a finite length. Additionally, the value of G needs to be evaluated.

The Hughes-Wroth-Windle method (Hughes, et al. 1977) takes into consideration the dilatancy of cohesionless soils. The method is based on the theoretical expression of the pressuremeter curve past the yield pressure. This expression is:

$$\log \left(\frac{\Delta R_c}{R_c} + \frac{C}{2} \right) = \left(\frac{K(1 - \sin \phi') + 1 + \sin \phi'}{2 \sin \phi'} \right) \log(p - u_0) + \text{const} \tan t \quad (7-14)$$

where R_c is the initial radius of the cavity, ΔR_c is the change in radius of the cavity, C is the intercept of the volumetric strain versus engineering shear strain plot, P is the total

pressuremeter pressure, u_0 is the pore water pressure, ϕ' is the peak friction angle and K is:

$$K = \tan^2 \left(45^\circ + \frac{\phi'_{CV}}{2} \right) \quad (7-15)$$

where ϕ'_{CV} is the friction angle at constant volume. For dense sand, the value of C is zero; for medium and loose sands, the value of C can be approximately assumed to be zero. Recommended values of ϕ'_{CV} are presented in Table 7-1. The results of the pressuremeter test are plotted as $\log(P-u_0)$ versus $\log(\Delta R_c / R_c)$, and the slope s of the line at large deformation is a function of ϕ' only, thus allowing determination of ϕ' .

$$s = \frac{2 \sin \phi'}{K(1 - \sin \phi') + 1 + \sin \phi'} \quad (7-16)$$

It should be noted that this technique was developed for self-boring pressuremeter test results and unproven for preboring pressuremeter tests.

Table 7-1 Preliminary estimates of ϕ'_{CV} (Robertson and Hughes, 1986)

Soil Type	ϕ'_{CV} (°)	Soil Type	ϕ'_{CV} (°)
Well-graded gravel-sand-silt	40	Uniform medium sand	34
Uniform coarse sand	37	Well-graded fine sand	34
Well-graded medium sand	37	Uniform fine sand	30
Assign lower values for well-rounded particles.			
Assign higher values for angular particles.			

For weak rock, Haberfield and Johnston (1993) presented a curve fitting technique to estimate the strength parameters. The method is based on the theory of expansion of an infinitely long cylindrical cavity in an elastic, perfectly plastic, homogeneous and isotropic Mohr-Coulomb material with cohesion c and internal friction angle ϕ .

The drained conditions are assumed and all parameters are expressed in effective stress parameters. Before yield, the expansion of the cavity is governed by:

$$\varepsilon_c = \frac{P - P_i}{2G} \quad (7-17)$$

where ε_c is the cavity strain, P is the probe pressure, P_i is the in situ horizontal stress and G is the shear modulus of the weak rock.

After yielding, the cavity expansion for pressure in excess of the yield pressure P_y is given by:

$$\varepsilon_c = \frac{1}{2G} \left[b_1 \left(\frac{r_y}{r_0} \right)^{(m-1)/m} + b_2 \left(\frac{r_y}{r_0} \right)^{(n-1)/n} + b_3 \right] \quad (7-18)$$

where r_y is the radius of the yield zone around the cavity, r_0 is the original radius of the cavity, and

$$b_1 = \frac{-2m}{m-1} \left[(1-\nu) \frac{(1+mn)}{(m+n)} - \nu \right] (P_y - P_i) \quad (7-19)$$

$$b_2 = 2n(1-\nu) \frac{(m+1)}{(m+n)} (P_y - P_i) \quad (7-20)$$

$$b_3 = (1-2\nu) \frac{(m+1)}{(m-1)} (P_y - P_i) \quad (7-21)$$

$$\frac{r_y}{r_0} = \left[\frac{P(m-1) + \hat{\sigma}}{P_y(m-1) + \hat{\sigma}} \right]^{m/(m-1)} \quad (7-22)$$

$$m = \frac{1 + \sin \phi}{1 - \sin \phi} \quad (7-23)$$

$$n = \frac{1 + \sin \psi}{1 - \sin \psi} \quad (7-24)$$

$$\hat{\sigma} = \frac{2c \cos \varphi}{1 - \sin \varphi} \quad (7-25)$$

where ψ is the dilation angle of the weak rock, and ν is the Poisson's ratio.

This method requires adjusting six parameters G , ν , c , φ , ψ , and P_i to fit pressuremeter curves. Given values of G , ν , ψ , and P_i , the values of c and φ can be obtained by fitting the pressuremeter test curve. However, this method is difficult to use without the aid of a computer program.

7.2 Deriving p-y Curves from Pressuremeter/Dilatometer Test Results

There are several methods available for deriving p-y curves from pressuremeter test results. However, all these methods were developed based on pressuremeter tests in soils. The applications of these methods for pressuremeter tests in rock have not been verified yet.

Menard et al. (1969) developed a method for deriving p-y curves from preboring pressuremeter test. This method was presented by Baguelin et al. (1978) in English. It considers that the p-y curve to be bilinear elastic and perfect plastic. Based on Menard's analysis on settlement of a strip footing, the value of first slope of p-y curve k was proposed as follows.

$$\frac{1}{k} = \frac{2}{9E} D_0 \left(2.65 \frac{D}{D_0} \right)^\alpha + \frac{\alpha}{6E} D \quad (D > 0.6 \text{ m or 2 feet}) \quad (7-26)$$

$$\frac{1}{k} = \frac{D}{E} \frac{4(2.65)^\alpha + 3\alpha}{18} \quad (D < 0.6 \text{ m or 2 feet}) \quad (7-27)$$

where D = the diameter of piles; the reference diameter $D_0 = 0.6$ m (2 feet); E = the modulus of soils from pressuremeter test; α = rheological factor, which is dependent on the soil type and the ratio E/P_1^* (P_1^* is the net limit pressure), as given in Table 7-2.

Near the ground surface, the soil reaction is less than at great depth because of possibility for soil heave. For soils above the critical depth z_c , which is in the order of $2D$ for cohesive soils and $4D$ for granular soils, the subgrade reaction will be reduced by a factor λ_z .

$$\lambda_z = \frac{1 + (z/z_c)}{2} \quad (7-28)$$

where z = depth.

Table 7-2 The Rheological Factor α for Various Soils (Baguelin et al., 1978)

Soil Type	Peat		Clay		Silt		Sand		Sand and gravel	
	E/P_1^*	α	E/P_1^*	α	E/P_1^*	α	E/P_1^*	α	E/P_1^*	α
Over-consolidated			>16	1	>14	2/3	>12	1/2	>10	1/3
Normally consolidated		1	9-16	2/3	8-14	1/2	7-12	1/3	6-10	1/4
Weathered and/or remolded			7-9	1/2		1/2		1/3		1/4
Rock	Extremely fractured		Other				Slightly fractured or extremely weathered			
	$\alpha = 1/3$		$\alpha = 1/2$				$\alpha = 2/3$			

The typical p - y curve by Menard et al. (1969) is shown in Fig. 7-6. When the soil pressure p/D (p is soil resistance per unit length of pile; and D is the shaft diameter) reaches the yield pressure P_y , the first linear line stops at this point. The slope value k_p of the second linear part is half of the k of the first part. The ultimate unit soil reaction p_u/D is equal to the limit pressure p_l of pressuremeter test for the depth greater than the critical depth. For soils above the critical depth, the value of k , k_p , and p_u should be reduced by

the factor λ_z . This method tends to give deflections larger than the measured deflection often by a factor of two (Baguelin et al., 1978).

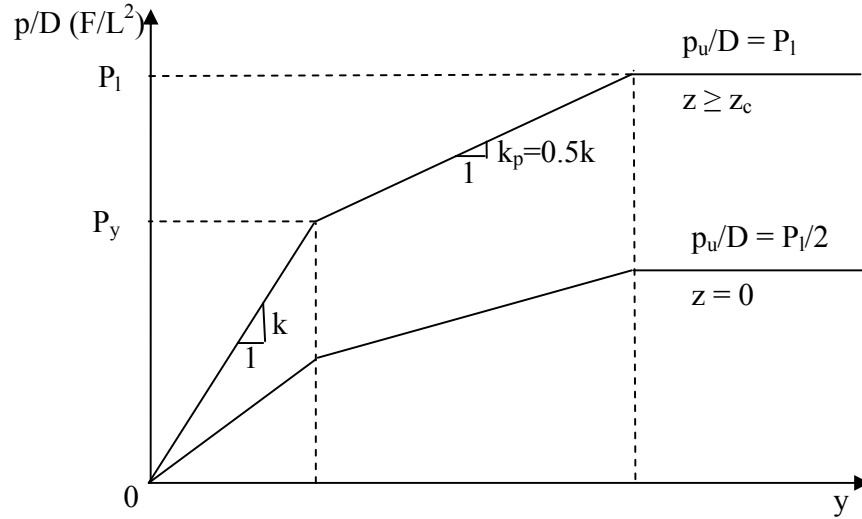


Figure 7-6 P-y curves from pressuremeter (Baguelin et al., 1978)

Baguelin, et al. (1978) method was incorporated in a more complete form in a design manual by the French Petroleum Institute in 1983. It uses the results of selfboring pressuremeter tests. The p-y curve at a depth z for the pile is obtained from the pressuremeter expansion curve at same depth z as follow:

$$p = \eta P^* D \quad (7-29)$$

$$y = \frac{1}{2} \frac{\Delta V}{V_0} R \quad (7-30)$$

where p is the soil resistance on the pile expressed as a force per unit length of pile, y is the pile horizontal displacement, η is the lateral resistance factor varying from 0.33 to 3, P^* is the net pressure ($P - P_i$) in the pressuremeter curve, R is the pile radius, V_0 is the initial volume of the probe, ΔV is the volume injected into the probe, and P_i is the in-situ at-rest horizontal stress.

Robertson et al. (1983) refined a method which was previously proposed by Hughes et al. (1979) to derive p-y curves directly from pressuremeter tests. The similarity of pressuremeter test and lateral loading of pile was the basis of the method. The effect of pile driving on soils was simulated with a self-driving pressuremeter.

For piles under lateral loading, the limiting lateral resistance from clay is approximately $9 S_u$, where S_u is the undrained shear strength. Whereas in the case of the pressuremeter, the limiting pressure ($P_l - P_i$) is approximately $5S_u$. Based on these assumptions on the relationship between limit resistance and undrained shear strength of clay, the following procedure was proposed by Robertson et al. (1983) and illustrated in Fig. 7-7.

$$p = \alpha P^* D \quad (7-31)$$

$$y = \frac{1}{4} \frac{\Delta V}{V_0} D \quad (7-32)$$

where D is the diameter of piles, α is 2 for clays and 1.5 for sands (Robertson et al., 1986). This method is similar to Baguelin et al. (1978) method except the value of coefficient α or η is different.

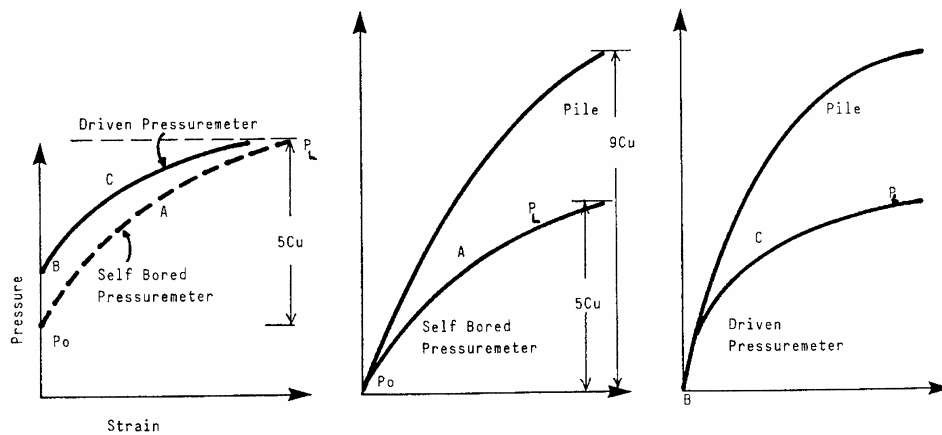


Figure 7-7 Steps for constructing p-y curve from pressuremeter test

Briaud, et al (1983) developed a method for deriving p-y curves from the results of pressuremeter test. This method considers that a p-y curve is made of a front resistance Q-y curve and a friction resistance F-y curve. This method is also applicable to test results of dilatometer.

The Q-y and F-y curves can be obtained point by point from the pressuremeter curve as follows:

$$Q = (SQ)(P^*)(D) \quad (7-32)$$

where Q = the frontal soil resistance on the pile,

D = pile diameter or width,

P^* = the net pressure which is equal to $(P-P_i)$,

SQ = shape factor for pressure reaction,

$$= \frac{\pi}{4} \text{ for circular piles,}$$

$$= 1.0 \text{ for square piles.}$$

$$F = (SF)(D)(X)(1 + X) \frac{\Delta P^*}{\Delta X} \quad (7-33)$$

in which, F = the frictional soil resistance on the pile,

SF = shape factor for shear reaction,

$$= 0.79 \text{ for circular piles,}$$

$$= 1.76 \text{ for square piles,}$$

ΔP^* = the increase of net pressure,

$X = \Delta V'/V_0'$ where V_0' is equal to $V_0 + V_i$ and $\Delta V'$ is the volume injected in the probe from V_0' point on.

$$y = \frac{D}{4} \frac{\Delta V'}{V'_0} \quad (7-34)$$

where y = the horizontal displacement of the pile,

After Q , F , and y values corresponding to each data point of pressure-volume curve are obtained, the p - y curve can be constructed from the summation of Q - y curve and F - y curve using the equation $p = Q + F$.

At shallow depth, the lack of vertical confinement influences the results of pressuremeters as well as the soil resistance to laterally loaded drilled shafts. The effects due to lack of vertical confinement was introduced by Smith (1983) as follow: no influence is considered for the F - y curve, while for the Q - y curve the critical depth D_c is determined from Fig. 7-8 and within that depth Q is multiplied by a reduction factor RF from Fig. 7-9. This reduction was developed for soils, it will not be considered for rock since for most cases a thick layer of soil exists above the rock mass.

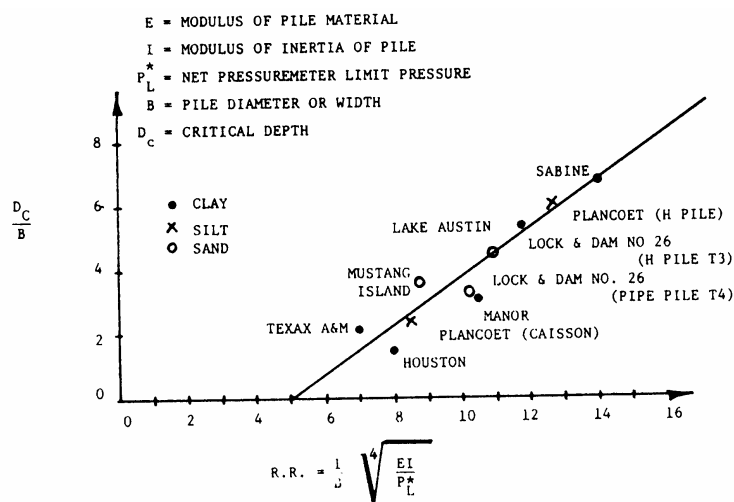


Figure 7-8 Determination of the critical depth (Smith, 1983)

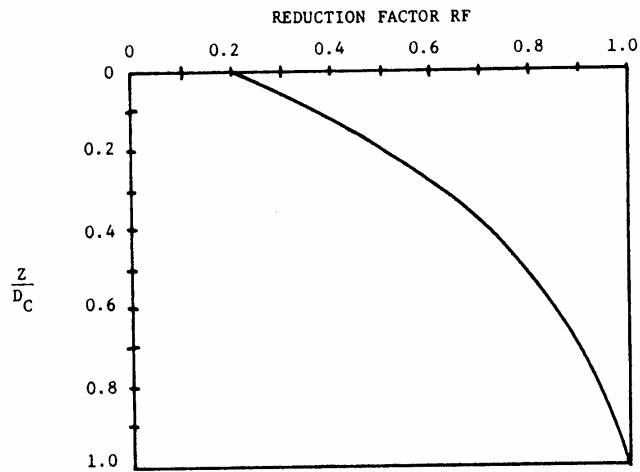


Figure 7-9 Reduction factor for depth within critical depth (Smith, 1983)

The above reviewed methods for deriving p-y curves from pressuremeter test results were developed for applications in soils. Briaud et al. (1983) method is considered as the most suitable method for applications in rock, as it does not require empirical coefficients and avoids the difficulty of determining the yield and limit pressure. Additionally, it considers both shear stress and normal stress as a result of soil or rock-shaft interaction. Therefore, it is decided to evaluate Briaud et al. (1983) method for applications to drilled shafts socketed in rock.

7.3 Evaluation

Briaud et al. (1983) method for deriving p-y curves from dilatometer test results is evaluated against field tests reported by Cho et al. (2001) and Gabr et al. (2002). The lateral load test by Cho et al. (2001) was performed on a free-head drilled shaft with a diameter of 30 inch and an embedment length of 168 inch. The shaft was embedded in soft weathered meta-argillite rock with 39 inch of overlying sandy silt and a 12 inch thick of dense sand.

The pertinent shaft and soil information are shown in Fig. 7-10. The average SPT N values of the sandy silt layer and dense sand layer were reported as 14 and greater than 100, respectively. Dilatometer (DM) tests were performed at depths of 8.5, 11.8, and 15 feet. The results of the dilatometer tests are provided in Fig. 7-11. P-y curves of the test site interpreted from DM test results using Briaud et al. (1983) method are shown in Fig. 7-12.

These interpreted p-y curves are input into LPILE program to predict the lateral response of the test drilled shaft. The sandy silt and dense sand is modeled using LPILE internal sand p-y curves. The friction angles of the sandy silt and dense sand layers were interpreted as 32° and 45° according to the SPT correlation table by Liang (2002). Nonlinear option of shaft stiffness is chosen for analysis. The predicted deflections at the top of the shaft are compared with the measured values, as shown in Fig. 7-13. It can be seen that the predicted deflections are little bitter smaller than the measured values.

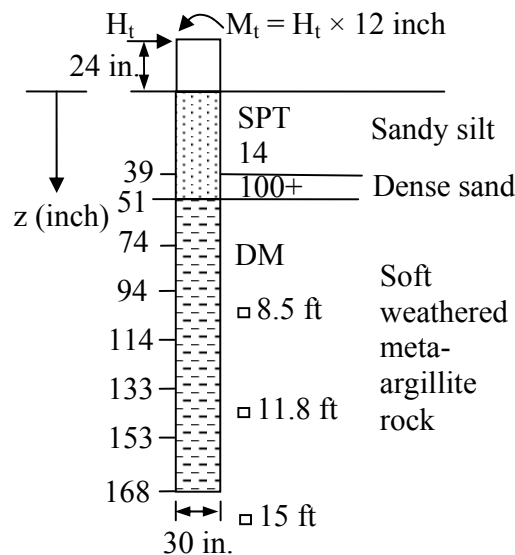


Figure 7-10 Shaft and soil profiles of the case study

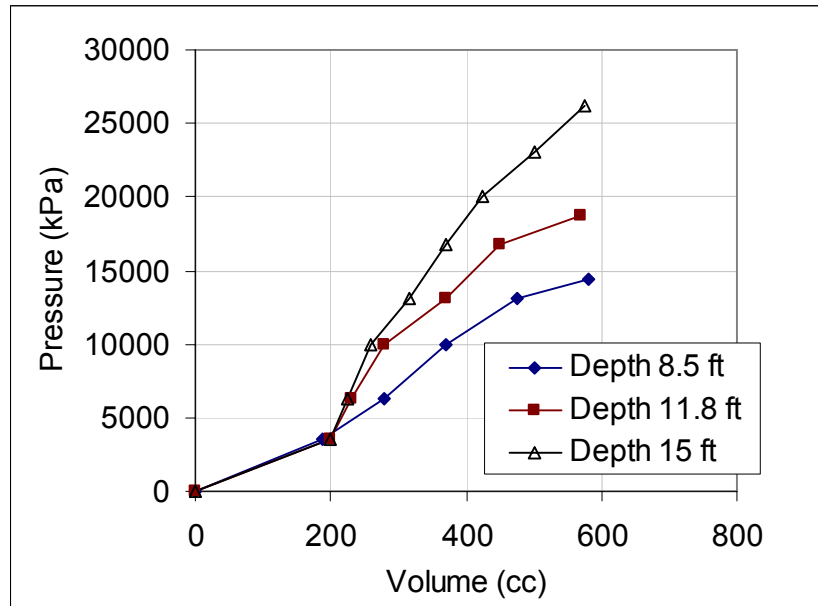


Figure 7-11 Dilatometer test results of the case study (after Cho et al., 2001)

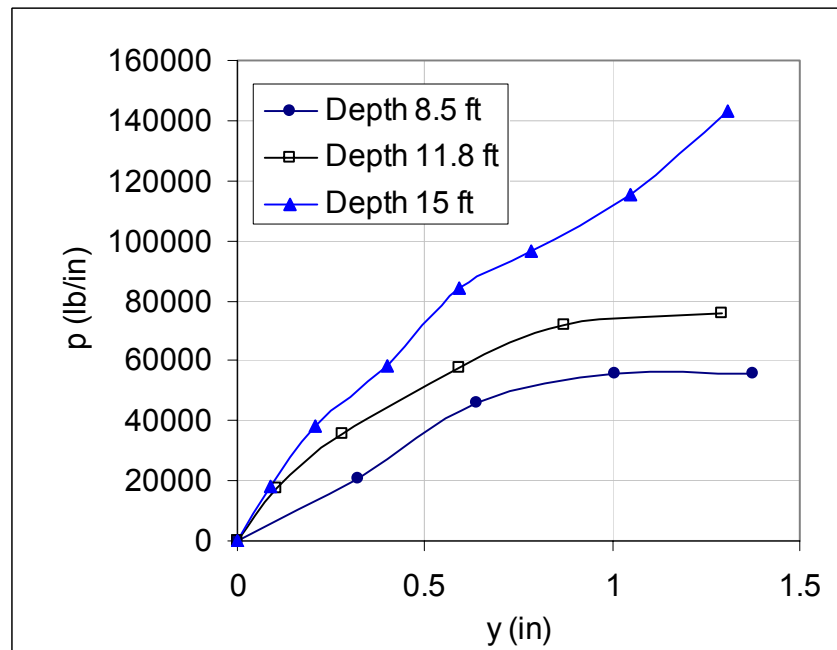


Figure 7-12 P-y curves from dilatometer tests of Cho et al. (2001)

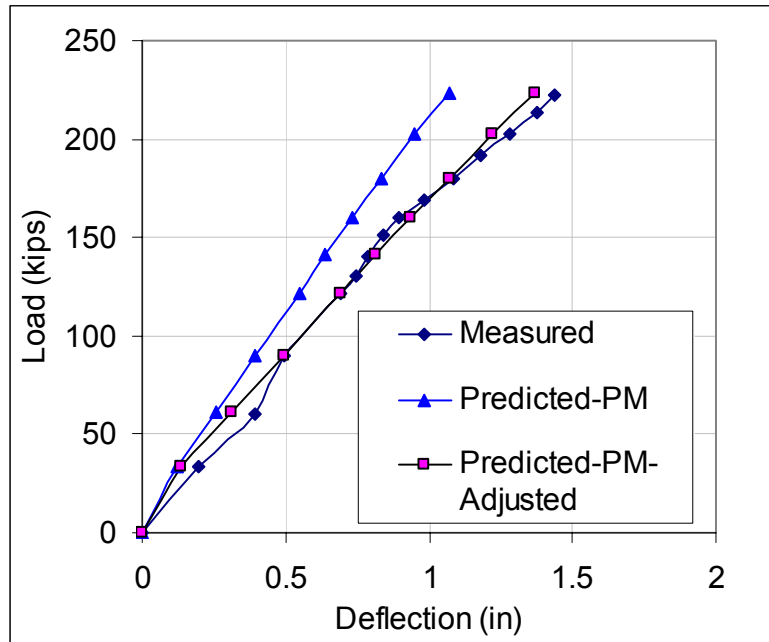


Figure 7-13 Comparison of the measured and predicted deflections at shaft top

The two lateral load tests, i.e., load tests at I-40 and I-85, reported by Gabr et al (2002) are also employed to evaluate Briaud et al. (1983) method. The test shaft and rock information have been described in Chapter VI. Dilatometer tests were performed at the two test sites. The derived p-y curves from dilatometer test results are provided in Figs. 7-14 to 7-17 for the four test shafts. The performance of these derived p-y curves are evaluated by inputting them into LPILE and comparing with the measured load-deflection curves, as shown in Figs. 7-18 to 7-21. It can be seen that the predicted deflections are smaller than the measured values. In order to match the measured deflections, a factor of 0.5 is multiplied to the calculated p values from dilatometer test results. The adjusted p-y curves are then input into LPILE to predict the deflections, as shown in Fig. 7-13 and Figs. 7-18 to 21. It can be seen that such adjustment on Briaud et al. (1983) method can make it works much better for most of the cases. Therefore, it is

concluded that the modified Briaud et al (1983) method (i.e., reducing the calculated value of p by 50%) can provide reasonable site-specific p - y curves.

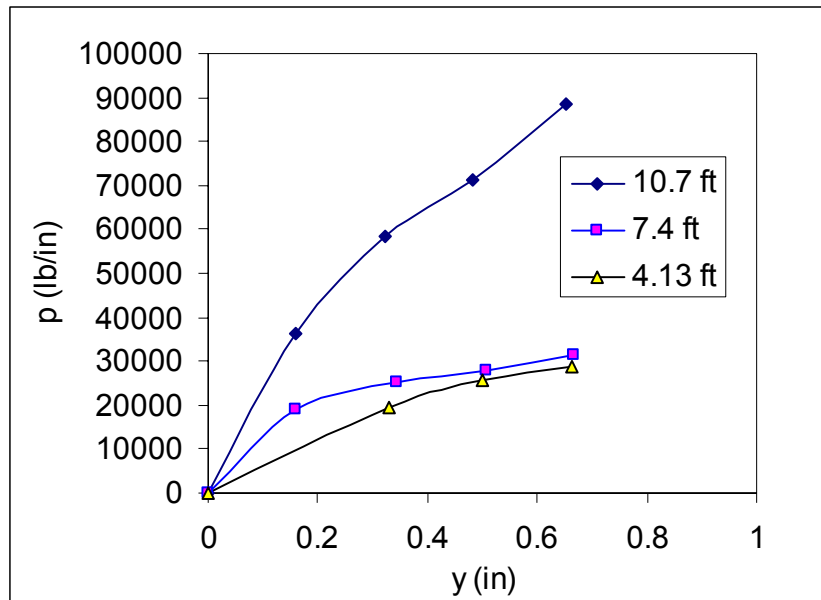


Figure 7-14 Derived p - y curves from dilatometers for I-40 short shaft

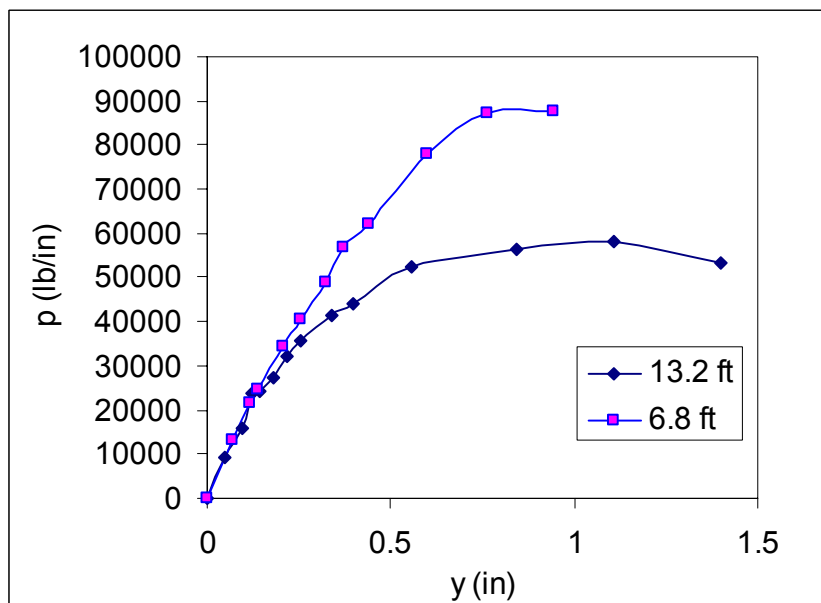


Figure 7-15 Derived p - y curves from dilatometers for I-40 long shaft

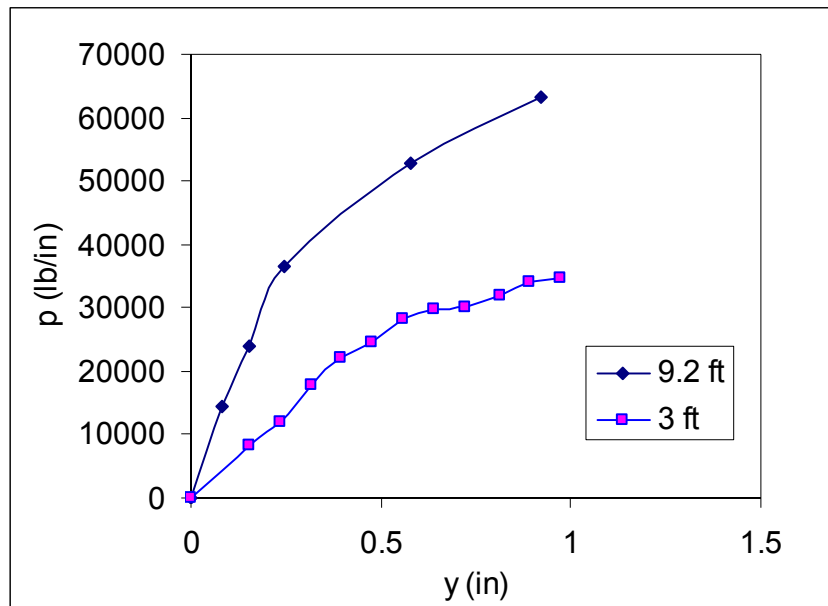


Figure 7-16 Derived p-y curves from dilatometers for I-85 short shaft

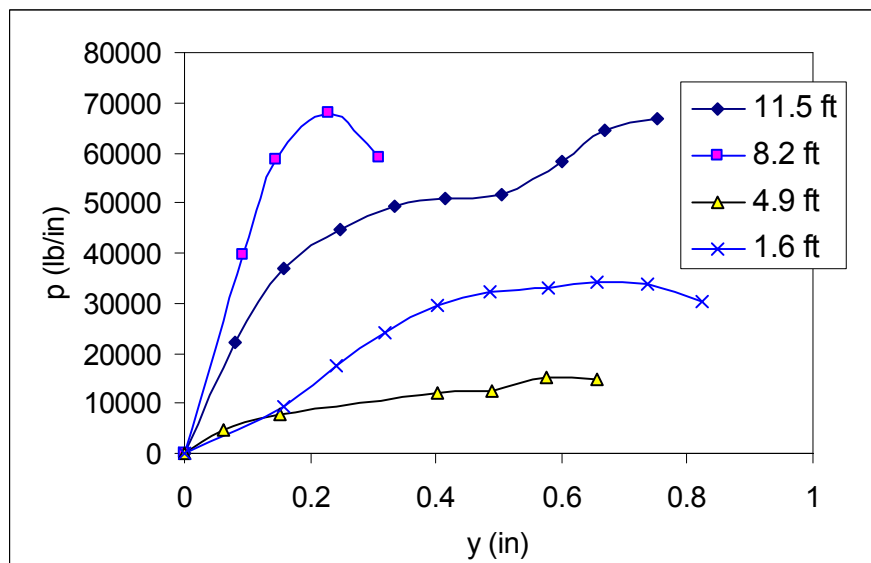


Figure 7-17 Derived p-y curves from dilatometers for I-85 long shaft

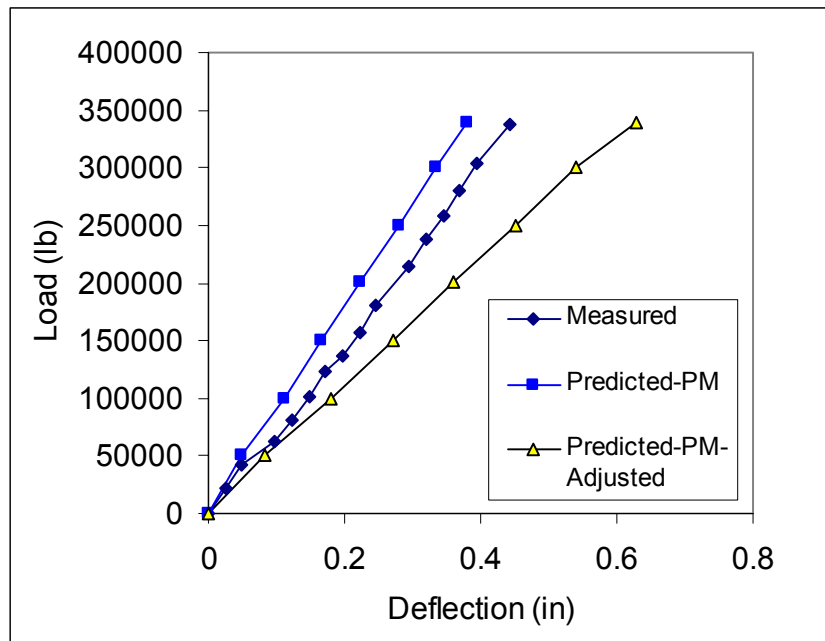


Figure 7-18 Comparison of load-deflection curves of I-40 short shaft

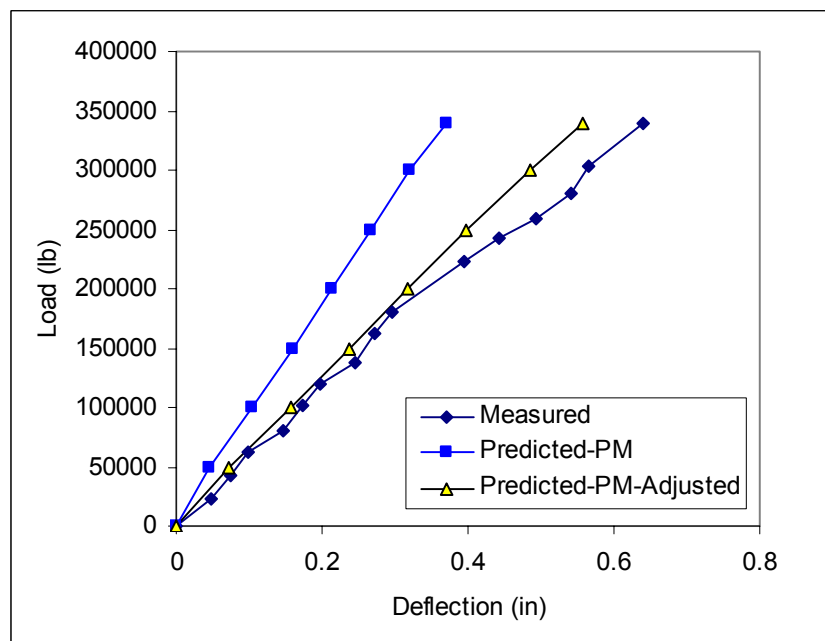


Figure 7-19 Comparison of load-deflection curves of I-40 long shaft

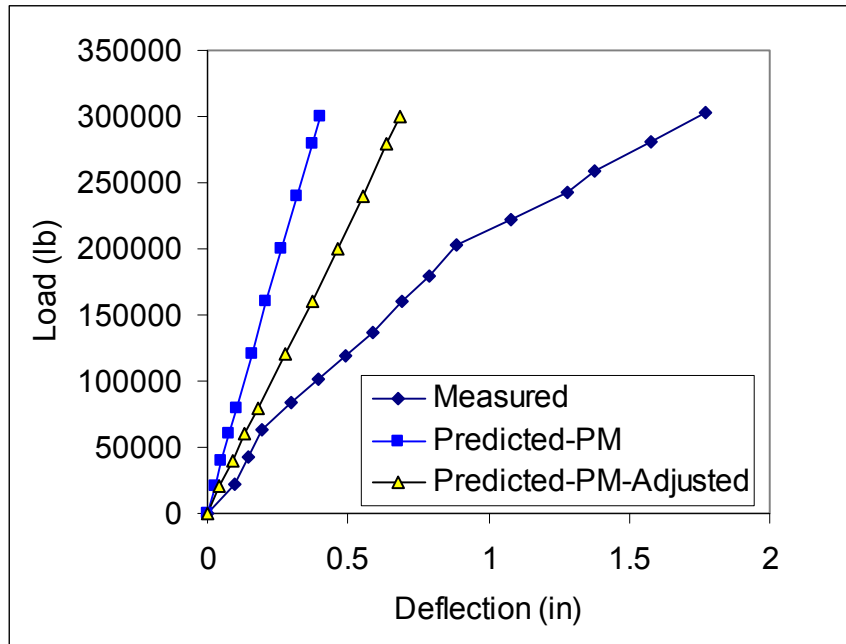


Figure 7-20 Comparison of load-deflection curves of I-85 short shaft

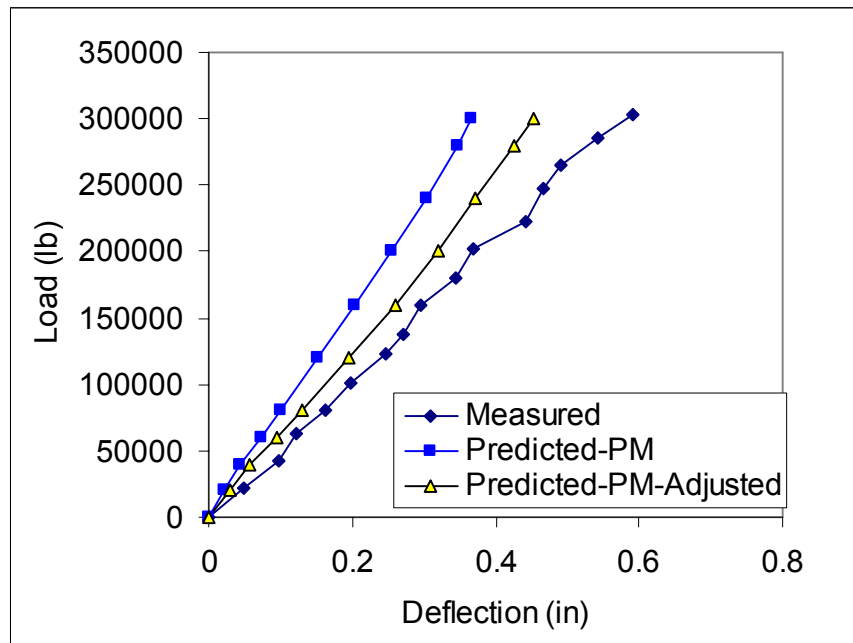


Figure 7-21 Comparison of load-deflection curves of I-85 long shaft

CHAPTER VIII

SUMMARIES AND CONCLUSIONS

8.1 Summaries

Towards the objective of developing a new p-y criterion of rock mass, a series of field work and theoretical work have been carried out. A detailed literature review was performed to study existing design and analysis methods of laterally loaded drilled shafts and piles in rock. A new hyperbolic p-y criterion of rock was proposed based on the field test data and extensive theoretical work.

A 3D finite element model simulating the response of laterally loaded drilled shafts in rock using ABAQUS was established to develop an empirical correlation equation for estimating the initial slope of a p-y curve of rock. Additionally, theoretical equations for determining the ultimate resistance of rock mass were derived based on failure modes of rock mass, a rock strength criterion, and an existing empirical equation for estimating the side shear resistance between rock and drilled shafts. The failure modes of rock mass were identified through a series of 3D FEM study.

In addition to the development of a p-y criterion of rock, a method for predicting lateral capacity of drilled shafts in rock and/or soils was developed. This estimate can be used to ensure adequate safety margin of a design of drilled shafts in rock. An elastic solution for predicting the lateral deflections of piles/drilled shafts embedded in a two-

layer soil/rock system was proposed. This solution allows a quick estimation of drilled shaft deflections under lateral loads. Furthermore, an evaluation of various existing methods for deriving p-y curves from the results of an instrumented lateral load test was carried out and the most suitable p-y curve derivation method was identified.

Finally, the existing methods for deriving site specific p-y curves of soils from pressuremeter and dilatometer tests were reviewed and examined with the lateral load test results of rock-socketed drilled shafts. Briaud et al. (1983) method, with a modification of reducing p value by 50%, was recommended for deriving p-y curves of rock from the pressuremeter and dilatometer tests.

8.2 Conclusions

Based on the research work performed in this study, the following conclusions can be drawn:

1. The evaluation on the interim p-y criterion (Reese, 1997) for weak rock using the two lateral load tests reveals that this p-y criterion tends to under-predict the deflections which may result in an unsafe design.
2. The suggested method for deriving experimental p-y curves from load test results, i.e. using high order polynomial curve fitting technique to obtain y and using piecewise polynomial curve fitting technique to obtain p, demonstrated its superiority against other methods by providing the smallest error on the predictions of the load-deflection curves.
3. The validation of the 3D FEM model using a field test suggests that it can be used to simulate the lateral response of drilled shafts in rock. This simulation has provided

- basic understanding of the mobilization mechanisms of lateral resistance of rock mass to the drilled shafts, from which analytical equations are derived for computing ultimate resistance of rock p_u .
4. The evaluation of the proposed method for estimating lateral capacity of drilled shafts in rock using field test results showed that this method can provide reasonable predictions of the lateral capacity of drilled shafts in rock. The average prediction error was around 21% which is acceptable for practice, considering the measured capacity may be under estimated due to a small deflection at the maximum applied lateral load. Additionally, the proposed capacity prediction method is versatile. It can be used for estimating the lateral capacity of drilled shafts in layered clay, sand, silts, and rock. Both short and long drilled shafts under free or fixed head condition can be considered.
 5. The comparisons with rigorous solutions and the validation against field lateral load test data have shown that the proposed elastic numerical solution can provide reasonable predictions of shaft deflection under small working loads. This solution provides an efficient way to estimate the deflections of a drilled shaft in a layered soil/rock profile under small working lateral loads. Additionally, the proposed empirical equation for estimating the deformation modulus of rock mass and the empirical equation for determining the modulus of subgrade reaction of rock can provide reasonable prediction results according to the validations against field test data.
 6. The hyperbolic p - y criterion for rock developed in this study can be used in conjunction with computer analysis programs, such as COM624P, LPLE, or FBPIER,

to predict the deflection, moment, and shear responses of a drilled shaft under the applied lateral loads. Considerations of the effects of joints and discontinuities on the rock mass modulus and strength are included in the p-y criterion. Evaluations based on comparisons between the predicted and measured responses of full-scale lateral load tests on fully instrumented drilled shafts have shown the practical uses of the proposed p-y criterion and the associated methods for determining the required input of rock parameters.

7. The Briaud et al. (1983) method with a modification of reducing the calculated p values by 50% for deriving the p-y curves from dilatometer tests is found to provide reasonable predictions on the lateral deflections of a drilled shaft in rock according to the evaluations against full-scale lateral field tests. The modified method is suggested for design of laterally loaded drilled shafts in rock using dilatometer test results.
8. The research findings of this study provide a complete solution for design of drilled shafts socketed in rock under lateral loads. The proposed elastic solution can be used for a preliminary design of shafts under service loads. The computer program LCPPILE can be used for limit state design to guarantee adequate safety against design loads. The proposed hyperbolic p-y curves can be used in conjunction of COM624P or LPILE for the final design. The modified Briaud et al. (1983) method can be used to validate the final design if dilatometer tests data are available.

8.3 Future Studies

More lateral load tests on drilled shafts socketed in various types of rock with the accompanying dilatometer tests at the load test sites should be performed to further

validate the developed p-y criterion, the capacity prediction method, and the validity of the modified Briaud et al. (1983) method for rock.

A preliminary design chart for selecting drilled shaft diameter and rock socketed length can be developed based on LCPILE and the elastic solutions to ensure both capacity and service limits criteria are met.

A future study on determining p-multipliers for a drilled shaft group in rock mass can be very helpful. This objective can be accomplished through a well-planned field test or a centrifuge test on drilled shafts groups socketed in rock mass. Additionally, a 3D finite element study may also be employed to determine p-multipliers for a drilled shaft group socketed in rock mass. Furthermore, the determination of group effect of lateral capacity of group drilled shafts in rock is of practical interest since drilled shafts are often constructed in a group.

A study on drilled shaft in rock under cyclic lateral loads will help seismic design of deep foundations socketed in rock mass. A field test or centrifuge test using displacement controlled loading will be very helpful for developing p-y curves of rock under cyclic loading.

Although the proposed hyperbolic p-y curves is suitable for weak and hard rock by considering the effects of joints and discontinuities of rock mass, it is not ready to be applied to intermediate geomaterials. Therefore, it is necessary to study the lateral response of drilled shafts socketed intermediate geomaterials, as these materials conform a significant portion of the supporting medium for drilled shafts.

REFERENCES

- ABAQUS (1998). *ABAQUS Standard User's Manual*, Version 5.8, Hibbitt, Karlsson & Sorensen, Inc.
- Afrouz, A.A. (1992). *Practical handbook of rock mass classification systems and modes of ground failure*, Florida, CRC Press, Inc.
- American Petroleum Institute (API). (1991). "Recommended practice for planning, designing and constructing fixed offshore platforms." API recommended practice 2A (RP2A), 19th Ed., Washington, D. C.
- ASTM D4719-00, (2000). "Standard test method for prebored pressuremeter testing in soils." ASTM International.
- Baguelin, F., Frank, R., and Said, Y. H. (1977). "Theoretical study of lateral reaction mechanism of piles." *Geotechnique*, 27, No. 3, p. 405-434.
- Baguelin, F., Jezequel, F. F., and Shields, D. H. (1978). *The Pressuremeter and Foundation Engineering*, Trans Tech Publications, Clausthal, Germany.
- Barton, N., Lien, R., and Lunde, J. (1974). "Engineering classification of rock masses for the design of tunnel support." *Rock Mechanics*, Vol. 6, No. 4, Vienna, Austria, p. 189-236.
- Bieniawski, Z. T. (1976). "Rock mass classifications in rock engineering." *Proceedings of the Symposium on Exploration for Rock Engineering*, Z. T. Bieniawski, ed., Vol. 1, A. A. Balkema, Rotterdam, Holland, p. 97-106.
- Bieniawski, Z.T., (1978). "Determining rock mass deformability: experience from case histories." *Int. J. Rock Mech. Min. Sci. & Geomech. Abstr.*, 15, p. 237-248.

Bieniawski, Z. T. (1989). *Engineering Rock Mass Classification*, p. 251. Wiley, New York.

Bishop, R. F., Hill, R., and Mott, N. F., (1945). "The theory of indentation and hardness tests." *The Proceedings of the Physical Society*, London, Vol. 57, No. 321, Part 3, May, p. 147-159.

Boghrat, A., 1990, "Sound Barrier Wall Foundations in Granular Material," *Transportation Research Record*, Issue: 1288, p. 158-167

Bowles, J. E. (1988). *Foundation analysis and design*, 4th Edition, McGraw Hill, New York, 1004.

Bowman, E. R. (1958). "Investigation of the lateral resistance to movement of a plate in cohesionless soil." *Unpublished thesis*, College of Engineering, The University of Texas at Austin.

Briaud, (1989). "The pressuremeter test for highway applications." *FHWA Publication No. FHWA-IP-89-008*. Department of Transportation, Federal Highway Administration, McLean, VA 22101-2296, USA.

Briaud, J.L., (1992) *The Pressuremeter*, published by A.A.Balkema, Rotterdam, Netherlands.

Briaud, J. L., Smith, T. D., and Meyer, B. J. (1983), "Using the Pressuremeter Curve to Design Laterally Loaded Piles." *Proceedings of Annual Offshore Technology Conference*, Vol. 8, p. 495-502.

Brinch Hansen, J. (1961). "The ultimate resistance of rigid piles against transversal forces." *Geoteknisk Institut. Bull.*, No.12, Copenhagen.

Brown, E. T. (1981). *Rock Characterization, Testing and Monitoring: ISRM Suggested Methods*, Pergamon Press, Oxford.

Brown, E.T. (1993). "The nature and fundamentals of rock engineering." *Comprehensive Rock Engineering – Principle, Practice and Projects*. Ed; J.A. Hudson, Pergamon Press, p.1-23.

Bukovansky, M. (1970). "Determination of elastic properties of rocks using various on-site and laboratory methods." *International Soc. Rock Mechanics, Proc., Vol. 1*, No 2-9, p. 329-332.

Carter, D. P. (1984). "A non-linear soil model for predicting lateral pile response." *Rep. No. 359*, Civil Engineering Dept., Univ. of Auckland, New Zealand.

Carter, J. P., Booker, J. R., and Yeung, S. K. (1986). "Cavity expansion in cohesive frictional soils." *Geotechnique*, 36(3), p. 349-358.

Carter, J. P., and Kulhawy, F. H. (1992). "Analysis of laterally loaded shafts in rock." *Journal of Geotechnical Engineering*, ASCE, 118(6), p. 839-855.

Cho, K. H., Clark, S. C., Keaney, B. D., Gabr, M. A., and Borden, R. H. (2001). "Laterally loaded drilled shafts embedded in soft rock." *Transportation Research Record* 1772, p. 3-11.

DiGioia, A. M., Jr., and Rojas-Gonzalez, L. F. (1993). "Discussion on 'Analysis of laterally loaded shafts in rock.'" *Journal of Geotechnical Engineering*, ASCE, 119(12), p. 2014-2015.

Dou, H. and Byrne, P. M., (1996). "Dynamic Response of Single Piles and Soil-pile Interaction," *Canadian Geotechnical Journal*, Vol. 33, p. 80-96.

Dunnavant, T. W., (1986). *Experimental and Analytical Investigation of the Behavior of Single Piles in Overconsolidated Clay Subjected to Cyclic Lateral Loads*, Ph.D. Dissertation of University of Houston, Texas.

Dykeman, P., and Valsangkar, A. J. (1996). "Model studies of socketed caissons in soft rock." *Canadian Geotechnical Journal*, v. 33 issue 5, p. 747-759.

Feldmann, R.M., and Hackathorn, M. (1996). *Fossils of Ohio*, Bulletin 70, Ohio Division of Geological Survey.

Fisher, S. P., Fanaff, A. S., and Picking, L. W. (1968). "Landslide of southeastern Ohio." *Ohio Journal of Science*, V. 68, p. 65-80.

Fleming, W. G. K., Weltman, A.J., Randolph, M. F., and Elson, W. K. (1992). *Piling Engineering*. Blackie, Glasgow, and London.

Frantzen, J., and Stratten, W. F. (1987). "Final report: p-y curve data for laterally loaded piles in shale and sandstone." *Rep. No. FHWA-KS-87-2*, Kansas Department of Transportation, Topeka, Kansas.

Gabr, M. A. (1993). "Discussion on 'Analysis of laterally loaded shafts in rock.'" *Journal of Geotechnical Engineering*, ASCE, 119(12), p. 2015-2018.

Gabr, M.A., Borden, R.H., Cho, K.H., Clark, S.C., and Nixon, J.B. (2002). "P-y curves for laterally loaded drilled shafts embedded in weathered rock." *FHWA/NC/2002-08*, North Carolina Department of Transportation.

Georgiadis, M., and Michalopoulos, A. P., (1986). "Dilatometer tests for the design of grouted piles in rock." *Use of In Situ Tests in Geotechnical Engineering, Proceedings of In Situ '86*, Blacksburg, VA, USA, p. 560-568.

Gibson, R. E., and Anderson, W. F. (1961). "In situ measurement of soil properties with the pressuremeter." *Civil Engineering and Public Works Review*, London, 56 No. 658.

Gokceoglu, C., Sonmez, H., and Kayabasi, A. (2003). 'Predicting the deformation moduli of rock masses' *International Journal of Rock Mechanics and Mining Sciences*, V. 40, p.701-710.

Goodman, R., and Shi, G. (1985). *Block theory and its application to rock engineering*, Prentice-Hall, Englewood Cliffs, N.J.

Guo, W. D. (2001). "Subgrade modulus for laterally loaded piles." *Proceedings of the Eighth International Conference on Civil and Structural Engineering Computing*, Vienna, Austria.

Haberfield, C. M., and Johnston, I. W. (1993). "Factors influencing the interpretation of pressuremeter tests in soft rock." *Proceedings of the international conference on geotechnical engineering of hard soils-soft rocks*, Athens, p. 525-531.

Hall, C. G., and M.C. Wang. (2000). Behavior of laterally loaded caissons in weak rock. *ASCE Geotechnical Special Publication*, Issue 100, New Technological and Design Developments in Deep Foundations, p. 240-253.

Hawk, D. J., and Ho, H. Y., (1980) "A study of the orthotropy of coal and other rock materials," *Final Report to U.S. Dept. of Interior and Bureau of Mines*, University of Colorado.

Hetenyi, M. (1946). *Beams on elastic foundations*. Ann Arbor: University of Michigan Press.

Heuze, F.E., (1984) "Suggested method for estimating the in-situ modulus of deformation of rock using the NX-borehole jack." *Geotechnical Testing Journal*, Vol.7, No. 4, p.205-210.

Heuze, F.E. and Amadei, B. (1985) "The NX-borehole jack: A lesson in trial and error" *International Journal of Rock Mechanics and Mining Science*, Vol. 22, No.2, p.105-112.

Heuze, F.E. and Salem A. (1976) "Plate bearing and borehole jack tests in rock- a finite element analysis." *Proc. 17th U.S. Symp. On Rock Mechanics*, Snowbird, Utah, p. 4B8-1 – 4B8-6.

Hoek, E. (1983). "Strength of jointed rock masses" *Geotechnique*, v. 33 issue 3, p. 187-223.

Hoek, E., (1990). "Estimating Mohr-Coulomb friction and cohesion values from the Hoek-Brown failure criterion." *Int. J. Rock Mech. Min. Sci. & Geomech. Abstr.*, Vol. 27, No. 3, p. 227-229.

Hoek, E. (1994). "Strength of rock and rock masses," *ISRM News Journal*, 2 (2), p. 4-16.

Hoek, E., and Brown, E. T. (1980). "Empirical strength criterion for rock masses." *American Society of Civil Engineers, Journal of the Geotechnical Engineering Division*, v. 106 issue 9, p. 1013-1035.

Hoek, E., and Brown, E.T. (1988). "The Hoek-Brown criterion – a 1988 update." 15th Canadian Rock Mechanics Symposium: *rock engineering for underground excavations*, University of Toronto, p. 31-38.

Hoek, E., and Brown, E.T. (1997). "Practical estimates of rock mass strength." *Int.J. Rock Mech. Min. Sci.*, 34(8), p. 1165-1186.

Hoek, E., Carranza-Torres, C., and Corkum, B. (2002) "Hoek-Brown failure criterion – 2002 edition." *Proc. North American Rock Mechanics Society Meeting in Toronto*.

Hughes, J. M. O., Wroth, G. P., and Windle, D. (1977). "Pressuremeter tests in sand." *Geotechnique*, Vol. 27, No. 4.

Hull, D.N. (1990) and Larsen, G.E. (2000) www.dnr.state.oh.us/geosurvey/pdf/stratcol.pdf, accessed on Aug. 2004.

Hustrulid, W. A. (1976) "An analysis of the Goodman jack." *Proc. 17th U.S. Symp. On Rock Mechanics*, Snowbird, Utah, p. 4B10-1 – 4B10-8.

Johnston, I. W. (1985). "Strength of intact geomechanical materials." *J.Geotech. Engrg.*, ASCE, vol. 111, p. 730-749.

Johnston, J. W. and Lam, T. S. K., (1989a), "Shear Behavior of Regular Triangular Concrete/Rock Joints—Analysis," *Journal of Geotechnical Engineering*, Vol. 115, No. 5, p. 711-727.

Johnston, J. W. and Lam, T. S. K., (1989b), "Shear Behavior of Regular Triangular Concrete/Rock Joints—Evaluation," *Journal of Geotechnical Engineering*, Vol. 115, No. 5, p. 728-740.

Kayabasi, A., Gokceoglu, C., and Ercanoglu, M. (2003). "Estimating the deformation modulus of rock masses: a comparative study." *International Journal of Rock Mechanics & Mining Science*, Vol. 40, p. 55-63.

Kulhawy, F. H. et al. (1983). "Transmission line structure foundations for uplift-compression loading." *Rep. No. EL-2870*, Electric Power Research Institute, Palo Alto, Calif.

Kulhawy, F. H. (1991). "Drilled shaft foundations." *Foundation Engineering Handbook*, 2nd Ed., Chap. 14, H. -Y. Fang ed., Van Nostrand Reinhold, New York.

Kulhawy, F. H., and Y. -J. Chen. (1995). "A thirty year perspective of Broms' lateral loading models, as applied to drilled shafts." *Bengt B. Broms Symposium on Geotechnical Engineering, Singapore*, p. 225-240.

Kulhawy, F. H. and Phoon, K. K. (1993), "Drilled Shaft Side Resistance in Clay Soil to Rock," *Proc. on Conf. On Design and Performance of Deep Foundation: Piles and Piers in Soil and Soft Rock*. ASEC, Geotechnical Special Publication 38, p. 172-183.

Lamborn, R.E., Austin, C. R., and Schaaf, D. (1938). *Shales and surface clays of Ohio*, Geological Survey of Ohio, fourth series, bulletin 39.

Liang, R. Y. (2002). "Drilled shaft foundations for noise barrier walls and slope stabilization." *Final Rep. FHWA/OH-2002/038*, Ohio Department of Transportation.

Littlechild, Brian D., et al.(2000) "Determination of rock mass modulus for foundation design." *Geotechnical Special Publication*, issue 97, p. 213-228.

Marinos, P., and Hoek, E. (2000). "GSI: A geologically friendly tool for rock mass strength estimation." *Proc. of the International Conference on Geotechnical and Geological Engineering (GeoEng 2000)*, Melbourne, Australia, p. 1422-1440.

Matlock, H. (1970). "Correlations for design of laterally loaded in soft clay." *Proc. 2nd Offshore Technology Conference*, Offshore Technology Conference, Houston, Vol.1, p. 577-594.

Matlock, H. and Ripperger, E. A., (1956). "Procedures and Instrumentation for Tests on a Laterally Loaded Pile," *Proceedings, Eighth Texas Conference on Soil Mechanics and Foundation Engineering*, Austin, Tex.

Meigh, A. C. (1979), "Design Parameters for Weak Rocks," *Proceedings, 7th Europe Conference on Soil Mechanics and Foundation*, p. 59-79.

Menard, L., Bourdon, G., and Gambin, M. (1969). "Methode Generale de Calcul d'un Rideau ou Pieu Sollicite Horizontalement en Fonction des Resultats Pressiometriques," *Sols-Soils*, No. 22/23.

Meyer, T. O. and McVey, J. R. (1974) "NX borehole jack modulus determinations in homogeneous, isotropic, elastic materials." *USBM RI 7855*.

Mezazigh, S. and Levacher, D., (1998). "Laterally Loaded Piles in Sand: Slope Effect on p-y Reaction Curves." *Canadian Geotechnical Journal*, Vol. 35, No. 3, p. 433-441.

Mokwa, R. L., Duncan, J. M., and Helmers, M. J. (2000). "Development of p-y curves for partly saturated silts and clays." *Proceedings of Geo-Denver 2000: New technological and design developments in deep foundations*, ASCE, p. 224-237.

Murchison, J. M. and O'Neill, M. W., 1984. "Evaluation of P-y Relationships in Cohesionless Soils," *Analysis and Design of Pile Foundations*, ASCE, Ed. J. R. Meyer, p.174-191.

Nicholson, G.A., Bieniawski, Z.T.(1990). "A nonlinear deformation modulus based on rock mass classification." *International Journal of Min Geol Eng.* Vol. 8, p. 181-202.

Nusairat, J., Engel, R. L., and Liang, R. Y. (2002). "Instrumentation, monitoring and testing at the ERI-60-3100 bridge project." *Rep. Prepared for Ohio Department of Transportation*, Columbus, OH.

Nusairat, J., Liang, R., Engel, R., Hanneman, D., Abu-Hejleh, N., and Yang, K. (2004). Drilled Shaft Design for Sound Barrier Walls, Signs, and Signals. *Final Report, CDOT-DTD-R-2004-8*, Colorado Department of Transportation.

O'Neill, M. W., and Reese, L. C. (1999). *Drilled Shafts: Construction Procedure and Design Methods*, FHWA-IF-99-025.

Pells, P. J. N. et al. (1980), "An Experimental Investigation into the Side Shear of Socketed in Sandstone," *Proceedings, International Conference on Structural Foundations in Rock*, Sydney, p. 291-302.

Pise, P. J. (1982). "Laterally loaded piles in a two-layer soil system." *Journal of the Geotechnical Engineering Division, ASCE*, Vol. 108, No. GT9, p. 1177-1181.

Poulos, H. G. (1971). "Behavior of laterally loaded piles. I: Single piles." *J. Soil Mech. Found. Div., ASCE*, 97(5), p. 711-731.

Ramamurthy, T., Rao, G. V., and Rao, K.S. (1985). "A strength criterion for rocks." *Proc. Indian Geotech. Conf., Roorkee, I*, p. 59-64.

Randolph, M. F. (1981). "The response of flexible piles to lateral loading." *Geotechnique*, 31(2), p. 247-259.

Reese, L. C. (1997). "Analysis of laterally loaded piles in weak rock." *J. Geotech. Envir. Engrg., ASCE*, 123(11), p. 1010-1017.

Reese, L. C., Cox, W. R. and Koop, F. D. (1974). "Analysis of laterally loaded piles in sand." *Proc. Of 6th offshore Tech. Conf., Houston, TX*, Vol. 2, p. 473-483.

Reese, L. C., Cox, W. R., and Koop, F. D. (1975). "Field testing and analysis of laterally loaded piles in stiff clay." *7th Offshore Technology Conference*, p. 671-690.

Reese, L. C., and Matlock, H. (1956). "Non-dimensional solutions for laterally loaded piles with soil modulus assumed proportional to depth." *Proceedings, Eight Texas Conference on Soil Mechanics and Foundation Engineering*, Austin, Texas, p. 1-23.

Reese, L. C., and Welch, R. C. (1975). "Lateral loadings of deep foundations in stiff clay." *Journal of Geotechnical Engineering, ASCE*, 101(7), p. 633-649.

Richardson, D. N., and Wiles, T. T., (1990) "Shale durability rating system based on loss of shear strength," *Journal of Geotechnical Engineering*, Vol. 116, No. 12, p. 1864-1880.

Robertson, P. K., and Hughes, J. M. O. (1986). "Determination of properties of sand from selfboring pressuremeter tests." *The pressuremeter and its Marine Applications: Second International Symp., ASTM STP 950*, Texas A&M University.

Robertson, P. K., Hughes, J. M. O., Campanella, R. G., and Sy, A. (1983). "Design of laterally loaded displacement piles using a driven pressuremeter." *ASTM SPT Symposium: Design & Performance of Laterally Loaded Piles and Pile Groups*.

Robertson, P. K., Hughes, J. M. O., Campanella, R. G., Brown, P. and McKeown, S. (1986). "Design of laterally loaded piles using the pressuremeter". *The pressuremeter and its Marine Applications: Second International Symp.*, ASTM STP 950, Texas A&M University.

Rocha, M., Silveira, A., Rodrigues, F. P., Silverio, A., and Ferreira, A. (1970). "Characterization of the deformability of rock masses by dilatometer tests." *International Soc Rock Mechanics, Proc.*, Vol. 1, No. 2-32, p. 509-516.

Rocscience (2002), RocLab, a free software from www.rocscience.com, Rocscience, Inc., Toronto, Canada.

Rosenberg, P. and Journeaux, N. L. (1976), "Friction and End Bearing Tests on Bedrock for High Capacity Socket Design," *Canadian Geotechnical Journal*, Vol. 13, p. 324-333.

Sargand, S. M, and Hazen, G. A. (1987). "Deformation behavior of shales" *Int. J. Rock Mech. Min. Sci. & Geomech. Abstr.*, Vol. 24, No. 6, p. 365-370.

Seidel, J. P. and Collingwood, B. (2001), "A new Socket Roughness Factor for Prediction of Rock Socket Shaft Resistance," *Can. Geotech. J.*, Vol. 38, p. 138-153.

Serafim J.L. and Pereira J.P. (1983). "Consideration of the geomechanical classification of Bieniawski." *Proceeding of International Symposium on Engineering Geology and Underground Construction*, Lisbon 1(II), p. 33-44.

Shen, W. Y., and Teh, C. I. (2002). "Analysis of laterally loaded pile groups using a variational approach." *Geotechnique*, 52(3), p. 201-208.

Shen, W. Y., and Teh, C. I. (2004). "Analysis of laterally loaded piles in soil with stiffness increasing with depth." *Journal of Geotechnical and Geoenvironmental Engineering*, Vol. 130, No. 8, p. 878- 881.

Shuri, F.S. (1981) "Borehole diameter as a factor in borehole jack results." *Proc. 22nd U.S. Symp. On Rock Mechanics*, Cambridge, Massachusetts, pp. 392-397, MIT Press, Cambridge.

Smith, T. D. (1983). "*Pressuremeter Design Method for Signal Piles Subjected to static Lateral Load.*" Ph. D. Thesis Texas A&M University.

Stout, Wilber (1941). *Dolomites and limestones of western Ohio*, Geological Survey of Ohio, fourth series, bulletin 42.

Sun, K. (1994). "Laterally loaded piles in elastic media." *Journal of Geotechnical Engineering, ASCE*, 120(8), p. 1324-1344.

Terzaghi, K. (1955). "Evaluation of coefficient of subgrade reaction." *Geotechnique*, 5(4), p. 297-326.

To, A. C., Ernst, H., and Einstein, H. H. (2003). "Lateral load capacity of drilled shafts in jointed rock." *Journal of Geotechnical and Geoenvironmental Engineering*, Vol. 129, No. 8, p. 711-726.

Toh, C. T. et. al. (1989), "Design Parameters for Bored piles in a Weathered Sedimentary Formation," *Procs. of the 12th International Conference on Soil Mechanics and Foundation Engineering*, Vol. 2, p. 1073-1078.

Trochianis, A., Bielak, J., and Christiano, P. (1988). "*A three-dimensional nonlinear study of piles leading to the development of a simplified model.*" Report R-88-176, Dept. of Civil Engr., Carnegie Inst. of Technology.

Vesic, A. S. (1961). "Beam on elastic subgrade and the Winkler hypothesis." *Proc. 5th Int. Conf. Soil Mechanics and Foundation Engineering*, Paris, Vol. 1, p. 845-850.

Wakai, A., Gose, S., and Ugai, K. (1999). "3-D elasto-plastic finite element analyses of pile foundations subjected to lateral loading." *Soils and Foundations*, Vol. 39, No. 1, p. 97-111.

Wallace, J. W. et al. (2002). "*Cyclic large deflection testing of shaft bridges part II: analytical studies.*" Report from California Dept. of Transportation.

Wang, S. T., and L. C. Reese. (1993). *COM624P – Laterally Loaded Pile Analysis Program for the Microcomputer*. Version 2.0, Federal Highway Administration Publication No. FHWA-SA-91-048.

Williams, A. F., Johnston, I. W., and Donald, I. B. (1980). "The Design of Socketed piles in weak rock," *Proceedings of International Conference on Structural Foundations on Rock*, Sydney, p. 327-347.

Williams, A. F., and Pells P. J. N. (1981). "Side Resistance Rock Sockets in Sandstone, Mudstone, and Shale," *Canadian Geotechnical Journal*, Vol. 18, p. 502-523.

Wilson, D. 1998. *Soil-pile-superstructure interaction in liquefying sand and soft clay*. Ph. D. Dissertation, University of California at Davis.

Wood, L. E., and Deo, P. (1975). "A suggested system for classifying shale materials for embankments," *Bulletin of the Association of Engineering Geologists*, Vol. XII, No. 1, p. 39-55.

Yang, K., and Liang, R. (2005). "Lateral Response of Large Diameter Drilled Shafts in Clay." *Proceedings of DFI 30th Annual Conference on Deep Foundations*, Chicago, IL.

Yang, K., Liang, R., and Liu, S. (2005). "Analysis and test of rock-socketed drilled shafts under lateral loads." *The 40th U.S. Symposium on Rock Mechanics*, Anchorage, Alaska.

Zhang, L. (1997). *Analysis and design of axially loaded drilled shafts socketed into rock*. MS thesis, Massachusetts Institute of Technology, Cambridge, MA.

Zhang, L., Ernst, H., and Einstein, H. H. (2000). "Nonlinear analysis of laterally loaded rock-socketed shafts", *Journal of Geotechnical and Geoenvironmental Engineering*. v. 126 issue 11, p. 955-968.

Zhang, L., Silva, F., and Grismala, R. (2005). "Ultimate lateral resistance to piles in cohesionless soils." *Journal of Geotechnical and Geoenvironmental Engineering*. v.131 No. 1, p. 78-83.